NEARBY M DWARF STARS AND THE WIDE MAIN SEQUENCE

by

Tiffany Danielle Clements

Under the Direction of Todd Henry, PhD

ABSTRACT

This dissertation addresses the underlying causes for the observed widening of the main sequence for low mass stars and presents the results of three different studies using two different astrophysical observing methods to assess the properties of a sample of nearby, M dwarf stars and how these properties affect a star's position on an H-R diagram.

The first study is the assessment of the activity of the internal magnetic fields of 76 southern nearby, M dwarf stars through measurements of the relative changes in their V magnitudes over time periods of years. This long-term variability is then analyzed with respect to the vertical positions of these stars on the main sequence to determine the effects of stellar activity on these positions.

The second study uses a similar technique as the first study (relative photometry) only on short-term timescales of only hours. This study serves to assess the effects of magnetic activity and variability at the surfaces of 120 low mass stars on their main sequence positions.

The final study presented here analyzes the high-resolution spectra of 80 nearby, M dwarf stars to assess their compositions and activity indicators and how these properties affect the placement of these stars above, below, or on the central distribution of the main sequence. This study also includes the use of published metallicity values for many of the stars in our sample to better assess the importance of this property on main sequence position.

We find that variability plays an important role in the elevation of stars, particularly young stars, above the main sequence, likely due to an extension of their chromospheres caused by heightened levels of stellar activity. For stars below the main sequence we find a strong connection between their positions and abundances, as low metallicity results in a temperature displacement that ultimately places these stars below the main sequence. These results suggest that while each property is important, heightened activity is a stronger influence for stars above the main sequence while low metallicity is the primary property that places these stars below the main sequence.

INDEX WORDS: astronomy, solar neighborhood, stars: low-mass, stars: subdwarfs, stars: abundances, stars: activity, stars: flare, techniques: photometric, techniques: spectroscopic

NEARBY M DWARF STARS AND THE WIDE MAIN SEQUENCE

by

Tiffany Danielle Clements

A Dissertation Submitted in Partial Fulfillment of the Requirements for the Degree of

Doctor of Philosophy

in the College of Arts and Sciences

Georgia State University

2017

NEARBY M DWARF STARS AND THE WIDE MAIN SEQUENCE

by

Tiffany Danielle Clements

Committee Chair:	Todd Henry
Committee:	Douglas Gies
	Russel White
	Brian Thoms
	Suzanne Hawley

Electronic Version Approved:

Office of Graduate Studies

College of Arts and Sciences

Georgia State University

December 2017

DEDICATION

This dissertation is dedicated to my wonderful husband and to my daughter. My husband, Keith Clements, has been my biggest supporter and has kept me going for the last six years. Between reassuring me that I can do this and picking up the extra work left while I was traveling or working well into the evenings he has kept me grounded and pushed me to do anything I set my mind to. He has kept me both sane and fed through the last six years and I am so grateful for all that he has done. My daughter, Artemis, while she may not be here yet, her constant kicks and stretches over the last several months have kept me motivated and sprinting for the finish line. I can't wait to finally meet her and guide her through the world until she finds her own place in it, as I have.

ACKNOWLEDGMENTS

Many thanks go to my adviser and mentor for the past six years, Dr. Todd Henry. Your to-do lists, guidance, and many paper edits have kept me on the path to this point and allowed me to evolve from "Protodoctor" to Dr. Clements.

The RECONS Team has always been a wonderful group that never questions working together and using observing time for each other to make sure we all succeed together. Wei-Chun Jao has always made himself available to answer my questions and taken the time to show me how to do something. Sergio Dieterich, Adric Riedel, and Jennifer Winters have all helped me to edit a paper, made their data readily available, used observing time to help with my projects, or answered any questions I've emailed them throughout my time at Georgia State. Michele Silverstein is the closest RECONS member to me and we've gone through a lot of this together. We've learned how to navigate our way through the group, attended conferences, and shared our observing time and expertise. I'm grateful to have had such a wonderful colleague and friend with whom to go through all of this.

My family and friends have always been supportive of my goals and taken the time to be there for both my complaints and successes. Thank you to my parents for raising me to know that if I want something badly enough and work hard enough, then I can do it, and for never doubting that I would make it this far. I love you both. Thank you to my sisters, Diana and Sara, and my brother, Josh, for being the best (and most complicated) family I could have asked for. You've all been so understanding about my missing so many family events and

gatherings because of the difficulty of traveling so far during grad school. Missing out on time with you has been one of the hardest parts of all of this, but I've cherished every moment I've had to visit or talk with you. Finally, to my friends, those of you not in Astronomy have found it so fascinating and "cool" to learn about what I do and your enthusiasm has always kept me motivated, those of you in Astronomy have understood how frustrating and complex this field can really be and have lamented with me, supported me, and always kept me grounded with how brilliant each of you are. Thank you all for your support, advice, and (Charlie) housing and feeding me for the past three years that I've lived out-of-state.

Finally, thanks to Alvin Das, the original creator of the LaTeX package for the preparation of a GSU dissertation, and the most recent editor of the package, Jeremy Jones. This dissertation would have probably never been written if it weren't for you as you've saved many Astronomy graduate students months of trying to find a way to format these daunting documents just right.

TABLE OF CONTENTS

LIST OF TABLES

LIST OF FIGURES

CHAPTER 1
INTRODUCTION

1.1 M Dwarf Stars

This research focuses on the properties and processes of the nearby population of M dwarf stars, where nearby is considered to be within 50 parsecs (pc) of our Solar System. M dwarfs are hydrogen fusing stars classified as "M" based primarily on molecular TiO bands evident in their spectra. These stars are very low mass, ranging from about 0.60 – 0.075 $M_{\odot}$, and are cooler, with effective temperatures from 2300 K to 3800 K, than higher mass stars like the Sun at 5800K (Tarter et al. 2007). For our study, we use photometric data in the V and K_s bands together as a proxy for stellar temperatures. For M dwarfs the $(V - K_s)$ colors range from about 3.5 to 8.8, the largest range of any spectral type.

M dwarfs represent at least 75% of stars in the solar neighborhood (Henry et al. 2006) and span larger ranges in luminosity and color than any other main sequence spectral type. These cool stars have main sequence lifetimes longer than the known age of the Universe, and M dwarfs are prime candidates for habitable planet hosts because although each M dwarf has a traditional habitable zone narrower and closer to the star than do solar-type stars, their ubiquity leads to them providing more aggregate habitable real estate than any other type of star (Cantrell et al. 2013). For instance, the closest star, the red dwarf Proxima Centauri, was recently discovered to have an orbiting terrestrial planet (Anglada-Escudé et al. 2016), and many other nearby red dwarfs are known to harbor planets as well (e.g., Bonfils et al. 2013).

1.2 The Wide Main Sequence

When the luminosities and temperatures of stars are plotted against each other (luminosity vs. temperature) – also known as a Hertzsprung-Russell (H-R) diagram – a majority of the stars fall into a diagonal, and slightly curved, line descending with descending temperature. This is what is known as the main sequence. Stars on the main sequence are hydrogen-burning stars that have finished contracting after their formation and are at a stable luminosity. Once these stars begin to run out of hydrogen to burn, they reach the ends of their stellar lives and begin to evolve off of the main sequence. This evolution begins by first moving the stars up and right – as their luminosities increase and temperatures decrease – until finally settling in the lower left region of this plot as white dwarfs. As shown on the H-R diagram in Figure 1.1, the main sequence significantly widens in the vertical (luminosity) direction for dwarfs of spectral class M0V through M5V. Figures 1.1 and 1.2 are the result of the RECONS[1] (REsearch Consortium On Nearby Stars) effort to measure and compile parallaxes and high quality $UBVRIJHK_s$ photometry values for more than 3000 stars within 25 pc using both RECONS data and values from the literature, supplemented with additional young stars and subdwarfs out to 50 pc. These data provide a precise representation of the observational H-R diagram shown in Figure 1.1, using absolute V magnitudes vs. $(V - K_s)$ colors – K_s magnitudes are sourced from 2MASS and are hereafter referred to only as "K". For comparison, an M_I vs. $(I - K)$ version of this H-R diagram is shown in Figure 1.2.

The region of the main sequence for the G and K spectral classes has an average width in

[1] *www.recons.org*

luminosity of ∼1 mag in M_V, as shown in Figure 1.1, so, for this work, we define an M dwarf to be "on" the main sequence if it lies within half a magnitude above or below this central fit of the distribution. The deviation, or distance, from the main sequence is determined by calculating an M_V value on the fit for the $(V - K)$ value of a given star, then subtracting the M_V of the fit from the known M_V of the star. For the sample of 657 stars in the three boxes for this study, 421 (64.1%) are within 0.5 mag of the fit, 590 (89.8%) are within 1.0 mag of the fit, and 622 (94.7%) are within 1.5 mag of the fit. Overall, stars in this study span the region from about 3 mag above (negative ΔM_V) to about 4 mag below (positive ΔM_V) for the most extreme young stars and subdwarfs, respectively.

From Figures 1.1 and 1.2 and other H-R diagram representations, such as the M_I vs. $(I - K)$ representation in Figure 1.2, it is clear that the main sequence drastically widens in luminosity for M dwarfs for various colors selected in the optical and near-infrared. The vertical width on these figures is ∼4 mag[2] through much of the M dwarf region, corresponding to a factor of ∼40 in luminosity. The Stefan-Boltzmann equation is used to determine stellar luminosities: $L = 4\pi R^2 \sigma T^4$ where L is luminosity (in Watts), R is radius (in meters), σ is the Stefan-Boltzmann constant ($5.67 \times 10^{-8} W m^{-2} K^{-4}$), and T is temperature (in Kelvin). Thus the luminosity is related to the size of the star via $L \propto R^2$. This implies that M dwarfs with similar spectral energy distributions (SEDs) vary by more than a factor of 6 in radius. The causes of this widening of the main sequence are still not fully understood, but there are several properties explored through this work that are likely to be contributing factors.

[2]In places, the widening extends to ∼6 mag, or a factor of ∼250 in luminosity.

- *Age*: Young red dwarfs with ages less than ∼200 Myr (Bell et al. 2015) are much brighter than their older counterparts of the same color. This is due primarily to their larger sizes, as they have not yet completed gravitational contraction to their final equilibrium radii (David et al. 2016). Stars with masses of 0.6 $M_{\odot}$ take ∼120 Myr to reach the zero age main sequence, while those with masses of only 0.1 $M_{\odot}$ take ∼1.5 Gyr (D'Antona & Mazzitelli 1985; Baraffe et al. 2015). In addition, red dwarfs remain in an elevated state of activity longer than the higher mass stars (West et al. 2008), which may also contribute to higher flux and/or variability levels. The opposite is true for older stars, known as cool subdwarfs, which have reached their ultimate size (at least for eons) and are typically less active (Jao et al. 2011).

- *Magnetic Fields*: The magnetic properties of early-type red dwarfs are generally correlated with age, but late-type red dwarfs exhibit the characteristic spots and flares due to magnetic activity presumably long after they have stopped contracting (West et al. 2004, 2008). For example, cluster surveys targeting the age-activity relation in low mass stars – such as those carried out by Stauffer et al. (1991) and Prosser (1992) – have produced various results. The work done by Stauffer on the Pleiades ($70 - 100$ Myrs) and Hyades ($\sim$ 600 Myrs) found through CaII K and Hα emission measurements that activity decay timescales increase toward lower mass stars, while Prosser's work on Alpha Perseids ($\sim$ 50 Myrs) found that Hα emission strength in M0V to M4.5V type stars decreases towards older systems, but with no mention of timescales for activity decay. Surveys of M dwarf stars in the solar neighborhood have found that there is no

age-activity relation for stars later than type M5V (Hawley 1993). Magnetic fields may affect stellar brightnesses, and thus vertical locations relative to the main sequence, in several ways, each of which can be observed over different timescales: (1) short-term effects can be seen via brightness changes due to solar flares over minutes to hours, (2) mid-term effects can be detected by measuring the rotation periods of stars as spots rotate in and out of view over hours to months, and (3) long-term effects of starspot cycles are studied via steady changes in brightness as the number of spots increases or decreases over years. Feiden & Chaboyer (2013, 2014) hypothesize that strong magnetic fields in low mass stars would inhibit convection in the stars, disrupting their thermodynamic equilibria and thus inflating their radii. However, their study used a small sample of detached eclipsing binaries and found that there is insufficient evidence to support this hypothesis for both fully convective stars and those with radiative cores, though the evidence was stronger for the latter.

- *Metallicity*: Often, the main sequence widening for M dwarfs has been solely attributed to varying metallicities in these stars (see e.g., Bonfils et al. (2005); Newton et al. (2014)). However, metallicity alone is not a complete solution to the issue, as illustrated in the H-R diagram for the Hyades in Figure 1.3. Data have been gathered from Goldman et al. (2013) and compiled using photometric data from the 2MASS and UCAC4 catalogs for stars with membership probabilities of at least 50% from van Altena (1969), Hanson (1975), or Reid (1993) (V photometry from Reid (1993) were used when UCAC4 values were not available). It is generally assumed that each Hyad

formed at the same time from the same interstellar material with a metallicity of [Fe/H] = +0.107, and there is no evidence of an [Fe/H] difference between Hyades dwarfs and giants (Taylor 1994); a modest abundance dispersion of 0.021 ± 0.003 dex (Liu et al. 2016) cannot account for the observed broadening of the main sequence. The current accepted age for the Hyades is 625 ±50 Myrs (Perryman et al. 1998), and a modest spread in age cannot explain the ∼2.5 mag spread in the central Box shown, which mimics our central Box 5 outlined for our sample in Figures 1.1 and 1.2. However, two Hyads with the same color, age, metallicity, and presumably mass do not necessarily have the same magnetic field properties, which can be indirectly studied by measuring photometric variability.

Metallicity variations are undoubtedly an important contributor to the widening of the main sequence for the heterogeneous sample of low mass stars within 25 pc. The stellar population in the solar neighborhood is a mixture of star formation events, resulting in significantly more low metallicity M dwarf stars than low metallicity high mass stars, which have relatively short stellar lifetimes and in many cases have joined the nearby white dwarf population. For a given mass, sub-solar metallicities result in bluer M dwarf stars, moving them significantly to the left and slightly up on the H-R diagram, and thus below the main sequence (Jao et al. 2008). Extremely high metallicity values could account for some of the spread above the main sequence, but this has not yet been confirmed for stars several magnitudes above the center of the distribution. Our work includes a spectroscopic assessment of metallicity across the luminosity spread

for stars in the sample (Chapter 5). There have been several spectroscopic efforts to assess the metallicity of M dwarfs, such as those of Bonfils et al. (2005), Rojas-Ayala et al. (2012), Neves et al. (2014), and Gaidos & Mann (2014) each of which has its own strengths.

- *Multiplicity*: Unresolved companions will certainly elevate points on an observational H-R diagram, boosting the location by 0.7 mag for an equal-luminosity binary. However, the sample of 25 pc stars and supplemental samples of young stars and subdwarfs in Figures 1.1 and 1.2 have been carefully vetted by the RECONS team for close multiples. While there will be a few close systems not yet resolved, the vast majority of stars plotted are known to be single; all known unresolved multiples have been removed from our sample and any newly resolved stars were removed as they were discovered. Even if the sample had not been vetted carefully, the overall M dwarf multiplicity fraction is only ∼28% (Winters 2015), which is insufficient to account for the dispersions seen in Figures 1.1 and 1.2.

- *Miscellaneous Properties*: Other properties that may contribute to the wide dispersion in brightness and radius of these stars include the depth of the convection zone (i.e., mixing length) and projected rotational velocity (vsin$i$). In the latter case, inclination may affect the brightness measured for the star if it is spinning rapidly, such as in the case for higher mass stars (McAlister et al. 2005). To date, no studies have been carried out to explore these properties and their relation to vertical main sequence position for a large number of M dwarf stars.

1.3 Activity in Low Mass Stars

This thesis focuses heavily on the activity of the nearby, low mass stars as it relates to their vertical positions relative to the center of the distribution of the main sequence. In order to better understand the ways in which we examine these activity levels and variability indicators we need to define activity in low mass stars and how it is studied. The activity of a star is linked to its magnetic field and the strength of the magnetic field can be studied through various activity indicators. These indicators include emission of the Hα and Ca II H and K lines in their spectra, as well as flares and starspots observed through photometric changes in brightness (the primary method used for this work).

The role activity plays in the H-R diagram position of a star above or below the main sequence is still not fully understood. While the brightness of the star is clearly affected, it is not clear what stellar properties are influenced by activity to cause this observed disparity. In Mann et al. (2015), methods were explored to constrain accurate stellar properties, such as mass, temperature, luminosity, and radius. They then assessed the various properties that may correlate with the errors in actual measurements versus their models. By measuring the strength of the Hα feature and using X-ray, NUV, and FUV fluxes from the literature, they were able to analyze whether or not there is any correlation between stellar activity and other observed stellar properties. What they found is that variations in magnetic activity appear to play no significant role in the offsets between the models and the observed temperatures and radii for the sample of M dwarf stars in their study.

Observing these stars through the V filter will show brightness changes as a result of

activity from the photospheres of these stars, where the effects of starspots and large flares can be observed (Cutispoto 1990). Studies done using the emission spectra of these stars as indicators of stellar activity are ideal for looking at activity in the chromospheres – Hα, in particular, responds to increasing temperatures in the chromosphere – where flares and prominences are more likely to be observed easily via emission features (Cutispoto & Giampapa 1988). While we use both methods to assess the activity in our sample of stars, we primarily focus on activity measurements through photometric variability, as detailed in Chapters 3 and 4.

1.4 Off-Main Sequence Stars in This Study: Young Stars and Subdwarfs

A primary aspect of this work is to gain a better understanding of the properties of the low mass star population. To accomplish this goal we need to observe these stars at all available stages of their long stellar lives. This means we need to include as many targets as we can from both the youngest low mass stars, representing the earliest stages of their evolution, and the subdwarf stars, representing the oldest available population. Closely studying these stars is also important as they generally lie on the extreme vertical ends of the main sequence, with young stars typically residing far above the main sequence and subdwarf stars along the bottom and below it. In order to enrich the sample of these important stars, our search radius was extended from 25 pc to 50 pc for these targets.

The extension of our search radius for these extreme stars has enriched our sample enough to include a total of 33 young stars and 33 subdwarfs. Of these young stars in the sample,

there are five located in Box 4, twenty in Box 5, and eight residing in Box 6. For the 33 subdwarfs[3] there are twenty-five in our Box 4 sample, five in the central region of Box 5, and only three in Box 6. These young and subdwarf stars have been labelled as the highest priority on our observing lists, to ensure enough would be observed for our ongoing studies, as they are in the extreme minority among the total of 657 stars in our target boxes, making up about 5% of the sample each.

The 33 stars residing within 50 pc that are elevated on the H-R diagram and show indications that they are younger than ∼200 Myr comprise our young sample. These M dwarfs were identified as nearby, young stars in Riedel et al. (2014) and references therein by (1) astrometric methods to determine moving cluster associations with young moving groups such as TW Hydra and β Pictoris, and/or (2) spectroscopy for the detection of the presence of lithium. By "young" we mean hydrogen fusing, pre-main sequence stars with ages of 200 Myrs or less (Bell et al. 2015), even though M dwarfs may remain active for much longer than this — about 1 Gyr for spectral type M0 and 7 Gyr for M5V according to West et al. (2008). Young stars are elevated above the main sequence due to their larger radii because they have not yet finished contracting.

The 33 stars within 50 pc classified as M-type subdwarfs lie below the main grouping of stars on the H-R diagram. Subdwarfs are relatively rare and are difficult to identify because they are intrinsically faint and high resolution spectra are typically required. These stars have

[3]We note that suspected, but not yet confirmed, subdwarfs included in this study are denoted as "(S)" in Tables 3.1, 4.1, and 5.1. These suspected subdwarfs are marked as such due to their positions more than one full magnitude below the main sequence and their metallicity values near or below $[m/H] - 0.5$ in one or more of the metallicity surveys mentioned in §1.2 and discussed in Chapter 5.

low metallicities of $[m/H] \leq -0.5$ and high space velocities – both characteristics are related to their advanced ages (Jao et al. 2011). Because of their low metallicities, M subdwarfs have lower atmospheric opacities than main sequence stars, revealing deeper, hotter layers that consequently move subdwarfs to bluer, hotter locations on the H-R diagram. Almost all of the subdwarf stars in our sample lie between 1–4 mag below the fit in Figure 1.1, but we note that this range is primarily caused by a temperature displacement and is not necessarily a result of smaller radii.

1.5 The Bigger Picture

The complexity of M dwarf stars and the driving mechanisms behind the observed disparity in luminosities at a given temperature will affect how these stars evolve as thermonuclear fusion ceases and they end their lives on the main sequence. Given the extreme lifetimes of these stars, which may last trillions of years (Adams et al. 2005), there are no observable examples of evolved M dwarf stars, so much of the knowledge of their evolutionary tracks is derived from theoretical models. Uncovering these mechanisms and their roles in the radii and brightnesses of M dwarf stars over time will help to improve these models. A better understanding of the roles of the various properties discussed in §1.2 will also enable theoretical astronomers to better model how changes in each property will affect how and when these stars will begin to evolve and end their stellar lives.

1.6 Overview of This Thesis

The remaining content of this thesis is divided between five chapters. In the next chapter, Chapter 2, we describe the sample for this work. This includes the properties and types of stars included as well as the origins of all of the data used for this work. We also discuss how we define the central area of the dispersion of the main sequence, as well as the regions of the main sequence that we focus on and why. In Chapter 3 we detail our long-term variability study, the stars in this study, and the results. This study assessed the activity levels of the interior magnetic fields of 76 stars over timescales of years. Chapter 4 discusses the procedure, stars, and results of our short-term variability study where we studied the variability of 120 stars over time periods of only hours to assess the surface magnetic field activity. Chapter 5 details the final study for this work outlining the methods, stars, and results for the spectroscopy component. For this study we have obtained high resolution spectra for 80 stars to assess their ages, activity indicators, and metallicities. In the final chapter, Chapter 6, we discuss our conclusions from all three studies and what we have discovered about the complexity of low mass stars and how these properties affect their positions above or below the main sequence.

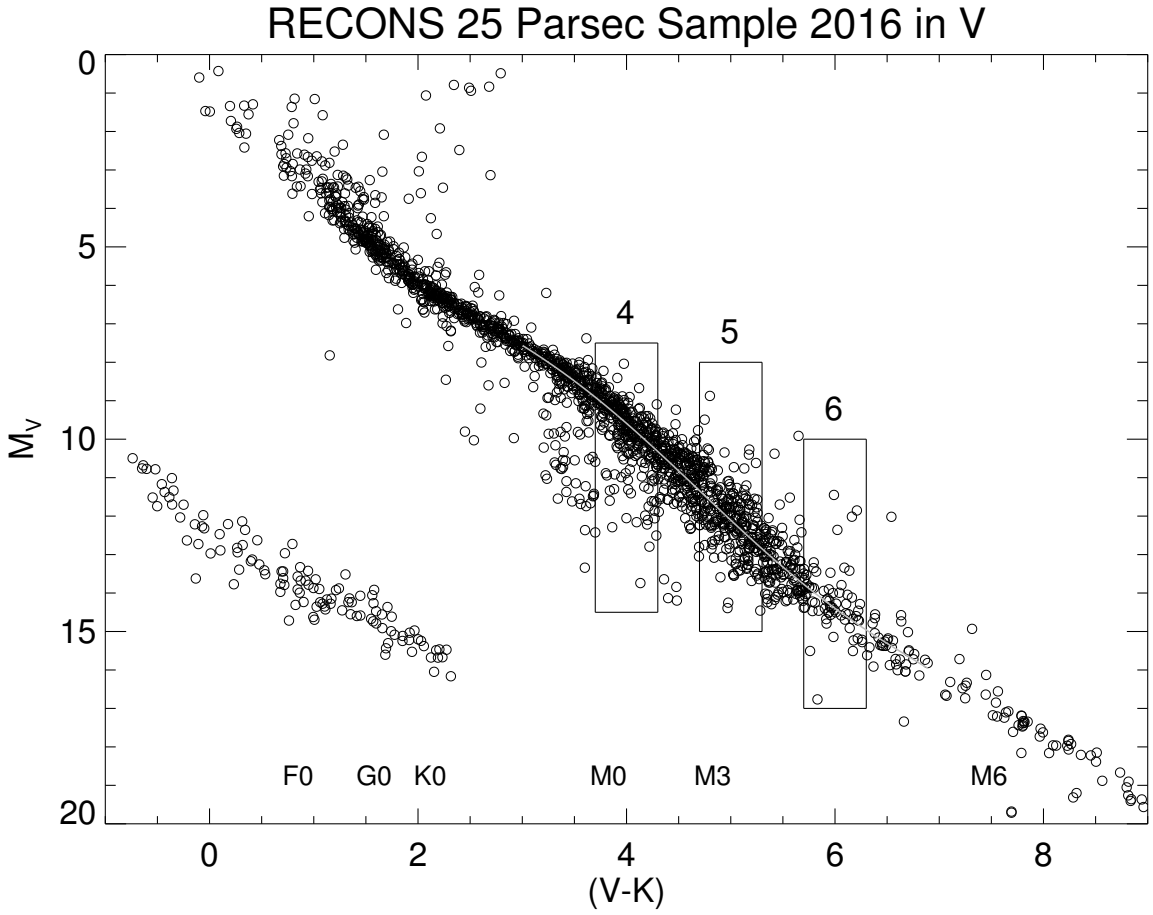

Figure 1.1: RECONS 25 pc sample H-R diagram created using stars with accurate parallaxes, V magnitudes, and 2MASS K_s magnitudes from both the literature and RECONS observations, supplemented with young stars and subdwarfs out to 50 pc. Our target Boxes 4, 5, and 6 (left to right), corresponding to their centers on the $(V-K)$ axis, are outlined. More details on these three boxes are given in Chapter 2. The gray line through the main sequence is our polynomial fit to the data from $(V-K) = 3-7$, excluding outlier, young, and subdwarf stars, and is our reference for a star's vertical distance from the center of the distribution. Stars to the lower left are white dwarfs and evolved stars are found in the region near $(V-K) \approx 2$ and $M_V \sim 2$. The errors here are smaller than the points, and are thus not displayed on the plot.

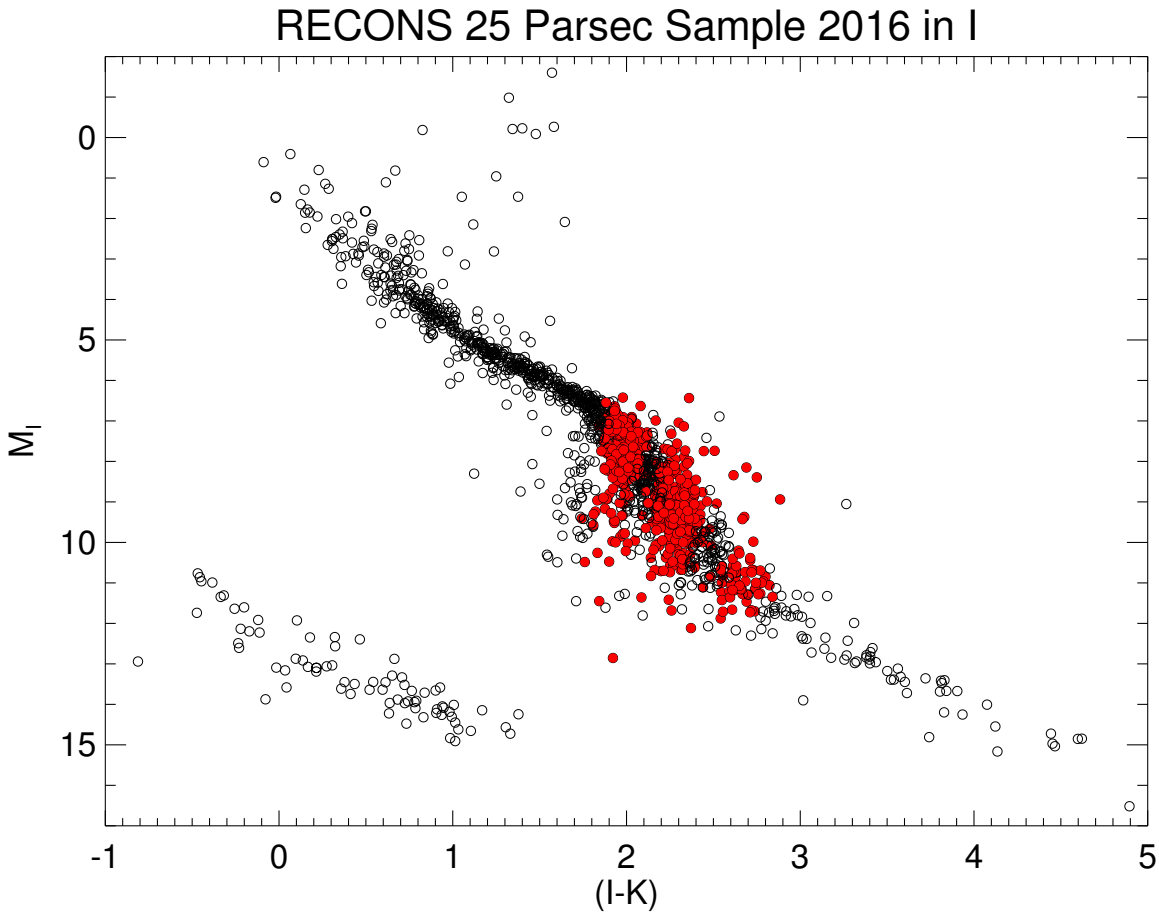

Figure 1.2: RECONS 25 pc sample H-R diagram created using stars with accurate parallaxes, I magnitudes, and 2MASS K_s magnitudes from both the literature and RECONS observations. Filled, red points indicate targets from the complete sample of 657 stars with reliable I photometry, located within the three boxes on Figure 1.1. This serves to confirm the observed broadening of the main sequence for M0V to M5V stars using different attributes other than M_V and $(V - K)$.

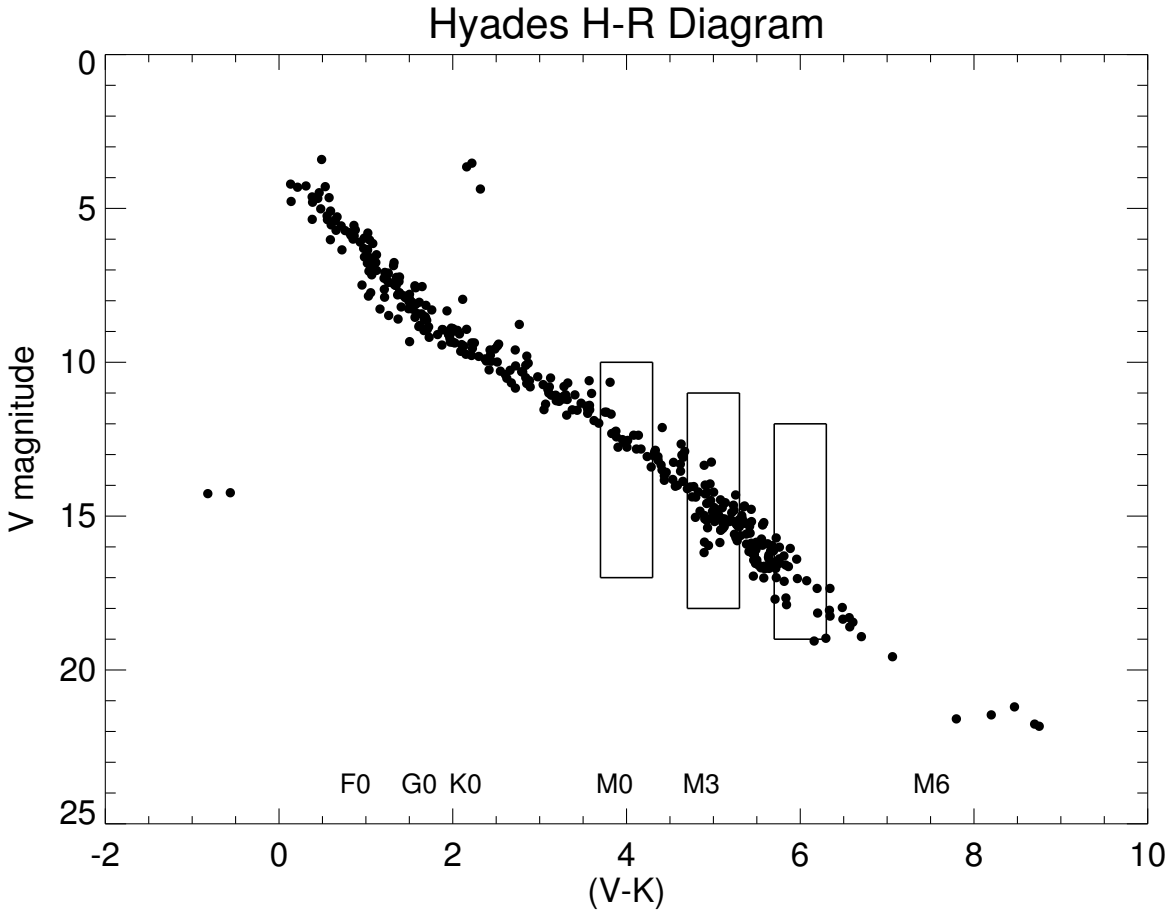

Figure 1.3: Members of the Hyades are shown on an H-R diagram created using accurate apparent V magnitudes and 2MASS K_s magnitudes from the literature for 400 high probability Hyades members. For comparison, the plot uses variables from the same filters as Figure 1.1, and our sample boxes are adjusted for apparent magnitudes and included. The Hyades main sequence begins to slightly widen past spectral type M0V, despite an assumed uniform metallicity and age throughout the star cluster. The data used to create this figure were gathered from the references described in §1.2.

CHAPTER 2
SELECTION OF TARGETS

2.1 Origin of the Data

The RECONS team has been gathering astrometric and photometric data for more than 3000 stars within 25 pc for the past two decades, with a key resource being the Small and Moderate Aperture Research Telescope System (SMARTS) 0.9 m telescope at the Cerro Tololo Interamerican Observatory (CTIO) near La Serena, Chile. These thousands of stars are compiled to create Figure 1.1, our precise 25 pc H-R diagram, using absolute V magnitudes for the luminosity and $(V - K)$ colors as a proxy for temperatures. These data are sourced from a combination of the RECONS published parallaxes and photometric magnitudes and carefully vetted sources from the literature. These sources include Bessel (1990), Weis (1994, 1996), Koen et al. (2010), and various references from the US Naval Observatory (USNO) for our V magnitudes, and K_s magnitudes from 2MASS (Skrutskie et al. 2006). Distances are calculated using the weighted mean trigonometric parallaxes from the CTIOPI (Cerro Tololo Inter-American Observatory Parallax Investigation) project (Jao et al. 2005, 2011; Henry et al. 2006; Riedel et al. 2010, 2011, 2014; Winters et al. 2015) and from the additional references as listed in the Tables 3.1, 4.1, and 5.1. These references include sources from the Yale Parallax Catalog (YPC) (van Altena et al. 1995), *Hipparcos* surveys (van Leeuwen 2007; Fabricius & Makarov 2000; Gould & Chanamé 2004), the Allegheny Observatory parallax program (Gatewood 2008), and others (Shkolnik et al. 2012; Smart et al. 2010, etc.). These surveys and studies together provide accurate parallax measurements for

thousands of stars in the solar neighborhood. These sources and our own observations provide parallax values with very low typical errors of only two milliarcseconds. This translates to an error in absolute V magnitude of only 0.04 mag for stars at 10 pc, and 0.11 mag for stars at 25 pc. As a result our errors in M_V are smaller than the point sizes in Figures 1.1 and 1.2, thus solidly placing the positions of our stars on the observational H-R diagrams. In Figure 2.1 we show a zoom-in of Figure 1.1 on the low-mass region of stars that are of interest for this work.

The data obtained for the long-term variability study were gathered over the last two decades using the CTIO SMARTS 0.9 m telescope as part of the parallax survey work.

The data obtained for the short-term variability study were gathered over four years on two different telescopes at two different sites. The light curves for our stars in the northern hemisphere were observed using the 0.5 m ARCSAT telescope at Apache Point Observatory (APO) in Sunspot, NM over 42 nights carried out remotely on the telescope, about ten of which were obtained while the telescope was still new and in the testing phase. The southern targets for this study were obtained using the 0.9 m telescope at CTIO, gathered over 36 nights on-site, 19 of which were obtained through NOAO granted observing time.

The spectroscopic data for this work were also gathered at both APO for our northern targets and CTIO for our southern targets. We were granted about 30 hours of queue time on the SMARTS 1.5 m telescope at CTIO using the CHIRON echelle spectrograph[1]. For our northern targets, we used the echelle spectrograph ARCES mounted on the 3.5 m telescope at APO, where we had ten successful nights of observations, three nights of which were carried

[1]We note that these spectra are not part of the analysis for this work, as detailed in Chapter 5.

out on-site, while the remaining nights were performed remotely. These two intsruments have similar resolutions – R ∼25000 for CHIRON vs. ∼31500 for ARCES – and wavelength ranges – $\lambda = 410 - 870$ nm vs. $350 - 1010$ nm – allowing us to rely on comparable results from each telescope. Each of the telescopes and instruments used for this work are detailed in Table 2.1.

Our observations were supplemented with additional data gathered from the literature in order to further support our results and test our hypotheses. These include ROSAT detections that were used for our long-term study, gathered from Voges et al. (1999) to support our variability results with an X-ray component. We have also supplemented our spectroscopy study with metallicity values pulled from various, reliable sources, including Bonfils et al. (2005), Rojas-Ayala et al. (2012), Neves et al. (2014), and Gaidos & Mann (2014) to assess the effects of metallicity on the H-R diagram placement of our stars.

2.2 Elimination of Close Binaries

Unresolved multiples would certainly influence the vertical width of the low mass main sequence as these multiple systems would be interpreted as single stars with the brightness of two or more. We eliminated such star systems as they were discovered throughout our research. Spectroscopic binaries were eliminated when they were discovered via literature searches on each target. Unresolved binaries or multiples that were previously unknown are often detected during our parallax observations using the CTIO 0.9 m telescope. Dozens of M dwarfs observed at the 0.9 m have been found to exhibit astrometric perturbations

due to unseen companions (e.g., Riedel et al. 2010; Winters et al. 2017); these have also been removed from our sample. If a close, unresolved system is suspected, due to the shape of the point spread function, it is then confirmed with subsequent observations and then removed from our sample for this work. The 0.9 m CTIO telescope is capable of resolving binaries for aperture photometry with an angular separation of about $2''$ and we conservatively exclude any targets at or closer than $5''$. As a result, only stars that (as far as we have been able to detect) have individual photometric measurements are included in this work. Studies using imaging to resolve close multiples find that stellar/substellar binaries are rare (Dieterich et al. 2012) and the small number of close, low mass companions that have been discovered using adaptive optics (Beuzit et al. 2004) have also been removed from our sample (see also Dieterich 2013 and Winters 2015). Through radial velocity searches for M dwarf companions, only 12 new companions were uncovered in a sample of 127 nearby stars ($\sim 9\%$) (Delfosse et al. 1999); these have also been removed from our sample. Wide binaries are either already known or are detected via their common proper motions and distances derived from parallaxes. Such stars are not eliminated from the sample so long as both stars lie within any of our three target boxes. Given the vast distances between the stars in such systems it is improbable that there would be any interactions between the stars that might affect the results of this project. The careful vetting carried out to remove any close binaries from this study has resulted in a large sample of effectively single low mass stars within the solar neighborhood; a total of 657 stars are part of this study.

2.3 Defining the Center of the Dispersion

In order to quantify a star's vertical distance from the main sequence, in absolute V magnitudes, we first have to define the center of the main sequence. This was done by fitting a polynomial line to the data on the H-R diagram in Figure 2.1. Due to the natural "S" shape of the main sequence, this was best done by fitting only the lower portion of the main sequence that concerns our study spanning the spectral range from about K5V to M6V (or a range in $(V - K)$ color of 3–7). We also only included stars that (a) are not known to be young, or (b) are subdwarf stars, and that (c) lie within one magnitude of the central distribution of the points along the main sequence, in order to avoid using outliers in the calculation of the fit. We chose stars within a width of one magnitude for our fit because this is the average width of the main sequence for stars of higher mass than spectral type K5V. We ran these data through the IDL *poly_fit* program and derived a fifth order polynomial fit to the curve, as an order greater than five had no further positive effect on the quality of the fit. To select the best polynomial fit we used the standard error between the M_V values of the points used for the fit and the M_V of the fit. For the fifth order this error was 0.48095 mag, the sixth order was 0.48104 mag, and the error of the seventh order fit was 0.48118 mag, therefore the quality of the fit was slightly degrading and the difference between the fifth order polynomial standard error and that of the sixth and seventh orders was negligible at less than 0.25 mmag. The resulting polynomial equation is:

$$M_V = -8.2673 + 17.1812(V-K) - 8.3311(V-K)^2 + 2.0744(V-K)^3$$
$$-0.2371(V-K)^4 + 0.0101(V-K)^5$$

Using this equation, we are able to quantify how far a star is above or below the central fit of the main sequence by calculating a star's vertical distance, or ΔM_V, as the difference between the absolute magnitude of the star from that of the fit at the same $(V-K)$ value. We use these ΔM_V values in our study to compare various properties of the stars to their main sequence positions to better understand the disparity in their luminosities, and presumably radii. The fit is also represented in Figures 1.1 and 2.1 as the light grey line along the central area of the data.

Due to the likely drifts in $(V-K)$ colors due to properties other than radii and temperature, such as starspots and clear atmospheres, we note that there is a need to measure accurate masses for these stars as well. With accurate masses we can better constrain their temperatures and radii in order to more accurately place their H-R diagram positions and measure their offsets from the central distribution of the main sequence.

2.4 Defining Our Boxes: What They Represent

Each of the three boxes illustrated in Figures 1.1 and 2.1 was carefully defined in order to include enough stars for a statistically significant study, provide a robust sample of each type of star, and to sample the three primary regions of the low mass H-R diagram – stars with radiative cores, those in the "transition" region, and fully convective stars. The boxes are

centered on $(V-K)$ values of 4, 5, and 6, and thus they are referred to as Boxes 4, 5, and 6. Each has a width in $(V-K)$ color of 0.6 magnitudes, the vertical range is arbitrary, as all stars within the $(V-K)$ range are included in the sample regardless of the absolute V magnitude. The first box, Box 4, ranges from $(V-K) = 3.7-4.3$ and contains 296 stars of spectral types K7V to M3V. These are stars in the region of the main sequence where all of the stars have radiative cores. Box 5, the central box, covers $(V-K) = 4.7-5.3$ and consists of 279 stars in the transition region, where the stars may or may not be fully convective. Current theoretical work estimates that stars become fully convective near a stellar mass of $0.35 M_{\odot}$ (Chabrier & Baraffe 1997), which corresponds to a spectral type of about M3.5V, and the stars in Box 5 range in spectral type from M2V to M4.5V. The last box, Box 6, ranges from $(V-K) = 5.7-6.3$ and spans spectral types from M4V to M6V. Box 6 contains 82 of the lowest mass stars in this study that are presumed to be fully convective, containing no radiative zones. The vertical spread in magnitude (ΔM_V) among all of these stars ranges from 3.83 magnitudes below (positive values) to 2.94 magnitudes above (negative values) the main sequence. These boxes have been carefully defined in order to include the most robust sample of spectral types, ΔM_V values, young stars, subdwarf stars, and stars with each type of primary energy transport method.

Table 2.1: Telescopes and Instruments Used.

Telescope	Site	Instrument	Filter	Wavelength(s)	# Nights	# Stars
0.5 m	APO	SurveyCam	V	541.1 nm	42	70
0.9 m	CTIO	Tek2K CCD	V	543.8 nm	36	54
3.5 m	APO	ARCES	$\cdots$	$350 - 1010$ nm	10	81
1.5 m	CTIO	CHIRON	$\cdots$	$410 - 870$ nm	5	25

Details of the four telescopes and instruments used for this work. Further details are provided in each chapter.

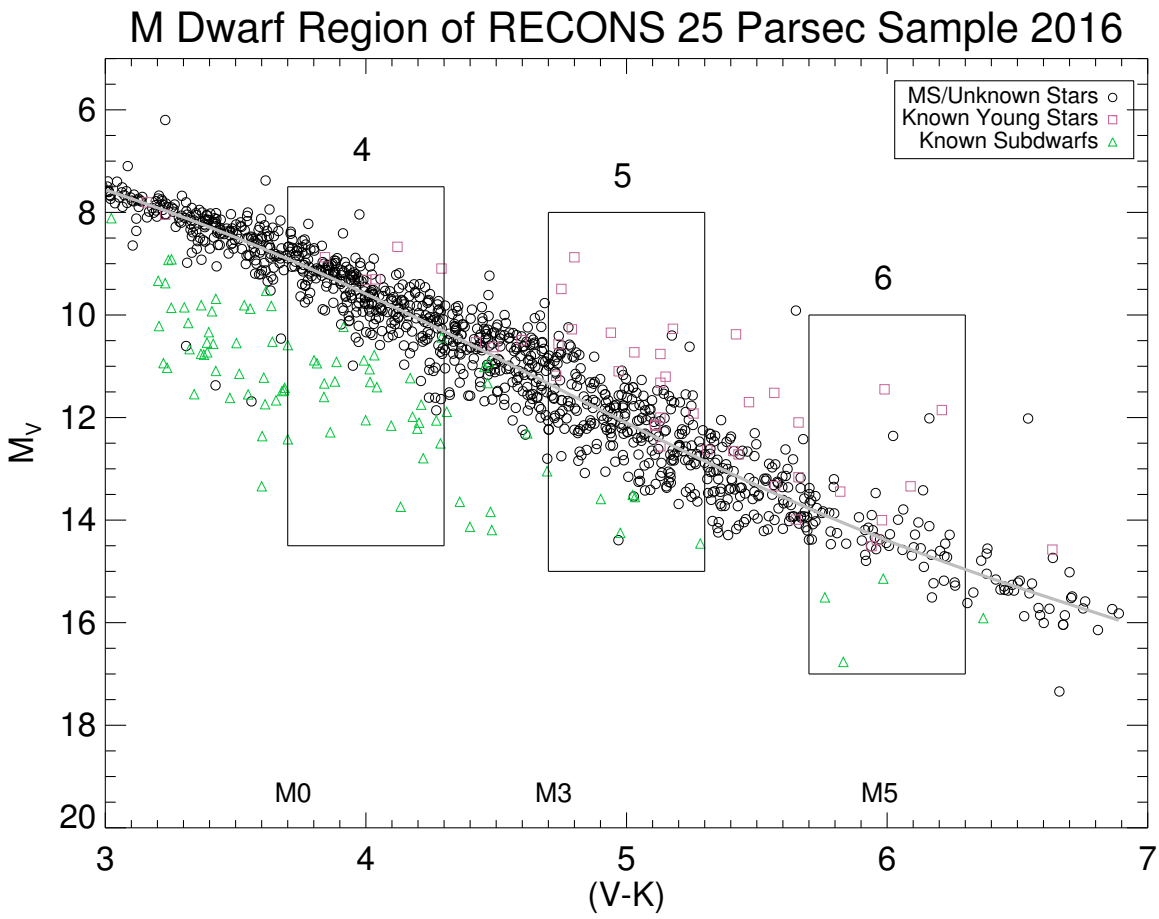

Figure 2.1: RECONS 25 pc sample H-R diagram from Figure 1.1 focused on the M dwarf region and our targets for this project. Our target Boxes 4, 5, and 6 (left to right), corresponding to their centers on the $(V-K)$ axis, are outlined. The gray line through the main sequence is our polynomial fit to the data from $(V-K) = 3-7$, excluding outlier, young, and subdwarf stars, and is our reference for a star's vertical distance from the center of the distribution. The sample horizon of 25 pc for the nearest stars (black circles) is extended to 50 pc for our young (pink squares) and subdwarf (green triangles) stars to increase the number of stars available for those samples.

CHAPTER 3
LONG-TERM VARIABILITY STUDY

3.1 Overview of the Long-Term Variability Study

By observing the photometric changes in these low-mass stars over long periods of time, we are able to analyze the effects their varying magnetic fields have on the vertical main sequence positions of the stars. The magnetic activity in low mass stars with radiative cores is thought to be driven, over the long term, primarily by an internal dynamo produced in the convection zone that moves in waves from the poles to the equator. This dynamo migration produces periods directly proportional to the time it takes these waves to complete their journeys from the poles, when starspot activity is low, to the equator, when starspot activity is high, before starting again (Parker 1955). For stars that are fully convective, the driving mechanisms behind the creation of their magnetic fields are still not well understood. Heightened periods of activity result in higher numbers of sunspots and thus more flare events relative to the strength of the magnetic field, which we can observe directly as changes in the surface brightnesses of the stars (Messina & Guinan 2002). The stronger a star's magnetic field activity is, the greater these changes in brightness are likely to be.

As described in Clements et al. (2017), in order to study the magnetic activity of our targets, we have used the RECONS parallax data gathered since 1999 and used relative photometric techniques to quantify any changes in brightness over time. The stars in this study were observed in the optical Johnson-Kron-Cousins V, R, and I filters two to three times per year for 3 to 18 years. For the purpose of our study, only stars observed in the

V filter were used because variations due to spots are more evident in V than in R or I. While we look for any evidence of cyclic activity among these stars, we are unable to pinpoint cycle periods for two reasons: (1) the lengths of their periods, and (2) inconsistent brightness changes from one cycle to the next and/or overlapping cycles. For example, given the average length of 11 years for the sunspot cycle of our Sun, we would ideally have at least 22 years of data to observe a repeating cycle. Because stellar cycles have never been carefully investigated for M dwarfs, which may have cycles even longer than the Sun's, all analysis is done via the measured variability for each star and visual inspections for evidence of cyclic activity or other trends. We will continue to monitor these stars through the CTIOPI program.

The 76 stars in this study and their properties are detailed in Table 3.1 where we provide their names and 2000.0 coordinates (columns 1, 2, and 3) as well as the V, I, and $(V-K)$ photometry for each star (4, 5, and 6). The distances to the stars and the distance references are also provided (7 and 8); these are used to derive the M_V values (9) needed to calculate the listed ΔM_V offsets (10) from the fit shown in Figures 1.1 and 2.1. The observational properties are then provided, including first and last dates of observations (11 and 12), as well as the duration of the observations and the number of frames (13 and 14). Each star was observed on 2 to 4 different nights a year, with typically five consecutive exposures per observation, over time periods of $3-17$ years. Our variability results (in mmag) are listed (15), as well as the rotational velocities (V_{rot}) from Newton et al. (2016) where available (16), with the notes for each star regarding their status as young stars (Y), suspected young

stars ((Y)), subdwarfs (S), or suspected subdwarfs ((S)) listed in the final column (17). The radial velocities are provided to show any correlation between variability and rotation rates, but the sample is too small for a robust analysis.

3.2 Stars in this Study

This portion of the project includes the long-term light curves for 76 nearby M dwarf stars. These stars range in spectral type from M2V to M5V and their ΔM_V values range from $+2.22$ to -2.94. We have been able to sample stars in each of our three target boxes, with the bulk of the targets lying in the central box, Box 5. In the first box, Box 4, we have light curves for 8 stars for this study, including one known young star and two known subdwarfs. Within Box 5 are nine young stars and three suspected subdwarfs among 57 stars in total. In our final box, Box 6, there are 11 stars that are included in this study, including three known young stars and no subdwarfs. This gives us a total sample of 13 known young stars, five subdwarf stars, and 58 stars that either lie on the main sequence, or are not yet identified to be young stars or subdwarfs. While we would have liked to include more subdwarf stars and more stars in Box 6, many of these stars are very faint and were thus observed in the R and I filters for the parallax program, rather than the more sensitive V filter used for stars in this study. It is known that young stars are more magnetically active, as was detailed in Chapter 1, so these stars are particularly important for this portion of the project as they will allow us to investigate this activity and its role in the placement of low mass stars on the H-R diagram. Given that subdwarf stars are generally older, their activity levels should have

calmed significantly, so we hypothesize that they will exhibit low photometric variability levels (Jao et al. 2011). The histogram in Figure 3.1 illustrates our sample of main sequence, young, and subdwarf stars as well as the spread in the duration of observations (in years) for the targets.

3.3 Observations and Reductions

Parallax program observations have been carried out by members of the RECONS team over two decades using the SMARTS 0.9 m telescope at CTIO for hundreds of stars within 25 pc. The images were collected using the rarely moved Tektronix 2048 $\times$ 2046 CCD detector in quarter chip mode, using the central quarter of the chip - field size $6.8' \times 6.8'$. As a regular part of the astrometric observations for the RECONS parallax study, each target is observed an average of two to three nights per year and three to five consecutive images each night, typically with integration times of 30 to 300 seconds (s). For optimal results the field of view (FOV) is kept the same for every image in order to maintain consistent reference stars for both astrometric and relative photometric comparisons. Targets are usually observed when the hour angle is within one hour of the meridian in order to avoid any changes in the positions of the stars in the field due to differential color refraction (DCR) for the astrometry portion of the RECONS work. Because this technique requires only relative magnitudes to the surrounding stars, observations can be carried out in non-photometric conditions, such as thin clouds and seeing as high as $2.5''$. This long-term study only uses those images in the Johnson-Krons-Cousins V filter as variability in the photosphere has been found to be more

apparent at shorter wavelengths, and these stars are too faint for regular observations in the U or B filters (Hosey et al. 2015). Images were taken through one of two Johnson V filters that peak at 5438Å and 5475Å. The two filters are photometrically identical to ∼7 mmag, as described in detail in Jao et al. (2011), where three non-pulsating white dwarfs with rich datasets in both V filters were tested and found to vary by less than ∼7 mmag. Several red dwarfs observed for this study with both V filters are found to vary by $6 - 8$ mmag, so the filters are effectively identical for red dwarfs as well. This provides our floor for long-term variability measurements of 7 mmag.

All observations undergo basic reductions using standard $IRAF$ procedures for photometry using the bias and flat frames taken for each night. Lower quality images are then removed from the data set prior to final analyses, such as those with trailing – due to wind or guiding problems –, high ellipticity, saturated target stars, too many missing reference stars, very poor seeing, filter problems, and an hour angle of more than two hours from the meridian. Following this initial processing, the data are then run through RECONS-developed programs for relative photometric comparisons using the methods outlined in Jao et al. (2011) and Hosey et al. (2015). These relative photometry techniques utilize a combination of IDL and $IRAF$ procedures to measure the photometric changes of the target star relative to a carefully chosen sample of the field stars. If, during analysis, a chosen reference star is found to be saturated or variable by more than ∼10 mmag, the star is removed from the sample and the variability calculation is run again. A comparison is made between the fluxes of the reference stars and that of the target, providing a single magnitude difference

between the target and the reference field for each frame. The resulting overall variability value in millimagnitudes (mmag), listed in column 15 of Table 3.1 is the mean absolute deviation of all of the frames from zero mmag. The mean absolute deviation (MAD) is the average of the absolute deviations of all of the points from a central point, in this case zero.

3.4 Analysis and Results

The results from the variability measurements in the V band for the 76 stars in this study are illustrated by Figures 3.2, 3.3, and 3.4. As described in §3.3, we find that the floor for our observations is the instrumental limit of 7 mmag and so we consider any measured variability of $\sim 3\sigma$ of this error, or about 20 mmag, to be considered a "variable" star, while anything below this limit is relatively quiescent. These limits are noted on Figure 3.2 where we show the variability of a star vs. its offset from the main sequence, the ΔM_V value. Dashed lines are used to represent the sharp cutoff at 7 mmag for our detection floor (Jao et al. 2011; Hosey et al. 2015) and at 20 mmag for our determination of obviously variable stars. We find that 60 out of the 76 stars (79%) are quiescent, showing variability less than 20 mmag, as can be seen in the histogram of Figure 3.3. These quiescent stars lie primarily below the main sequence, with ΔM_V values greater than zero, while each of the remaining 16 stars is positioned on or above the main sequence. In fact *every* star with $\Delta M_V > 0$ varies by less than 20 mmag over the long term. While there certainly are stars that show low levels of cyclic activity (below 20 mmag), such as G 099-049 and GJ 299 (see §3.4.1), we do not see evidence of these stars exhibiting strong magnetic activity. These results are

further supported by the H-R diagram in Figure 3.4, in which the symbol size is directly proportional to each star's measured long-term variability value. We also show the model tracks from Baraffe et al. (2015) for M stars between 0.1 and 0.5 $M_{\odot}$ for 100 Myrs (solid line) and 1 Gyrs (dashed line). We note that these tracks are significantly lower than our main sequence, particularly in the region of Box 5. Because it is reasonable to assume that the majority of our stars are not less than 100 Myrs old, then we can only assume that the models require revision. We have outlined some of the variability properties for a subsample of our 76 stars and provided their light curves in Figures 3.7 and 3.8, with further discussion in §3.4.1.

As was briefly discussed in §3.1, many of these stars exhibit visual evidence of cyclic activity and we attempted to investigate these cycles by running periodograms for each star. Using the Infrared Processing and Analysis Center (IPAC) periodogram tool provided by the NASA Exoplanet Archive, each long-term lightcurve was processed and analyzed to extract a stellar cycle period and the power level of any detected period. Unfortunately, no usable results were produced through this analysis because the calculated periods were simply either the exact length of the duration of the observations or the average time between observations with very low power, indicating the calculated period is not very likely. We predict this is due to successful periodogram techniques requiring more than one cycle for an accurately measured period with a strong detection power. Our data contain, on average, less than one cycle when a sinusoidal trend is present. For the remaining targets, there was either no sinusoidal trend present, brightness changes throughout the years of observations were

inconsistent, or there were large gaps in the data where observations were not obtained for time periods of up to two years. Only two of the 76 targets produced periods that seemed likely by visually comparing it to the lightcurve, but the power values for these results were also very low, and thus unusable. With more time, and thus more full cycles, this work could potentially be carried out in future analyses, but unfortunately we will need several more years of observations to produce better results.

To illustrate the quality of our variability values we have run a comparison of the apparent magnitude of each star against its variability value, to ensure that these values are not noise driven. Our results are shown in Figure 3.5, where we see no trend in the comparison of these two parameters. We expect to see such results because observation integration times are increased to up to at least 300 seconds for fainter stars to ensure consistent total counts among the targets.

We have also run our variability data through one of the equations derived by Stetson (1996) to assess the variability of a target using photometric data. For our work we determined that the best Stetson Index to use would be the Welsh/Stetson variability index I, which uses the deviation of the photometry in an individual frame from the average for two filters (if only one filter is used, as in our case, then the frames are compared to each successive frame) and the error of each photometric value. We do not have distinct errors for each image because relative photometric techniques were used, so we used our floor of 7 mmag as our error. The equation from Stetson (1996) and the method in which we used it

are as follows:

$$I = \sqrt{\frac{1}{n(n-1)}} \sum_{i=1}^{n} \left(\frac{b_i - \bar{b}}{\sigma_{b,i}} \right) \left(\frac{v_i - \bar{v}}{\sigma_{v,i}} \right),$$

$$I = \sqrt{\frac{1}{n(n-1)}} \sum_{i=1}^{n-1} \left(\frac{dv_i}{0.007} \right) \left(\frac{dv_{i+1}}{0.007} \right)$$

In both equations n is the number of frames in each filter. In the original I-index equation b and v represent the photometric value of each frame in one of two filters, $\bar{b}$ and $\bar{v}$ are the average of the photometric values of all frames in each filter, and the σ values are the errors for each frame. For our modification only one filter is used, the V filter. Because we have used relative photometry, we apply the difference between the value of the frame and the average (dv) and use 0.007 magnitudes as our error. The results are shown in Figure 3.6 as our variability values versus the Welsh/Stetson I-index. We see a clear increase in the values as the variability increases, confirming that our variability measurements are due to true stellar variability.

3.4.1 Individual Stars

The long-term variability light curves for 12 of the target stars in this study are shown in Figures 3.7 and 3.8 to provide context for our findings. Each panel shows the change in brightness at V in magnitudes over time for a star, in the sense that as a star brightens the points move upwards in a panel. In Figure 3.7 we show the results for six of our quiescent targets showing no variability or low level cyclic activity. In Figure 3.8 are six light curves of the more interesting targets with noticeable trends and higher levels of variability. The

low variability stars in Figure 3.7 range from being far below to just above the center of the main sequence, which is consistent with our hypothesis that only stars above the main sequence would demonstrate higher levels of variability.

In the top two panels of Figure 3.7 are the stars **GJ 480.1** and **GJ 643**, the latter a member of a multiple star system with a total of five red dwarfs, with little to no detected variability at values of 8.7 and 9.4 mmag, respectively. Their light curves are relatively flat and given their main sequence positions at $\Delta M_V = +1.07$ mag and $+0.50$ mag, these results are to be expected.

The middle panels of Figure 3.7 show the light curves for **G 099-049** and **L 032-008**. Both of these stars display low levels of cyclic activity despite their respective photometric variability values of only 17.1 mmag and 15.0 mmag, placing them below the 20 mmag threshold. G 099-049 is located on the main sequence, at $\Delta M_V = -0.06$, even though it is classified as a flare star with spectral type M3.5Ve (Davison et al. 2015). Also lying almost directly on the main sequence, at $\Delta M_V = -0.12$, L 032-008 is the secondary component in a binary system with L 032-009 with a separation of $23''$. With $(V - K) = 4.58$, L 032-009 falls between target Boxes 4 and 5; however, we note that it varies by an amount similar to that of L 032-008 (13.9 mmag at V). These stars are each interesting in their own way, despite showing very low activity, and the evidence of possible cyclic activity warrants further observations.

Within the last two panels of Figure 3.7 are the results for the very quiescent stars **LHS 2010** and **LHS 3746**. These stars are virtually identical in color with $(V - K)$ values

of 4.99 and 5.04, but they lie on opposite vertical sides of the center of the main sequence at $\Delta M_V = -0.90$ and $+0.19$, respectively. They each show almost no activity, nor evidence of any cyclic activity or other trends with variability measurements of only 11.0 mmag and 13.2 mmag, respectively.

The next set of panels, in Figure 3.8, represents a sample of six of the stars that show higher levels of variability or distinct trends in their brightness changes. Five of the six stars lie above the center of the main sequence, confirming our hypothesis that such stars would show higher levels of activity. The measured variability values for these five stars are above the variability threshold of 20 mmag. The one star that varies by less than 20 mmag, **GJ 299** at 16.5 mmag, exhibits an interesting trend in its brightness over time.

LHS 1610 is located on the main sequence at $\Delta M_V = -0.22$ and shows significant variability (29.0 mmag) with a flux decrease of $\sim$10% from 2003$-$2008. This star also exhibits large short-term variations that are superimposed on the longer cycle, likely indicative of large spots on its surface.

AP Col is the nearest (8.4 pc) known pre-main sequence star (Riedel et al. 2011), with an estimated age of $12 - 50$ Myr. With $\Delta M_V = -1.23$, this star lies well above the main sequence, appears to have a cycle lasting longer than the 11 years over which we have data, and a measured variability of 21.1 mmag. What is somewhat surprising is that it is not more variable on long timescales, as might be expected if the star consistently exhibited a few large spots. Alternatively, it could be that its surface typically has *many* spots, so that long term variations are muted.

GJ 299 shows a long-term decrease over 6 years of observations from $2010 - 2016$, although the formal variability measurement of 16.5 mmag is not large. It is located far below the main sequence at $\Delta M_V = +1.08$ and is likely a subdwarf, so we do not expect extreme variability. Nonetheless, the long term fading that is observed is worthy of continued monitoring as this may be indicative of a long stellar cycle.

GJ 2006B is part of a young binary separated by $18''$. At $\Delta M_V = -1.67$, this star is well above the main sequence and the large observed photometric variations (36.2 mmag) are consistent with its elevated H-R diagram location. In the 11 years of observations in-hand, we do not detect an obvious periodicity or trend. A similar result is observed for its primary GJ 2006A ($\Delta M_V = -1.61$), which exhibits more than twice the variability value at 76.8 mmag, with no obvious trend.

GJ 358 exhibits strong cyclic activity, for which we measure a variability of 30.2 mmag and a possible period on the order of 10 years. It lies above the main sequence at $\Delta M_V = -0.50$.

GJ 1284 is a known flare star and potential young star according to recent work by Shkolnik et al. (2017); who classify it as a likely member of the young moving group β Pictoris. However, past work by Torres et al. (2006) has classified this star as a potential SB2 spectroscopic binary with a note that rapidly rotating, spotted stars can appear as SB2's. There is no mention or verification of a spectroscopic binary status for this star in any later publications and so its status as young is currently suspected, but unconfirmed. This star lies well above the main sequence, with $\Delta M_V = -1.29$, and we find a variability

of 27.1 mmag. The brightness at V changed rather abruptly by $\sim$5% from late 2006 to late 2007 and the star has continued to gradually get brighter.

3.4.2 ROSAT Study

Flare activity in these stars would be more obvious and more easily detected at shorter wavelengths such as in the X-ray or UV range of the spectrum. Unfortunately, these stars are far too faint to allow for regular monitoring in these bands on smaller telescopes. To further investigate the long-term results, we have cross-referenced our targets with detections from the ROSAT All-Sky Bright Source Catalog found in Voges et al. (1999) to determine if any of our high variability stars exhibit high X-ray luminosity. For this study we used a search radius of $1'$ and all sources were matched within $20''$ of the target star and confirmed visually. The ROSAT fluxes and luminosities are presented in Table 3.2.

We find that 19 of the 76 stars can be matched to ROSAT sources, including nine out of the 13 known young stars in our study. These nine stars are noted as "Young" in Table 3.2. Data for the remaining young stars were unavailable; there were no ROSAT observations for SCR 0757-7114 or LP 993-115A, but there was for its companion (not in this study) LP 993-116(B), in Voges et al. (1999), and GJ 2006B and TWA 8B appear not to have separate values from their A components. Among the remaining ten stars, two are known flare stars (GJ 358 and GJ 1154) that are about half a magnitude above the main sequence. Of the remaining eight stars, four are known flare stars, but their positions relative to the main sequence differ: G 188-038 is 0.41 mag above the main sequence, GJ 1156, at $\Delta M_V = -0.11$ is effectively on the main sequence, GJ 1207 lies 0.13 mag below the main

sequence, and GJ 729 is, curiously, at +0.71 mag *below* the main sequence. We measure only 11 mmag of variability in V over 15 years for GJ 729, and the X-ray luminosity for this star is much lower than those of the other targets that are located above the main sequence. Finally, the remaining four stars that have not been identified to be young or flare stars are all within 0.25 mag of the center of the main sequence and have $L_{Xray} \leq 0.44 \times 10^{29} erg\ s^{-1}$.

Figure 3.9 illustrates the results of this X-ray search, where the X-ray luminosity is plotted vs. the ΔM_V value and the point size is indicative of our variability results presented here. The X-ray luminosity (denoted as L_{XRay}) was calculated using the published ROSAT stellar flux values (f), given in W/m^2 and converted to $erg\ s^{-1}$ using the distances (D) given in Table 3.2 via the equation:

$$L_{XRay} = 1.20 \times 10^{38} \times f \times D^2$$

Figure 3.9 shows that the X-ray luminosity increases for stars located above the main sequence. Thus we find a correlation between X-ray luminosity and our V photometric variability values, indicating a clear link between X-ray flux levels and the rather more easily obtained V band variability measurements.

3.5 Conclusions

The results from this study show that not only are stars above the main sequence (ΔM_V from 0.0 to -3.5 mag) more active over the long term than their smaller radii counterparts (as discussed in §1.2), but no stars that lie on or below the central fit of the main sequence

(ΔM_V from +2.5 to 0.0 mag) show a variability measurement greater than our threshold of 20 mmag in V. We also find that stars classified as young are almost always variable by more than this 20 mmag threshold and our subdwarf targets show very low variability measurements. We observe a clear increase in long-term variability, as illustrated in Figures 3.2, 3.3 and 3.4, primarily for stars that are known to be young. These results support our hypothesis that overluminous red dwarfs are more photometrically variable in V over the long-term than their main sequence counterparts. We propose that this variability is due to activity caused by the internal workings of the magnetic fields that result in the cyclic occurrence of spots and flares on the stars. We infer that these stars' radii are larger than their lower luminosity counterparts due to strong magnetic fields that either support the outer layers of the star or suppress convection and to allow energy to escape the stars must expand, consequently resulting in higher luminosities. Finally, we find a link between our long-term photometric variability measurements at V made from the ground and X-ray fluxes measured from space. Thus, we have also discovered a relatively straightforward method for identifying young red dwarfs in the solar neighborhood: V band photometric measurements over the long term. However, we are unable to draw any firm conclusions about the role of the method of energy transport (e.g., convection) in the level of observed activity at this time, due to our limited sample in Boxes 4 and 6 where comparisons need to be made. When more long-term data are available in these regions, we will explore the role of convection's effects on position relative to the main sequence.

Table 3.1: Properties of the Low Mass Stars in the Long-Term Variability Study.

Star Name (1)	R.A. (2)	Dec. 2000.0 (3)	V (4)	I (5)	$V-K$ (6)	dist. (pc) (7)	dist. ref. (8)	M_V (9)	ΔM_V (10)	Obs. Date First (11)	Obs. Date Last (12)	Duration (years) (13)	# Frames (14)	Var. (mmag) (15)	V_{Rot} (km/s) (16)	Notes[a] (17)
SCR 0017-6645	00:17:23	−66:45:12	12.45	10.00	4.75	39.0	Rie14	9.49	−1.97	2010 Jul 07	2015 Jul 24	5.05	70	34.8	···	Y
G 266-089A	00:19:37	−28:09:46	14.27	11.44	4.80	31.8	Jao11	11.76	+1.23	2000 Nov 15	2005 Sep 12	4.83	62	7.6	···	(S)
GJ 2006A	00:27:50	−32:33:06	12.95	10.29	4.94	33.2	Rie14	10.34	−1.61	2000 Jul 27	2010 Oct 27	10.25	69	76.8	···	Y
GJ 2006B	00:27:50	−32:33:24	13.25	10.48	5.13	31.5	Rie14	10.76	−1.67	2000 Jul 27	2010 Oct 27	10.25	69	36.2	···	Y
GJ 1025	01:00:56	−04:26:56	13.36	10.55	5.14	11.4	Jao05	13.08	+0.63	2000 Jul 28	2015 Oct 31	15.26	80	18.5	···	
GJ 105B	02:36:04	+06:53:12	11.71	8.88	5.14	7.2	vLe07	12.42	+0.05	2010 Dec 19	2015 Dec 18	15.00	40	12.5	···	
L 174-028	02:37:52	−58:45:11	12.47	9.76	4.96	15.0	vLe07	11.59	−0.35	2012 Dec 15	2016 Aug 17	3.67	33	15.8	···	
LP 993-115A	02:45:10	−43:44:32	12.38	9.61	5.11	11.2	Rie14	12.13	−0.24	1999 Aug 16	2016 Aug 14	17.0	87	21.1	···	Y
LP 771-095A	03:01:51	−16:35:36	11.22	8.66	4.72	7.0	vLe07	11.99	+0.61	1999 Aug 21	2015 Dec 17	16.32	211	17.7	···	
LHS 1491	03:04:04	−20:22:43	12.84	10.13	5.09	14.8	Rie10	11.99	−0.35	1999 Sep 15	2016 Jan 24	16.36	86	17.7	···	
LHS 178	03:42:29	+12:31:34	12.87	10.78	3.99	24.3	YPC95	10.94	+1.32	2009 Dec 04	2015 Sep 04	15.75	64	9.4	113.7	S
GJ 1065	03:50:43	−06:05:10	12.82	10.04	5.07	9.5	Dav15	12.93	+0.66	2004 Nov 01	2015 Oct 27	8.99	111	15.9	···	
LHS 1610	03:52:41	+17:01:04	13.85	10.66	5.80	9.9	Hen06	13.87	−0.11	1999 Sep 18	2016 Jan 17	16.33	183	29.0	0.1	
GJ 166C	04:15:22	−07:39:35	11.24	8.31	5.28	5.0	vLe07	12.75	−0.04	2012 Sep 12	2015 Jan 27	6.36	54	24.9	···	
LP 776-025	04:52:24	−16:49:21	11.63	9.12	4.74	16.2	Shk12	10.58	−0.87	2004 Sep 23	2008 Feb 15	3.39	55	15.6	···	Y
LHS 1731	05:03:20	−17:22:25	11.69	9.16	4.75	9.2	Jao05	11.87	+0.39	1999 Dec 22	2015 Dec 20	15.99	215	13.6	···	
BD 21-01074A	05:06:50	−21:35:09	10.41	8.45	4.29	18.3	Rie14	9.10	−1.20	2000 Jan 24	2012 Feb 29	12.10	72	52.9	···	Y
GJ 203	05:28:00	+09:38:38	12.47	9.80	4.93	9.7	vLe07	12.53	+0.57	2009 Dec 08	2015 Dec 18	6.03	76	15.1	···	
LHS 1767	05:31:04	−30:11:44	13.11	10.45	4.92	15.3	Rie10	12.19	+0.28	2003 Dec 15	2016 Jan 07	12.06	88	14.0	···	
GJ 213	05:42:09	+12:29:21	11.54	8.74	5.15	5.8	vLe07	12.72	+0.18	2010 Mar 01	2015 Dec 05	5.76	62	13.3	1.4	
G 099-049	06:00:03	+02:42:23	11.31	8.43	5.27	5.2	Dav15	12.73	−0.06	1999 Nov 27	2016 Mar 04	16.25	406	17.1	6.9	
AP Col	06:04:52	−34:33:36	12.97	9.60	6.10	8.4	Rie11	13.35	−1.23	2004 Sep 28	2016 Jan 17	11.30	223	21.1	···	Y
GJ 1088	06:10:52	−43:24:17	12.28	9.61	4.97	11.4	Rie10	12.00	−0.05	2000 Nov 16	2016 Jan 21	15.18	105	20.9	···	
L 032-008	06:33:46	−75:37:30	11.43	8.82	4.87	9.0	vLe07	11.66	−0.12	2003 Dec 13	2016 Jan 21	12.11	197	15.0	···	
GJ 273	07:27:24	+05:13:32	9.85	7.17	4.99	3.8	Gat08	11.95	−0.11	2010 Jan 03	2016 Mar 13	6.19	81	14.4	···	
LHS 1932	07:36:12	−51:55:21	12.48	9.92	4.73	16.1	Rie10	11.37	+0.04	2000 Nov 15	2003 Feb 19	2.26	93	10.4	···	
L 034-026	07:49:12	−76:42:06	11.31	8.79	4.73	10.6	Rie14	11.18	−0.23	2006 Mar 16	2012 Nov 18	6.67	94	18.0	···	Y
SCR 0757-7114	07:57:32	−71:14:54	12.45	9.77	5.03	22.1	Rie14	10.73	−1.45	2008 Feb 14	2012 Nov 17	4.76	63	7.1	···	Y
GJ 299	08:11:58	+08:46:23	12.86	9.91	5.20	6.8	YPC95	13.70	+1.08	2010 Feb 28	2015 Dec 20	5.81	83	16.5	9.1	(S)
LHS 2010	08:27:11	−44:59:21	11.86	9.19	4.99	13.7	Rei10	11.18	−0.90	2001 Feb 21	2015 Mar 19	14.08	173	11.0	···	
GJ 1123	09:17:05	−77:49:23	13.15	10.16	5.70	9.0	Jao05	13.38	−0.40	2002 Mar 24	2015 Apr 23	13.08	132	20.3	···	
GJ 358	09:39:46	−41:04:03	10.78	8.27	4.72	9.5	vLe07	10.89	−0.50	2004 Dec 27	2015 Jan 23	10.07	143	30.2	···	
GJ 1128	09:42:46	−68:53:06	12.74	9.65	5.70	6.5	Lur14	13.68	−0.11	2000 Mar 24	2015 Jan 21	14.83	197	16.9	···	
LHS 272	09:43:46	−17:47:06	13.16	10.87	4.29	13.5	Jao11	12.51	+2.22	2001 Feb 22	2016 Jan 20	14.91	93	12.5	···	S
GJ 1129	09:44:47	−18:12:48	12.46	9.67	5.20	10.6	Jao11	12.33	−0.29	2000 Jan 23	2015 Apr 17	15.23	90	14.0	···	
GJ 402	10:50:52	+06:48:29	11.70	8.85	5.33	6.8	vLe07	12.54	−0.33	2010 May 23	2015 Apr 24	4.92	59	15.0	···	
LP 491-051	11:03:21	+13:37:57	12.96	10.24	5.05	15.4	Shk12	12.02	−0.25	2009 Apr 26	2016 Mar 15	6.05	52	12.9	0.4	
LHS 2401	11:23:57	−18:21:48	13.10	10.54	4.78	18.3	Rei10	11.79	+0.24	2001 Feb 23	2009 Apr 28	8.18	76	13.5	···	

[a] Notes in Column 17: Y = known young stars, (Y) = suspected young star, S = known subdwarf stars, (S) = suspected, but unconfirmed subdwarf stars.

Distance references: (Cos05) Costa et al. (2005); (Cos06) Costa et al. (2006); (Dav15) Davison et al. (2015); (Gat08) Gatewood (2008); (Hen06) Henry et al. (2006); (Jao05) Jao et al. (2005); (Jao11) Jao et al. (2011); (Lur14) Lurie et al. (2014); (Rie10) Riedel et al. (2010); (Rie11) Riedel et al. (2011); (Rie14) Riedel et al. (2014); (Shk12) Shkolnik et al. (2012); (vLe07) van Leeuwen (2007); (YPC95) van Altena et al. (1995).

Table 3.1: Properties of the Low Mass Stars in the Long-Term Variability Study.

Star Name	R.A.	Dec.	V	I	$V-K$	dist. (pc)	dist. ref.	M_V	ΔM_V	Obs. Date First	Obs. Date Last	Duration (years)	# Frames	Var. (mmag)	V_{Rot} (km/s)	Notes[a]
	2000.0															
(1)	(2)	(3)	(4)	(5)	(6)	(7)	(8)	(9)	(10)	(11)	(12)	(13)	(14)	(15)	(16)	(17)
TWA 8A	11:32:41	−26:51:56	12.23	9.79	4.80	46.9	Rie14	8.87	−2.72	2000 Feb 21	2011 Feb 28	11.02	65	78.6	···	Y
TWA 8B	11:32:41	−26:52:09	15.22	11.76	6.21	47.1	Rie14	11.85	−2.94	2000 Feb 21	2011 Feb 28	11.02	65	124.1	···	Y
GJ 438	11:43:19	−51:50:25	10.35	8.27	4.03	10.8	Rie10	10.18	+0.51	2000 Jan 25	2012 Feb 08	12.04	97	7.9	···	
LHS 2520	12:10:05	−15:04:16	12.09	9.30	5.23	12.8	Rie10	11.55	−1.12	2000 Jan 25	2015 May 25	15.33	95	15.0	···	
SCR 1214-2345	12:14:08	−23:45:17	13.96	10.78	5.73	10.9	Rie14	13.77	−0.07	2010 Feb 26	2015 May 29	5.26	82	23.1	···	
GJ 1154	12:14:16	+00:37:26	13.64	10.31	6.10	8.4	YPC95	14.02	−0.58	2010 May 26	2015 Apr 24	4.91	65	14.4	6.7	
GJ 1156	12:18:59	+11:07:34	13.80	10.34	6.23	6.5	YPC95	14.73	−0.11	2010 May 22	2015 May 26	5.01	60	17.4	18.5	
GJ 1157	12:23:01	−46:37:08	13.59	10.71	5.23	16.0	Rie10	12.57	−0.11	2001 Feb 21	2015 Mar 21	14.08	112	13.3	···	
GJ 480.1	12:40:46	−43:33:59	12.24	9.58	4.83	8.0	vLe07	12.72	+1.07	2003 Jul 05	2015 Apr 25	11.80	102	8.7	···	(S)
GJ 486	12:47:56	+09:45:05	11.40	8.68	5.04	8.4	vLe07	11.78	−0.40	2010 May 22	2015 May 30	5.02	69	11.6	···	
LHS 346	13:09:20	−40:09:27	12.86	10.24	4.87	16.1	Jao05	11.83	+0.04	2001 Feb 21	2004 Jun 11	3.31	71	8.3	···	
LHS 2718	13:20:03	−35:24:44	12.84	10.24	4.86	13.6	Rie10	12.17	+0.41	2001 Feb 23	2005 May 30	4.27	70	10.7	···	
GJ 545	14:20:07	−09:37:13	12.84	10.15	4.86	14.0	Jao05	12.11	+0.35	2000 Feb 21	2003 Apr 20	3.16	48	9.4	···	
LHS 2899	14:21:15	−01:07:19	13.12	10.39	5.03	13.3	Rie10	12.50	+0.31	2000 Feb 22	2015 Apr 25	15.17	94	17.0	···	
GJ 581	15:19:26	−07:43:20	10.55	8.04	4.71	6.2	Lur14	11.59	+0.20	2000 Jul 29	2015 Jul 19	14.97	279	14.6	···	
GJ 609	16:02:50	+20:35:21	12.58	9.73	5.21	10.0	YPC95	12.58	−0.03	2010 May 26	2015 Jul 18	5.14	69	11.9	···	
LHS 3169	16:14:21	−28:30:36	12.95	10.29	4.84	18.7	Rie10	11.59	−0.10	2000 Jul 30	2010 Mar 13	9.62	67	10.9	···	
GJ 628	16:30:18	−12:39:45	10.07	7.37	5.00	4.3	Dav15	11.90	−0.17	2003 Jul 05	2014 Jun 09	10.93	160	11.5	···	
GJ 643	16:55:25	−08:19:21	11.77	9.05	5.05	6.5	Cos05	12.70	+0.50	2003 Jul 09	2015 Apr 23	11.79	142	9.4	···	
GJ 1207	16:57:05	−04:20:56	12.25	9.43	5.13	8.7	Hen06	12.55	+0.13	1999 Aug 16	2014 Jun 14	14.83	247	18.4	···	
LHS 3295	17:29:27	−80:08:57	12.18	9.53	4.95	12.5	Rie10	11.70	−0.11	2000 Jul 27	2004 Mar 31	3.68	74	8.9	···	
GJ 2130A	17:46:12	−32:06:09	10.50	···	4.25	14.1	Hen06	9.75	−0.43	1999 Aug 21	2005 Sep 15	6.07	73	11.8	···	
GJ 693	17:46:34	−57:19:08	10.77	8.20	4.75	5.8	vLe07	11.95	+0.48	2003 Jul 06	2015 Apr 25	11.80	191	11.1	···	
LTT 07419A	18:43:12	−33:22:31	10.25	8.28	3.92	15.2	Cos06	9.34	−0.07	2000 Jul 27	2003 Apr 19	2.73	53	9.5	···	
GJ 729	18:49:49	−23:50:10	10.50	7.68	5.13	3.0	Dav15	13.11	+0.71	1999 Aug 16	2014 Aug 29	15.04	134	10.6	···	
LHS 3443	19:13:07	−39:01:53	12.39	9.85	4.73	20.5	Rie10	10.83	−0.60	2000 Jul 29	2009 Sep 29	9.17	69	9.4	···	
LHS 475	19:20:54	−82:33:16	12.69	10.00	5.00	12.0	Jao11	12.29	+0.17	2000 Jul 27	2015 May 29	14.84	158	10.8	···	
LHS 499	20:51:41	−79:18:39	11.81	9.64	4.15	17.5	Jao11	10.59	+0.65	2003 Dec 14	2007 Oct 02	3.80	62	6.3	···	
LP 816-060	20:52:33	−16:58:29	11.50	8.64	5.30	5.7	vLe07	12.72	−0.04	2003 Jul 08	2014 Aug 25	11.13	164	19.0	···	
LHS 512	21:38:43	−33:39:55	12.55	9.89	4.98	12.1	Jao05	12.14	+0.08	2000 Jul 27	2015 May 27	14.83	94	11.2	···	
G 188-038	22:01:13	+28:18:24	12.05	9.17	5.27	9.0	vLe07	12.28	−0.41	2009 Jul 22	2015 Jul 20	5.99	66	19.0	32.5	
LHS 3746	22:02:29	−37:04:51	11.76	9.04	5.04	7.4	Hen06	12.41	+0.19	1999 Sep 16	2015 Jul 18	15.84	335	13.2	···	
GJ 849	22:09:40	−04:38:26	10.38	7.87	4.79	9.0	Lur14	10.61	−0.94	2003 Jul 09	2015 Oct 26	12.30	148	12.7	···	
LHS 3799	22:23:07	−17:37:01	13.30	10.04	5.98	7.4	Rie14	13.95	−0.38	2003 Jul 08	2014 Sep 03	11.15	131	13.2	···	Y
GJ 876	22:53:16	−14:15:49	10.18	7.40	5.17	4.7	Lur14	11.82	−0.69	2003 Jul 09	2014 Oct 21	11.28	76	28.1	···	
GJ 1277	22:56:24	−60:03:49	14.00	10.79	5.89	10.2	Jao11	13.96	−0.23	2001 Nov 15	2015 Oct 28	13.95	120	10.4	···	
GJ 1284	23:30:13	−20:23:27	11.12	8.59	4.79	16.1	Rie14	10.13	−1.29	2003 Jul 05	2011 Jul 06	8.00	95	27.1	···	(Y)
LHS 4058	23:59:51	−34:06:42	12.84	10.08	5.09	15.8	Rie10	11.85	−0.49	2000 May 30	2015 Nov 04	15.43	84	11.5	···	

[a] Notes in Column 17: Y = known young stars, (Y) = suspected young star, S = known subdwarf stars, (S) = suspected, but unconfirmed subdwarf stars.

Distance references: (Cos05) Costa et al. (2005); (Cos06) Costa et al. (2006); (Dav15) Davison et al. (2015); (Gat08) Gatewood (2008); (Hen06) Henry et al. (2006); (Jao05) Jao et al. (2005); (Jao11) Jao et al. (2011); (Lur14) Lurie et al. (2014); (Rie10) Riedel et al. (2010); (Rie11) Riedel et al. (2011); (Rie14) Riedel et al. (2014); (Shk12) Shkolnik et al. (2012); (vLe07) van Leeuwen (2007); (YPC95) van Altena et al. (1995).

Table 3.2: ROSAT Detection Data.

Star Name	ROSAT Flux $mW/m^2(\times 10^{-12})$	L_{XRay} $(10^{29} erg\ s^{-1})$	ΔM_V	Variability (mmag)	Star Type
SCR 0017-6645	1.68	3.07	−1.97	34.8	Young
GJ 2006AB	2.56	3.39	−1.61	76.8	Young
LP 776-025	3.08	0.97	−0.87	15.6	Young
BD 21-01074A	8.62	3.46	−1.20	52.9	Young
G 099-049	2.93	0.10	−0.06	17.1	
AP Col	3.70	0.31	−1.23	21.1	Young
L 032-008	0.340	0.03	−0.12	15.0	
L 034-026	4.25	0.57	−0.23	18.0	Young
GJ 358	1.17	0.13	−0.50	30.2	Flare
LP 491-051	1.53	0.44	−0.25	12.9	
TWA 8AB	2.71	7.15	−2.72	78.6	Young
SCR 1214-2345	0.932	0.13	−0.07	23.1	
GJ 1154	0.697	0.06	−0.58	14.4	Flare
GJ 1156	0.913	0.05	−0.11	17.4	Flare
GJ 1207	2.20	0.20	+0.13	18.4	Flare
GJ 729	5.68	0.06	+0.71	10.6	Flare?
G 188-038	2.85	0.28	−0.41	19.0	Flare
LHS 3799	1.27	0.08	−0.38	13.2	Young
GJ 1284	3.65	1.14	−1.29	27.1	Young?

The 19 stars with ROSAT detections in Voges et al. (1999), their X-ray values, and other important parameters used to create Figure 3.9.

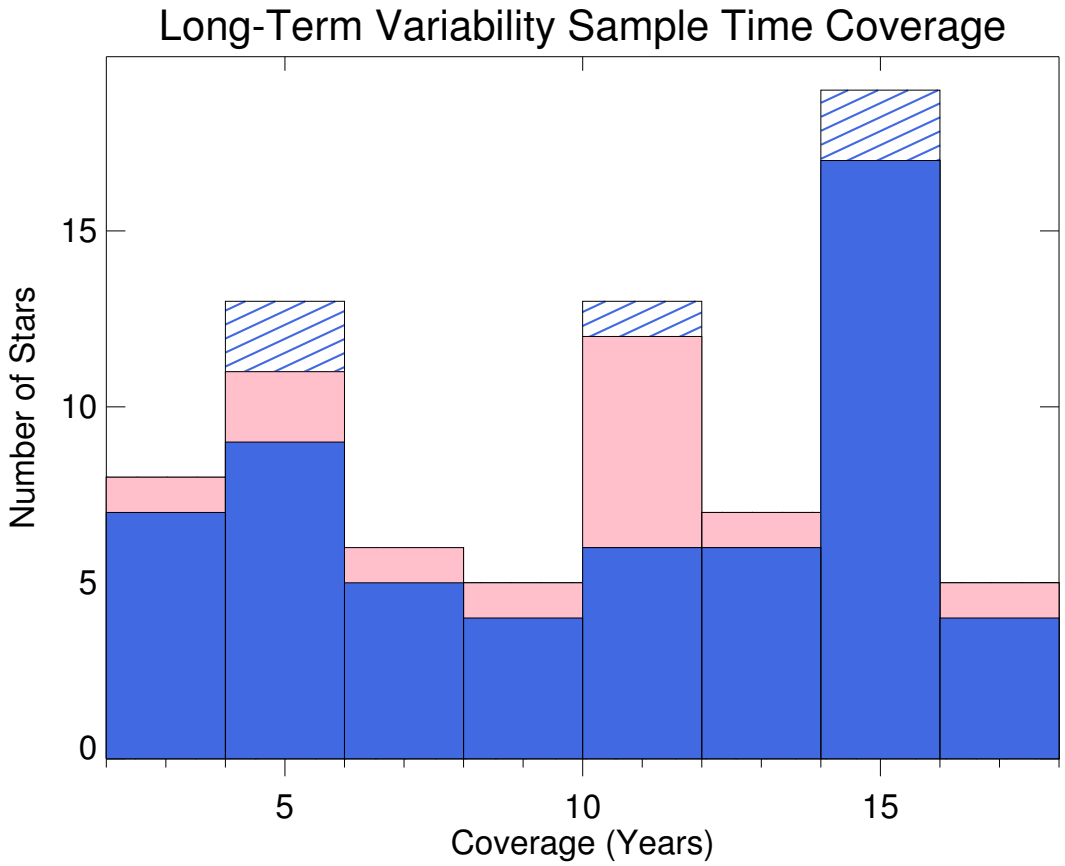

Figure 3.1: Histogram demonstrating the coverage, from $3 - 17$ years, of the 76 stars included in this study. Solid blue represents main sequence or stars not confirmed to be young or subdwarfs. Pink represents known young stars. Blue and white lined represents subdwarfs. The bin sizes are 2 years, starting at 2 years and ending at 18 years.

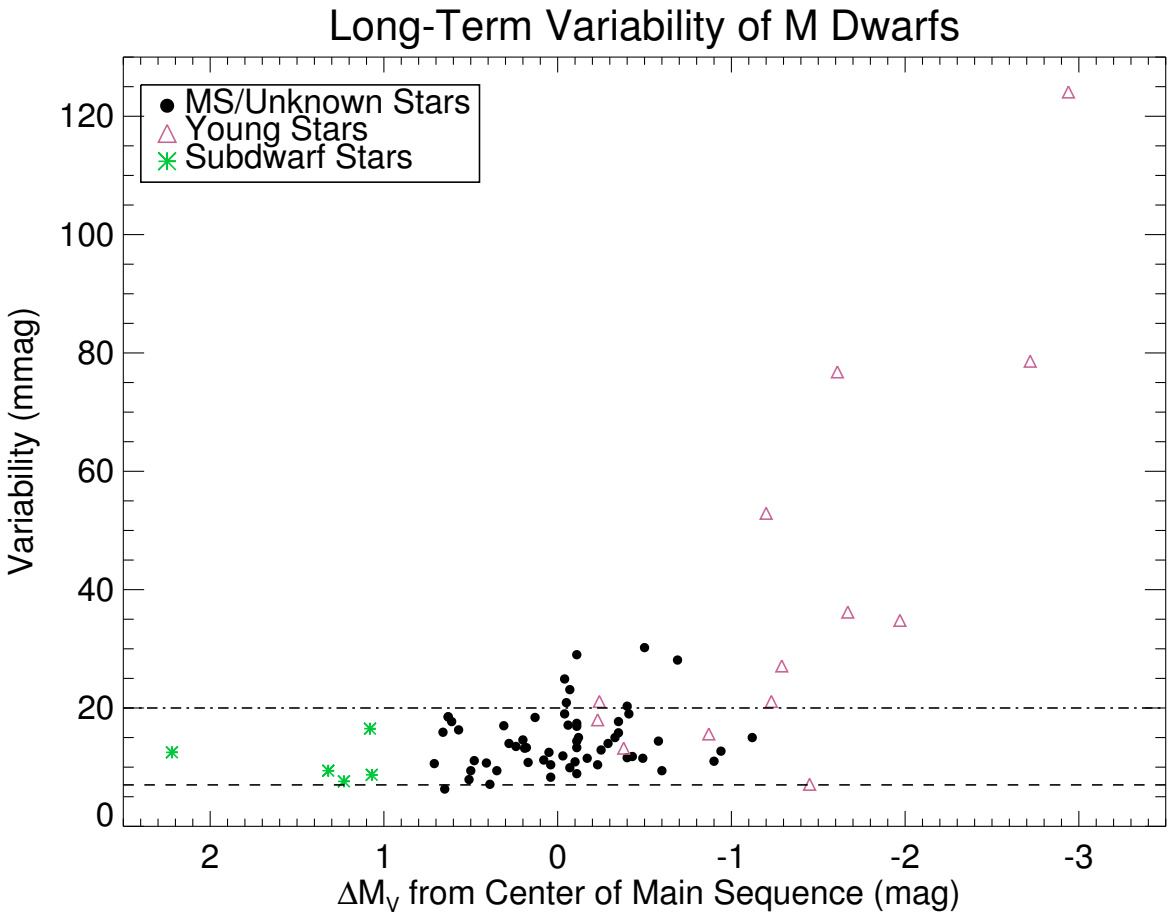

Figure 3.2: Scatter plot of stellar variability in the V filter vs. offset from the fit to the distribution of stars in the H-R diagram of Figure 2.1. Stars are shown with solid black points, unless they are known to be young (pink triangles) or subdwarfs (green asterisks). The dashed line is at our lower detection threshold of 7 mmag and the dashed-dotted line is at our lower limit of 20 mmag for non-quiescent variability. The high values for long-term variability for stars above the main sequence, but not below, supports our hypothesis that the elevated stars are more magnetically active.

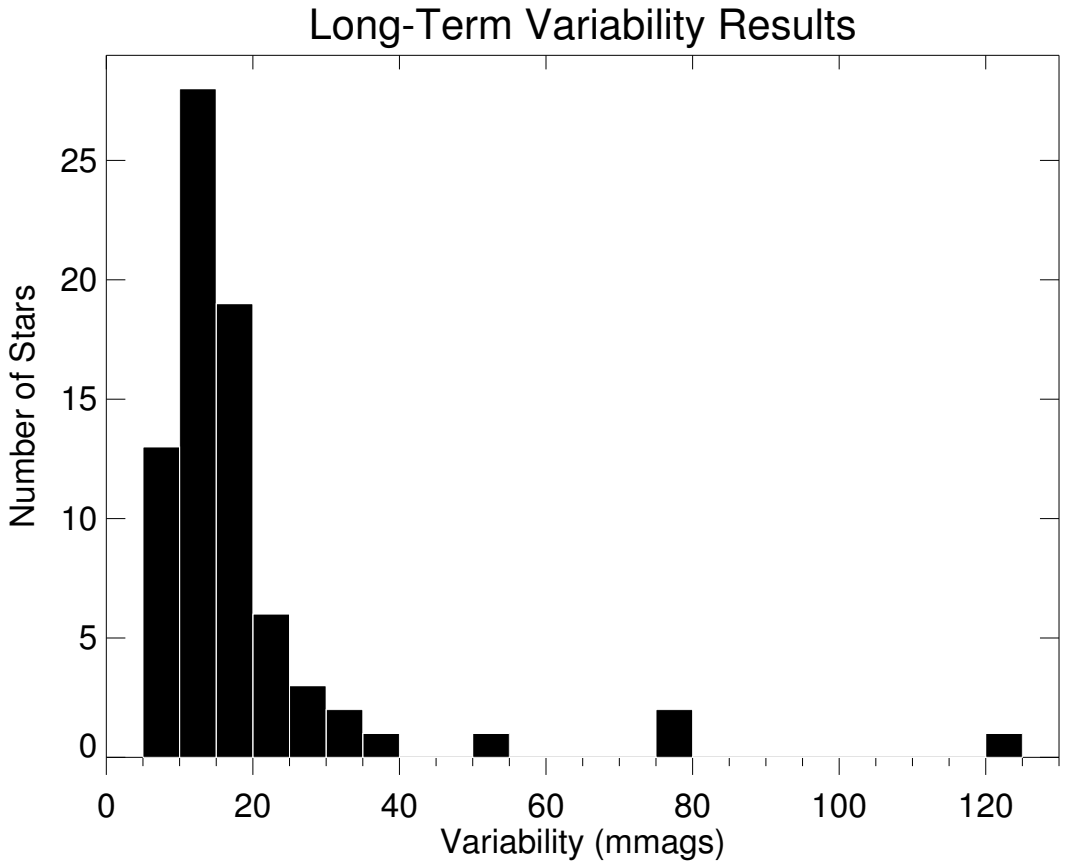

Figure 3.3: Histogram showing our range of long-term variability values. The bins are 5 mmag in width, from $5-10$ mmag to $120-125$ mmag. Sixteen of 76 stars (21%) vary by more than 20 mmag, our threshold for a clearly variable star.

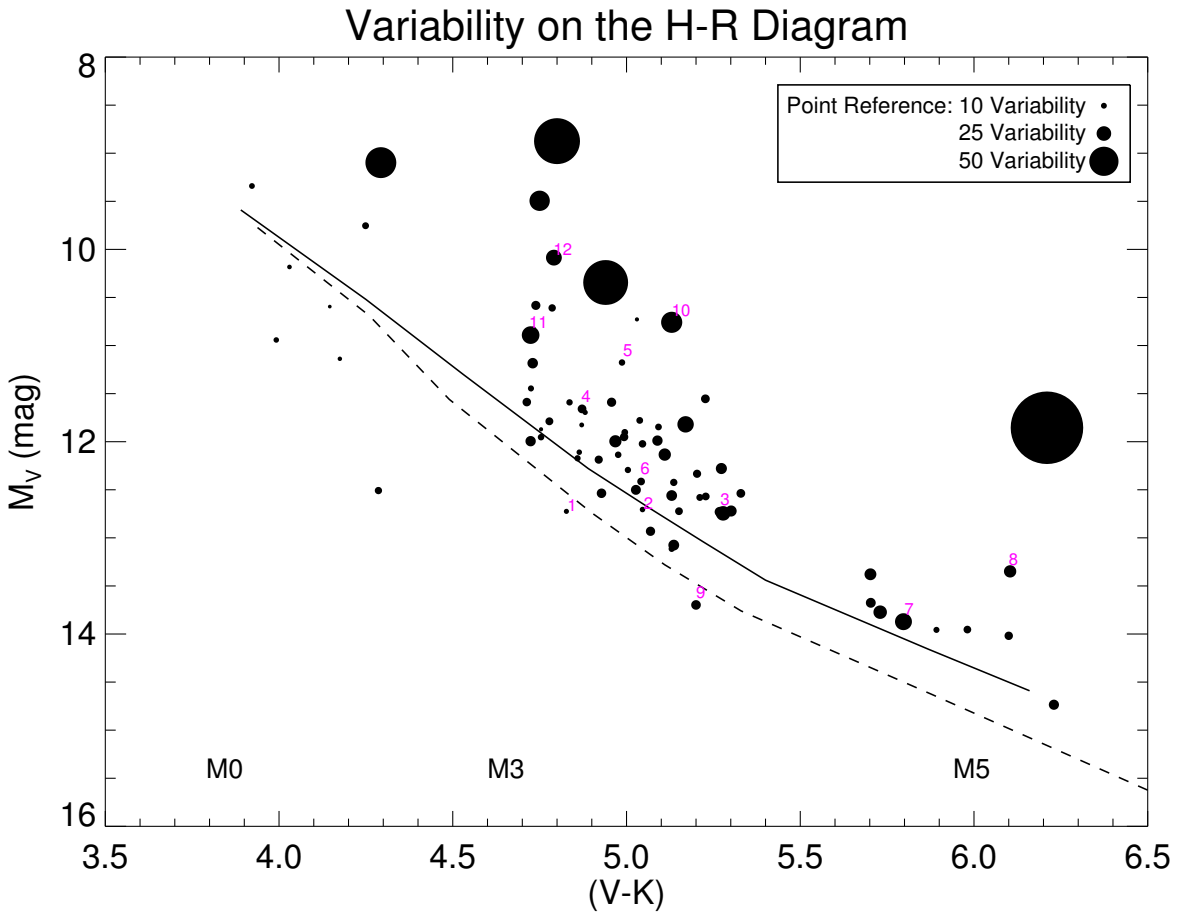

Figure 3.4: The stars are plotted on an H-R diagram where point sizes are scaled to indicate each star's variability in V. Reference points for variability of 10, 25, and 50 mmag are given in the legend. Numbers correspond to stars with light curves presented in Figures 3.7 and 3.8. The largest point at $M_V = 11.85$ and $(V - K) = 6.21$, is TWA 8B, for which we measure a variability of 124 mmag. We also plot the model tracks from Baraffe et al. (2015) for M stars at 100 Myrs (solid) and 1 Gyr (dashed).

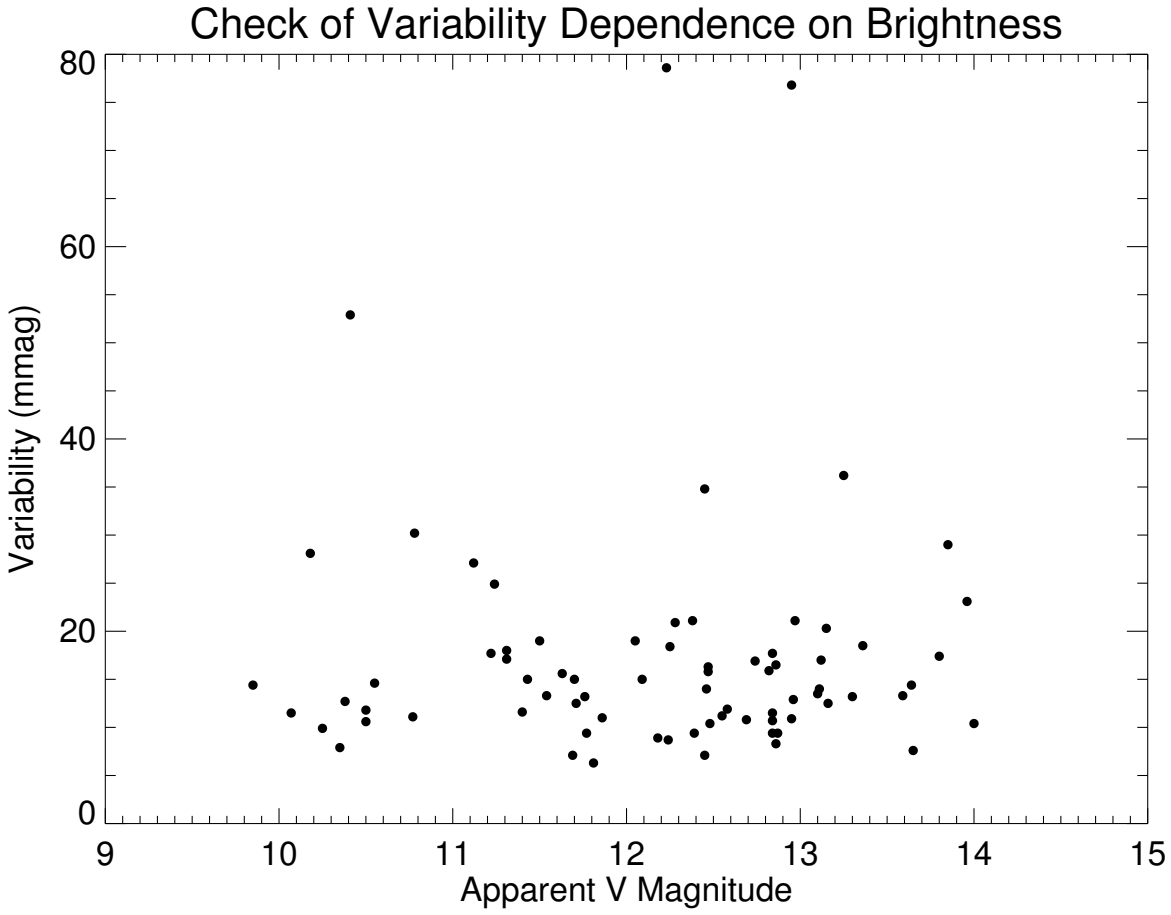

Figure 3.5: The random scatter of the apparent magnitude of each star versus its variability. This provides further evidence of the quality of our variability calculations and results because there is no trend of increasing variability for fainter stars simply because of lower SNR.

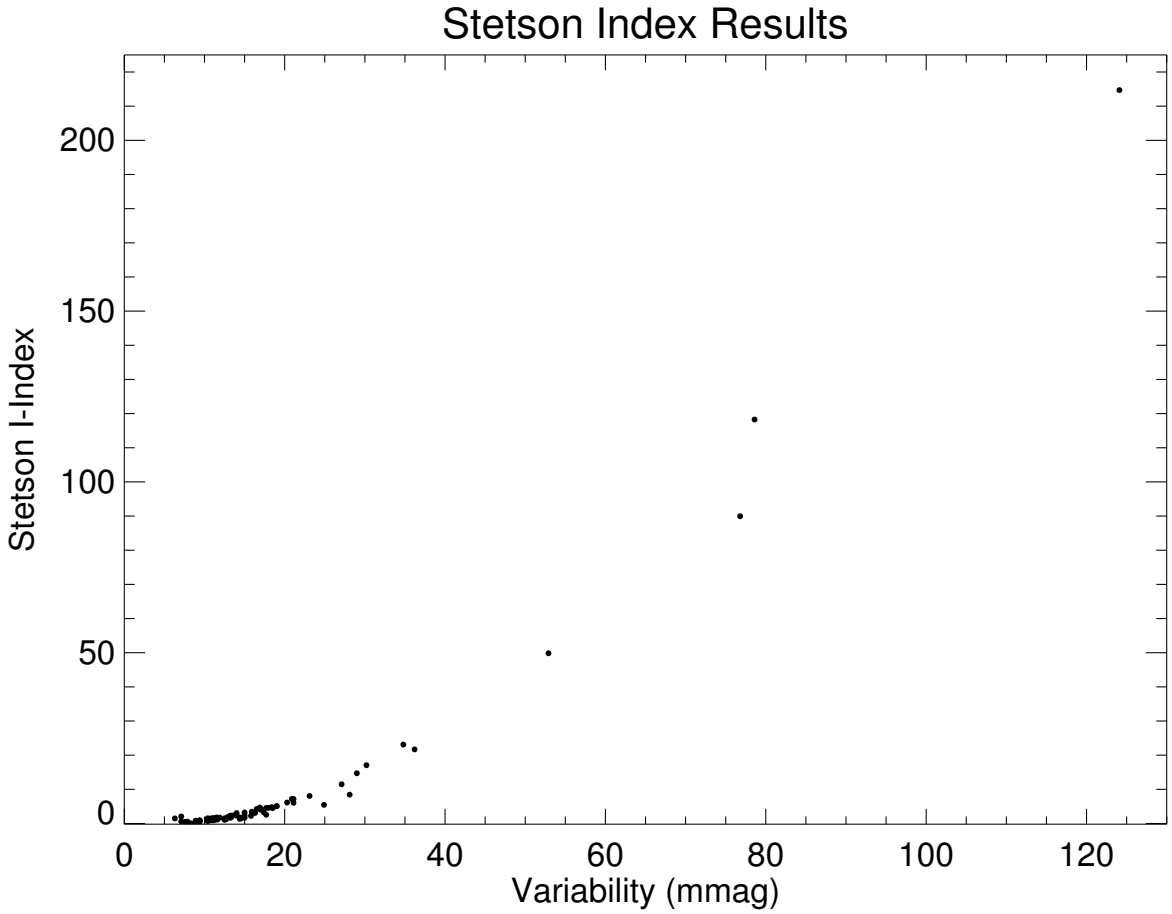

Figure 3.6: The results of our Welsh/Stetson I-index calculations described in §3.4. This shows a distinct and steady increase in the I-index as the variability increases, confirming that our variability measurements are due to true stellar variability.

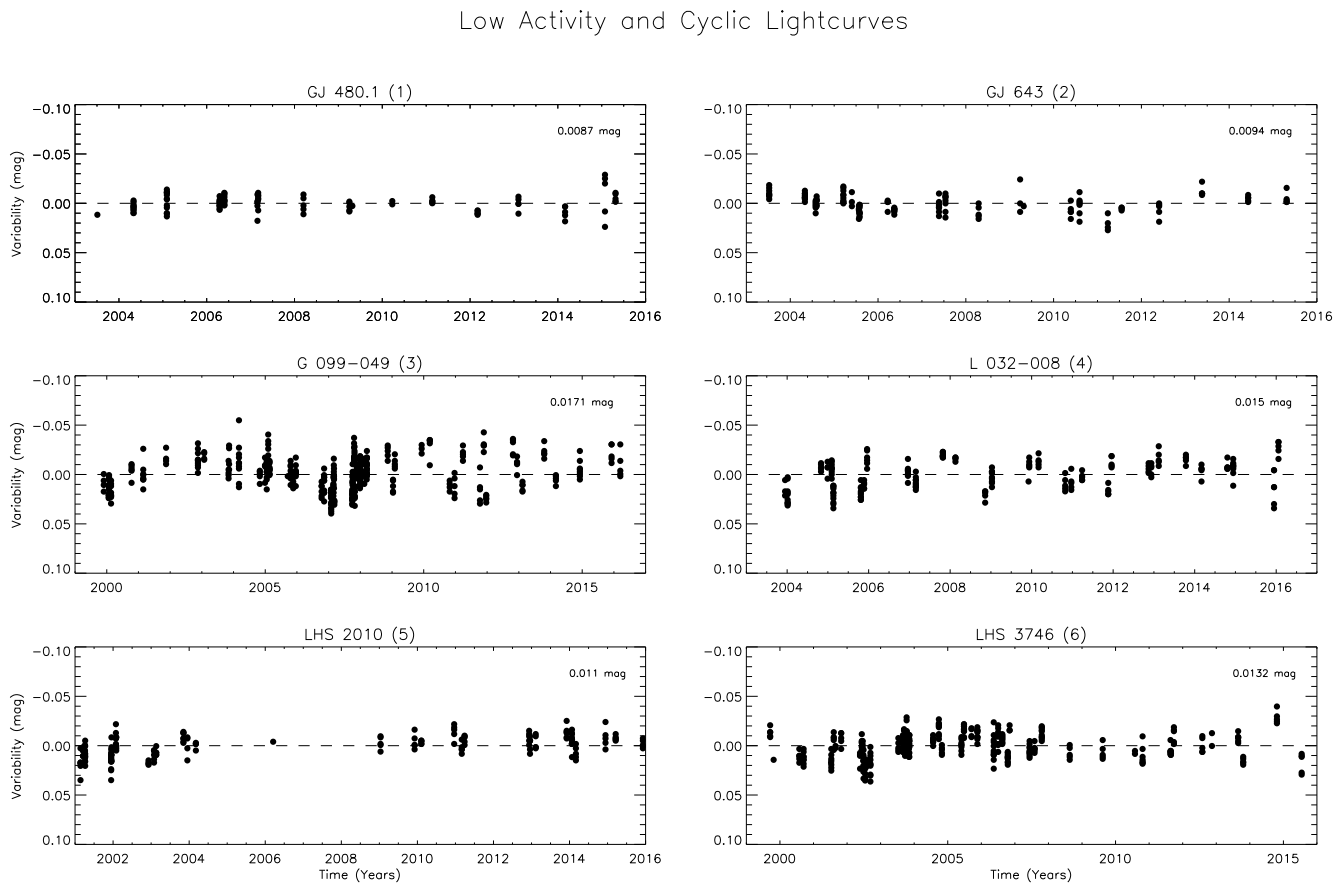

Figure 3.7: Each panel shows a light curve for the title star with the change in apparent V magnitude vs. time in years. In the upper right corner of each plot is the calculated value for the overall variability of each star. These light curves show a sample of our relatively inactive targets, a few of which still show evidence of low level cyclic activity. The stars are numbered 1 through 6 and are noted as such on Figure 3.4 and are detailed in §3.4.1.

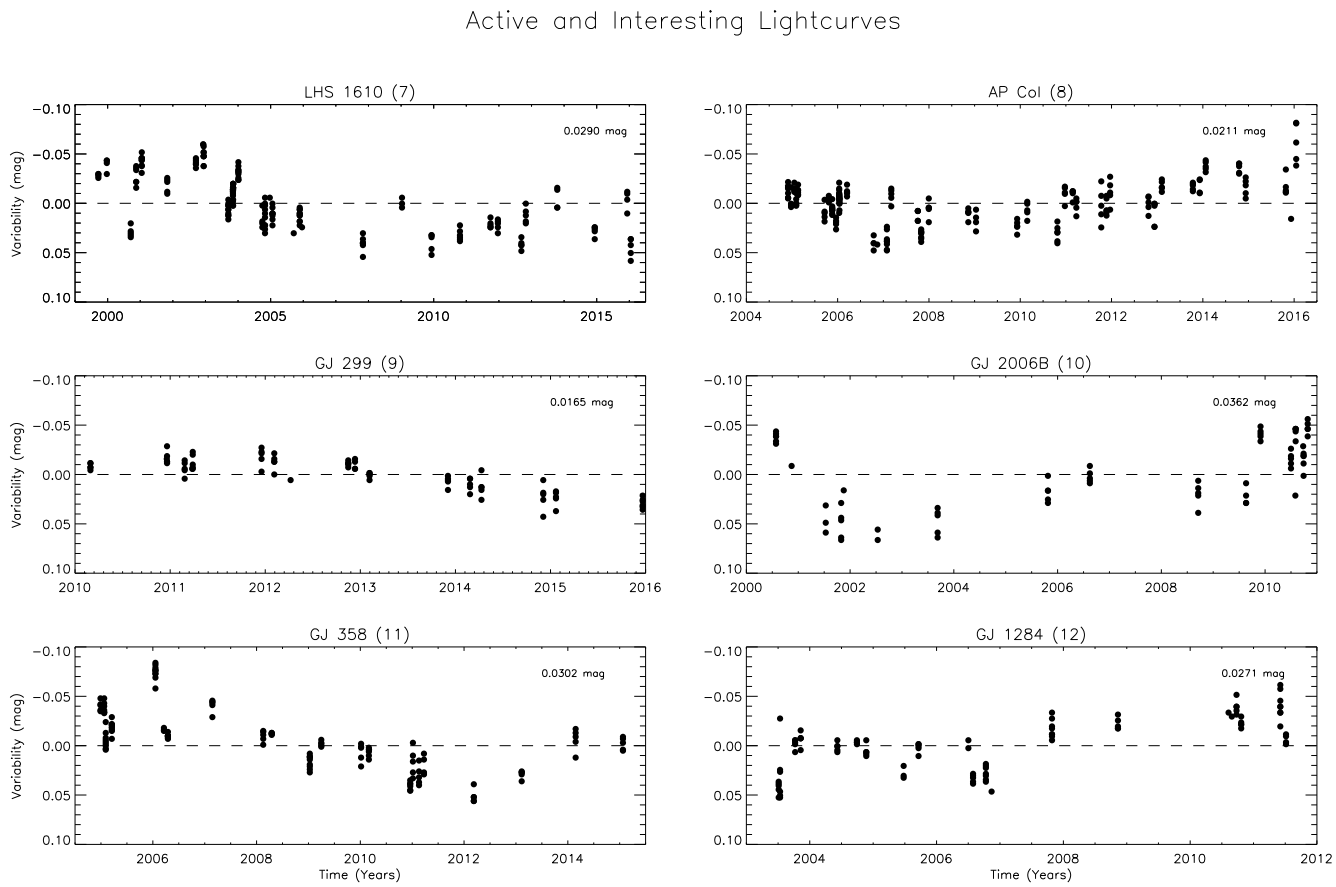

Figure 3.8: Each panel shows a light curve for the title star with the change in apparent V magnitude vs. time in years. In the upper right corner of each plot is the calculated value for the overall variability of each star. These light curves show active targets that are of particular interest. The stars are numbered 7 through 12 and are noted as such on Figure 3.4 and are detailed in §3.4.1.

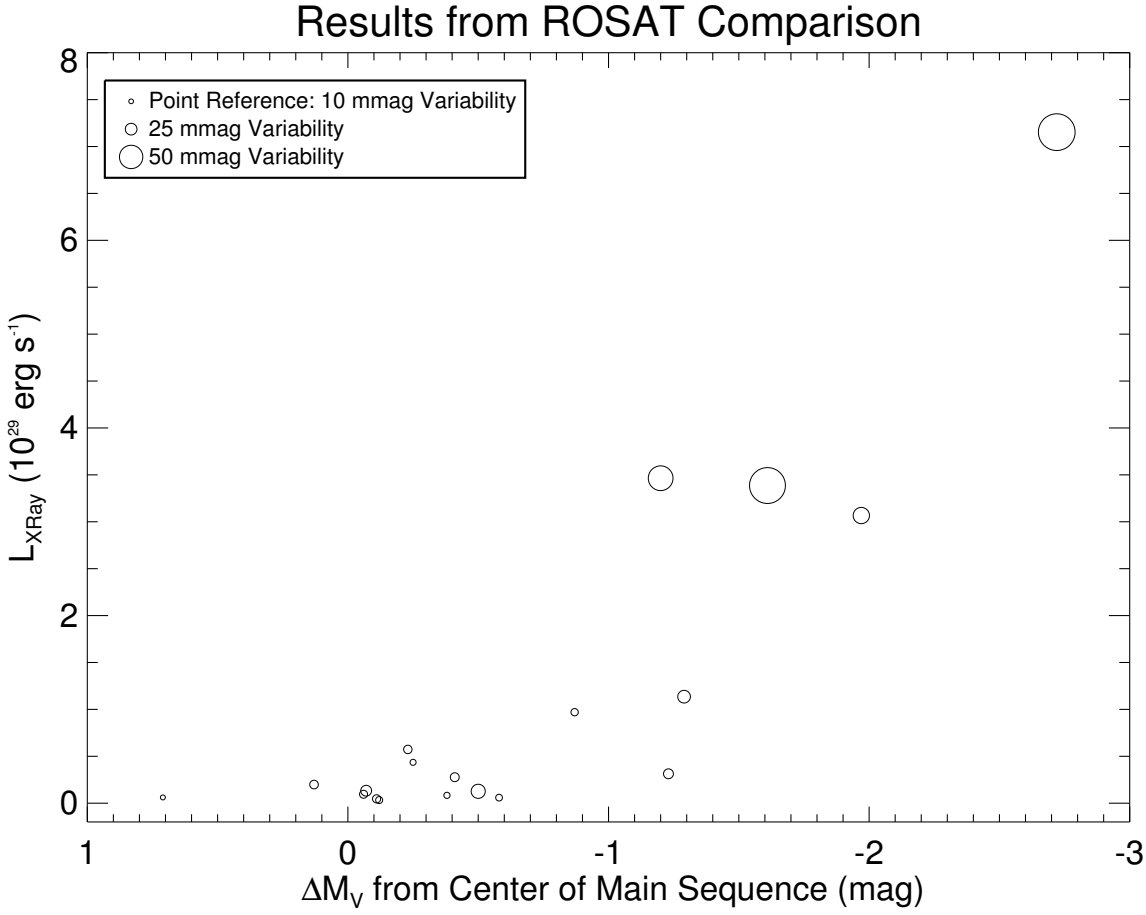

Figure 3.9: The ROSAT All-Sky Bright Source Catalog data for nineteen of our stars. The X-ray luminosity on the y-axis is derived from the published ROSAT fluxes using the distances in Table 3.1. The luminosities are plotted against their ΔM_V values, and the point sizes represent the long-term variability for each target, as in Figure 3.4, with reference points for variability of 10, 25, and 50 mmag given in the legend.

CHAPTER 4
SHORT-TERM VARIABILITY STUDY

4.1 Overview of the Short-Term Variability Study

Low mass stars remain youthfully active for significantly longer periods of time than higher mass stars. As discussed in Chapter 1, the lifetimes for this heightened activity increase quickly as the stellar types advance from M0V to M9V (West et al. 2004, 2008). This implies that stellar activity and magnetic fields may be a key contributing factor to the width of the main sequence for these stars. We study this activity directly by photometrically monitoring these stars in the V band over various time periods. Our goal for such studies is to identify changes in brightness that are related to interior magnetic activity via the appearance and disappearance of starspots over long term monitoring, and surface magnetic activity via small and large flare events over the short term. The study described in this chapter is focused on the short term monitoring for flares and small changes in brightness due to the activity levels of the magnetic fields at the surfaces of these stars. We determine any variability above 3σ of the threshold, as described in §4.4, for a given night to indicate a positive detection of short-term variability for a given star.

Flares occur when the magnetic field lines of a star become twisted, due to the differential rotation of the layers within the star, and then snap apart quickly resulting in a violent explosion at the surface hurling very high energy radiation and stellar material out into space as a flare (Kopp & Pneuman 1976). Similar to observations of such activity in the Sun, magnetically active stars are also found to have small prominences and filaments, or

microflares, rising and falling at the surface over small timescales of only seconds, which very slightly affect the brightness of the stars at shorter wavelengths (Robinson et al. 1995). It is also reasonable to hypothesize that younger, more active stars would exhibit larger changes in brightness due to stronger and higher numbers of microflares at the surface. Our previous work discussed in Chapter 3 has shown that low-mass stars classified as "young" are more magnetically active on long-term time scales (Clements et al. 2017). The effort outlined in this chapter aims to investigate whether or not the same is true, and observable, on short-term time scales. We have successfully observed 120 stars in the V band over short time periods of only two to six hours to detect small changes in brightness, with the intent of assessing whether or not there is a relation between the surface magnetic field activity and the vertical main sequence positions (or radii) of these stars. Figure 4.1 shows a histogram of time coverage for the 131 total observations. Five stars were observed multiple times to determine whether or not similar results were obtained at different epochs (and one – GJ 490A – was unintentionally observed twice). The stars observed for this study, their properties, and results are detailed in Table 4.1.

Table 4.1 contains all of the relevant properties for the 120 stars in this study used to create the various Figures in this chapter (as well as those in Chapter 1). The names and 2000.00 coordinates of each star are listed in columns 1, 2 and 3. The photometry values for each star are listed in columns 4 (apparent V magnitudes), 5 (apparent I magnitudes), and 6 (their $(V - K)$ colors). Columns 7 and 8 of Table 4.1 contain the distances and their references for each star. The distance in column 7 for each target was determined using

either RECONS published parallax values or those from the literature, as indicated by the references in column 8. Some of these distances were calculated using the weighted mean parallax value from more than one reference, as is indicated by YV (YPC95 and vLe07) or YVO (YPC95, vLe07, and other). The absolute magnitude (M_V) and distance from the main sequence (ΔM_V) for each star are listed in columns 9 and 10, respectively. The next three columns – 11, 12 and 13 – contain the observing information for each star; the telescope, date, and duration (in hours) for each set of observations for the given star. Columns 14, 15, and 16 contain the results of this study, including the variability measurements for each star, a reference baseline value – which is the variability measurement of a carefully chosen reference star –, and the σ value for each star– which is the variability of the target star divided by that of the baseline reference star . We also include the rotational velocities in km/s for 17 (14%) of our stars also found in Newton et al. (2016) from the MEarth Project, using only the northern data (17). These numbers were provided to show any correlation between variability and rotation rates, but the sample is too small for a robust analysis. The final column, 18, lists the notes for each star indicating if the star is known to be young (Y) or a subdwarf (S), or is suspected to be a young star ((Y)) or subdwarf ((S)).

4.2 Stars in Study

Our target boxes – outlined in Figures 1.1 and 1.2 – are described in detail in Chapter 2. These boxes, Box 4, 5 and 6, are centered around $(V-K)$ values of 4, 5, and 6 with a width in $(V-K)$ color of 0.6 mag. For this study we have observed 120 stars continuously to

produce lightcurves for short-term variability. Of these 120 stars, 50 are located in Box 4, 62 in Box 5, and only four are in Box 6. The remaining four stars of the 120 lie somewhere in between the three target boxes[1]. This sample includes 24 stars that appear to be younger than 200 million years, and are thus more active, and ten stars classified as low metallicity subdwarfs (both discussed in more detail below). We have obtained a large range in the spectral types for our sample, from K7 to M5.5 to allow us to determine if later spectral types exhibit different levels of variability during this experiment than earlier types. We note that the apparent magnitude of each star will affect the cadence of the observations, as brighter stars will require shorter exposure times while the faintest stars will be observed for a maximum of 300 s. These stars range from $V = 8.08 - 15.44$ in apparent magnitude.

Our target volume was expanded to 50 pc in order to include more stars at the extreme edges of the main sequence – subdwarfs and young stars. The low metallicity subdwarf stars included in this study range from $\Delta M_V = +0.62$ to $+2.38$. These stars are important to observe as they represent much of the lower portion of the main sequence, where we theorize most of the spread is dominated by metallicity effects. These stars are generally fainter, and thus more difficult to observe using exposure times of 300 s or less to still obtain sufficient counts. As a result, there are only ten subdwarf stars for which we have successfully obtained lightcurves. We note that two of these stars are suspected to be subdwarf stars (GJ 232 and GJ 1248), but are not yet confirmed, based on their positions more than one full magnitude below the main sequence and published metallicity values of $[m/H] \leq -0.5$ in

[1]These four stars were initially located on the inner edge of a box and updated photometry barely pushed them just outside of one, or they are a low mass primary or secondary to a target star and its lightcurve was also observed within the same field.

Dittmann et al. (2016). We would expect these stars to show little to no short-term activity as they are presumably much older than their counterparts on or above the main sequence. Subdwarf stars have had time to cease contracting to their final main sequence radii and to settle magnetically.

Many of the stars located significantly above the main sequence ($\Delta M_V = -1.00$ or more) are known young stars with ages less than 200 Myrs and are thus important targets for this study, considering their likely heightened levels of youthful activity. The ages of these stars were estimated based on either associations with young moving groups, the presence of lithium in their spectra, or both (as described in §1.4). These young stars are also generally fainter, as many of them are more than 25 pc away, and so were more difficult to observe for this study than the closer, brighter central main sequence stars. We have, in total, lightcurves for 24 nearby, young stars with a range in ΔM_V of -0.12 to -2.94. We would expect any detected variability on a short-term scale to come from these stars, as was the case for the long-term variability study, and so including more young stars in our sample is vital to better understanding the role of activity in the enhanced radii of these stars.

The histograms in Figures 4.1 and 4.2 serve to illustrate our sample for this study. In Figure 4.1 we show the range in duration for our observations of the stars and we see that a majority of targets were observed at our goal duration of four to five hours, including both the young and subdwarf stars in our study. Only five stars were observed for less than three hours, including one young star. These shorter observations occurred due to a sudden decline in the sky conditions that forced an end to the observations. Figure 4.2 illustrates the

distribution of our variability detections, most of which show no detected variability above our threshold of 3σ, on a short-term timescale.

4.3 Observations and Reductions

Observations were carried out using small telescopes at both CTIO and APO. Southern targets were observed at CTIO with the 0.9 m telescope in Chile, using the TekTronix 2048×2046 CCD camera in quarter chip mode. For our northern targets we utilized the 0.5 m ARCSAT telescope at APO in New Mexico with the *SurveyCam* 4096×4096 CCD detector. The V filters used for each telescope are almost identical. The CTIO 0.9 m uses a Johnson V filter centered at 5438Å, while ARCSAT uses a Johnson-Cousins V filter centered at 5411Å. All observations were taken using only the V filter for each instrument and basic calibrations, including bias and flat field frames, were taken at the beginning of each night. The lightcurve for each individual star was acquired during a single night, as it was continuously observed for two to six hours in order to increase our chances of observing micro-fluctuations in brightness or flares, if the star has heightened magnetic activity. Observations carried out at CTIO took advantage of the guiding feature available due to the smaller field-of-view (FOV); at only $6.8'$ on a side it was necessary to maintain enough consistent reference stars in the field. The FOV of $31.1' \times 31.1'$ on the ARCSAT *SurveyCam* was sufficient to maintain at least ten consistent reference stars in each image, and so no guiding was required. Our integration times were limited to $30 - 300$ s, to reduce our chances of missing any flares or prominences that may dissipate after only a few minutes

with the upper limit and to allow for sufficient counts in the surrounding reference stars with the lower limit. We aimed to acquire at least one million total counts for our target star, so long as the exposure time did not exceed 300 s. If a star was too bright and began to saturate in less than 30 s, we defocused the telescope in order to avoid saturation but still acquire our desired minimum counts and enough counts for the surrounding reference stars. We also aimed to keep the peak counts ∼20,000 counts below the saturation level of the CCD, this way we could avoid saturation if the star were to flare during observations. Our fields were carefully chosen to include a minimum of seven bright comparison stars that have $20\% - 100\%$ of the total counts of the target star.

We also acquired multiple light curves, over several different nights, for five control stars: LHS 178 (three nights), GJ 179 (two nights), GJ 203 (two nights), GJ 1125 (five nights), and GJ 480 (three nights). We chose one star at each location relative to the main sequence – one each at more than a magnitude below and above, between three-quarters and half a magnitude below and above, and within a tenth of a magnitude of the main sequence. These stars were each observed using the method outlined above more than once over the duration of this study to verify the quality and consistency of our observing method for this experiment. These results are discussed in §4.4.1. Thus, in total, we have 131 observations of 120 stars for this study.

The data were initially reduced using the bias and flat frames obtained for each night following standard *IRAF* procedures, and then run through the cosmic ray removal package *(cosmicray)* in order to reduce the chance of any false detections of variability due to cosmic

rays within the apertures. After cosmic ray removal, the images were all visually inspected to ensure their quality, eliminating any poor quality images, such as those that were clouded out, where trailing was present (due to a telescope shift), or where the target star was saturated. The images were then aligned using *imalign* to ensure all targets used are consistently in the same pixel location in each frame for a given lightcurve. After the images are properly inspected and aligned, the reference stars were carefully chosen and the images were run through the *phot* package in *IRAF* using aperture sizes that comfortably fit around each star while avoiding contact with any surrounding stars (this was usually between $12''$ and $19''$). The target star was run separately from the reference stars to allow for a different aperture size, as it is generally brighter and will require a larger aperture than the reference stars.

Following the *IRAF* reduction procedures, the remaining analysis was done using *IDL* programs written by the RECONS team for the purpose of producing short-term time-domain lightcurves. The program takes the fluxes and magnitudes from each *.mag* file created for the reference stars using the *phot* package and calculates the mean changes across each frame, eliminating any reference stars that vary by more than 2σ relative to the other reference stars, ensuring that only non-variable reference stars are used in the normalization of the lightcurves for relative photometry. The mean change calculated for each frame is then used to normalize the light curve of the target star, as well as a chosen reference star that serves as the baseline value for the dataset, and the fluxes are then converted to magnitudes and normalized around zero. The mean absolute deviation of the target star's magnitude (in millimagnitudes) is our calculated variability value and our baseline is given as the mean

absolute deviation of the magnitude of a carefully chosen, low variability reference star with fewer total counts than our target star, so as to provide a conservative estimate of the sensitivity of this method. Our lightcurves are then produced using *IDL* to create the plots for each target; examples are shown in Figures 4.8, 4.9, and 4.10.

4.4 Analysis and Results

With the 131 lightcurves in hand, the analysis using the calculated variability values was carried out. The results are illustrated in Figures 4.3, 4.4, and 4.5, where we plot the variability of each star against its main sequence position. In Figures 4.3 and 4.4 we show two different methods for determining whether or not there is a trend in variability for stars as they move from far below to far above the main sequence. Figure 4.3 shows our calculated variability values (in mmag) with the calculated variability of our chosen reference star as the baseline error bar – as this value would indicate our threshold detection for a given set of observations – versus the ΔM_V value for each star. Figure 4.4 better illustrates any trend that may be observed, as we instead use the σ detection of variability by dividing the variability of our target star by that of the reference star plotted against the ΔM_V value for each star. The points in Figure 4.4 flatten down to below 3σ for almost every star, with the exception of a handful of stars, discussed in §4.4.2, indicating that this study was unable to detect clear micro-fluctuations in the brightnesses of most of these 120 stars on short timescales of hours. Figure 4.5 is created in the same format as Figure 3.4, where the targets are plotted on an H-R diagram, with the point sizes indicating the σ detection level

of variability for each star. In mirroring the format of Figure 3.4, we also show the model tracks from Baraffe et al. (2015) for M stars between 0.1 and 0.5 $M_{\odot}$ for 100 Myrs (solid line) and 1 Gyrs (dashed line). We note that these tracks are significantly lower than our main sequence, particularly in the region of Box 5. Because it is reasonable to assume that the majority of our stars are not less than 100 Myrs old then we can only assume that the models may need revision.

A slight increasing trend is made more evident by showing the distributions of different variability σ ranges (excluding outliers above 5σ) over the range in ΔM_V values, as shown in Figure 4.6. The four panels of histograms show the ranges in σ of less than 1σ, 1σ to 2σ, 2σ to 3σ, and 3σ to 5σ for ΔM_V bins of 2 to 1, 1 to 0, 0 to -1, and -1 to -2. Due to the large number of stars between 1σ and 2σ the second panel has twice the scale in number of stars as the other three panels, which show the number of stars from 0 to 20. We see that there are no stars less than $\Delta M_V = -1$ with a variability measurement below 1σ and no stars greater than $\Delta M_V = 1$ with a variability measurement above 3σ. We also observe a gradual shift towards stars above the main sequence with increasing σ detection values.

In Figure 4.7, we show for four fields how the measured variabilities depend on star brightnesses, and the consequent signal-to-noise ratios. Here the variability of the target star is plotted against the curve of the data for the reference stars, with fainter reference stars exhibiting higher levels of variability. This allows us to determine if the measured value is due primarily to noise or an actual variability detection. If the target star (blue triangle) lies within the curve of the other data points, its variability value can be deemed to be

effectively along the baseline, non-detection envelope. If it lies far above the curve, as seen in the case of **G 141-029**, we can identify this measured variability as a positive detection of stellar activity. Any reference stars lying above the curve of the rest of the data, varying by 2σ or more when compared to the other reference stars, were automatically removed from the calculations of the reference star set used for normalizing the lightcurves. The four stars used to create Figure 4.7 were all taken using ARCSAT, and thus have richer fields due to the larger FOV. This allowed us to choose our maximum of 20 reference stars for each data series, to create an ideal representation of the curves. The red squares in each panel are the reference stars chosen to be indicative of our error, as they had similar (but fewer) total counts as the target star and they exhibited similar, or lower variability measurements.

In order to better determine the presence or strength of any trend in these results we calculated the average variability σ for each group of young stars, main sequence stars, and subdwarf stars and then did the same for each major grouping of main sequence positions (ΔM_V values) – excluding the single outlier at 22.3σ. As shown in Figure 4.11, these results did demonstrate a trend in the activity levels for each group of stars. For the known young stars the average σ detection value is 2.2, for main sequence (or yet unidentified) stars we find a 1.5σ average, and the subdwarfs are (predictably) the lowest at 1.4σ. When broken down to an analysis of the range in ΔM_V values this trend is even clearer. For the stars furthest below the central distribution of the main sequence, $\Delta M_V = +2.5$ to $+1.5$, the average variability is 1.4σ, the lowest average. For those at $\Delta M_V = +1.5$ to $+0.5$ this average is 1.5σ and for those within a magnitude of the central distribution, at $\Delta M_V = +0.5$ to -0.5,

the variability average is 1.6σ. Stars located above the main sequence at $\Delta M_V = -0.5$ to -1.5 exhibit an average variability that is actually the same as the last grouping, at 1.6σ. For the stars furthest above the main sequence we use the range of $\Delta M_V = -1.5$ to -3.0, as there are only five stars in this group, and these stars have the highest variability average at 2.9σ. These slight increasing trends do imply that stars are more active, on short-term timescales, the further they are above the main sequence, and for young stars in particular. These results reflect those of our long-term study and support our hypothesis that stars above the main sequence are likely over-luminous due to inflated radii supported by increased magnetic activity.

4.4.1 Control Stars Results

As described in §4.3, we acquired multiple lightcurves, on each telescope and on different nights for five stars at different ΔM_V values to assess the consistency and accuracy of our results. Among these five stars is the known subdwarf **LHS 178** at $\Delta M_V = +1.40$ for which we obtained 3 lightcurves, one on ARCSAT and two on the CTIO 0.9 m. These lightcurves showed mildly consistent variability values well below our 3σ threshold of 1.5σ, 1.2σ, and 0.8σ, this variance is due mainly to the lower quality of the two CTIO observations because they had significantly fewer good reference stars in each frame. Our control star located below the main sequence is **GJ 203** at $\Delta M_V = +0.67$ and was observed on two different occasions, once at each telescope. These results were also consistent, with variability detections of only 1.0σ and 1.1σ. The star within the central distribution of the main sequence, **GJ 1125**, at $\Delta M_V = +0.08$ showed very stable results over five different nights, at 1.0σ, 1.2σ, 1.2σ, 1.2σ,

and 1.1σ. Our control star results remained stable after moving above the main sequence to **GJ 179** at $\Delta M_V = -0.60$ with two lightcurves (one at each telescope) at variability values of 1.1σ and 0.9σ. The final control star was the highest of these above the main sequence at $\Delta M_V = -0.81$ and this star, **GJ 480**, also showed the highest deviation in its results, though still well below the 3σ threshold. The three observations for this over-luminous star consist of two carried out on ARCSAT and one at CTIO with variability values of 1.3σ, 0.9σ, and 1.6σ. The results of this control experiment confirm the stability of our observing and reduction methods for this study and show that our results presented here are reliable.

4.4.2 Individual Variability Detections

Of the 120 stars observed for this study there were only 11 stars (9%) that exhibited interesting trends, flares, or a variability σ detection above our threshold of 3σ. Here we discuss these targets and their results individually. Of these 11 stars, seven have a variability measurement greater than 3σ. The remaining four stars, below 3σ, include one star (**G 141-029**) that had two small flares but measured at only 2.6σ – likely limited by either saturation of the frames or the long cadence – and another (**GJ 275.1**) that is just under the 3σ threshold at 2.9σ. Of the last two stars, one (**LHS 1976**) is decreasing in brightness throughout the observations at 2.7σ variability and the other (**GJ 534.2**) exhibits a slight sinusoidal trend with a 2.1σ detection, possibly indicating a rotation period of about four hours. The lightcurves for each of the 11 stars are shown in Figures 4.8, 4.9, and 4.10.

The seven stars with variability detections of 3σ or greater include five known young stars, one main sequence star within Box 6, and, surprisingly, one star half a magnitude below the

main sequence (**GJ 643**). Figure 4.8 shows the lightcurves for three of the known young stars – **SCR 0017-6645**, **TWA 8B**, and **G 141-029** – and **SCR 1214-2345**, each of which flared during the observations. We note that the young star **SCR 0017-6645**, located far above the main sequence at $\Delta M_V = -1.92$, was observed early in the program and saturated during the flare event, making those frames unusable, so the strength in variability of this flare was likely much higher than reported here at 3.2σ, as shown in the first panel of Figure 4.7. In the next panel we show the strongest flare observed, on **SCR 1214-2345** an M4.5V class star at $\Delta M_V = +0.07$ inside Box 6. This star is not known to be young, but it is a known X-ray source (as shown in §3.4.2). SCR 1214-2345 is also, presumably, fully convective and so the mechanisms driving its magnetic field activity are not fully known and it is interesting to observe such a strong flare event from this star. The star also continued to brighten significantly during the entire 4.5 hours of observations, both before and after the flare event, giving the highest variability detection of 22.3σ. The known young star **TWA 8B**, at $\Delta M_V = -2.74$, also flared strongly and appears to have begun flaring again at the end of the 4.5 hours of observations with a high variability measurement of 7.9σ. In the last panel **G 141-029**, at $\Delta M_V = -0.12$, shows a variability detection of only 2.6σ, but had two small flares during the four hours of observations. It is likely that with a smaller cadence (exposures were 300 s) these flares would have peaked higher, resulting in a higher variability measurement.

As shown in Figure 4.9, two of the other young stars, **AP Col** and **G 190-028** as well as **LHS 1976** and **GJ 643**, are all slightly decreasing in brightness for the duration of their

observations. The young star **AP Col** above the main sequence at $\Delta M_V = -1.06$ was steadily decreasing by about 25 mmag over 4.5 hours with a measured variability of 3.3σ. It is worth noting that while **G 190-028**, at $\Delta M_V = -0.54$, was decreasing steadily for about five hours at a measured variability of 3.1σ, it is part of an M dwarf binary system and the primary component, **G 190-027**, did begin to flare at the very end of the observations but it was not enough to increase the measured variability to above 3σ over 4.5 hours. The detection for **LHS 1976**, $\Delta M_V = -0.49$, was below our threshold of 3σ, but it shows a decrease in brightness over 4.0 hours at 2.7σ. The last star with a variability detection greater than 3σ is **GJ 643**, located 0.55 magnitudes below the main sequence. This star was also very slightly decreasing in brightness throughout the observations. Each of these decreases in brightness are likely the result of one of two scenarios. The first, and most likely, is that we are observing a portion of these stars' rotation period light curves as a result of starspots moving into or out of view. The other, and less likely, is that these stars had flared prior to the start of the observations and we observed them during the decay, or "cool down" period of their flare events, though the decay time after the peak of a typical flare is unlikely to last for four or more hours.

In Figure 4.10 we show three stars that exhibited other interesting trends, two with less than a 3σ variability detection. These are **GJ 275.1**, a star with $\Delta M_V = -0.76$, **GJ 534.2**, another star above the main sequence at $\Delta M_V = -0.43$, and **GJ 871.1B** a known young star at $\Delta M_V = -1.84$. The first star, **GJ 275.1** started out the observations dimming slightly before settling and remaining consistent for the other half of the five hours of observations.

This star was also just below our threshold for a variable star at $\sigma = 2.9$, so the initial dimming was significant. **GJ 534.2**, with a variability measurement of only 2.1σ, showed a very slight sinusoidal trend – slightly decreasing, then increasing, and decreasing again throughout the observations – that could be indicative of a full rotation period of only four hours. The last star, **GJ 871.1B**, was brightening by about 40 mmag throughout the 4.5 hours of observations at a high measured variability value of 5.0σ.

4.5 Conclusions

It is important to note that this is the first study of its kind and the capabilities and results for such a study were previously unknown. Similar studies have been performed, but used faster cadences (of less than one second) or utilized photometric observations at higher energy wavelengths, such as X-ray and UV (see e.g., Robinson et al. 1995, Wargelin et al. 2008, and Schmitt et al. 2016). These studies have been able to successfully detect micro-fluctuations in the magnitudes of such stars due to high-speed microflares and prominences at their surfaces. There have also been multiple flare studies on M dwarf flare stars carried out at the University of Washington Department of Astronomy. These studies are similar to this study, though they use much faster cadences for only a handful of stars in combination with high cadence spectra (see e.g., Kowalski et al. 2013, 2016). They also carried out a much larger survey to assess the flare rates in M dwarf stars using SDSS Stripe 82 data with long cadences of several days, over years, for over 50,000 M dwarf lightcurves and identified 271 flares. From this study they found that flaring strongly correlated with the presence of Hα

emission and that the flaring fraction strongly increased for redder stars (Kowalski et al. 2009).

As part of earlier RECONS studies, Hosey et al. (2015) compared their long-term variability efforts to *Kepler* data and found that while *Kepler* observed thousands of northern M dwarfs, most are not in the solar neighborhood and none were in their (nor in our) long-term study. Through their investigation they found that of the extracted variability rates for more than 2000 M dwarfs from *Kepler* with magnitudes between $M_{Kepler} = 14 - 16$, only 7% varied by more than 10 mmag. Of the smaller number of M dwarfs closer in brightness to those in our short-term variability sample ($M_{Kepler} = 12 - 14$), only 9% varied by more than 10 mmag. When compared to the results of our short-term study, we find that only about 6% of our 120 stars vary by more than our conservative variability estimate of 3σ. We also note that our average variability floor for a given lightcurve is less than 3 mmag, meaning a 10 mmag detection would (on average) be more than 3σ. Though the timescales for the observations of each study are different (*Kepler* observed each star every 30 minutes for up to 33 days) our resulting variability rates are similar to what is found for M dwarfs from *Kepler*.

While we were able to successfully detect large flare events, three of which occurred on young stars, as well as a handful of other slight changes in brightness, we were not able to detect microflares or small fluctuations that have been detected at shorter wavelengths and with much faster cadences of subseconds to microseconds. From this study we find that with slower cadences on timescales of minutes, there is only a slight trend in the short-

term variability for stars above the main sequence relative to those below. In addition, the majority of the 120 stars in this study showed no variability detections. We did, however, find that almost all of the stars with measurable variability on these timescales were either young or positioned above the main sequence. The one variable star positioned below the main sequence (**GJ 643**) was dimming very slightly throughout the observations, possibly because a large spot rotated into view. We also find that none of the subdwarfs are variable by more than 2.2σ, with a majority around 1σ, meaning they exhibited no measured variability on short-term timescales.

At the very least, this study supports our hypothesis that younger stars would be more active on short timescales, as three of the four stars in which flares were detected are known young stars, resulting in higher σ variability values than the other types of stars. Though this study was unsuccessful in uncovering a clear, strong trend in the short-term variability with the vertical main sequence position of low mass stars, it is possible that with a larger aperture telescope – allowing for much shorter integration times and cadences – such a study may be better designed to detect variability due to the surface magnetic field activity of these stars.

Table 4.1: Properties of the Low Mass Stars in the Short-Term Variability Study.

Star Name	R.A.	Dec.	V	I	$V-K$	dist.	dist.	M_V	ΔM_V	Telescope	Obs.	Dur.	Var.	Base.	σ	V_{Rot}	Notes[a]
	2000.0					(pc)	ref.				Date	(hours)	(mmag)		km/s		
(1)	(2)	(3)	(4)	(5)	(6)	(7)	(8)	(9)	(10)	(11)	(12)	(13)	(14)	(15)	(16)	(17)	(18)
GJ 7	00:09:04	−27:07:19	11.69	9.78	3.83	22.9	vLe07	9.89	+0.71	CTIO-0.9	2016.1029	4.0	2.2	2.4	0.9	···	
LHS 1054	00:17:20	+29:10:58	11.52	9.35	4.28	22.8	vLe07	9.73	−0.51	ARCSAT	2014.1115	5.0	2.0	1.9	1.1	···	
SCR 0017-6645	00:17:23	−66:45:12	12.45	10.00	4.75	39.0	Rie14	9.49	−1.92	CTIO-0.9	2014.1026	5.0	10.4	3.3	3.2	···	Y
GJ 15A	00:18:23	+44:01:24	8.08	6.45	4.06	3.6	YVO	10.30	+0.59	ARCSAT	2015.1215	3.5	14.8	5.2	2.8	0.6	
GJ 15B	00:18:26	+44:01:42	11.06	8.24	5.11	3.6	YVO	13.28	+0.97	ARCSAT	2015.1215	4.5	7.4	5.9	1.3	0.1	
LHS 5004A	00:21:37	−46:05:33	12.24	9.73	4.79	19.3	vLe07	10.81	−0.70	CTIO-0.9	2015.0911	4.0	3.7	3.3	1.1	···	
GJ 2006A	00:27:50	−32:33:06	12.95	10.29	4.94	33.2	Rie14	10.34	−1.54	CTIO-0.9	2015.0902	4.5	10.5	9.3	1.1	···	Y
GJ 2006B	00:27:50	−32:33:24	13.25	10.48	5.13	31.5	Rie14	10.76	−1.59	CTIO-0.9	2015.0902	4.5	9.6	9.3	1.0	···	Y
G 001-021B	00:45:17	+01:40:34	14.04	11.85	4.20	23.1	YPC95	12.22	+2.18	CTIO-0.9	2016.1025	4.0	3.4	3.1	1.1	···	S
GJ 46	00:58:27	−27:51:25	11.77	9.17	4.88	12.3	vLe07	11.32	−0.42	CTIO-0.9	2015.0904	4.5	2.7	1.2	2.3	···	
GJ 1025	01:00:56	−04:26:56	13.36	10.55	5.14	11.4	Jao05	13.08	+0.70	CTIO-0.9	2015.0903	4.5	3.8	2.8	1.4	···	
GJ 49	01:02:38	+62:20:42	9.56	7.44	4.19	9.9	vLe07	9.58	−0.44	ARCSAT	2014.1203	6.0	10.3	3.8	2.7	37.3	
GJ 1030	01:06:41	+15:16:22	11.40	9.23	4.24	21.8	vLe07	9.64	−0.50	ARCSAT	2014.1205	4.0	4.4	2.7	1.6	···	
LHS 1289	01:43:15	+27:50:31	10.40	8.55	3.80	21.4	vLe07	8.75	−0.36	ARCSAT	2014.1206	4.5	3.0	2.2	1.4	···	
GJ 82	01:59:23	+58:31:16	12.21	9.48	5.25	12.2	vLe07	11.78	−0.86	ARCSAT	2014.1113	2.5	5.4	1.9	2.8	···	Y
GJ 93	02:17:34	−53:59:20	11.40	9.51	3.75	22.5	vLe07	9.64	+0.64	CTIO-0.9	2015.0910	4.5	4.6	3.4	1.4	···	
GJ 96	02:22:14	+47:52:48	9.41	7.51	3.86	11.8	vLe07	9.05	−0.19	ARCSAT	2014.1201	5.0	7.4	4.1	1.8	···	
LTT 17413	02:45:39	+44:56:55	10.85	9.10	3.87	23.0	vLe07	9.04	−0.23	ARCSAT	2015.1121	5.0	2.7	1.5	1.8	29.5	
GJ 118.2C	02:55:39	+26:52:23	13.90	11.06	5.24	23.5	vLe07	12.04	−0.57	ARCSAT	2015.1220	4.0	8.1	4.4	1.8	···	
GJ 1058	03:22:04	+02:56:35	14.78	11.82	5.27	16.9	YPC95	13.64	+0.95	CTIO-0.9	2016.1027	4.0	6.9	6.8	1.0	17.2	
GJ 1062	03:38:18	−11:29:49	13.01	10.79	4.18	16.0	YPC95	11.99	+2.00	CTIO-0.9	2016.1024	4.0	7.8	7.8	1.0	···	S
LHS 178	03:42:29	+12:21:34	12.87	10.78	3.99	24.3	YPC95	10.94	+1.40	ARCSAT	2014.1130	5.0	4.3	2.8	1.5	···	S
LHS 178	03:42:29	+12:21:34	12.87	10.78	3.99	24.3	YPC95	10.92	+1.40	CTIO-0.9	2016.1026	4.0	7.0	6.0	1.2	···	S
LHS 178	03:42:29	+12:21:34	12.87	10.78	3.99	24.3	YPC95	10.94	+1.40	CTIO-0.9	2016.1207	4.6	6.4	8.0	0.8	···	S
GJ 1065	03:50:43	−06:05:10	12.82	10.04	5.07	9.5	YPC95	12.93	+0.72	ARCSAT	2015.1118	4.5	2.3	4.1	0.6	···	
LP 834-032	04:35:36	−25:27:34	12.44	9.74	5.03	17.3	Win15	11.25	−0.86	CTIO-0.9	2016.1029	4.0	6.1	3.0	2.0	···	Y
GJ 179	04:52:05	+06:28:35	11.98	9.33	5.04	12.3	vLe07	11.53	−0.60	ARCSAT	2016.0131	4.2	2.0	1.8	1.1	···	
GJ 179	04:52:05	+06:28:35	11.98	9.33	5.04	12.3	vLe07	11.53	−0.60	CTIO-0.9	2016.1025	4.0	1.6	1.7	0.9	···	
LP 776-025	04:52:24	−16:49:21	11.63	9.12	4.74	16.2	Shk12	10.58	−0.81	CTIO-0.9	2016.1028	4.0	3.3	2.8	1.2	···	Y
GJ 1074	04:58:45	+50:56:37	10.98	9.01	3.94	19.2	vLe07	9.56	+0.14	ARCSAT	2016.0125	2.0	3.6	3.7	1.0	···	
GJ 203	05:28:00	+09:38:38	12.47	9.78	4.93	9.7	YV	12.54	+0.67	ARCSAT	2015.1122	4.5	3.1	3.1	1.0	···	
GJ 203	05:28:00	+09:38:38	12.47	9.78	4.93	9.7	YV	12.54	+0.67	CTIO-0.9	2017.0124	4.3	1.9	1.8	1.1	···	
GJ 212	05:41:30	+53:29:23	9.76	7.75	4.00	12.2	vLe07	9.33	−0.24	ARCSAT	2016.0129	4.5	5.9	4.4	1.3	···	Y
GJ 213	05:42:09	+12:29:21	11.54	8.68	5.25	5.8	vLe07	12.72	+0.08	ARCSAT	2016.0204	5.0	2.5	1.6	1.6	1.4	
GJ 220	05:53:14	+24:15:32	10.84	8.71	4.01	19.4	YPC95	9.40	−0.19	ARCSAT	2015.1120	4.0	2.9	2.0	1.5	···	
G 099-049	06:00:03	+02:42:23	11.31	8.43	5.27	5.2	Hen06	12.73	+0.04	ARCSAT	2015.1121	4.5	2.4	1.5	1.6	6.9	
AP Col	06:04:52	−34:33:36	12.97	9.60	6.10	8.4	Rie11	13.35	−1.06	CTIO-0.9	2014.1210	4.5	5.6	1.7	3.3	···	Y
GJ 232	06:24:41	+23:25:59	13.16	10.21	5.25	8.4	YPC95	13.54	+0.90	ARCSAT	2015.1220	3.5	2.7	2.9	0.9	···	(S)

[a]Notes in Column 18: Y = known young stars, (Y) = suspected young star, S = known subdwarf stars, (S) = suspected, but unconfirmed subdwarf stars.

Distance references: (Ang12) Anglada-Escudé et al. (2012); (Cos05) Costa et al. (2005); (Cos06) Costa et al. (2006); (Dav15) Davison et al. (2015); (Fab00) Fabricius & Makarov (2000); (Gat08) Gatewood (2008); (Gou04) Gould & Chanamé (2004); (Hen06) Henry et al. (2006); (Jao05) Jao et al. (2005); (Jao11) Jao et al. (2011); (Lur14) Lurie et al. (2014); (Rie10) Riedel et al. (2010); (Rie11) Riedel et al. (2011); (Rie14) Riedel et al. (2014); (Shk12) Shkolnik et al. (2012); (Sma10) Smart et al. (2010); (vLe07) van Leeuwen (2007); (Win15) Winters et al. (2015); (YPC95) van Altena et al. (1995).

Table 4.1: Properties of the Low Mass Stars in the Short-Term Variability Study.

Star Name	R.A.	Dec.	V	I	$V-K$	dist. (pc)	dist. ref.	M_V	ΔM_V	Telescope	Obs. Date	Dur. (hours)	Var. (mmag)	Base. (mmag)	σ km/s	V_{Rot}	Notes[a]
	2000.0																
(1)	(2)	(3)	(4)	(5)	(6)	(7)	(8)	(9)	(10)	(11)	(12)	(13)	(14)	(15)	(16)	(17)	(18)
G 108-021(A)	06:42:11	+03:34:53	12.06	9.55	4.73	10.4	YPC95	11.97	+0.61	ARCSAT	2015.1215	4.5	1.9	1.7	1.1	0.2	
GJ 2050	06:44:45	+71:53:15	10.95	8.99	3.95	22.0	vLe07	9.24	−0.21	ARCSAT	2016.0205	5.5	4.9	1.8	2.7	···	
LTT 11918	06:47:18	+23:46:44	12.66	11.15	3.95	21.5	YPC95	11.00	+1.55	ARCSAT	2014.1115	2.5	4.4	2.5	1.8	···	
LHS 1882	06:56:22	+54:57:38	12.47	10.24	4.21	17.2	YPC95	11.29	+1.23	ARCSAT	2014.1206	4.5	3.4	1.9	1.8	···	
GJ 270	07:19:31	+32:49:48	10.08	8.27	3.70	19.1	vLe07	8.67	−0.22	ARCSAT	2016.0130	4.5	4.9	4.6	1.1	···	
GJ 273	07:27:24	+05:13:32	9.85	7.14	4.99	3.8	Gat08	11.95	−0.06	ARCSAT	2014.1201	5.0	4.7	3.4	1.4	···	
GJ 277B	07:31:57	+36:13:47	11.78	9.06	5.03	11.8	vLe07	11.42	−0.69	ARCSAT	2016.0207	4.5	1.8	1.6	1.1	···	
GJ 275.1	07:32:02	+68:37:15	10.89	8.89	4.03	24.9	vLe07	8.91	−0.73	ARCSAT	2016.0128	5.0	5.0	1.7	2.9	···	
LHS 1932	07:36:12	−51:55:21	12.48	9.92	4.72	16.1	Rie10	11.45	+0.11	CTIO-0.9	2015.0127	5.0	3.7	2.2	1.7	···	
GJ 289	07:48:16	+20:22:05	11.45	9.34	4.05	14.8	YV	10.60	+0.92	ARCSAT	2016.0125	4.0	2.0	1.5	1.3	···	
SCR 0757-7114	07:57:32	−71:14:54	12.45	9.77	5.03	22.1	Rei14	10.73	−1.38	CTIO-0.9	2015.0321	4.0	2.0	1.5	1.3	···	Y
LHS 1976	08:03:20	+52:50:38	11.38	9.26	4.14	24.8	Sma10	9.41	−0.49	ARCSAT	2015.1118	4.5	6.2	2.3	2.7	···	
LHS 2010	08:27:11	−44:59:21	11.86	9.19	4.99	13.7	Rie10	11.18	−0.84	CTIO-0.9	2015.0128	4.5	3.0	2.2	1.4	···	
GJ 317	08:40:55	−23:28:00	12.01	9.37	4.98	15.3	Ang12	11.09	−0.90	CTIO-0.9	2016.0311	4.0	2.2	2.3	1.0	···	
LHS 2122	09:16:25	−62:04:16	12.57	9.94	5.03	17.0	Rie10	11.42	−0.69	CTIO-0.9	2016.0310	4.0	1.9	1.8	1.1	···	
GJ 1125	09:30:44	+00:19:22	11.72	9.13	4.85	9.9	vLe07	11.74	+0.08	ARCSAT	2016.0206	4.0	1.7	1.7	1.0	···	
GJ 1125	09:30:44	+00:19:22	11.72	9.13	4.85	9.9	vLe07	11.74	+0.08	CTIO-0.9	2017.0125	4.3	2.4	2.0	1.2	···	
GJ 1125	09:30:44	+00:19:22	11.72	9.13	4.85	9.9	vLe07	11.74	+0.08	CTIO-0.9	2017.0315	4.5	3.4	2.8	1.2	···	
GJ 1125	09:30:44	+00:19:22	11.72	9.13	4.85	9.9	vLe07	11.74	+0.08	ARCSAT	2017.0405	4.1	2.6	2.2	1.2	···	
GJ 1125	09:30:44	+00:19:22	11.72	9.13	4.85	9.9	vLe07	11.74	+0.08	CTIO-0.9	2017.0509	4.0	4.7	4.3	1.1	···	
GJ 358	09:39:46	−41:04:03	10.78	8.27	4.72	9.5	vLe07	10.89	−0.45	CTIO-0.9	2016.0317	2.5	1.7	1.9	0.9	···	
LHS 277	10:01:10	−30:23:24	11.44	8.98	4.74	16.0	vLe07	10.42	−0.97	CTIO-0.9	2016.0312	4.0	1.7	1.6	1.1	···	
LHS 2317	10:50:26	+33:05:19	13.07	10.38	5.06	22.9	YPC95	11.27	−0.91	ARCSAT	2015.1215	3.5	2.7	2.4	1.1	···	
GJ 412A	11:05:28	+43:31:36	8.77	6.70	4.00	4.8	vLe07	10.36	+0.80	ARCSAT	2016.0419	4.5	6.1	3.8	1.6	4.7	
GJ 414B	11:11:05	+30:26:45	9.98	7.82	4.25	11.9	vLe07	9.60	−0.56	ARCSAT	2016.0202	4.7	7.8	3.7	2.1	···	
GJ 424	11:20:04	+65:50:47	9.32	7.43	3.79	8.9	vLe07	9.57	+0.48	ARCSAT	2016.0207	4.5	6.1	2.6	2.3	···	
GJ 430.1	11:31:43	+22:40:01	10.27	8.29	3.95	15.9	vLe07	9.26	−0.19	ARCSAT	2016.0129	5.0	5.5	4.1	1.3	···	
TWA 8A	11:32:41	−26:51:56	12.23	9.79	4.80	46.9	Rie14	8.87	−2.66	CTIO-0.9	2015.0515	4.5	4.7	2.2	2.1	···	Y
TWA 8B	11:32:41	−26:52:09	15.22	11.76	6.21	47.1	Rie14	11.85	−2.74	CTIO-0.9	2015.0515	4.5	17.3	2.2	7.9	···	Y
GJ 1148	11:41:44	+42:45:07	11.92	9.18	5.10	11.2	YV	11.67	−0.61	ARCSAT	2016.0128	5.5	2.8	2.4	1.2	···	
GJ 445	11:47:41	+78:41:28	10.79	8.13	4.84	5.3	vLe07	12.17	+0.53	ARCSAT	2016.0130	4.5	3.2	2.6	1.2	···	
LHS 2497	12:02:18	+28:35:14	12.86	10.36	4.47	20.2	YPC95	11.33	+0.62	ARCSAT	2015.0509	4.2	2.7	2.7	1.0	5.6	S
SCR 1214-2345	12:14:08	−23:45:17	13.96	10.78	5.73	10.9	Rie14	13.77	+0.07	CTIO-0.9	2015.0517	4.5	42.3	1.9	22.3	···	
GJ 458.2	12:15:08	+48:43:57	10.53	8.70	3.76	24.8	vLe07	8.56	−0.46	ARCSAT	2016.0204	4.8	4.7	1.7	2.8	···	
LHS 2567	12:29:54	−05:27:24	13.08	10.33	5.12	20.9	Rie10	11.48	−0.85	CTIO-0.9	2015.0516	4.5	5.1	2.6	2.0	···	
GJ 480	12:38:52	+11:41:46	11.51	8.98	4.82	14.0	vLe07	10.78	−0.81	ARCSAT	2016.0205	4.0	3.0	2.4	1.3	···	
GJ 480	12:38:52	+11:41:46	11.51	8.98	4.82	14.0	vLe07	10.78	−0.81	ARCSAT	2017.0408	4.5	11.6	12.8	0.9	···	
GJ 480	12:38:52	+11:41:46	11.51	8.98	4.82	14.0	vLe07	10.78	−0.81	CTIO-0.9	2017.0516	4.2	4.3	2.7	1.6	···	
GJ 490A	12:57:40	+35:13:30	10.68	8.81	4.13	19.8	vLe07	9.20	−0.68	ARCSAT	2015.0510	4.5	3.7	2.4	1.5	···	

[a]Notes in Column 18: Y = known young stars, (Y) = suspected young star, S = known subdwarf stars, (S) = suspected, but unconfirmed subdwarf stars.

Distance references: (Ang12) Anglada-Escudé et al. (2012); (Cos05) Costa et al. (2005); (Cos06) Costa et al. (2006); (Dav15) Davison et al. (2015); (Fab00) Fabricius & Makarov (2000); (Gat08) Gatewood (2008); (Gou04) Gould & Chanamé (2004); (Hen06) Henry et al. (2006); (Jao05) Jao et al. (2005); (Jao11) Jao et al. (2011); (Lur14) Lurie et al. (2014); (Rie10) Riedel et al. (2010); (Rie11) Riedel et al. (2011); (Rie14) Riedel et al. (2014); (Shk12) Shkolnik et al. (2012); (Sma10) Smart et al. (2010); (vLe07) van Leeuwen (2007); (Win15) Winters et al. (2015); (YPC95) van Altena et al. (1995).

Table 4.1: Properties of the Low Mass Stars in the Short-Term Variability Study.

Star Name	R.A.	Dec.	V	I	$V-K$	dist. (pc)	dist. ref.	M_V	ΔM_V	Telescope	Obs. Date	Dur. (hours)	Var. (mmag)	Base. (mmag)	σ km/s	V_{Rot}	Notes[a]
	2000.0																
(1)	(2)	(3)	(4)	(5)	(6)	(7)	(8)	(9)	(10)	(11)	(12)	(13)	(14)	(15)	(16)	(17)	(18)
GJ 490A	12:57:40	+35:13:30	10.68	8.81	4.13	19.8	vLe07	9.20	−0.68	ARCSAT	2016.0206	4.0	3.9	2.7	1.4	···	
GJ 1169	13:16:30	+27:52:44	13.26	10.64	4.82	15.8	YPC95	12.27	+0.68	ARCSAT	2016.0528	4.0	2.9	2.8	1.0	···	
GJ 507.1	13:19:40	+33:20:47	10.62	8.49	4.23	17.0	vLe07	9.47	−0.65	ARCSAT	2016.0421	4.6	6.5	3.4	1.9	···	
LHS 350	13:22:54	+24:28:00	12.96	10.21	5.00	13.6	YPC95	12.29	+0.26	ARCSAT	2017.0405	4.5	3.5	3.2	1.1	0.1	
LHS 2729	13:23:38	−25:54:45	12.89	10.14	5.11	13.9	Rie10	12.17	−0.13	CTIO-0.9	2015.0518	4.5	2.8	1.4	2.0	···	Y
GJ 534.2	13:53:47	+78:51:06	10.61	8.76	3.80	24.1	vLe07	8.70	−0.41	ARCSAT	2016.0527	4.0	3.5	1.7	2.1	···	
LHS 2852	14:02:47	−24:31:50	12.13	9.85	4.29	17.2	Win15	10.95	+0.69	CTIO-0.9	2016.0316	4.0	4.7	4.3	1.1	···	S
GJ 540	14:08:12	+80:35:50	10.35	8.33	4.02	16.8	vLe07	9.22	−0.39	ARCSAT	2017.0409	4.0	2.7	2.4	1.1	···	
LHS 2866	14:08:16	+75:51:14	11.59	9.51	4.03	24.9	YPC95	9.61	−0.03	ARCSAT	2016.0529	2.8	1.9	1.7	1.1	···	
GJ 548A	14:25:43	+23:37:01	9.76	7.91	3.79	16.1	vLe07	8.73	−0.36	ARCSAT	2015.0505	4.5	4.4	4.3	1.0	···	
GJ 548B	14:25:46	+23:37:13	10.01	8.07	3.92	16.1	vLe07	8.98	−0.41	ARCSAT	2015.0505	4.5	4.3	4.3	1.0	···	
GJ 1185	14:47:53	−03:09:15	13.33	10.99	4.27	19.7	YPC95	11.86	+1.64	ARCSAT	2016.0523	4.3	5.0	5.1	1.0	···	
GJ 563.2B	14:49:31	−26:06:42	12.07	9.92	4.18	22.3	vLe07	10.33	+0.33	CTIO-0.9	2015.0519	3.7	1.7	2.0	0.9	···	
GJ 563.2A	14:49:32	−26:06:20	11.68	9.62	4.04	22.3	vLe07	9.94	+0.28	CTIO-0.9	2015.0519	3.7	1.8	2.0	0.9	···	
LHS 3018	15:04:18	+60:23:04	10.99	8.88	4.10	17.8	vLe07	9.74	−0.06	ARCSAT	2017.0407	4.0	4.5	4.8	0.9	···	
LHS 3073	15:28:14	+16:43:11	13.92	12.47	3.52	58.8	YPC95	10.07	+1.56	ARCSAT	2017.0406	4.5	4.5	4.8	0.9	···	S
GJ 2116	15:43:18	−20:15:32	13.06	10.93	4.04	21.3	Jao05	11.42	+1.76	CTIO-0.9	2015.0515	4.5	4.0	1.8	2.2	···	S
LHS 3130B	15:53:06	+34:44:47	13.17	10.50	4.99	22.3	YPC95	11.43	−0.58	ARCSAT	2016.0419	4.5	4.5	3.6	1.3	···	
GJ 609	16:02:50	+20:35:21	12.58	9.70	5.21	10.0	YPC95	12.58	+0.03	ARCSAT	2017.0404	4.3	3.2	2.4	1.3	···	
GJ 615.2D	16:13:56	+33:46:24	12.33	—–	3.99	22.7	vLe07	10.55	+1.01	ARCSAT	2016.0525	4.0	3.6	2.5	1.4	···	
GJ 625	16:25:24	+54:18:14	10.11	7.89	4.27	6.5	vLe07	11.05	+0.83	ARCSAT	2016.0421	4.5	2.2	2.1	1.0	···	
GJ 2121	16:30:13	−14:39:49	12.35	9.84	4.75	22.4	vLe07	10.60	−0.81	CTIO-0.9	2015.0516	4.5	3.0	1.2	2.5	···	
GJ 643	16:55:25	−08:19:21	11.77	9.01	5.05	6.5	vLe07	12.71	+0.55	CTIO-0.9	2015.0517	4.5	3.9	1.2	3.3	···	
GJ 1207	16:57:05	−04:20:56	12.25	9.43	5.13	8.7	Hen06	12.55	+0.20	ARCSAT	2015.0509	3.5	2.9	1.8	1.6	···	
GJ 1219	17:27:39	+14:29:02	13.73	11.11	4.77	19.9	YPC95	12.24	+0.77	ARCSAT	2016.0523	4.0	5.5	5.8	0.9	0.1	
GJ 676A	17:30:11	−51:38:13	9.59	7.76	3.77	16.3	vLe07	8.53	−0.52	CTIO-0.9	2015.0514	4.0	4.1	3.2	1.3	···	Y
GJ 676B	17:30:11	−51:38:13	13.31	10.50	5.29	16.3	vLe07	12.25	−0.48	CTIO-0.9	2015.0514	4.0	5.0	3.2	1.6	···	Y
L 1422-015(B)	17:39:32	+27:46:37	12.72	10.32	4.75	24.9	vLe07	10.74	−0.67	ARCSAT	2015.0510	4.0	2.0	2.0	1.0	···	Y
G 141-029	18:42:45	+13:54:17	12.84	9.96	5.29	11.1	Rie14	12.61	−0.12	ARCSAT	2016.0525	4.0	6.8	2.6	2.6	1.6	Y
GJ 729	18:49:49	−23:50:10	10.50	7.68	5.13	3.0	vLe07	13.11	+0.76	CTIO-0.9	2015.0518	4.7	4.1	2.6	1.6	···	
GJ 745A	19:07:05	+20:53:17	10.78	8.54	4.26	8.7	vLe07	11.08	+0.89	ARCSAT	2016.0527	4.0	2.0	1.6	1.3	···	
GJ 745B	19:07:13	+20:52:37	10.76	8.53	4.24	8.7	vLe07	11.06	+0.92	ARCSAT	2016.0527	4.0	3.0	1.6	1.9	80.7	
LHS 3445	19:14:39	+19:19:04	11.59	9.05	4.78	18.6	Sma10	10.24	−1.25	ARCSAT	2016.0528	4.0	8.1	3.6	2.3	82.9	Y
GJ 1236	19:22:02	+07:02:31	12.39	9.86	4.70	10.7	YPC95	12.24	+0.96	CTIO-0.9	2015.0903	4.5	1.7	1.5	1.1	11.7	
LHS 3499	19:55:52	+51:16:22	11.86	9.79	4.01	24.7	vLe07	9.90	+0.31	ARCSAT	2014.0724	5.0	9.5	3.4	2.8	···	
GJ 1248	20:03:51	+05:59:44	12.11	9.84	4.24	12.5	YPC95	11.63	+1.49	ARCSAT	2014.0723	5.0	4.2	3.2	1.3	40.5	(S)
GJ 774A	20:04:02	−65:36:48	11.35	9.06	4.29	13.1	Fab00	10.76	+0.50	CTIO-0.9	2015.0904	4.8	4.8	1.7	2.8	···	
GJ 774B	20:04:02	−65:36:48	12.83	10.24	4.70	13.1	Fab00	12.24	+0.96	CTIO-0.9	2015.0904	4.5	4.7	1.7	2.8	···	
GJ 781.1A	20:07:44	−31:45:14	12.22	9.73	4.82	15.5	vLe07	11.27	−0.32	CTIO-0.9	2015.0519	4.0	1.3	1.7	0.8	···	

[a]Notes in Column 18: Y = known young stars, (Y) = suspected young star, S = known subdwarf stars, (S) = suspected, but unconfirmed subdwarf stars.

Distance references: (Ang12) Anglada-Escudé et al. (2012); (Cos05) Costa et al. (2005); (Cos06) Costa et al. (2006); (Dav15) Davison et al. (2015); (Fab00) Fabricius & Makarov (2000); (Gat08) Gatewood (2008); (Gou04) Gould & Chanamé (2004); (Hen06) Henry et al. (2006); (Jao05) Jao et al. (2005); (Jao11) Jao et al. (2011); (Lur14) Lurie et al. (2014); (Rie10) Riedel et al. (2010); (Rie11) Riedel et al. (2011); (Rie14) Riedel et al. (2014); (Shk12) Shkolnik et al. (2012); (Sma10) Smart et al. (2010); (vLe07) van Leeuwen (2007); (Win15) Winters et al. (2015); (YPC95) van Altena et al. (1995).

Table 4.1: Properties of the Low Mass Stars in the Short-Term Variability Study.

Star Name	R.A.	Dec.	V	I	$V-K$	dist.	dist.	M_V	ΔM_V	Telescope	Obs.	Dur.	Var.	Base.	σ	V_{Rot}	Notes[a]
	2000.0					(pc)	ref.				Date	(hours)	(mmag)		km/s		
(1)	(2)	(3)	(4)	(5)	(6)	(7)	(8)	(9)	(10)	(11)	(12)	(13)	(14)	(15)	(16)	(17)	(18)
GJ 781.1B	20:07:48	−31:45:28	12.51	9.70	4.92	15.5	vLe07	11.56	−0.28	CTIO-0.9	2015.0519	4.0	3.3	1.6	2.1	···	
GJ 784.2A	20:13:58	+06:41:25	13.33	10.55	5.16	22.3	YPC95	11.59	−0.84	CTIO-0.9	2015.0901	4.5	1.8	1.4	1.3	···	
GJ 803A	20:45:09	−31:20:27	8.65	6.61	4.12	9.9	vLe07	8.67	−1.18	CTIO-0.9	2015.0902	4.5	3.3	3.0	1.1	···	Y
GJ 812A	20:56:48	−04:50:49	11.94	9.27	4.88	16.7	YV	10.83	−0.91	CTIO.0.9	2015.0910	4.5	2.4	3.1	0.8	···	
LTT 16412	21:57:26	+08:08:13	11.03	8.91	4.18	21.1	vLe07	9.41	−0.59	ARCSAT	2014.0729	4.5	4.0	2.7	1.5	···	
LHS 3739A	21:58:50	−32:28:17	14.72	11.88	5.16	19.6	Rie10	13.26	+0.83	CTIO-0.9	2016.1026	4.3	12.1	6.6	1.8	···	
SCR 2204-3347	22:04:02	−33:47:39	15.44	13.41	3.84	58.6	Cos05	11.60	+2.40	CTIO-0.9	2016.1028	4.0	7.4	4.7	1.6	···	S
LHS 3799	22:23:07	−17:37:01	13.30	10.04	5.98	7.4	YPC95	13.95	−0.24	CTIO-0.9	2016.1027	4.0	5.1	6.1	0.8	···	Y
GJ 871.1A	22:44:57	−33:15:01	12.11	9.32	5.18	23.3	vLe07	10.27	−2.20	CTIO-0.9	2014.1025	4.5	4.9	2.2	2.2	···	Y
GJ 871.1B	22:45:00	−33:15:26	13.36	10.33	5.57	23.3	vLe07	11.52	−1.84	CTIO-0.9	2014.1025	4.5	10.9	2.2	5.0	···	Y
LHS 543	23:21:37	+17:17:25	11.65	8.89	5.14	10.8	vLe07	11.48	−0.89	CTIO-0.9	2016.1024	4.0	3.7	3.3	1.1	···	
G 190-027	23:29:25	+41:27:48	12.42	9.56	5.25	14.7	YPC95	11.58	−1.06	ARCSAT	2015.1120	5.0	4.8	2.1	2.3	···	Y
G 190-028	23:29:26	+41:28:20	11.89	9.31	4.82	14.7	YPC95	11.05	−0.54	ARCSAT	2015.1120	5.0	6.6	2.1	3.1	···	Y
GJ 1284	23:30:13	−20:23:27	11.12	8.60	4.79	16.1	Rie14	10.09	−1.43	CTIO-0.9	2015.0907	4.5	5.7	3.8	1.5	···	(Y)
GJ 1290	23:44:23	+21:36:14	13.29	10.66	5.07	22.0	YPC95	11.58	−0.63	ARCSAT	2015.1122	5.0	6.6	6.2	1.1	···	

[a]Notes in Column 18: Y = known young stars, (Y) = suspected young star, S = known subdwarf stars, (S) = suspected, but unconfirmed subdwarf stars.

Distance references: (Ang12) Anglada-Escudé et al. (2012); (Cos05) Costa et al. (2005); (Cos06) Costa et al. (2006); (Dav15) Davison et al. (2015); (Fab00) Fabricius & Makarov (2000); (Gat08) Gatewood (2008); (Gou04) Gould & Chanamé (2004); (Hen06) Henry et al. (2006); (Jao05) Jao et al. (2005); (Jao11) Jao et al. (2011); (Lur14) Lurie et al. (2014); (Rie10) Riedel et al. (2010); (Rie11) Riedel et al. (2011); (Rie14) Riedel et al. (2014); (Shk12) Shkolnik et al. (2012); (Sma10) Smart et al. (2010); (vLe07) van Leeuwen (2007); (Win15) Winters et al. (2015); (YPC95) van Altena et al. (1995).

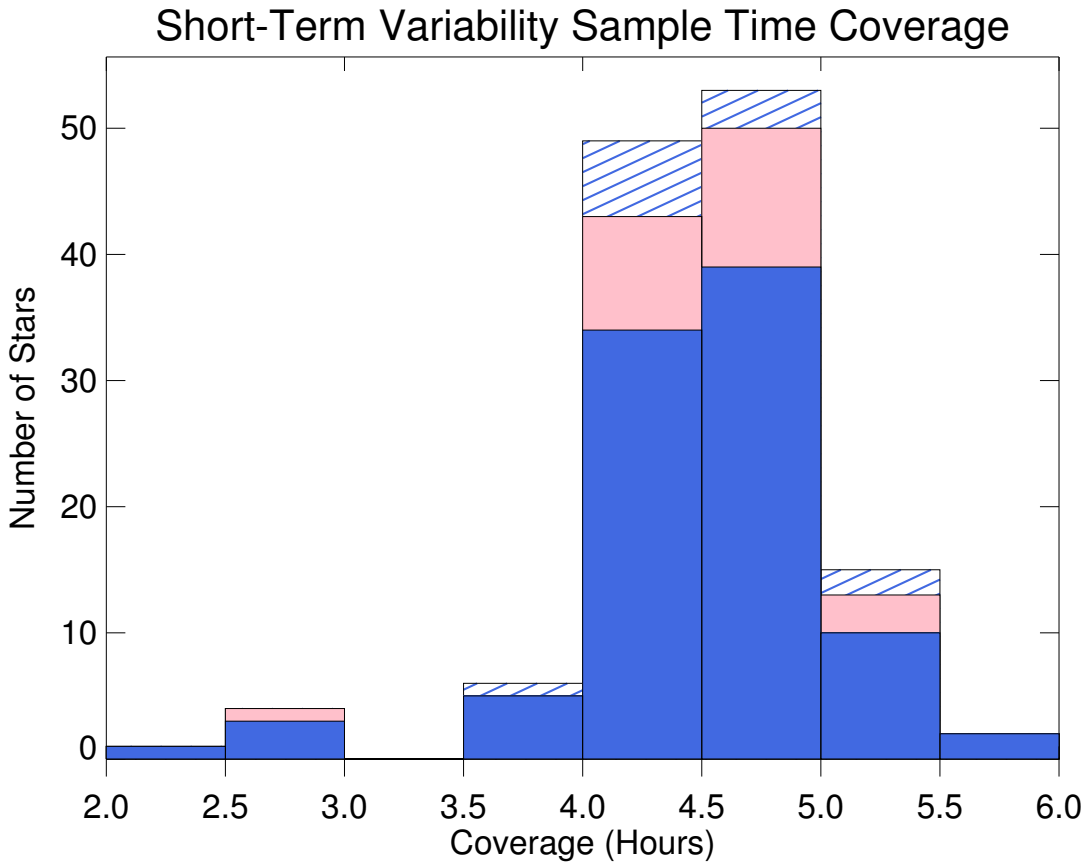

Figure 4.1: Histogram illustrating the coverage, from 2−6 hours, of the 120 stars included in this study. Solid blue represents main sequence or stars not confirmed to be young or subdwarfs. Pink represents known young stars. Blue and white lined represents subdwarfs. The bin sizes are 0.5 hours, starting at 2 hours and ending at 6 hours.

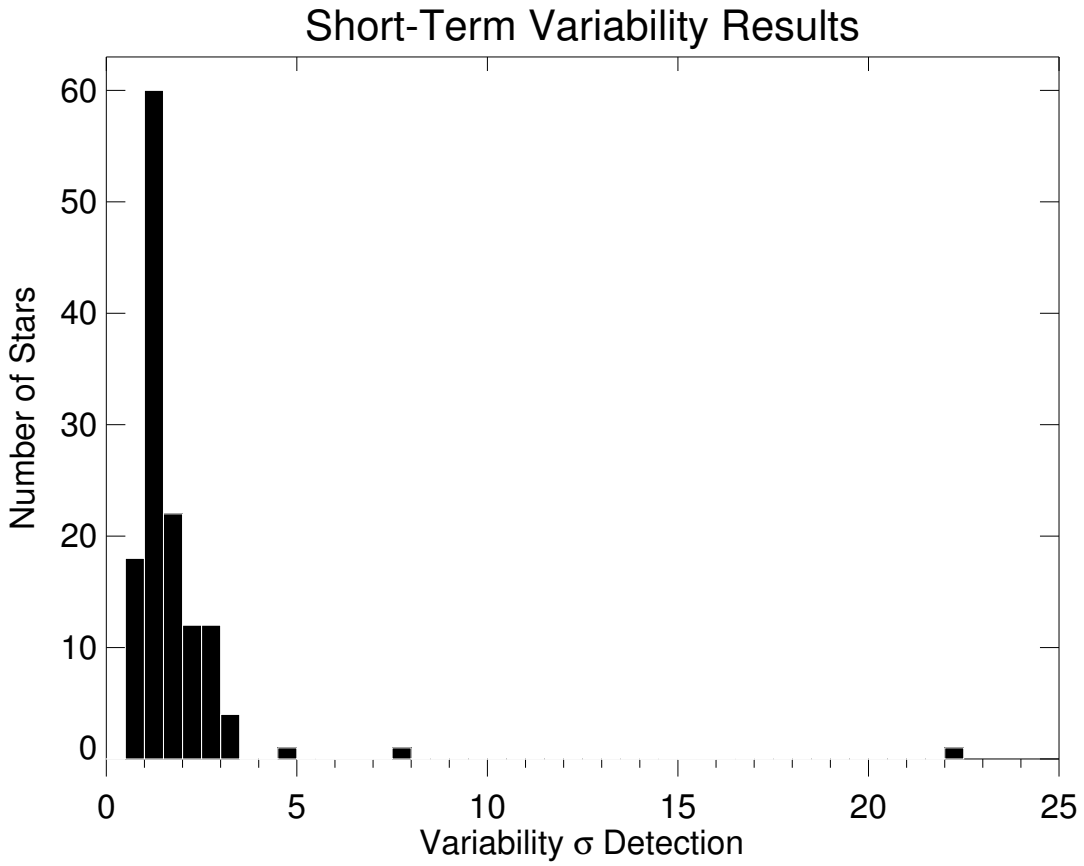

Figure 4.2: Histogram showing our range of short-term variability σ values. The bins are 0.5σ in width, from $0 - 0.5\sigma$ to $24.5 - 25\sigma$. Most stars vary by less than our adopted threshold for a clearly variable star of 3σ.

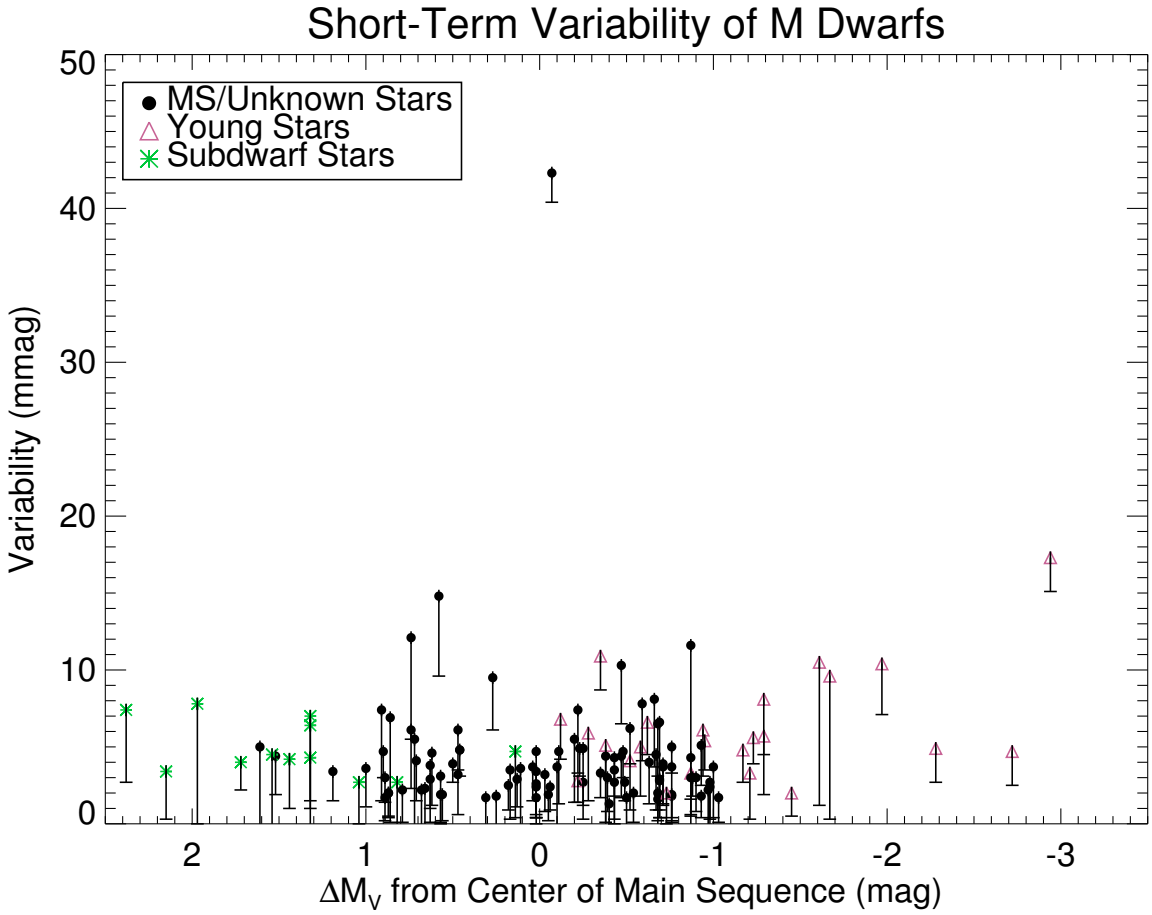

Figure 4.3: Scatter plot of the stellar variability, in the V filter, versus the ΔM_V for each target star. The variability (in mmag) is the value calculated using the methods described in §4.4 and the baseline error bars are derived from the variability of the chosen reference star for each set of observations. Main sequence (or not yet identified to be young or subdwarfs) stars are indicated by circles (black), known young stars by triangles (pink), and subdwarf stars by asterisks (green).

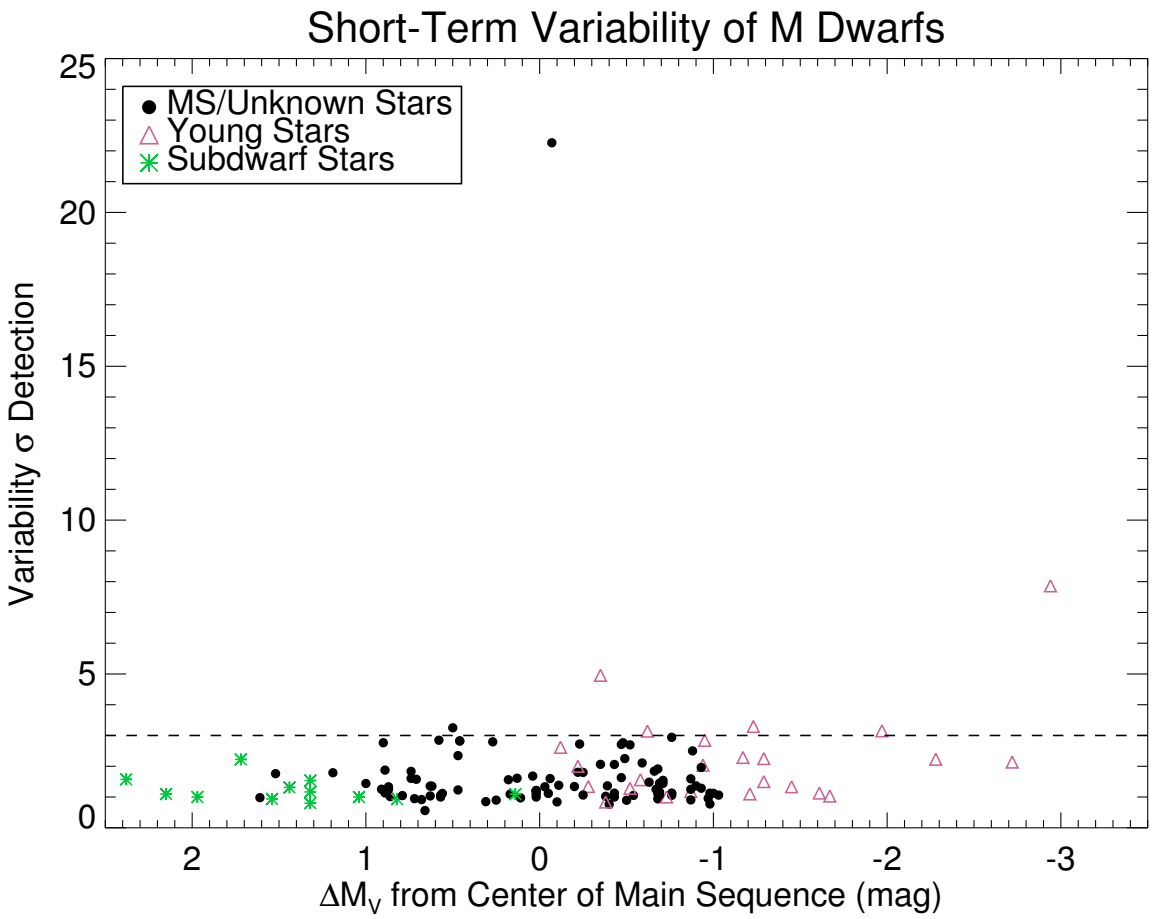

Figure 4.4: Scatter plot of the σ detection of stellar variability, in the V filter, versus the ΔM_V for each target star. The variability σ value is calculated by dividing the variability measurement for each star by that of its reference star. Main sequence (or not yet identified to be young or subdwarfs) stars are indicated by circles (black), known young stars by triangles (pink), and subdwarf stars by asterisks (green). This figure clearly shows that a majority of stars vary by less than our adopted threshold for a variable star of 3σ, indicated by the dashed line.

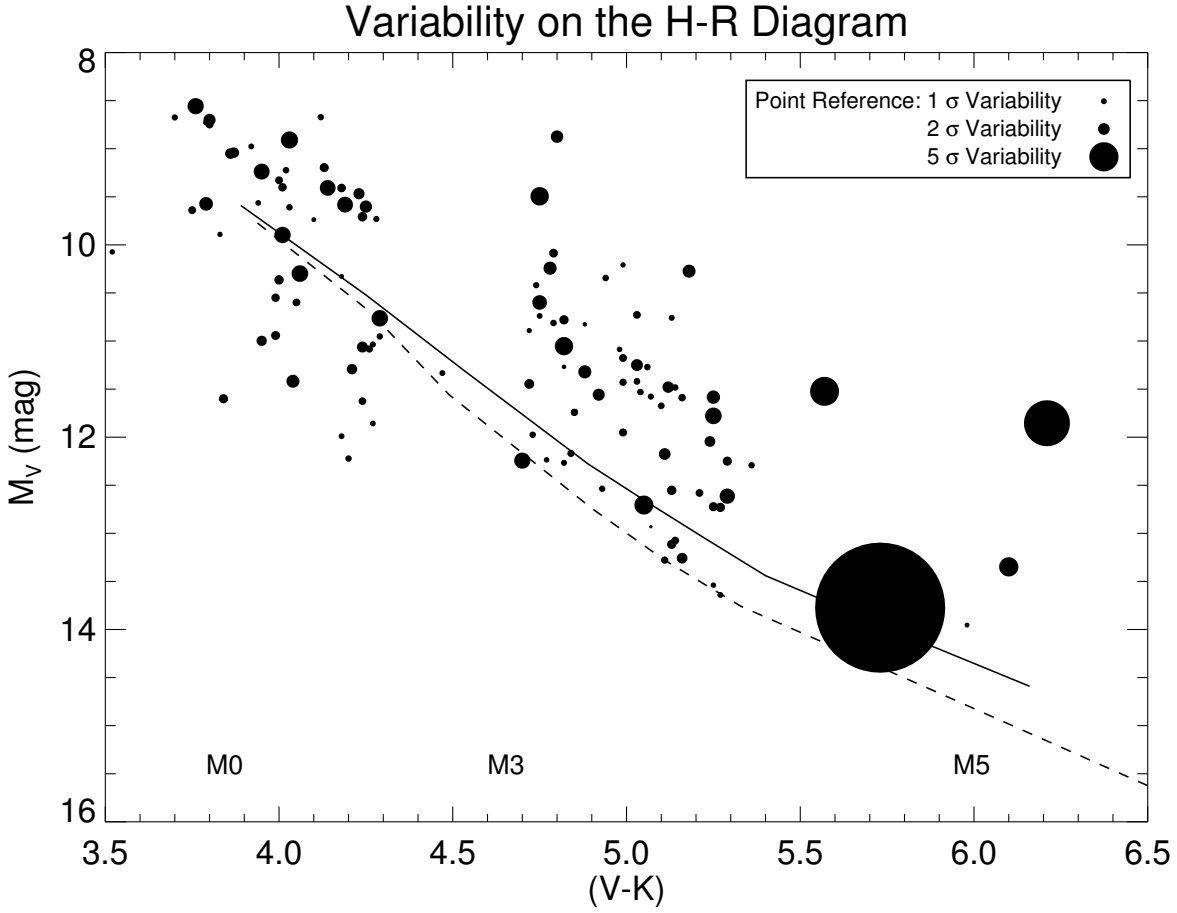

Figure 4.5: The stars are plotted on an H-R diagram where point sizes are scaled to indicate each star's variability in V using the sigma values illustrated in Figure 4.4. Reference points for variability of 1, 2, and 5 mmag are given in the legend. We also plot the model tracks from Baraffe et al. (2015) for M stars at 100 Myrs (solid) and 1 Gyr (dashed). The largest point at $M_V = 13.77$ and $(V - K) = 5.73$, is SCR 1214-2345, for which we measure a variability σ value of 22.3. This star is one of a very few that flared during observations.

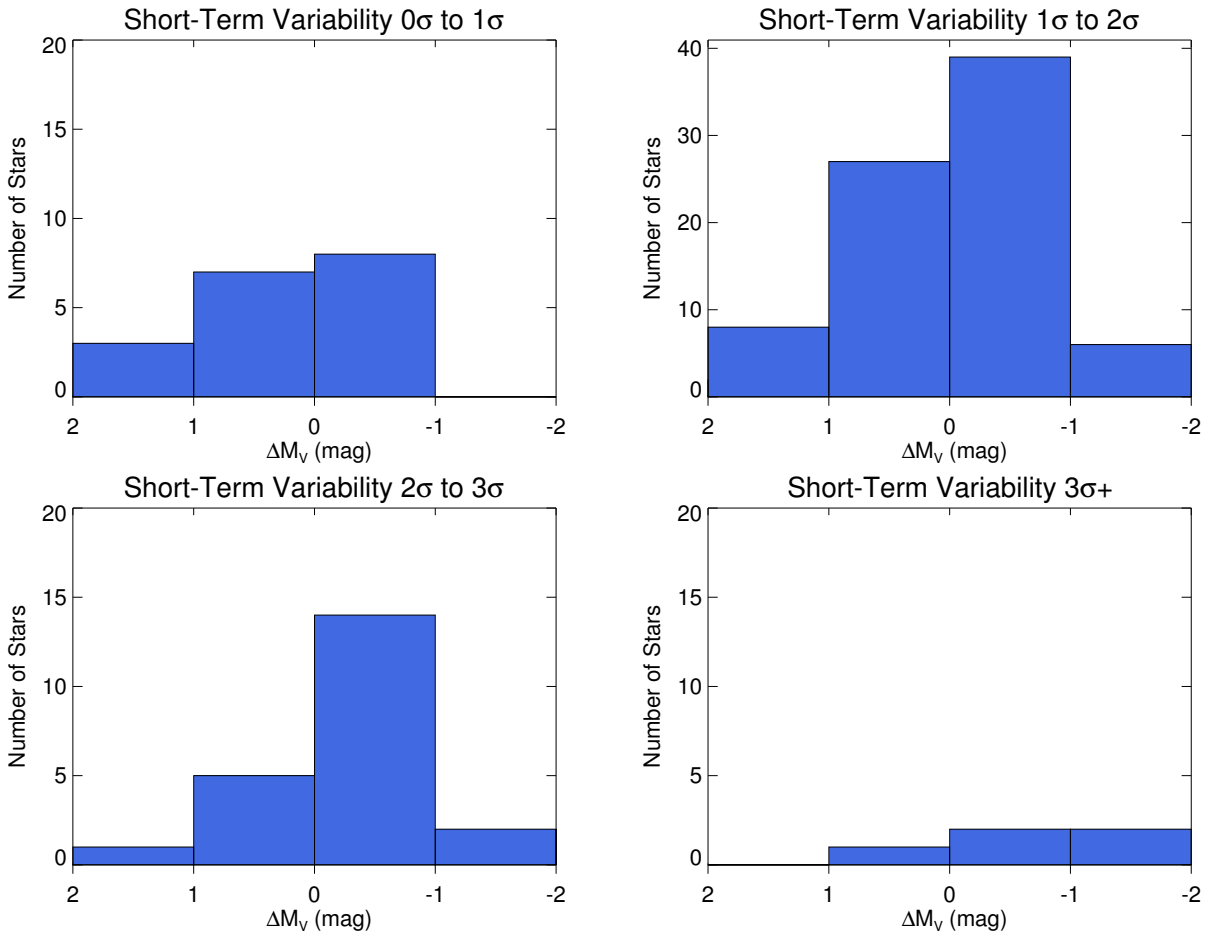

Figure 4.6: These histograms show the distribution of different variability σ value detections across the range of ΔM_V values in this study. The upper left shows the results for variability below 1σ, the upper right has twice the scale of the other three and shows the majority of our results from 1σ to 2σ. The lower left shows the distribution for stars with variability measurements from 2σ to 3σ, and the lower right panel shows our variable stars above 3σ. We note that the three outliers above 5σ are excluded from these results.

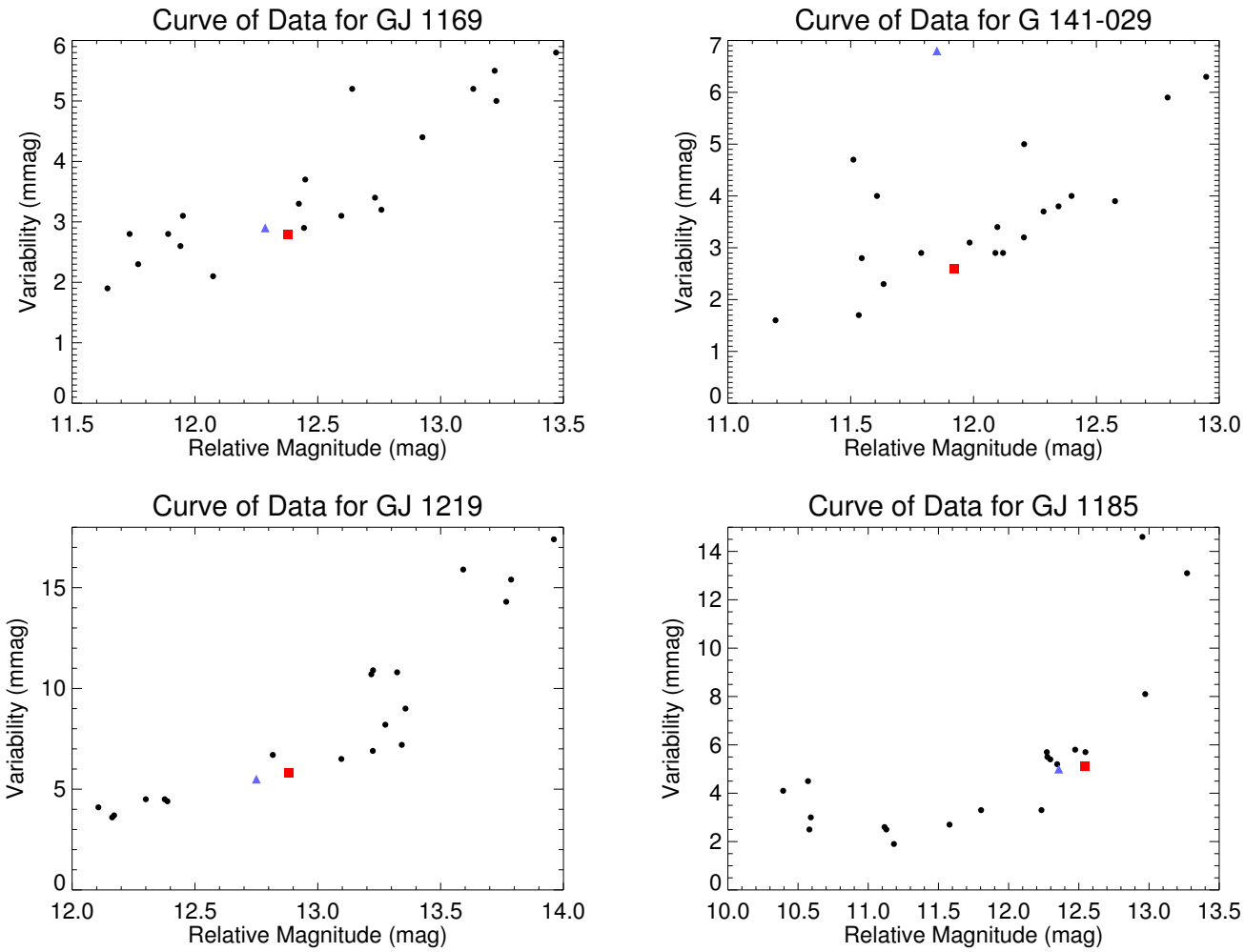

Figure 4.7: This figure shows the data curves for four stars with rich enough fields to use 20 reference stars in the variability calculations. In each panel the blue triangle indicates the target star, the red square the chosen reference star used to determine the baseline, and the remaining reference stars are indicated by the black circles.

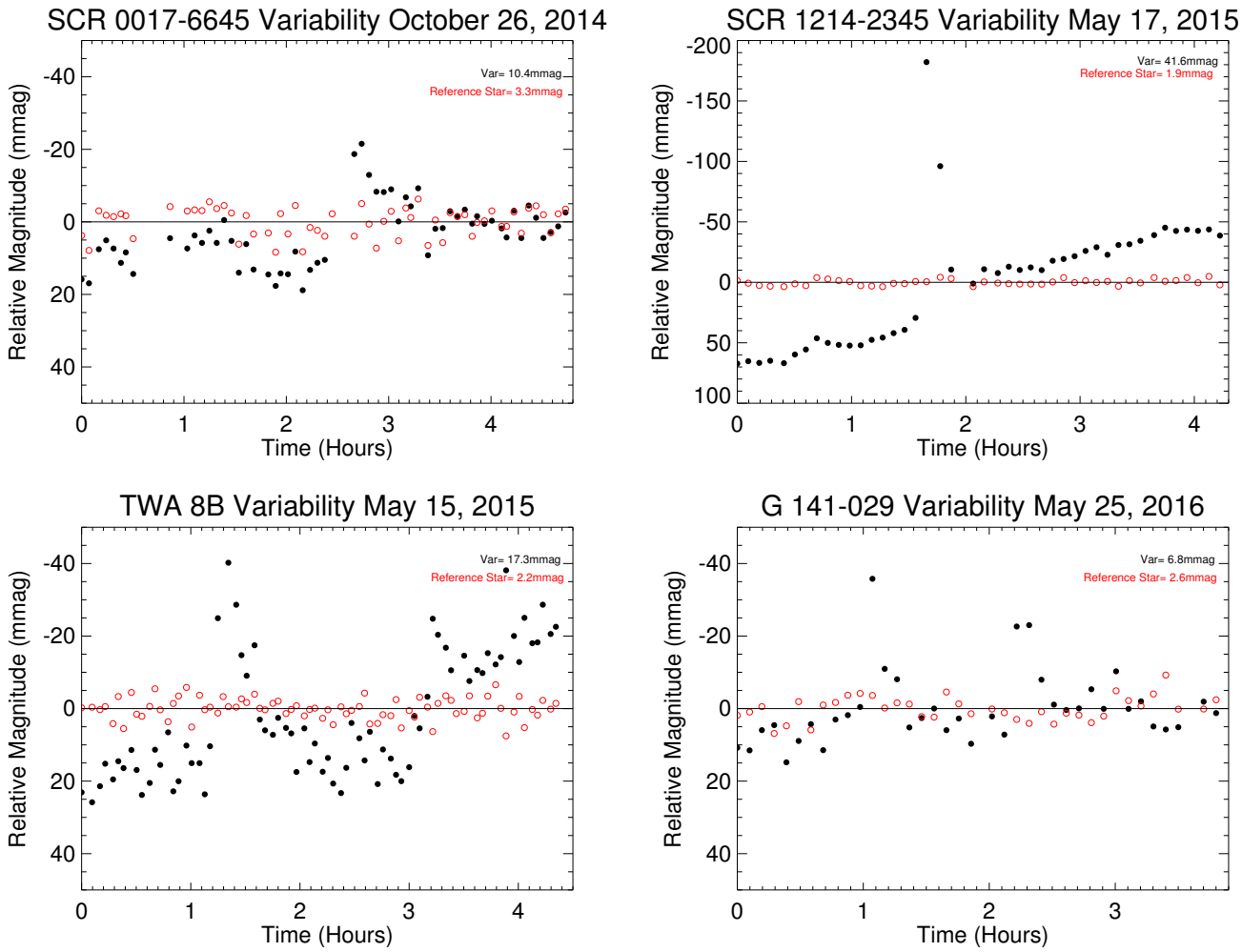

Figure 4.8: This figure shows the lightcurves for four stars that experienced flare events during their observations. The black circles indicate the lightcurve data points for the target star, while the red circles are those for the chosen reference star.

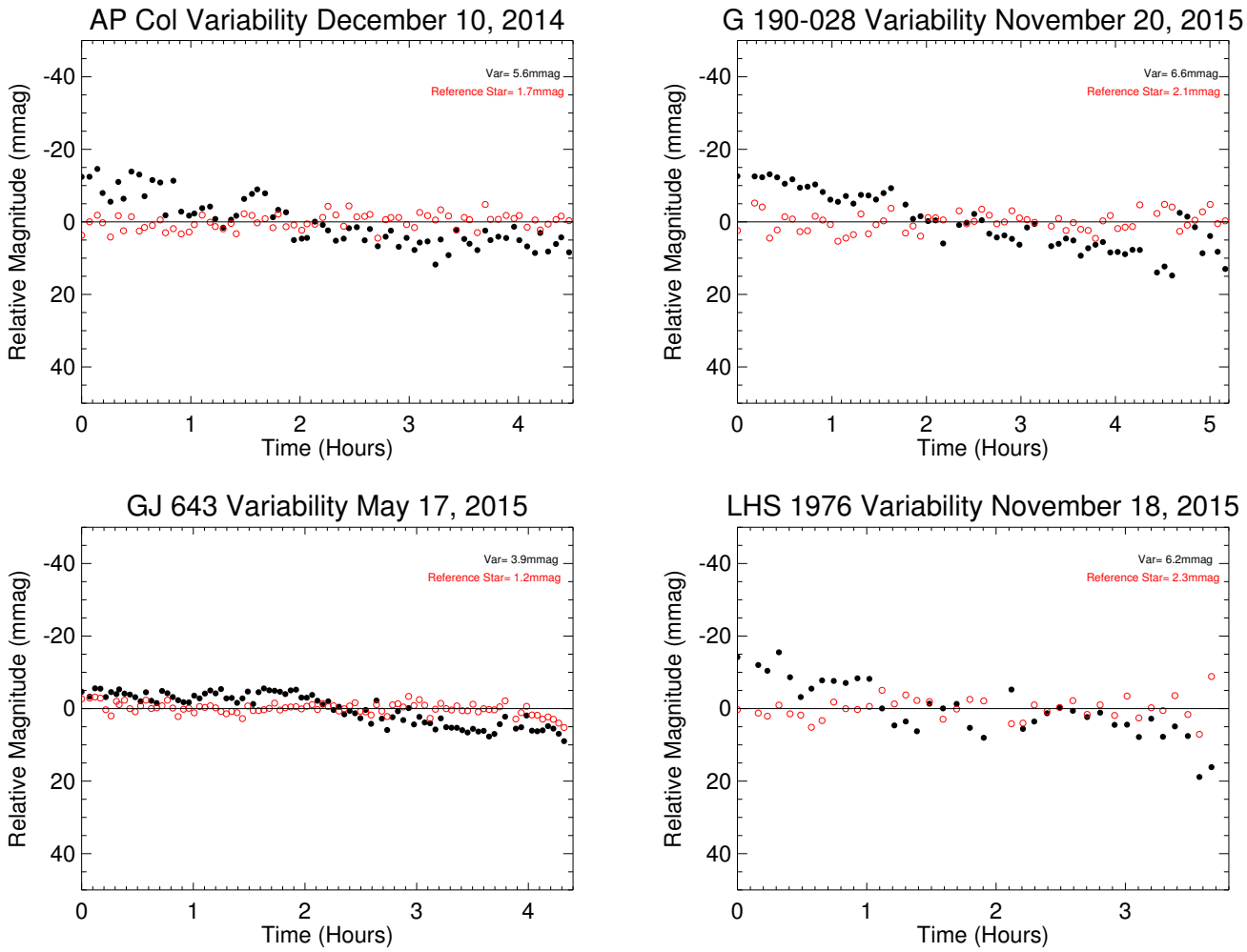

Figure 4.9: This figure shows the lightcurves for four stars that demonstrated a slight, but steady decrease in brightness throughout the observations. The black circles indicate the lightcurve data points for the target star, while the red circles are those for the chosen reference star.

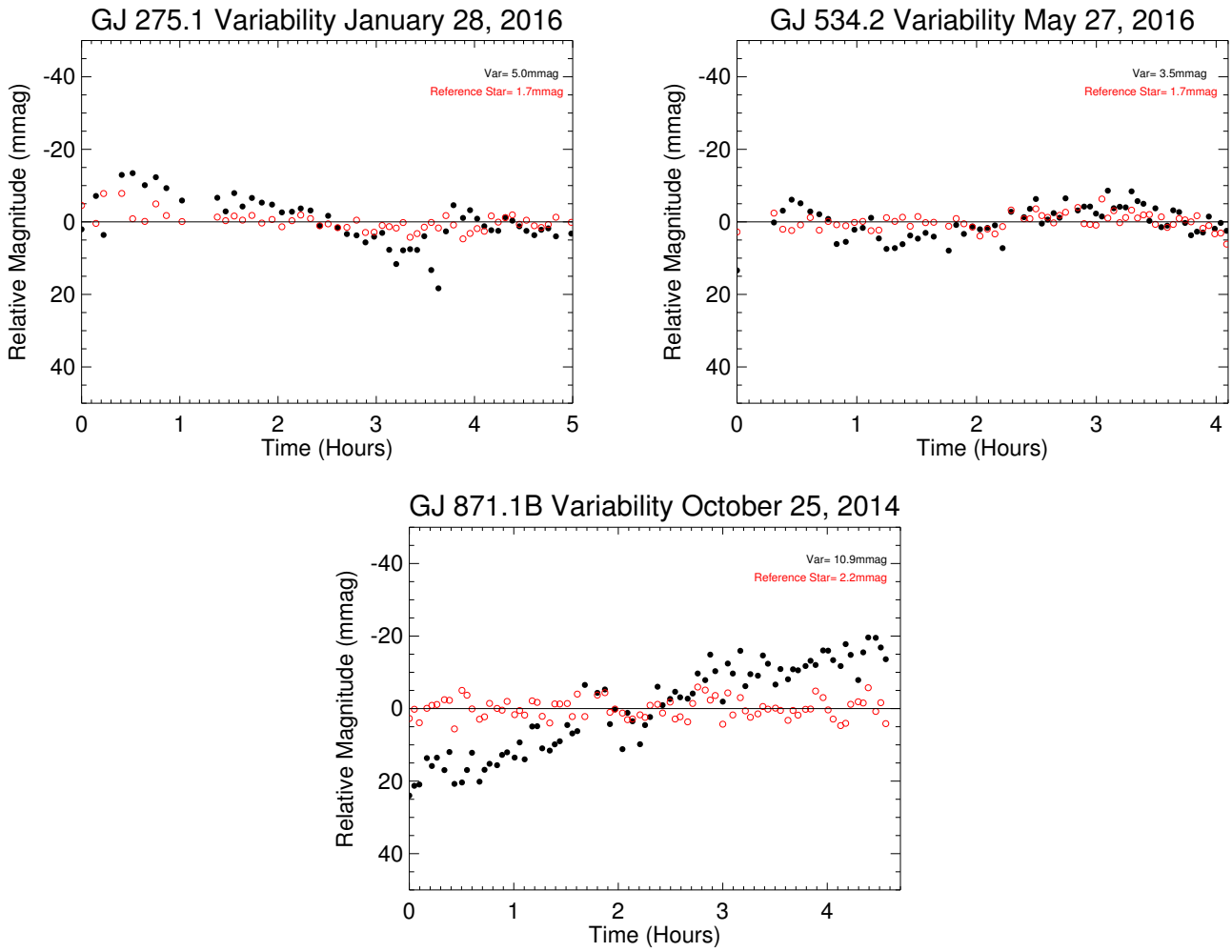

Figure 4.10: This figure shows the lightcurves for three stars, GJ 275.1, GJ 534.2, and GJ 871.1B, that showed other interesting trends discussed in §4.4.2. The black circles indicate the lightcurve data points for the target star, while the red circles are those for the chosen reference star.

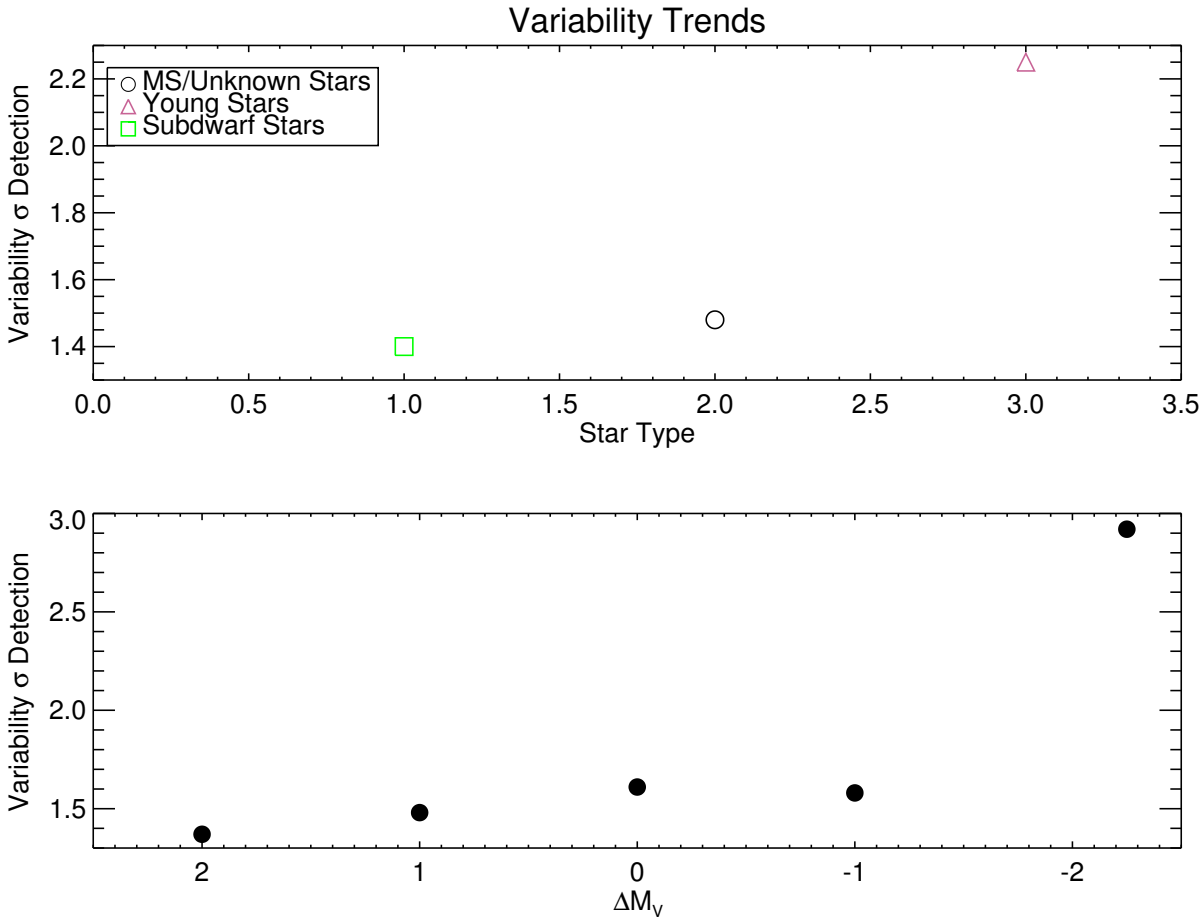

Figure 4.11: The observed variability trend for each group of stars. The top panel shows the trend broken down by type of star, where the black circle represents main sequence (or not yet identified to be young or subdwarfs), the green square represents the known subdwarfs, and the pink triangle indicates the known young stars. The bottom panel illustrates the increasing trend by ΔM_V position for the stars, as described in §4.4.

CHAPTER 5
SPECTROSCOPY STUDY

5.1 Overview of the Spectroscopy Study

The goal of the spectroscopy component of this study was to gather high resolution spectra, in a broad wavelength range, for at least 100 of our target stars in order to accurately assess their (1) ages via the presence of strong Hα emission and/or lithium absorption at 6708Å, (2) radial velocities via wavelength offsets, (3) metallicities via line ratio measurements, and (4) trends in any other spectral features (e.g. Ca, Fe, K, Na, CaH, and MgH) that may relate to the position of the target star above or below the main sequence. These spectra were obtained with the 1.5 m SMARTS telescope at CTIO using the echelle spectrograph CHIRON for southern targets and the 3.5 m telescope at APO using the echelle spectrograph ARCES for northern targets. Most of these goals are accomplished by measuring the equivalent widths (EWs) of the various notable spectral features for each target star and performing different analyses from there to obtain the desired information about the presence of emission as indicators of activity, line ratios, and metallicity values.

5.2 Stars In Study

For this study we have observed a total of 104 stars in our target boxes, focusing on stars far above or below the main sequence when possible. Of these stars, the 80 observed using the ARCES instrument at APO are presented here while the remaining 25 observed using CHIRON at CTIO will be presented in future work (one of the 104 stars was observed on

each telescope for a total of 105 observations). These 104 observed stars include three known subdwarfs and two potential subdwarfs, all more than one full V magnitude below the main sequence. In addition, eight known young stars and two possibly young stars that are one V magnitude or more above the main sequence were observed. There are also 23 stars residing above the central main sequence distribution by $\Delta M_V \leq -0.5$, not classified as young and 27 stars below by $\Delta M_V \geq +0.5$ not classified as subdwarfs. The remaining 40 stars lie within 0.5 magnitudes of the central M_V distribution, and are thus considered "on" the main sequence and have no confirmed or potential status as a young star or subdwarf. The targets range in magnitude from 7.34 to 15.87 in V with spectral types ranging from K7V to M4.5V. This spectroscopic study has concentrated on bright stars to increase SNR in the spectra. In Box 4 there are 68 stars, including four confirmed young stars, three of the confirmed subdwarfs, and both of the suspected subdwarfs. There are 35 stars in Box 5 with four stars classified as young and both of the two suspected young stars. The last box, Box 6, has only one star in this study because the faint nature of the stars within Box 6 made it difficult to observe many of them. The stars observed for this study and their properties are detailed in Table 5.1 where we provide their names (column 1), 2000.0 coordinates (2 and 3), photometric parameters (4, 5, and 6), distances and references (7 and 8), absolute magnitudes (9), ΔM_V values (10), spectral types and references (11 and 12), observation details (13 and 14), and notes indicating whether a star is young (Y), suspected to be young ((Y)), a subdwarf (S), or suspected subdwarf ((S)) in the last column (15). All of the stars observed for this study, including the 25 obtained at CTIO for which results are not presented in this dissertation,

are detailed in Table 5.1.

5.3 Observations and Reductions

The observations for this study were carried out on two different telescopes and instruments with similar properties. Northern targets were observed using the echelle spectrograph (ARCES) on the APO 3.5 m telescope. ARCES has a wavelength range of about $3500 - 10100$Å on a 2048×2048 SITe CCD with a resolution of about 31,500. Each spectrum consists of 107 orders distributed across the chip. The default slit of $1.6'' \times 3.2''$ was used and – with the exception of three nights on-site for training – observations were carried out remotely using the Telescope User Interface (TUI) to control the telescope and software. The 25 southern targets in this study were obtained using the echelle spectrograph (CHIRON) on the 1.5 m telescope at CTIO. These data are provided in a different format that did not allow us to analyze the results using the same methods as for the ARCES data and so they will be presented in future work. The properties for CHIRON are similar to those of ARCES, with a wavelength range of $4100 - 8700$Å and a resolution of about 25,000 in fiber mode. The instrument utilizes a 4096×4096 CCD detector with the spectrum divided across 59 orders. These southern targets were obtained in queue mode by the telescope operator at CTIO.

For the data gathered at APO, standard flat and bias calibrations were taken for each night of observations and ThAr lamp exposures were obtained periodically throughout the night, primarily before any major slew, for proper wavelength calibrations. The brighter

targets in this study ($V < 11$) were observed once with exposure times long enough to obtain a signal-to-noise ratio (SNR) of at least 50, while fainter targets were observed two to three times for an SNR of 15 to 30 and the images were coadded in order to reduce the noise for a SNR closer to 50. We also obtained multiple spectra of A0V class stars at various airmasses to map telluric lines contributed by the atmosphere of the Earth that could then be removed from the spectra. However, it was ultimately decided that such a telluric template would not be necessary, as many of the atmospheric features were generally not intruding on any of the spectral features we were interested in measuring and the large oxygen band at $\sim$7500Å overlying the TiO band (often used for measuring abundances) was too strong to be properly removed from the spectra.

The spectra obtained with ARCES at APO were reduced following the reduction guide created and provided by Karen Kinemuchi at the NMSU Astronomy Department using the following standard *IRAF* packages: *noao*, *imred*, *ccdred*, *echelle*, *crutil*, *astutil*, *images*, *imgeom*, *twodspec*, *apextract*, and *onedspec*. These reductions included bias subtraction, flat fielding, cosmic ray removal, tracing the apertures, correcting scattered light between apertures, wavelength calibration, continuum fitting, and finally combining the orders. Targets with two or more spectra, to reduce noise, were then coadded using *scombine*. The data obtained by the observers at CTIO using queue time with CHIRON were reduced prior to being provided to us, using a different procedure with *IDL*. These spectra were then flattened by fitting the continuum for each frame using a *python* pipeline provided by RECONS member Leonardo Paredes. Unfortunately, due to the format of the pre-reduced data,

they are incompatible with *IRAF* and we were unable to complete further processing and analysis in the same manner as was carried out for the ARCES data, detailed in §5.4. We plan to include these data in further work for this study, but are unable to present results for these 25 spectra in this dissertation.

5.4 Analysis and Results

Upon the completion of basic reductions, a total of 24 lines and features in the 80 spectra obtained using ARCES were measured using two methods. Smaller absorption features, such as the Fe I and K lines, as well as the molecular features due to MgH and CaH, were measured interactively using the *IDL* program Tool for the Automatic Measurement of Equivalent width (TAME), which is used for the measurement of EWs in high resolution spectra (Kang & Lee 2012). Broader lines and emission lines, such the Ca II H and K lines, Hα, the Na I doublet, and Ca I lines, could not be properly measured using TAME and were thus carefully measured using the *IRAF splot* task. Both of these methods interactively use a Gaussian fit to measure the EWs (in Å) of the features with respect to the normalized continuum. We list the measured EWs for the measured spectral features discussed here in Table 5.2. Only 13 of these 24 measured lines are listed in the Table because the remaining were either contaminated by water lines (as in the case of the Fe I line at 8387Å) or they produced only a random scatter when plotted against the ΔM_V values. Each feature was not always present (or at least detectable amongst the noise) in each spectrum, these instances are left empty in the Table. These 13 features are discussed in detail in §5.4.1, in addition

to Li at 6708Å as it is an important feature but this feature was not present in any of our spectra.

5.4.1 Trends in Spectral Features

- *Hα*: The presence of the Hα Balmer line ($\lambda = 6563$Å) emission feature, shown in Figure 5.1 for the known young star LP 776-025, is an indicator of heightened activity within the chromosphere of a star. As the stellar matter in the chromosphere increases, the absorption of the Hα feature deepens until reaching a massive enough chromosphere that emission wings form, before becoming a strong emission line (Cram & Mullan 1979; Stauffer & Hartmann 1986). The presence of strong, extremely broad Hα emission is often indicative of accretion due to the presence of a circumstellar disk, indicating a star is younger than 10 Myr (Barrado y Navascués & Martín 2003). Stassun et al. (2012) found that for active M dwarfs there is a correlation between the strength of the measured Hα emission and how much the temperature is suppressed and the radius is inflated for these stars. While this effect maintains a star's bolometric luminosity, this correlation (if confirmed) would serve to allow for accurate corrections to stellar masses, temperatures, and radii for active low mass stars using the relatively easily measured Hα feature. We carefully measured this feature for each of our 80 ARCES spectra using the *IRAF splot* task. Our results, illustrated in Figure 5.2, show that many stars above the main sequence ($\Delta M_V < 0$) exhibit Hα emission that is particularly strong for many of the known young stars, while most of the other stars measured show weak absorption. We also observe that the known subdwarf, **LHS 482** at (+1.59, −1.81),

presents Hα in emission as well. Upon further investigation it is found that this known subdwarf is also known to be an active flare star, making this star uniquely interesting and worthy of much closer analysis, as subdwarfs are generally inactive (Gizis 1998).

- *Li*: The lithium feature at 6708Å is often used as an indicator of youth in low mass stars; its presence determines that an early-type M star is younger than 10 Myr, an M3.5 type star is younger than 40 Myr, and a late-type M (around M6) star is younger than 90 Myr, as this is generally the amount of time it takes low mass stars to burn their primordial lithium (Chabrier et al. 1996; Stauffer et al. 1998). We were unable to detect the presence of lithium absorption among the noise at or near wavelength 6708Å in any of the 80 measured spectra – including our known young stars – and are thus unable to comment on the ages of our stars regarding the presence of lithium absorption at this time. We may need a better SNR, resolution, or the use of larger aperture telescopes to acquire any such results from this important feature, if it is present at all.

- *Na lines*: Andretta et al. (1997) determined that the sodium doublet lines Na D_1/D_2 (also known as the Fraunhofer D lines) at 5890/5896Å, shown in Figure 5.3 for the known young star LP 776-025, are formed within the chromosphere and are dependent on the conditions in the middle-to-lower chromosphere for low mass stars. The emission cores in these features, when present, are dependent on both the density and the thickness of active chromospheres, while the depth of the absorption component of the feature between an emission core and the wings of the surrounding absorption appears

to be temperature dependent. So, we would expect to observe a trend in these features due to both the increasing thickness of the chromosphere and the heightened activity levels of stars above the central main sequence distribution. We measured EWs for both lines separately and show the results in Figure 5.4. We observe a trend where the Na D_1/D_2 lines are decreasing in measured EW – generally due to the presence of emission cores – as the stars move above the central distribution of the main sequence, but this trend is not very tightly constrained, likely due to a spread resulting from temperature effects. Because the ΔM_V values are dependent on luminosity variations for stars of the same color, or temperature, the temperature effects on the Na D_1/D_2 lines would result in increased scatter when the EWs are plotted against ΔM_V values.

- *Ca lines*: The Ca II H and K lines at 3933Å and 3968Å, shown in Figure 5.5 for the known young star LP 776-025, are produced within the photosphere of a low mass star in absorption and present with an emission core when the star has heightened activity within the chromosphere (Rauscher & Marcy 2006). Young and active flare stars often present strong emission in the Ca II H and K lines in their spectra. The ratio of the EWs of the emission cores (in the sense of K_{EW}/H_{EW}) of these two lines also decreases with increasing activity as the line formation region becomes optically thick (Houdebine & Stempels 1997). Thus, the measurements of these two features are ideal for deducing activity levels within the chromospheres of our stars. In Figure 5.6 we observe an increase in the strengths of the emission cores for stars above the main sequence with a dissipating trend for stars below the main sequence. In Figure 5.7 we

also see a modest decrease in the ratio of the two lines with decreasing ΔM_V. Each of these trends indicates an increase in activity within the chromospheres of stars above the main sequence.

- *Fe lines*: We measured three strong Fe I lines in each of our spectra at 8046Å, 8075Å, and 8327Å, shown in Figure 5.8 for the known young star LP 776-025, for analysis. We also attempted to measure the strong Fe I line at 8387Å but a nearby water line moving in and out of the feature with varying blue- and red-shifts of the spectral features rendered the EW measurements unreliable. We predict these lines to be strongly metallicity dependent, as optical Fe I and Fe II lines have been used to derive metallicities in previous studies such as Bonfils et al. (2005) and Nissen et al. (2014). As shown in Figure 5.9, we see distinct trends in the strengths of the absorption features from $\Delta M_V = 2.0$ to -0.5 for the stars, where the EWs for each of the three Fe I lines measured increases (we presume due to increasing [Fe/H] values) with decreasing ΔM_V values. This increasing trend breaks down around $\Delta M_V = -0.5$, particularly for the Fe I line at 8327Å. This figure is divided between stars within Box 4 and those in Boxes 5 and 6 in order to reduce the effects of stellar temperature on these features, so the trend is driven primarily by metallicity. This is a similar trend to what we observe for the published metallicity values discussed in §5.4.2.

- *K lines*: The potassium resonance doublet at 7665Å and 7699Å, shown for the known young star LP 776-025 in Figure 5.10, is a prominent atomic feature in low mass stars and is very useful in the determination of spectral types. Reid et al. (2000) found that

this feature increases in equivalent width for increasing spectral types from M3 to M7 before decreasing and then broadening for later types (M7 to L0), inferring that these changes are likely due to the formation of dust in the cooler atmospheres. They propose that at lower temperatures, the presence of dust would serve to reduce scattering at optical wavelengths, thereby weakening the lines. We measured these features due to their prominence in M dwarf stars, but find no trend in the measured EWs of these features with decreasing ΔM_V values as seen in Figure 5.11.

- *Molecular bands (CaH & MgH)*: For this study we also measured the molecular features CaH and MgH, and found particularly interesting results for the CaH molecular bands at 6382Å and 6830Å, shown for the known subdwarf GJ 1062 in Figure 5.12, and a less defined increase in the EW of the MgH band at 5200Å, shown for the known subdwarf GJ 1062 in Figure 5.15. The spectra of low metallicity stars are dominated by hydride bands because as abundance decreases the number density of neutral hydrogen atoms increases, resulting in stronger absorption of these hydride bands (Rojas-Ayala et al. 2012). The CaH bands are particularly sensitive to metallicity changes below [Fe/H] = +0.05 dex, and $\log(g)$ and can be used to discern between subdwarfs and main sequence stars (Jao et al. 2008). As shown in Figures 5.13 and 5.14 we observe a notable decrease in the measured CaH EW values for stars moving from below to above the main sequence, likely due to increasing metallicity. The MgH molecular band at 5200Å is also a useful metallicity indicator, often used relative to the strengths of TiO bands (Ake & Greenstein 1980). This feature is also temperature sensitive (Pettersen

et al. 1985), likely causing much of the scatter seen in Figure 5.16. With this feature we see a grouping of about ten stars above the main sequence at $\Delta M_V < -0.5$ that show an increase in the EW measurement for the MgH feature, otherwise we see no trend. Much of the scatter in Figures 5.13, 5.14, and 5.16 is likely due to a combination of temperature dependence and measurement errors. While we aimed for consistency in how each feature was measured via TAME, the molecular bands span large ranges in wavelength, making it sometimes difficult to extract accurate EW values.

5.4.2 Metallicities

We have supplemented the data in our spectroscopy study with metallicities from four papers published in refereed journals: Bonfils et al. (2005), Rojas-Ayala et al. (2012), Neves et al. (2014), and Gaidos & Mann (2014). We cross-referenced the stars in these papers to our sample of 657 stars by names and/or coordinates, as some papers only provided names for their targets. We found [Fe/H] values for 124 stars ($\sim$ 19% of our total sample). Each of these papers used either spectroscopic or a combination of spectroscopic and photometric techniques to determine metallicities for the nearby, M dwarf stars. While each study used different features and techniques to derive metallicities, many of the overlapping stars in these studies have similar values that fall within the given errors. We discuss each of the efforts in the following paragraphs.

We found [Fe/H] values for 17 stars in the Bonfils et al. (2005) study that are also included within the three target boxes for our study. The metallicities provided by Bonfils et al. (2005) were determined using high resolution spectra gathered with the spectrographs ELODIE on

the 1.93 m telescope at Observatoire de Haute Provence (France), and CORALIE on the 1.20 m Swiss telescope at La Silla Observatory ESO (Chile). They used the *IRAF splot* task to measure the EWs of 39 Fe I and 12 Fe II lines, then derived the stellar parameters using the MOOG code with a grid of model atmospheres.

The work done by Rojas-Ayala et al. (2012) provided metallicities for 50 of our target stars. Their study utilized near-infrared K-band spectra obtained with the TripleSpec spectrograph on the 200 inch Hale Telescope at Palomar Observatory. They derived their metallicities using Ca I and Na I line EWs calculated using an *IDL* pipeline. To remove the temperature dependence of these features they used a water index (H_2O-K2) that samples the overall shapes of M dwarf spectra from 2.07-2.38 μm, where H_2O is absorbed. The Ca I and Na I line strengths and the temperature determined by the H_2O-K2 index were then used to determine [Fe/H] values for early to mid-M stars using a linear equation derived by the team and revised in their most recent work. They compared their results with those from other techniques (including those of Bonfils et al. 2005) to ensure the quality of their results. They determined their metallicity estimates are accurate to 0.17 dex.

From the work of Neves et al. (2014) we gathered [Fe/H] values for 68 of the stars in our sample. The spectroscopic data used to derive these metallicities were gathered in the optical wavelengths $530-690$ nm from La Silla Observatory using the HARPS instrument on the ESO 3.6 m telescope. For their metallicity determinations they measured pseudo-EWs of most of the lines/features in each spectrum and then correlated these EWs with reference photometric scales for [Fe/H] from previous work (Neves et al. 2012; Casagrande et al. 2008).

These scales are based on [Fe/H] determinations for M dwarf secondaries to F-,G-, and K-primaries.

The most recent work used comes from Gaidos & Mann (2014) and provided metallicities for 59 stars from our sample. Their work utilized near-infrared spectra from two instruments: the SpeX spectrograph on the 3.0 m NASA Infrared Telescope (IRTF) and the SuperNova Integral Field Spectrograph (SNIFS) on the University of Hawaii 2.2 m telescope at Mauna Kea. To derive the [Fe/H] values for the stars observed with SpeX the strengths of atomic lines in the H- and K-band spectra were used and calibrated using wide binaries. For the SNIFS data they utilized a procedure to determine the best-fit match between the stellar spectra and model spectra.

These 124 stars and their published metallicities are detailed in Table 5.3 where we give their names (column 1), 2000.00 coordinates (2 and 3), V magnitudes, and $V - K$ values (4 and 5). We also provide the parameters used to create Figure 5.17, the ΔM_V values (6), and [Fe/H] metallicities and errors from each study (7–13). These results are illustrated in Figure 5.17, where we observe a clear trend, illustrated with a linear fit, of increasing metallicity with decreasing ΔM_V (as stars move from below to above the main sequence). Given that this relationship has has been previously noted for metallicity values, we expect to see these results. However, we note that the trend appears to taper off slightly for stars around $\Delta M_V < -0.3$ and with more data for stars above the main sequence we would be able to better observe whether or not this "drop" is authentic. This observation would support our theory that, while metallicity does play an important role, these over-luminous stars are

also driven to higher luminosities by magnetic activity that would be less of a factor for their counterparts below the main sequence.

5.4.3 Radial Velocity Measurements

TAME also calculates the radial velocity measurements (in km s^{-1}) for each star based on the difference between the given resting wavelength for a feature and the measured wavelength of that feature. We calculate each radial velocity using the mean of the derived values for only the atomic lines that were not crowded by water lines from the Earth's atmosphere or in the blue end of the spectrum, where the SNR was much lower. These lines include the Hα Balmer line, three Fe I lines, two K I lines, Na I doublet lines, and other Ca I features measured but not used or discussed in §5.4.1 (at 8498Å, 8542Å, and 8662Å). These values were then corrected for the heliocentric velocity by adding the values calculated by the *IRAF* procedure *rvcorrect* from our measured radial velocity measurements. The error for each star's radial velocity measurement is simply the standard deviation of the radial velocities used to calculate the mean radial velocity for the star, divided by the square root of the number of radial velocity measurements used for each mean. Using this method the majority of our calculated errors are less than 3 km s^{-1} with a few that are between about 4 and 8 km s^{-1}. While these errors are relatively high, our current goals for this study are not to provide precise radial velocity measurements, but to assess these values in reference to their main sequence positions.

As illustrated by Figure 5.18 our radial velocity measurements and their dispersion show no indication of a clear trend in relation to their ΔM_V values. We also note that the subdwarf

flare star LHS 482 demonstrates the highest radial velocity measurement at -147 km s^{-1}.

Though it is difficult to see amongst the spread in radial velocity on Figure 5.18, we do note that the known subdwarfs have a higher average radial velocity measurement than both the main sequence/unknown stars and the young stars, as is summarized in Table 5.4. Subdwarfs are expected to have higher space velocities in general due to their longer lifetimes. With more time these stars have experienced more gravitational interactions with their surroundings, resulting in a ramp up in the velocity of their space motions (Jao et al. 2017). We find that the average radial velocity for the five subdwarfs in this study is almost 50 km s^{-1} with the median measurement at about 18 km s^{-1}. For the main sequence (or stars not yet identified as young or subdwarf) stars and the young stars the average radial velocities differ by about 10 km s^{-1} with the main sequence stars exhibiting a mean radial velocity at almost 27 km s^{-1} and a median at 17.6 km s^{-1} while the young stars are higher at a mean of almost 38 km s^{-1} and a median of 25.9 km s^{-1}. The higher radial velocity of the subdwarfs at almost twice that of the main sequence stars makes sense as these stars are older and have presumably had more time for gravitational interactions to accelerate their movements through the Galaxy. The radial velocities only provide one direction of stellar motion for these stars. Combined with proper motions we can accurately assess the UVW space motions of these stars to better analyze the link between main sequence position and space motion velocities, as they relate to stellar ages.

In order to check the quality of our radial velocity measurements we have cross referenced our targets with those that have radial velocities provided in Newton et al. (2016) (from the

references therein). Most of the radial velocity measurements from Newton et al. (2016) have errors of 5.0 km s^{-1} while ours are generally less than 3.0 km s^{-1}. We show the results of these comparisons in Figure 5.19, where we plot our values for 14 stars against those from the literature. We see a clear linear trend where all of our measurements fall within the errors (of 5.0 km s^{-1}) of the previously published measurements, a one-to-one linear fit is included to demonstrate this quality.

5.4.4 Notable Stars

There are several stars in this study that exhibited interesting results in the Hα and Ca II H and K plots of Figures 5.2 and 5.6. These stars are primarily the known subdwarf stars and a handful of stars elevated above the main sequence whose spectra show indicators that they may be young. Here we discuss the six stars not identified as young that show strong Hα emission in Figure 5.2 and are elevated above the main sequence, the two subdwarfs that show relatively strong Ca II H and K emission in Figure 5.6, the three stars in the same Figure that show strong Ca II H and K absorption despite being elevated above the main sequence, and the remaining subdwarfs observed for this study and their results.

In Figure 5.2 there are six stars that have notably strong Hα emission lines and have not been identified as young. These stars are **GJ 82** at $\Delta M_V = -0.86$, **GJ 166C** at $\Delta M_V = +0.03$, **GJ 388** at $\Delta M_V = -0.45$, both **GJ 490A** and **B** at $\Delta M_V = -0.71$ and -0.86, respectively, and **GJ 875.1** with $\Delta M_V = -0.69$. Each of these stars, except GJ 490A in Box 4, is located in Box 5. GJ 82 is a known flare star with spectral type M4.0Ve, as noted in Table 5.1. This star is also given an age estimate between $35 - 300$ Myr in Klutsch

et al. (2014), though they also identify it as a possible Pleiades member, which seems unlikely given its distance of only 12.2 pc. The next potentially young star, GJ 166C, is also known to be a flare star but given its location only 0.03 mag below the main sequence M_V it is unlikely to be young. The star is discussed in Zhao et al. (2011), where it is given an age estimate of 5 Gyr, though its spectral type of M4.5V indicates that this star is fully convective so the mechanisms behind this star's activity are currently not fully understood. Klutsch et al. (2014) give an age estimate of $25 - 300$ Myr for GJ 388, an M4.5Ve flare star, though they estimate a very low probability of a membership (43%) in the young moving group Castor. The double star system GJ 490A and B are both listed as possible members of Tucana-Horologium (at 65%), another young moving group, with an age estimate of $15 - 150$ Myr, making these two stars likely to be young. For the last star with strong Hα emission we find that GJ 875.1 is known to be a variable star and Klutsch et al. (2014) gives it an age estimate of $20 - 300$ Myr with only a 24% probability for membership in the young moving group AB Dor. In summary, each of these stars, except GJ 166C, is potentially young but needs further investigation to better constrain their ages.

The results from the Ca II H and K measurements in Figure 5.6 uncovered five noteworthy stars that show results opposite to what might be expected. Two subdwarf stars, **LHS 482** and **GJ 1062** presented these features in emission while three main sequence, or unknown, stars – **GJ 105B**, **LHS 3056**, and **GJ 2121** – exhibited strong Ca II absorption, despite being elevated above the main sequence. As previously noted, LHS 482 at $\Delta M_V = +1.59$, is also a known flare star in Box 6. The heightened activity of this star seems unusual and

makes it an excellent candidate for closer study. We also note that LHS 482 shows CaH measurements that do not align with those of the other four subdwarfs. As for GJ 1062, with $\Delta M_V = +1.97$ this star is rapidly rotating with vsin$i$ = 9.8 km s^{-1} and a measured rotation period of only 1.92 days (Houdebine et al. 2017). This is quite fast, given the median rotation period for M dwarfs of about 15.4 days (Nielsen et al. 2013). This may lead to elevated levels of activity given the correlation between high rotation and heightened activity (Houdebine et al. 2017). The three stars with unexpectedly strong absorption in these features are all located in Box 5 and are relatively faint with $V = 11.7 - 12.9$ and, as a result, may have poor quality Ca II measurements due to low SNRs and lack of flux in the blue end of their spectra, where these features are located. Because the Hα features in each of these spectra are also lacking emission it is possible that, though we would expect more active chromospheres from these elevated stars, during the time of these observations they were simply quiescent – particularly for LHS 3056 and GJ 2121 given their ΔM_V values of -1.29 and -0.88, respectively.

There were seven stars for which we were unable to measure the Ca II H and K lines and, rarely, some other features due to the low SNR and noise in the blue end of their spectra. These stars are listed in Table 5.2 and their EW measurements were simply left empty when measurements were not possible. These include one of the five subdwarf stars, **GJ 907**, which is why Figures 5.6 and 5.7 only show results for four of the five subdwarfs. The other stars lacking measurements include several stars located below the main sequence – in these cases the features weren't strong enough to distinguish from noise – and two very faint stars

above the main sequence whose spectra were simply too noisy in the $3000 - 4000$Å range to clearly define the Ca II lines. The other two subdwarf stars with measurements that have not yet been discussed individually are **LHS 178** and suspected subdwarf **GJ 1248**. Each of these two stars is predictably quiescent and shows indications of low metallicity in its Fe I line and CaH band measurements.

5.5 Conclusions

In conclusion, we find that by measuring the EWs of various spectral features for our 80 stars obtained using ARCES and analyzing the trends of these measurements with respect to their ΔM_V values we are able to discern how the mechanisms behind some of these features may be driving the increased width of the main sequence for low mass stars. **Our results support our hypothesis that for stars below the main sequence offsets are driven mainly by metallicity effects, while stars above the main sequence are likely elevated due to a combination of both metallicity and heightened magnetic activity.**

We find that spectral features indicative of heightened chromospheric activity support our hypothesis that stars elevated above the main sequence are more active than their counterparts with lower luminosities, and likely smaller radii. These features that form within the chromospheres of low mass stars include Hα, Ca II H and K, and the Na D doublet. Each of these features demonstrates an increase in the strength of emission (or at least a decrease in absorption for Na I) for stars located above the central distribution of the main sequence. We have also compared our Hα measurements to our long-term variability results

from Chapter 3, 11 stars have results in both studies, to explore the connection between the Hα emission and photometric variability. These results are shown in Figure 5.20, where we see the onset of a trend of increasing emission strength with increasing long-term variability. More data points are needed for a robust analysis of these results.

We also observe slight trends in the CaH spectral features that are often used to determine abundances in low mass stars. The Fe I absorption lines grow stronger with decreasing ΔM_V, likely as a result of increasing metallicity, and this trend seems to be more prominent for stars below the main sequence. We see the opposite effect for the CaH molecular bands, where their EW measurements decrease with decreasing ΔM_V. We also find a distinct trend in the published [Fe/H] metallicities for our stars, where the metallicity increases as stars are selected from below to above the main sequence, and this trend appears to taper off a bit for stars above the central distribution of the main sequence. It is known that much of the spread in the H-R diagram below the main sequence is due to the effects of low metallicity, where the lack of heavier elements results in a decreased opacity and thus blue-shifted $(V - K)$ colors (i.e., hotter temperatures) for these stars.

We do not find any distinct trend in the radial velocity measurements for our 80 stars besides the higher measured average radial velocities for the five subwarfs.

Table 5.1: Properties of the Low Mass Stars in the Spectroscopy Study.

Star Name (1)	R.A. (2)	Dec. 2000.0 (3)	V (4)	I (5)	$V-K$ (6)	dist. (pc) (7)	dist. ref. (8)	M_V (9)	ΔM_V (10)	Spectral Type (11)	SpTy (ref) (12)	Telescope (13)	Obs. Date (14)	Notes[a] (15)
GJ 2	00:05:11	+45:47:11	9.95	7.87	4.10	11.2	vLe07	9.70	−0.10	M1.0V	Rei95	APO	2015.1216	
GJ 1	00:05:24	−37:21:26	8.54	6.41	4.02	4.3	vLe07	10.37	+0.76	M1.5V	Haw96	CTIO	2015.0724	
NLTT 372	00:08:52	+20:49:08	15.87	13.12	5.15	85.8	Rie14	11.21	−1.20	M4.5V	Rei95	APO	2014.1027	Y
GJ 1006A	00:16:14	+19:51:37	12.26	9.46	5.17	15.1	YPC95	11.37	−1.08	M3.6V	Shk12	APO	2015.1220	Y
LHS 1054	00:17:20	+29:10:58	11.52	9.35	4.28	22.8	vLe07	9.73	−0.51	M2.0V	Rei95	APO	2015.1216	
GJ 15A	00:18:23	+44:01:24	8.08	6.45	4.06	3.6	vLe07	10.30	+0.59	M1.5V	Hen94	APO	2013.1012	
GJ 15B	00:18:26	+44:01:42	11.06	8.24	5.11	3.6	vLe07	13.28	+0.97	M3.5V	Hen94	APO	2013.1012	
GJ 22B	00:32:29	+67:14:08	12.40	···	6.02	10.1	YVO	12.38	−1.88	M3.0V	Kir91	APO	2014.1027	
GJ 49	01:02:38	+62:20:42	9.56	7.44	4.19	9.9	YPC95	9.58	−0.44	M1.5V	Alo15	APO	2015.1216	
GJ 1030	01:06:41	+15:16:22	11.40	9.23	4.24	21.8	vLe07	9.71	−0.43	M2.0V	Rei95	APO	2015.1220	
GJ 52.2	01:07:49	+34:12:54	13.37	11.06	4.29	22.1	YPC95	11.65	+1.39	M2.5V	Rei95	APO	2015.1216	
L 797-030	01:17:15	−13:15:47	10.79	8.86	3.88	23.3	vLe07	8.95	−0.34	M1.0V	Koe10	CTIO	2015.0723	
LHS 1289	01:43:15	+27:50:31	10.40	8.55	3.80	21.4	vLe07	8.75	−0.36	M1.0V	Gra03	APO	2015.1220	
GJ 78	01:51:48	−10:48:12	11.80	9.59	4.17	16.2	vLe07	10.75	+0.78	M2.0V	Rei95	APO	2015.1216	
GJ 79	01:52:49	−22:26:05	8.88	7.08	3.70	11.0	vLe07	8.67	−0.22	K9.0V	Gra06	CTIO	2015.0725	
GJ 82	01:59:23	+58:31:16	12.21	9.48	5.25	12.2	vLe07	11.78	−0.86	M4.0Ve	Rei95	APO	2015.1216	
GJ 84.1A	02:05:23	−28:04:11	10.88	9.04	3.72	23.1	vLe07	9.06	+0.13	M1+V	Gra06	CTIO	2015.0725	
GJ 91	02:13:53	−32:02:28	10.31	8.15	4.22	12.4	vLe07	9.84	−0.25	M2.0V	Gra06	CTIO	2015.0724	
GJ 96	02:22:14	+47:52:48	9.41	7.51	3.86	11.8	YV	9.05	−0.19	M0.5V	Rei95	APO	2013.1011	
GJ 105B	02:36:04	+06:53:12	11.71	8.88	5.14	7.5	vLe07	12.33	−0.04	M3.5V	Hen94	APO	2013.1023	
GJ 114.1	02:50:05	−53:08:20	10.72	8.55	4.23	13.0	vLe07	10.15	+0.03	M1.5V	Haw96	CTIO	2015.0724	
GJ 119A	02:56:34	+55:26:14	10.48	8.55	3.89	20.7	YPC95	8.90	−0.41	M1.0V	Rei95	APO	2015.1216	
LHS 1499	03:08:23	+43:02:09	14.79	12.17	4.75	24.5	YPC95	12.84	+1.43	M4.0V	New14	APO	2014.1027	
LHS 1521	03:15:29	+57:51:33	15.24	12.53	4.97	14.7	YV	14.40	+2.44	M3.5V	Alo15	APO	2014.1027	
GJ 1062	03:38:18	−11:29:49	13.01	10.79	4.18	16.0	YPC95	11.99	+2.00	M2.5VI	Giz97	APO	2015.1216	S
LHS 178	03:42:29	+12:31:34	12.87	10.78	3.99	24.3	YPC95	10.94	+1.40	M1.5VI	Giz97	APO	2013.1023	S
GJ 154	03:46:20	+26:12:55	9.58	7.75	3.74	14.6	vLe07	8.76	−0.22	M1.0V	Gra03	APO	2013.1023	
GJ 1065	03:50:43	−06:05:10	12.82	10.04	5.07	9.5	YPC95	12.93	+0.72	M3.5V	Rei95	APO	2015.1216	
GJ 157.1	03:59:53	+26:05:24	12.62	10.09	4.80	22.8	YPC95	10.83	−0.71	M3.0V	Rei95	APO	2015.1220	
GJ 166C	04:15:22	−07:39:35	11.24	8.31	5.28	5.0	vLe07	12.75	+0.03	M4.5V	Rei95	APO	2014.1027	
LP 776-025	04:52:24	−16:49:21	11.63	9.12	4.74	16.3	Shk12	10.57	−0.82	M3.3V	Shk09	APO	2015.1220	Y
GJ 184	05:03:23	+53:07:42	9.98	8.10	3.81	13.7	vLe07	9.30	+0.16	M0.5V	Rei95	APO	2015.1216	
BD 21-1074A	05:06:50	−21:35:09	10.41	8.25	4.29	18.3	Rie14	9.10	−1.16	M1.5Ve	Rie14	APO	2013.1011	Y
GJ 205	05:31:27	−03:40:38	7.95	5.88	3.91	5.7	YV	9.17	−0.19	M1.5V	Hen94	APO	2015.1216	
GJ 212	05:41:30	+53:29:23	9.76	7.75	4.00	12.2	YV	9.34	−0.22	M0.5V	Rei95	APO	2013.1011	Y
GJ 220	05:53:14	+24 15 32	10.84	8.71	4.21	19.4	YPC95	9.40	−0.67	M2.0V	Kir91	APO	2015.1220	
G 099-049	06:00:03	+02:42:23	11.31	8.43	5.27	5.2	Hen06	12.73	+0.04	M3.5Ve	Hen06	APO	2014.1027	Y
GJ 232	06:24:41	+23:25:59	13.16	10.21	5.25	8.4	YPC95	13.54	+0.90	M4.0V	Kir91	APO	2014.1027	
G 108-021	06:42:09	+03:35:41	12.06	9.55	4.73	10.4	YPC95	11.97	+0.61	M3.5V	Rei95	APO	2015.1220	
G 108-022	06:42:09	+03:35:41	13.33	10.61	5.05	10.4	YPC95	13.24	+1.09	M4.0V	Rei95	APO	2015.1220	
LTT 11918	06:47:18	+23:46:44	12.65	11.15	3.94	21.5	YPC95	10.99	+1.56	···	···	APO	2015.1220	
GJ 273	07:27:25	+05:13:32	9.85	7.14	4.99	3.8	Gat08	11.95	−0.06	M3.5V	Hen94	APO	2013.1011	
GJ 275.1	07:32:02	+68:37:15	10.89	8.89	4.03	24.9	vLe07	8.91	−0.73	M1.0V	Rei95	APO	2015.1220	
GJ 282C	07:36:07	−03:06:38	9.87	7.92	3.94	14.1	YVO	9.12	−0.30	M1.0V	Alo15	APO	2013.1023	
GJ 281	07:39:23	+02:11:01	9.58	7.80	3.71	14.5	vLe07	8.77	−0.14	M0.0Ve	Lep13	APO	2013.1023	
GJ 334	09:06:45	−08:48:24	9.50	7.68	3.74	14.4	YV	8.71	−0.27	K7.0V	Rei95	APO	2015.1220	
GJ 373	09:56:08	+62:47:18	8.97	7.11	3.77	10.7	YV	8.82	−0.22	M0.0V	Rei95	APO	2015.1220	
GJ 383	10:12:08	−18:37:04	9.95	8.14	3.76	17.9	VO	8.69	−0.34	K7.0V	Rei95	CTIO	2015.1220	
GJ 382	10:12:17	−03:44:44	9.29	7.11	4.28	7.9	vLe07	9.80	−0.44	M1.5V	Rei95	CTIO	2015.1220	
GJ 382	10:12:17	−03:44:44	9.29	7.11	4.28	7.9	vLe07	9.80	−0.44	M1.5V	Rei95	APO	2015.1220	

[a] Notes in Column 15: Y = known young stars, (Y) = suspected young stars, S = known subdwarf stars, (S) = suspected, but unconfirmed subdwarf stars.

Only the 80 stars observed at APO are presented in this dissertation.

Distance references: (Cos06) Costa et al. (2006); (Fab00) Fabricius & Makarov (2000); (Gat08) Gatewood (2008); (Hen06) Henry et al. (2006); (Rie11) Riedel et al. (2011); (Rie14) Riedel et al. (2014); (Shk12) Shkolnik et al. (2012); (vLe07) van Leeuwen (2007); (YPC95) van Altena et al. (1995).

Spectral type references: (Alo15) Alonso-Floriano et al. (2015); (Bid85) Bidelman (1985); (Giz97) Gizis (1997); (Gra03) Gray et al. (2003); (Gra06) Gray et al. (2006); (Haw96) Hawley et al. (1996); (Hen94) Henry et al. (1994); (Kir91) Kirkpatrick et al. (1991); (Koe10) Koen et al. (2010); (Lep13) Lépine et al. (2013); (New14) Newton et al. (2014); (Rei95) Reid et al. (1995); (Rie14) Riedel et al. (2014); (Shk09) Shkolnik et al. (2009); (Shk12) Shkolnik et al. (2012)

Table 5.1: Properties of the Low Mass Stars in the Spectroscopy Study.

Star Name	R.A.	Dec.	V	I	$V-K$	dist.	dist.	M_V	ΔM_V	Spectral	SpTy	Telescope	Obs.	Notes[a]
	2000.0					(pc)	ref.			Type	(ref)		Date	
(1)	(2)	(3)	(4)	(5)	(6)	(7)	(8)	(9)	(10)	(11)	(12)	(13)	(14)	(15)
GJ 2079	10:14:19	+21:04:29	10.04	8.24	3.78	23.0	vLe07	8.23	−0.84	M0.7V	Shk09	APO	2015.1220	
GJ 388	10:19:36	+19:52:11	9.29	6.78	4.70	4.9	YPC95	10.84	−0.45	M3.0V	Hen94	APO	2013.1011	
GJ 411	11:03:20	+35:58:11	7.46	4.79	4.21	2.5	YV	10.47	+0.40	M2.0V	Hen94	APO	2013.1011	
GJ 412A	11:05:28	+43:31:36	8.77	6.70	4.00	4.8	YV	10.36	+0.80	M1.0V	Hen94	APO	2013.1011	
GJ 1148	11:41:44	+42:45:07	11.92	9.18	5.10	11.2	YV	11.67	−0.61	M4.0V	Rei95	APO	2016.0520	
LHS 2520	12:10:05	−15:04:16	12.09	9.30	5.23	12.8	Rie10	11.55	−1.04	M3.5V	Rei95	APO	2016.0520	
GJ 480	12:38:52	+11:41:46	11.51	8.98	4.82	14.0	YV	10.78	−0.81	M3.0V	Rei95	APO	2016.0520	
GJ 490B	12:57:39	+35:13:19	13.20	10.48	5.18	19.8	YV	11.72	−0.76	M4.0V	Rei95	APO	2015.1220	
GJ 490A	12:57:40	+35:13:30	10.68	8.81	4.13	19.8	YV	9.20	−0.68	M0.5V	Rei95	APO	2015.1220	
GJ 512A	13:28:21	−02:21:37	11.42	8.93	4.81	13.7	vLe07	10.74	−0.83	M3.0V	Rei95	APO	2016.0520	
GJ 1185	14:47:53	−03:09:15	13.33	10.99	4.27	19.7	YPC95	11.86	+1.64	M2.0V	Rei95	APO	2016.0520	
LHS 3056	15:19:12	−12:45:06	12.87	11.63	5.29	21.2	Win15	11.24	−1.50	M4.0V	Rei95	APO	2016.0520	
GJ 615.2D	16:13:56	+33:46:24	12.33	···	3.99	22.7	YVO	10.55	+1.01	M2.5V	Rei95	APO	2016.0520	
GJ 625	16:25:24	+54:18:14	10.11	7.89	4.28	6.5	vLe07	11.05	+0.81	M1.5V	Hen94	APO	2016.0520	
GJ 2120	16:27:33	−10:00:28	10.85	8.84	4.02	22.8	vLe07	9.06	−0.55	M1.0V:	Koe10	CTIO	2015.0723	
GJ 2121	16:30:13	−14:39:49	12.35	9.84	4.75	22.4	vLe07	10.60	−0.81	M2.5V	Gra06	APO	2016.0520	
GJ 628	16:30:18	−12:39:45	10.07	7.37	5.00	4.3	YV	11.90	−0.13	M3.0V	Hen94	CTIO	2015.0723	
GJ 643	16:55:25	−08:19:21	11.77	9.01	5.05	6.5	YPC95	12.70	+0.55	M3.5V	Hen94	APO	2016.0524	
GJ 1216	17:20:46	+49:15:20	14.53	11.70	5.15	17.0	YPC95	13.38	+0.98	M4.0V	Rei95	APO	2016.0520	
GJ 676A	17:30:11	−51:38:13	9.59	7.76	3.77	16.3	vLe07	8.53	−0.52	M0.0V	Haw96	CTIO	2015.0723	
GJ 693	17:46:34	−57:19:08	10.77	8.20	4.75	5.8	YV	11.95	+0.54	M2.0V	Haw96	CTIO	2015.0724	
GJ 701	18:05:07	−03:01:52	9.37	7.30	4.06	7.8	vLe07	9.91	+0.20	M0.0V	Hen94	CTIO	2015.0723	
LHS 461B	18:18:03	+38:46:36	13.54	10.71	5.17	11.3	YPC95	13.27	+0.82	M4.0V	Rei95	APO	2016.0524	
LTT 07419A	18:43:12	−33:22:31	10.25	8.28	3.92	15.2	Cos06	9.34	−0.04	M2.0V	Bid85	CTIO	2015.0723	
GJ 729	18:49:49	−23:50:10	10.50	7.68	5.13	3.0	vLe07	13.11	+0.76	M3.5V	Hen94	CTIO	2015.0723	
GJ 731	18:51:51	+16:34:59	10.15	8.28	3.83	15.2	vLe07	9.24	+0.06	M0.0V	Rei95	APO	2015.0930	
GJ 740	18:58:00	+05:54:29	9.21	7.31	3.85	10.9	vLe07	9.02	−0.20	M0.5V	Rei95	APO	2015.0930	
GJ 745A	19:07:05	+20:53:17	10.78	8.54	4.26	8.7	vLe07	11.08	+0.89	M1.5V	Rei95	APO	2016.0520	
GJ 745B	19:07:13	+20:52:37	10.76	8.53	4.24	8.7	vLe07	11.06	+0.92	M2.0V	Rei95	APO	2016.0520	
LHS 3445	19:14:39	+19:19:04	11.59	9.05	4.78	18.6	vLe07	10.24	−1.25	M3.5V	Rei95	APO	2015.0930	(Y)
GJ 1236	19:22:02	+07:02:31	12.39	9.86	4.70	10.7	YPC95	12.24	+0.96	M3.0V	Rei95	APO	2016.0520	
LP 869-042	19:39:36	−26:45:07	10.48	8.58	3.83	23.2	vLe07	8.65	−0.53	M1.0V	Gra06	CTIO	2015.0723	
LTT 15769	19:45:49	+32:23:13	10.86	8.91	4.09	12.1	Fab00	10.45	+0.67	M1.0V	Rei95	APO	2015.0930	
GJ 1248	20:03:51	+05:59:44	12.11	9.84	4.24	12.5	YPC95	11.63	+1.49	M1.5V	Rei95	APO	2015.0930	(S)
LHS 482	20:05:02	+54:26:03	12.00	9.98	3.89	16.5	YPC95	10.91	+1.60	M1.5VI	Giz97	APO	2015.0930	S
GJ 806	20:45:04	+44:29:56	10.77	8.57	4.24	12.2	vLe07	10.34	+0.20	M2.0V	Kir91	APO	2015.0930	
GJ 803A	20:45:09	−31:20:27	8.65	6.61	4.12	9.9	YV	8.67	−1.18	M0.0V	Haw96	APO	2013.1012	Y
GJ 809	20:53:19	+62:09:15	8.56	6.58	3.94	7.1	YV	9.30	−0.12	M0.0V	Hen94	APO	2013.1012	
GJ 828.2	21:27:16	−06:50:39	11.10	9.15	3.93	16.4	vLe07	10.03	+0.62	M0.5V	Rei95	CTIO	2015.0725	
GJ 832	21:33:33	−49:00:32	8.66	6.48	4.16	4.9	vLe07	10.21	+0.26	M1.5V	Haw96	CTIO	2015.0725	
HIP 106803	21:37:55	−63:42:42	10.62	8.62	3.98	21.2	vLe07	8.99	−0.53	M0.0V	Haw96	CTIO	2015.0725	
LTT 16412	21:57:26	+08:08:13	11.03	8.91	4.19	21.1	YPC95	9.41	−0.61	M1.5V	Rei95	CTIO	2015.0725	
GJ 846	22:02:10	+01:24:00	9.17	7.27	3.85	10.2	YV	9.13	−0.10	M0.5V	Kir91	APO	2013.1012	
LTT 08848	22:05:51	−11:54:51	10.11	8.28	3.71	22.2	vLe07	8.38	−0.54	M0.0V	Rei95	CTIO	2015.0726	
GJ 849	22:09:40	−04:38:26	10.38	7.87	4.79	9.0	YV	10.61	−0.90	M3.5V	Rei95	CTIO	2015.0726	
GJ 863	22:33:02	+09:22:40	10.38	8.34	4.02	13.3	YV	9.76	+0.15	M1.0V	Rei95	APO	2015.0930	
GJ 875	22:50:19	−07:05:24	9.86	8.02	3.76	14.1	vLe07	9.11	+0.09	M0.5V	Gra03	CTIO	2015.0725	
GJ 875.1	22:51:53	+31:45:15	11.62	9.11	4.75	14.8	YV	10.77	−0.64	M3.0V	Rei95	APO	2015.0930	
GJ 876	22:53:16	−14:15:49	10.18	7.40	5.17	4.7	YV	11.82	−0.63	M3.5V	Hen94	CTIO	2015.0726	
GJ 880	22:56:34	+16:33:12	8.65	6.55	4.13	6.8	YV	9.49	−0.39	M1.5V	Hen94	APO	2013.1012	
GJ 887	23:05:52	−35:51:11	7.34	5.32	3.88	3.3	vLe07	9.75	+0.46	M0.5V	Haw96	CTIO	2015.0725	

[a]Notes in Column 15: Y = known young stars, (Y) = suspected young stars, S = known subdwarf stars, (S) = suspected, but unconfirmed subdwarf stars.

Only the 80 stars observed at APO are presented in this dissertation.

Distance references: (Cos06) Costa et al. (2006); (Fab00) Fabricius & Makarov (2000); (Gat08) Gatewood (2008); (Hen06) Henry et al. (2006); (Rie11) Riedel et al. (2011); (Rie14) Riedel et al. (2014); (Shk12) Shkolnik et al. (2012); (vLe07) van Leeuwen (2007); (YPC95) van Altena et al. (1995).

Spectral type references: (Alo15) Alonso-Floriano et al. (2015); (Bid85) Bidelman (1985); (Giz97) Gizis (1997); (Gra03) Gray et al. (2003); (Gra06) Gray et al. (2006); (Haw96) Hawley et al. (1996); (Hen94) Henry et al. (1994); (Kir91) Kirkpatrick et al. (1991); (Koe10) Koen et al. (2010); (Lep13) Lépine et al. (2013); (New14) Newton et al. (2014); (Rei95) Reid et al. (1995); (Rie14) Riedel et al. (2014); (Shk09) Shkolnik et al. (2009); (Shk12) Shkolnik et al. (2012)

Table 5.1: Properties of the Low Mass Stars in the Spectroscopy Study.

Star Name (1)	R.A. 2000.0 (2)	Dec. 2000.0 (3)	V (4)	I (5)	$V-K$ (6)	dist. (pc) (7)	dist. ref. (8)	M_V (9)	ΔM_V (10)	Spectral Type (11)	SpTy (ref) (12)	Telescope (13)	Obs. Date (14)	Notes[a] (15)
HIP 114066	23:06:04	+63:55:34	10.82	8.99	3.84	24.5	vLe07	8.87	−0.33	M0.5V	Rei95	APO	2015.0930	Y
GJ 1284	23:30:13	−20:23:27	11.12	8.60	4.79	16.1	vLe07	10.09	−1.43	M3.0Ve	Rei95	APO	2013.1012	(Y)
GJ 907	23:48:03	+49:00:57	12.08	9.92	4.15	16.6	YV	10.98	+1.06	M1.0V	Rei95	APO	2015.0930	(S)
GJ 908	23:49:12	+02:24:04	8.98	6.95	3.94	6.0	YV	10.09	+0.66	M1.0V	Hen94	APO	2013.1012	

[a] Notes in Column 15: Y = known young stars, (Y) = suspected young stars, S = known subdwarf stars, (S) = suspected, but unconfirmed subdwarf stars.

Only the 80 stars observed at APO are presented in this dissertation.

Distance references: (Cos06) Costa et al. (2006); (Fab00) Fabricius & Makarov (2000); (Gat08) Gatewood (2008); (Hen06) Henry et al. (2006); (Rie11) Riedel et al. (2011); (Rie14) Riedel et al. (2014); (Shk12) Shkolnik et al. (2012); (vLe07) van Leeuwen (2007); (YPC95) van Altena et al. (1995).

Spectral type references: (Alo15) Alonso-Floriano et al. (2015); (Bid85) Bidelman (1985); (Giz97) Gizis (1997); (Gra03) Gray et al. (2003); (Gra06) Gray et al. (2006); (Haw96) Hawley et al. (1996); (Hen94) Henry et al. (1994); (Kir91) Kirkpatrick et al. (1991); (Koe10) Koen et al. (2010); (Lep13) Lépine et al. (2013); (New14) Newton et al. (2014); (Rei95) Reid et al. (1995); (Rie14) Riedel et al. (2014); (Shk09) Shkolnik et al. (2009); (Shk12) Shkolnik et al. (2012)

Table 5.2: Measured Equivalent Widths in the Spectroscopy Study.

Star Name (1)	R.A. 2000.0 (2)	Dec. 2000.0 (3)	ΔM_V (mag) (4)	CaII K 3933Å (5)	CaII H 3968Å (6)	MgH 5200Å (7)	NaI D_1 5890Å (8)	NaI D_2 5896Å (9)	CaH 6382Å (10)	Hα 6563Å (11)	CaH 6830Å (12)	KI 7665Å (13)	KI 7699Å (14)	FeI 8046Å (15)	FeI 8075Å (16)	FeI 8327Å (17)	RV avg km s^{-1} (18)	RV err km s^{-1} (19)	Note[a] (20)
GJ 2	00:05:11	+45:47:11	−0.10	−5.944	−4.476	0.096	4.812	3.722	0.228	0.436	0.042	0.489	0.444	0.099	0.094	0.321	0.68	1.54	
NLTT 372	00:08:52	+20:49:08	−1.20	···	···	0.067	0.883	0.937	0.137	−0.042	0.103	0.591	0.543	0.165	0.168	0.287	-26.60	2.63	Y
GJ 1006A	00:16:14	+19:51:37	−1.08	−6.214	−10.011	0.069	3.472	2.908	0.278	−3.969	0.047	0.652	0.700	0.087	0.186	0.397	1.79	2.45	Y
LHS 1054	00:17:20	+29:10:58	−0.51	−4.677	−3.712	···	4.334	3.698	0.291	0.513	0.042	0.489	0.480	0.113	0.103	0.296	-6.33	1.46	
GJ 15A	00:18:23	+44:01:24	+0.59	−2.557	−1.534	0.088	4.998	4.908	0.295	0.371	0.046	0.462	0.445	0.075	0.075	0.299	12.77	1.74	
GJ 15B	00:18:26	+44:01:42	+0.97	−2.755	−4.522	0.021	6.494	7.481	0.384	0.131	0.029	0.792	0.602	0.112	0.089	0.272	13.18	6.02	
GJ 22B	00:32:29	+67:14:08	−1.88	0.739	0.559	0.125	6.089	5.520	0.310	0.381	0.048	0.856	0.495	0.027	0.080	0.279	1.42	1.82	
GJ 49	01:02:38	+62:20:42	−0.44	−8.547	−5.656	0.093	4.688	4.087	0.249	0.392	0.037	0.773	0.439	0.111	0.097	0.340	-3.56	1.48	
GJ 1030	01:06:41	+15:16:22	−0.43	−3.946	−2.882	0.118	3.740	3.177	0.246	0.512	0.041	0.182	0.451	0.109	0.098	0.273	19.25	1.49	
GJ 52.2	01:07:49	+34:12:54	+1.39	···	···	0.022	5.501	5.131	0.323	0.428	0.056	0.486	0.535	0.028	0.060	0.219	-11.33	2.00	
LHS 1289	01:43:15	+27:50:31	−0.36	−5.576	−4.394	0.084	6.777	5.954	0.228	0.599	0.019	0.463	0.545	0.176	0.117	0.365	0.88	1.36	
GJ 78	01:51:48	−10:48:12	+0.78	−2.458	−1.931	0.106	4.011	3.528	0.247	0.394	0.052	0.428	0.502	0.062	0.104	0.273	-10.11	1.78	
GJ 82	01:59:23	+58:31:16	−0.86	−9.443	−15.792	0.148	1.729	1.668	0.053	−8.804	···	0.433	0.249	0.046	0.101	0.138	4.70	1.66	
GJ 96	02:22:14	+47:52:48	−0.19	−3.760	−3.419	0.082	4.946	5.289	0.199	0.603	0.029	0.700	0.523	0.143	0.106	0.282	-37.27	1.53	
GJ 105B	02:36:04	+06:53:12	−0.04	11.912	13.045	0.045	2.926	2.162	0.011	1.057	0.010	0.340	0.288	0.164	0.084	0.279	28.08	1.37	
GJ 119A	02:56:34	+55:26:14	−0.41	−4.074	−3.111	0.106	4.268	3.604	0.177	0.633	0.041	0.507	0.435	0.118	0.101	0.363	80.78	1.45	
LHS 1499	03:08:23	+43:02:09	+1.29	0.557	0.593	0.116	3.358	3.075	0.307	0.296	0.084	0.896	0.540	0.050	0.091	0.241	22.64	6.28	
LHS 1521C	03:15:29	+57:51:33	+2.37	···	···	0.083	2.153	2.749	0.249	0.359	0.066	0.611	0.459	0.121	0.119	0.234	74.72	8.16	
GJ 1062	03:38:18	−11:29:49	+1.97	−3.592	−1.741	0.095	7.046	5.771	0.337	0.321	0.064	0.706	0.616	0.023	0.059	0.240	-82.53	2.00	S
LHS 178	03:42:29	+12:31:34	+1.32	0.945	1.376	0.075	5.215	4.300	0.304	0.344	0.070	0.077	0.448	0.043	0.046	0.222	-52.77	2.12	S
GJ 154	03:46:20	+26:12:55	−0.24	−0.526	−.366	0.095	4.629	3.818	0.141	0.586	0.048	0.402	0.471	0.120	0.111	0.281	33.14	3.83	
GJ 1065	03:50:43	−06:05:10	+0.66	−3.209	−1.958	0.108	4.711	3.632	0.358	0.352	0.058	0.955	0.584	0.054	0.090	0.308	-10.48	2.69	
GJ 157.1	03:59:53	+26:05:24	−0.76	···	···	0.165	3.290	2.755	0.266	0.464	0.054	0.542	0.442	0.112	0.100	0.258	58.14	2.09	
GJ 166C	04:15:22	−07:39:35	+0.03	−0.528	−1.191	0.014	3.567	3.096	0.324	−1.757	0.013	0.999	0.778	0.046	0.022	0.321	-36.34	6.81	
LP 776-025	04:52:24	−16:49:21	+1.52	−8.128	−10.650	0.027	3.473	3.141	0.281	−3.287	0.036	0.911	0.650	0.097	0.195	0.415	24.93	4.24	Y
GJ 184	05:03:23	+53:07:42	+0.14	−3.633	−2.318	0.098	4.108	3.473	0.196	0.534	0.028	0.513	0.486	0.107	0.075	0.273	65.97	1.61	
BD 21-1074A	05:06:50	−21:35:09	−1.20	−2.759	−7.424	0.088	3.836	3.909	0.211	−3.407	0.033	0.815	0.540	0.123	0.162	0.431	22.12	4.06	Y
GJ 205	05:31:27	−03:40:38	−0.20	−6.204	−4.145	0.088	5.043	4.425	0.274	0.573	0.036	0.765	0.494	0.138	0.135	0.332	7.96	2.22	
GJ 212	05:41:30	+53:29:23	−0.28	−3.707	−3.137	0.075	4.608	4.760	0.280	0.374	0.042	0.451	0.428	0.125	0.102	0.349	-0.38	2.07	Y
GJ 220	05:53:14	+24 15 32	−0.69	−6.137	−4.376	0.098	4.907	4.278	0.221	0.496	0.043	0.190	0.452	0.110	0.098	0.298	26.54	1.58	
G 099-049	06:00:03	+02:42:23	−0.06	−0.948	−1.131	0.015	4.598	4.723	0.327	−1.591	0.026	0.228	0.624	0.023	0.138	0.375	29.74	2.71	Y
GJ 232	06:24:41	+23:25:59	+0.82	···	···	0.104	4.309	3.481	0.307	0.429	0.052	0.855	0.637	0.081	0.101	0.252	0.69	5.05	
G 108-021	06:42:09	+03:35:41	+0.56	−1.228	−1.256	0.295	3.596	3.092	0.274	0.400	0.070	0.789	0.448	0.084	0.106	0.265	82.80	2.06	
G 108-022	06:42:09	+03:35:41	+1.00	−4.374	−1.865	0.182	3.767	3.345	0.355	0.297	0.058	0.849	0.462	0.109	0.104	0.260	82.16	2.13	
LTT 11918	06:47:18	+23:46:44	+0.03	0.726	0.362	0.077	3.894	3.141	0.258	0.510	0.034	0.253	0.431	0.104	0.085	0.263	57.59	1.59	
GJ 273	07:27:25	+05:13:32	−0.11	−2.876	−1.625	0.018	3.906	3.434	0.308	0.239	0.053	0.297	0.555	0.105	0.093	0.300	17.69	1.82	
GJ 275.1	07:32:02	+68:37:15	−0.76	−3.336	−4.264	0.274	−5.097	−4.289	0.205	0.675	0.072	0.491	0.261	0.111	0.109	0.199	-14.09	2.01	
GJ 282C	07:36:07	−03:06:38	−0.32	−1.648	−2.600	0.079	4.680	3.924	0.213	−0.178	0.041	0.595	0.406	0.101	0.101	0.320	-13.16	3.28	
GJ 281	07:39:23	+02:11:01	−0.16	−3.121	−3.222	0.071	5.168	4.930	0.195	0.598	0.037	0.758	0.453	0.157	0.104	0.323	20.18	1.38	

[a]Notes in Column 20: Y = known young stars, (Y) = suspected young stars, S = known subdwarf stars, (S) = suspected, but unconfirmed subdwarf stars.

Table 5.2: Measured Equivalent Widths in the Spectroscopy Study.

Star Name (1)	R.A. 2000.0 (2)	Dec. 2000.0 (3)	ΔM_V (mag) (4)	CaII K 3933Å (5)	CaII H 3968Å (6)	MgH 5200Å (7)	NaI D_1 5890Å (8)	NaI D_2 5896Å (9)	CaH 6382Å (10)	Hα 6563Å (11)	CaH 6830Å (12)	KI 7665Å (13)	KI 7699Å (14)	FeI 8046Å (15)	FeI 8075Å (16)	FeI 8327Å (17)	RV avg km s^{-1} (18)	RV err km s^{-1} (19)	Note[a] (20)
GJ 334	09:06:45	−08:48:24	−0.30	−7.207	−4.833	0.068	5.750	3.841	0.225	0.550	0.050	0.209	0.439	0.155	0.110	0.338	37.99	1.55	
GJ 373	09:56:08	+62:47:18	−0.25	−6.217	−4.904	0.094	5.744	4.661	0.194	0.517	0.030	0.790	0.547	0.159	0.115	0.363	17.88	1.42	
GJ 382	10:12:17	−03:44:44	−0.46	−5.040	−5.761	0.028	4.487	3.836	0.281	0.431	0.042	0.233	0.443	0.116	0.100	0.339	9.73	1.60	
GJ 2079	10:14:19	+21:04:29	−0.86	−5.396	−3.891	0.065	4.581	4.142	0.206	0.489	0.036	0.438	0.563	0.167	0.138	0.456	7.04	1.92	
GJ 388	10:19:36	+19:52:11	−0.45	−4.597	−5.281	0.024	3.982	3.096	0.323	−3.434	0.051	0.494	0.631	0.147	0.162	0.463	15.68	3.70	
GJ 411	11:03:20	+35:58:11	+0.30	2.365	2.284	0.088	4.133	4.160	0.299	0.462	0.042	0.481	0.429	0.075	0.067	0.281	-80.80	3.22	
GJ 412A	11:05:28	+43:31:36	+0.74	2.279	2.826	0.075	5.917	5.798	0.275	0.412	0.046	0.927	0.521	0.065	0.081	0.278	68.94	1.61	
GJ 1148	11:41:44	+42:45:07	−0.69	−2.143	−1.980	0.149	3.392	3.039	0.265	0.338	0.044	0.457	0.530	0.102	0.094	0.222	-10.90	3.07	
LHS 2520	12:10:05	−15:04:16	−1.12	−1.165	−2.233	0.149	3.309	2.602	0.246	0.384	0.049	0.558	0.516	0.112	0.096	0.397	81.95	2.38	
GJ 480	12:38:52	+11:41:46	−0.87	−3.901	−2.640	0.158	3.073	2.606	0.250	0.566	0.047	0.492	0.507	0.102	0.107	0.295	-2.58	1.59	
GJ 490B	12:57:39	+35:13:19	−0.86	−12.530	−13.626	0.056	3.170	2.204	0.012	−4.531	···	0.104	0.301	0.005	0.035	0.066	-10.17	1.27	
GJ 490A	12:57:40	+35:13:30	−0.71	−7.262	−12.915	0.181	4.894	4.418	0.053	−2.265	0.030	0.488	0.632	0.010	0.139	0.082	1.18	2.31	
GJ 512A	13:28:21	−02:21:37	−0.88	−5.844	−4.308	0.090	3.124	2.902	0.274	0.554	0.046	0.445	0.515	0.119	0.102	0.277	-37.90	1.66	
GJ 1185	14:47:53	−03:09:15	+1.61	5.363	5.182	0.130	4.738	4.497	0.355	0.309	0.060	0.766	0.524	0.053	0.054	0.213	-57.71	3.49	
LHS 3056	15:19:12	−12:45:06	−1.29	8.662	7.622	0.030	1.759	1.333	0.136	0.776	0.021	0.664	0.326	0.109	0.091	0.235	-21.86	2.21	
GJ 615.2D	16:13:56	+33:46:24	+1.00	−4.258	−3.432	0.098	3.992	3.345	0.263	0.202	0.046	0.864	0.496	0.098	0.096	0.271	-11.03	2.06	
GJ 625	16:25:24	+54:18:14	+0.79	−6.045	−4.641	0.086	6.948	5.986	0.327	0.319	0.051	···	0.474	0.095	0.081	0.318	-13.36	1.95	
GJ 2121	16:30:13	−14:39:49	−0.88	5.281	6.124	0.087	2.613	2.472	0.163	0.425	0.034	0.419	0.456	0.074	0.084	0.242	-118.08	1.39	
GJ 643	16:55:25	−08:19:21	+0.50	−1.052	−.964	0.111	5.966	5.460	0.336	0.399	0.057	0.492	0.545	0.075	0.088	0.242	17.60	1.93	
GJ 1216	17:20:46	+49:15:20	+0.88	1.602	0.983	0.108	4.414	3.892	0.331	0.329	0.058	0.612	0.644	0.083	0.095	0.262	-20.90	1.89	
LHS 461B	18:18:03	+38:46:36	+0.74	−1.820	−1.030	0.123	4.539	4.438	0.329	0.407	0.055	0.922	0.650	0.063	0.098	0.223	-0.23	2.34	
GJ 731	18:51:51	+16:34:59	+0.04	−2.920	−2.588	0.073	5.570	4.496	0.202	0.511	0.034	0.502	0.426	0.110	0.087	0.287	-12.27	1.40	
GJ 740	18:58:00	+05:54:29	−0.23	−0.588	−4.049	0.090	5.801	5.343	0.198	0.610	0.032	0.748	0.441	0.118	0.100	0.337	13.26	1.48	
GJ 745A	19:07:05	+20:53:17	+0.87	6.305	8.062	0.079	6.385	5.688	0.315	0.291	0.047	0.391	0.488	0.072	0.068	0.261	32.79	1.93	
GJ 745B	19:07:13	+20:52:37	+0.89	8.886	7.598	0.072	5.307	4.203	0.282	0.373	0.040	0.361	0.419	0.060	0.064	0.240	32.77	1.89	
LHS 3445	19:14:39	+19:19:04	−0.87	−7.798	−9.405	0.034	3.047	3.027	0.052	−4.967	0.019	0.081	0.395	0.058	0.024	0.004	-83.29	4.80	(Y)
GJ 1236	19:22:02	+07:02:31	+0.89	−2.708	−1.450	0.101	4.438	4.104	0.316	0.328	0.060	0.867	0.538	0.067	0.082	0.272	25.90	1.52	
LTT 15769	19:45:49	+32:23:13	+0.64	−7.879	−3.871	0.027	5.150	4.012	0.269	0.484	0.050	0.752	0.431	0.083	0.106	0.244	-11.82	1.38	
GJ 1248	20:03:51	+05:59:44	+1.44	1.536	1.985	0.103	6.972	5.995	0.290	0.440	0.060	0.356	0.531	0.056	0.075	0.254	32.04	1.47	(S)
LHS 482	20:05:02	+54:26:03	+1.59	−6.009	−8.538	0.007	5.691	5.378	0.096	−1.809	0.012	0.109	0.226	0.014	0.028	0.199	-147.27	6.50	S
GJ 806	20:45:04	+44:29:56	+0.17	−3.188	−3.033	0.111	5.417	4.521	0.289	0.466	0.041	0.303	0.531	0.118	0.107	0.342	-23.40	1.51	
GJ 803A	20:45:09	−31:20:27	−1.21	···	−4.175	0.017	4.794	3.508	0.265	−3.139	0.024	0.318	0.548	0.122	0.160	0.424	-2.57	3.80	Y
GJ 809	20:53:19	+62:09:15	−0.14	−3.091	−3.414	0.087	4.943	3.742	0.260	0.540	0.035	0.375	0.441	0.126	0.108	0.344	-15.26	1.34	
GJ 846	22:02:10	+01:24:00	−0.11	−3.537	−4.071	0.089	4.826	4.929	0.203	0.536	0.035	0.624	0.434	0.111	0.095	0.275	18.30	2.16	
GJ 863	22:33:02	+09:22:40	+0.11	−4.434	−4.417	0.100	5.476	4.486	0.291	0.379	0.044	0.764	0.449	0.110	0.091	0.271	-4.18	1.41	
GJ 875.1	22:51:53	+31:45:15	−0.69	−3.195	−7.557	0.152	3.619	3.132	0.273	−4.006	0.003	0.880	0.002	0.065	0.063	0.010	0.56	3.53	
GJ 880	22:56:34	+16:33:12	−0.42	−3.789	−4.170	0.090	4.073	4.102	0.247	0.592	0.035	0.216	0.440	0.118	0.097	0.334	-25.79	1.64	
HIP 114066	23:06:04	+63:55:34	−0.35	−4.764	−7.234	0.094	6.026	4.342	0.068	−2.276	0.038	0.467	0.072	0.178	0.162	0.055	-17.31	2.50	Y
GJ 1284	23:30:13	−20:23:27	−1.29	−3.966	−3.634	0.136	4.601	4.163	···	−4.345	0.043	0.169	0.248	0.072	0.087	0.258	35.64	4.63	(Y)
GJ 907	23:48:03	+49:00:57	+1.03	···	···	0.093	7.246	5.710	0.279	0.464	0.057	0.410	0.490	0.065	0.081	0.256	20.06	1.74	S
GJ 908	23:49:12	+02:24:04	+0.67	−5.544	−2.434	0.097	3.868	3.441	0.056	0.491	0.038	0.527	0.427	0.062	0.062	0.257	-70.22	1.89	

[a]Notes in Column 20: Y = known young stars, (Y) = suspected young stars, S = known subdwarf stars, (S) = suspected, but unconfirmed subdwarf stars.

Table 5.3: Published Metallicities for Nearby M Dwarfs.

Star Name	RA	Dec	V	$(V\text{-}K)$	ΔM_V	Bon05		Roj12[a]	Nev14		Gai14	
	2000.0					[Fe/H]	err	[Fe/H]	[Fe/H]	err	[Fe/H]	err
(1)	(2)	(3)	(4)	(5)	(6)	(7)	(8)	(9)	(10)	(11)	(12)	(13)
GJ 2	00:05:11	+45:47:11	9.95	4.10	−0.09	···	···	···	···	···	−0.01	0.08
GJ 1	00:05:24	−37:21:26	8.54	4.02	+0.77	···	···	···	−0.45	0.09	−0.39	0.08
GJ 12	00:15:49	+13:33:22	12.62	4.81	+0.75	···	···	···	−0.29	0.09	···	···
GJ 15A	00:18:23	+44:01:24	8.08	4.06	+0.59	···	···	···	···	···	−0.26	0.08
GJ 15B	00:18:26	+44:01:42	11.06	5.11	+0.97	···	···	···	···	···	−0.20	0.08
GJ 1010B	00:23:28	+77:11:21	14.10	4.99	+0.82	···	···	+0.00	···	···	···	···
GJ 22B	00:32:29	+67:14:08	12.40	6.02	−1.70	···	···	−0.27	···	···	···	···
GJ 27.1	00:39:58	−44:15:12	11.39	4.00	−0.09	···	···	···	···	···	+0.01	0.09
LHS 1134	00:43:25	−41:17:39	13.01	5.30	+0.07	···	···	···	−0.13	0.09	···	···
GJ 1021B	00:45:46	−47:33:07	12.43	4.79	+0.01	−0.08	0.09	···	···	···	···	···
GJ 49	01:02:38	+62:20:42	9.56	4.19	−0.43	···	···	···	+0.15	0.08	···	···
GJ 53.1B	01:07:37	+22:57:17	13.60	4.93	+0.13	+0.07	0.12	+0.21	···	···	···	···
GJ 87	02:12:20	+03:34:32	10.04	3.96	+0.47	···	···	···	−0.32	0.09	−0.36	0.08
GJ 96	02:22:14	+47:52:48	9.41	3.86	−0.19	···	···	···	+0.14	0.08	···	···
GJ 105B	02:36:04	+06:53:12	11.71	5.14	+0.06	−0.19	0.07	···	−0.02	0.09	−0.11	0.08
GJ 107B	02:44:11	+49:13:42	10.06	4.20	−0.20	−0.03	0.09	···	···	···	···	···
LP 993−115	02:45:10	−43:44:32	12.38	5.11	−0.17	···	···	···	−0.07	0.09	···	···
LTT 01445A	03:01:51	−16:35:36	11.22	4.72	+0.65	···	···	···	−0.34	0.09	···	···
GJ 1057	03:13:22	+04:46:29	13.94	6.11	−0.13	···	···	···	−0.10	0.09	···	···
GJ 1065	03:50:43	−06:05:10	12.82	5.07	+0.73	···	···	···	−0.23	0.09	···	···
LHS 1610	03:52:41	+17:01:04	13.85	5.80	+0.03	···	···	−0.07	···	···	···	···
GJ 163	04:09:15	−53:22:25	11.84	4.71	−0.34	···	···	···	+0.07	0.09	···	···
GJ 1068	04:10:28	−53:36:08	13.60	5.70	+0.73	···	···	···	−0.43	0.20	···	···
GJ 166C	04:15:22	−07:39:35	11.24	5.28	+0.03	−0.33	0.06	−0.15	−0.12	0.20	···	···
GJ 173	04:37:41	−11:02:19	10.34	4.25	−0.03	···	···	···	···	···	−0.04	0.08
GJ 1072	04:50:50	+22:07:22	15.20	6.22	−0.14	···	···	+0.21	···	···	···	···
GJ 179	04:52:05	+06:28:35	11.98	5.04	−0.60	···	···	+0.23	+0.12	0.09	+0.20	0.09
LHS 1731	05:03:20	−17:22:25	11.69	4.75	+0.45	···	···	···	−0.19	0.09	−0.12	0.08
GJ 191	05:11:40	−45:01:06	8.85	3.80	+1.78	−0.99	0.04	···	−0.85	0.09	···	···
GJ 192	05:12:42	+19:39:56	10.75	4.28	−0.07	···	···	···	···	···	−0.09	0.09
GJ 203	05:28:00	+09:38:38	12.47	4.93	+0.68	···	···	···	−0.22	0.09	···	···
GJ 205	05:31:27	−03:40:38	7.95	3.91	−0.19	+0.21	0.13	+0.35	+0.19	0.09	+0.43	0.08
LTT 11684	05:34:51	+13:52:25	11.81	4.87	−0.38	···	···	···	···	···	+0.02	0.08
GJ 212	05:41:30	+53:29:23	9.76	4.00	−0.24	+0.04	0.11	+0.03	···	···	+0.11	0.08
GJ 213	05:42:09	+12:29:21	13.32	4.99	−0.20	···	···	−0.25	−0.11	0.09	−0.21	0.08
G 099−049	06:00:03	+02:42:23	11.31	5.27	+0.04	···	···	+0.08	···	···	···	···
LHS 1805	06:01:11	+59:35:01	11.71	5.07	+0.10	···	···	···	···	···	+0.03	0.08
LHS 1809	06:02:29	+49:50:58	14.53	6.10	+0.28	···	···	−0.01	···	···	···	···
LP 838−016	06:07:43	−25:44:41	11.89	4.72	+0.28	···	···	···	···	···	−0.15	0.08
GJ 229A	06:10:34	−21:51:52	8.14	3.97	−0.18	···	···	···	−0.03	0.09	+0.12	0.10
L 032−008	06:33:46	−75:37:30	11.43	4.87	−0.06	···	···	···	−0.06	0.09	···	···
GJ 239	06:37:10	+17:33:53	9.64	3.78	+0.62	···	···	···	···	···	−0.34	0.09
G 108−021	06:42:09	+03:35:41	12.06	4.73	+0.62	···	···	···	−0.02	0.09	···	···
GJ 1092	06:49:05	+37:06:51	13.78	5.01	+1.10	···	···	−0.35	···	···	···	···
GJ 251	06:54:48	+33:16:05	10.02	4.75	−0.13	···	···	−0.07	···	···	+0.00	0.08
GJ 273	07:27:24	+05:13:32	9.85	4.99	−0.06	···	···	−0.17	−0.01	0.09	−0.11	0.08
GJ 1097	07:28:45	−03:17:53	11.43	4.73	−0.25	···	···	···	···	···	−0.01	0.08
GJ 277.1	07:34:27	+62:56:29	10.49	3.93	+0.72	···	···	···	···	···	−0.37	0.08
GJ 299	08:11:58	+08:46:23	12.86	5.20	+1.18	···	···	−0.46	−0.53	0.09	···	···
GJ 317	08:40:55	−23:28:00	12.01	4.98	−0.91	···	···	···	+0.22	0.09	···	···
GJ 1123	09:17:05	−77:49:23	13.15	5.70	−0.27	···	···	···	+0.15	0.09	···	···
GJ 341	09:21:37	−60:16:55	9.49	3.90	+0.06	···	···	···	−0.14	0.09	···	···
GJ 1125	09:30:44	+00:19:22	11.72	4.85	+0.08	···	···	···	−0.09	0.09	−0.10	0.08
GJ 353	09:31:56	+36:19:12	10.22	3.92	+0.11	···	···	···	···	···	−0.20	0.08

[a] Errors on Rojas-Ayala et al. (2012) [Fe/H] values are all 0.17 dex.
Metallicity references: Bon05: Bonfils et al. (2005); Roj12: Rojas-Ayala et al. (2012); Nev14: Neves et al. (2014); Gai14: Gaidos & Mann (2014).

Table 5.3: Published Metallicities for Nearby M Dwarfs.

Star Name	RA	Dec	V	(V-K)	ΔM_V	Bon05		Roj12[a]	Nev14		Gai14	
	2000.0					[Fe/H]	err	[Fe/H]	[Fe/H]	err	[Fe/H]	err
(1)	(2)	(3)	(4)	(5)	(6)	(7)	(8)	(9)	(10)	(11)	(12)	(13)
GJ 358	09:39:46	−41:04:03	10.78	4.72	−0.46	···	···	···	−0.01	0.09	···	···
GJ 361	09:41:10	+13:12:34	10.40	4.27	−0.08	···	···	···	···	···	−0.05	0.08
GJ 1129	09:44:47	−18:12:48	12.46	5.20	−0.20	···	···	···	+0.05	0.09	···	···
GJ 373	09:56:08	+62:47:18	8.97	3.77	−0.22	···	···	···	···	···	+0.11	0.08
GJ 382	10:12:17	−03:44:44	9.29	4.28	−0.42	···	···	···	+0.02	0.09	+0.11	0.08
GJ 388	10:19:36	+19:52:11	9.29	4.70	−0.45	···	···	+0.28	+0.12	0.20	+0.16	0.08
GJ 390	10:25:10	−10:13:43	10.17	4.14	−0.15	···	···	···	···	···	−0.02	0.08
LHS 288	10:44:21	−61:12:35	13.90	6.17	+0.96	···	···	···	−0.55	0.20	···	···
GJ 402	10:50:52	+06:48:29	11.70	5.33	−0.29	···	···	+0.20	+0.03	0.09	+0.20	0.08
LP 731−076	10:58:28	−10:46:30	14.44	5.80	−0.09	···	···	···	+0.08	0.11	···	···
GJ 411	11:03:20	+35:58:11	7.46	4.21	+0.40	−0.42	0.07	−0.41	···	···	−0.30	0.08
GJ 412A	11:05:28	+43:31:36	8.77	4.00	+0.80	−0.43	0.05	−0.40	···	···	···	···
GJ 414B	11:11:05	+30:26:45	9.98	4.25	−0.55	+0.02	0.11	···	···	···	···	···
GJ 424	11:20:04	+65:50:47	9.32	3.79	+0.49	···	···	···	···	···	−0.41	0.08
GJ 433	11:35:26	−32:32:23	9.84	4.22	+0.01	···	···	···	−0.17	0.09	···	···
GJ 1148	11:41:44	+42:45:07	11.92	5.10	−0.61	···	···	+0.05	···	···	−0.04	0.08
GJ 438	11:43:19	−51:50:25	10.35	4.03	+0.55	···	···	···	−0.36	0.09	···	···
GJ 445	11:47:41	+78:41:28	10.79	4.84	+0.53	···	···	−0.25	···	···	···	···
GJ 1156	12:18:59	+11:07:34	13.80	6.23	+0.11	···	···	+0.15	···	···	···	···
GJ 480.1	12:40:46	−43:33:59	12.24	4.83	+1.12	···	···	···	−0.48	0.09	···	···
GJ 486	12:47:56	+09:45:05	11.40	5.04	−0.35	···	···	···	+0.03	0.09	···	···
GJ 505B	13:16:51	+17:01:01	9.60	3.85	+0.15	−0.25	0.05	···	···	···	···	···
GJ 514	13:29:59	+10:22:37	9.05	4.01	+0.05	···	···	···	···	···	−0.08	0.08
GJ 526	13:45:43	+14:53:29	8.46	4.05	+0.11	−0.10	0.07	−0.30	−0.22	0.09	−0.18	0.09
GJ 536	14:01:03	−02:39:17	9.68	4.00	+0.12	···	···	···	−0.14	0.09	···	···
GJ 581	15:19:26	−07:43:20	10.55	4.71	+0.28	···	···	−0.10	−0.20	0.09	−0.10	0.08
GJ 611B	16:04:47	+39:09:35	14.23	5.07	+1.22	···	···	−0.45	···	···	···	···
LP 804−027	16:12:41	−18:52:31	11.37	4.78	−0.90	···	···	+0.46	···	···	···	···
GJ 625	16:25:24	+54:18:14	10.11	4.28	+0.81	···	···	−0.23	···	···	−0.36	0.08
GJ 628	16:30:18	−12:39:45	10.07	5.00	−0.13	···	···	−0.02	−0.02	0.09	−0.02	0.08
GJ 643	16:55:25	−08:19:21	11.77	5.05	+0.55	···	···	−0.22	−0.26	0.09	···	···
GJ 649	16:58:08	+25:44:39	9.69	4.07	−0.08	···	···	−0.04	···	···	+0.00	0.08
LTT 15087	17:11:34	+38:26:33	11.61	4.81	−0.35	···	···	···	···	···	+0.03	0.08
GJ 1214	17:15:18	+04:57:50	14.71	5.93	+0.06	···	···	+0.20	+0.05	0.09	···	···
GJ 676A	17:30:11	−51:38:13	9.59	3.77	−0.50	···	···	···	+0.26	0.09	···	···
GJ 678.1A	17:30:22	+05:32:54	9.30	3.88	+0.04	···	···	···	−0.14	0.09	···	···
GJ 686	17:37:53	+18:35:30	9.61	4.04	+0.41	···	···	−0.28	−0.35	0.09	−0.25	0.08
GJ 2130A	17:46:12	−32:06:09	10.50	4.25	−0.41	···	···	···	···	···	+0.12	0.08
GJ 693	17:46:34	−57:19:08	10.77	5.05	−0.40	···	···	···	−0.28	0.09	···	···
GJ 699	17:57:48	+04:41:36	9.57	5.05	+1.13	···	···	−0.39	−0.51	0.09	−0.32	0.08
GJ 701	18:05:07	−03:01:52	9.37	4.06	+0.19	−0.20	0.08	···	−0.27	0.09	−0.24	0.08
GJ 1224	18:07:31	−15:58:15	13.51	5.68	+0.54	···	···	−0.05	−0.25	0.20	···	···
G 141−029	18:42:45	+13:54:17	12.84	5.29	−0.12	···	···	···	−0.08	0.20	···	···
LHS 3409	18:45:44	+52:28:20	15.13	4.91	+1.78	···	···	−0.52	···	···	···	···
GJ 729	18:49:49	−23:50:10	10.50	5.13	+0.76	···	···	···	−0.40	0.20	−0.12	0.08
GJ 745B	19:07:13	+20:52:37	10.76	4.24	+0.91	···	···	···	···	···	−0.33	0.08
GJ 1236	19:22:02	+07:02:31	12.39	4.70	+0.95	···	···	···	−0.47	0.09	···	···
LHS 482	20:05:02	+54:26:03	12.00	3.89	+1.60	···	···	−0.64	···	···	···	···
GJ 783.2B	20:11:06	+16:11:16	13.98	5.10	+0.15	−0.16	0.08	−0.29	···	···	···	···
GJ 1253	20:26:05	+58:34:23	14.04	5.95	+0.06	···	···	+0.16	···	···	···	···
GJ 1254	20:33:40	+61:45:14	12.54	5.14	−0.83	···	···	+0.24	···	···	···	···
GJ 1256	20:40:33	+15:29:59	13.45	5.70	−0.15	···	···	+0.20	+0.06	0.09	···	···
GJ 806	20:45:04	+44:29:56	10.77	4.24	+0.20	···	···	−0.11	···	···	···	···
LP 816−060	20:52:33	−16:58:29	11.50	5.30	−0.03	···	···	+0.06	−0.07	0.09	···	···
GJ 809	20:53:19	+62:09:15	8.56	3.94	−0.12	−0.13	0.10	−0.21	···	···	−0.01	0.08

[a] Errors on Rojas-Ayala et al. (2012) [Fe/H] values are all 0.17 dex.
Metallicity references: Bon05: Bonfils et al. (2005); Roj12: Rojas-Ayala et al. (2012); Nev14: Neves et al. (2014); Gai14: Gaidos & Mann (2014).

Table 5.3: Published Metallicities for Nearby M Dwarfs.

Star Name	RA	Dec	V	$(V\text{-}K)$	ΔM_V	Bon05		Roj12[a]	Nev14		Gai14	
	2000.0					[Fe/H]	err	[Fe/H]	[Fe/H]	err	[Fe/H]	err
(1)	(2)	(3)	(4)	(5)	(6)	(7)	(8)	(9)	(10)	(11)	(12)	(13)
LTT 16135	20:58:41	+34:16:27	11.06	3.81	+0.02	···	···	−0.05	···	···	···	···
GJ 821	21 09 17	−13 18 09	10.87	3.96	+0.98	···	···	···	···	···	−0.45	0.09
GJ 832	21:33:33	−49:00:32	8.66	4.16	+0.27	···	···	···	−0.17	0.09	···	···
GJ 846	22:02:10	+01:24:00	9.17	3.85	−0.09	···	···	···	+0.01	0.09	+0.03	0.08
LHS 3746	22:02:29	−37:04:51	11.76	5.04	+0.27	···	···	···	−0.13	0.09	···	···
GJ 849	22:09:40	−04:38:26	10.38	4.79	−0.90	···	···	+0.31	+0.22	0.09	+0.35	0.09
LHS 3799	22:23:07	−17:37:01	13.30	5.98	−0.24	···	···	+0.38	+0.10	0.20	···	···
GJ 873	22:46:49	+44:20:02	10.22	4.92	−0.11	···	···	−0.01	···	···	−0.03	0.09
GJ 876	22:53:16	−14:15:49	10.18	5.17	−0.63	···	···	+0.19	+0.14	0.09	+0.17	0.08
GJ 880	22:56:34	+16:33:12	8.65	4.13	−0.38	···	···	···	+0.03	0.09	+0.17	0.08
GJ 887	23:05:52	−35:51:11	7.34	3.88	+0.47	−0.22	0.09	···	−0.24	0.09	−0.15	0.08
GJ 891	23:10:15	−25:56:52	11.27	4.28	+0.04	···	···	···	···	···	−0.22	0.08
LHS 543	23:21:37	+17:17:25	11.65	5.14	−0.90	···	···	···	+0.23	0.09	+0.19	0.08
GJ 895	23:24:30	+57:51:15	10.00	4.13	−0.44	···	···	···	···	···	+0.24	0.08
GJ 908	23:49:12	+02:24:04	8.98	3.94	+0.89	···	···	−0.59	−0.44	0.09	−0.47	0.08

[a]Errors on Rojas-Ayala et al. (2012) [Fe/H] values are all 0.17 dex.
Metallicity references: Bon05: Bonfils et al. (2005); Roj12: Rojas-Ayala et al. (2012); Nev14: Neves et al. (2014); Gai14: Gaidos & Mann (2014).

Table 5.4: Radial Velocities by Star Type.

Star Type	# of Stars	RV Avg. (km s^{-1})	RV Med. (km s^{-1})	RV SD (km s^{-1})
Subdwarf	5	49.8	18.3	56.7
Main Sequence	65	26.7	17.6	25.8
Young	10	37.9	25.8	34.5

Average and median radial velocities and the standard deviations in radial velocities by star type: subdwarfs, main sequence/unknown stars, and young stars. Discussed in §5.4.3.

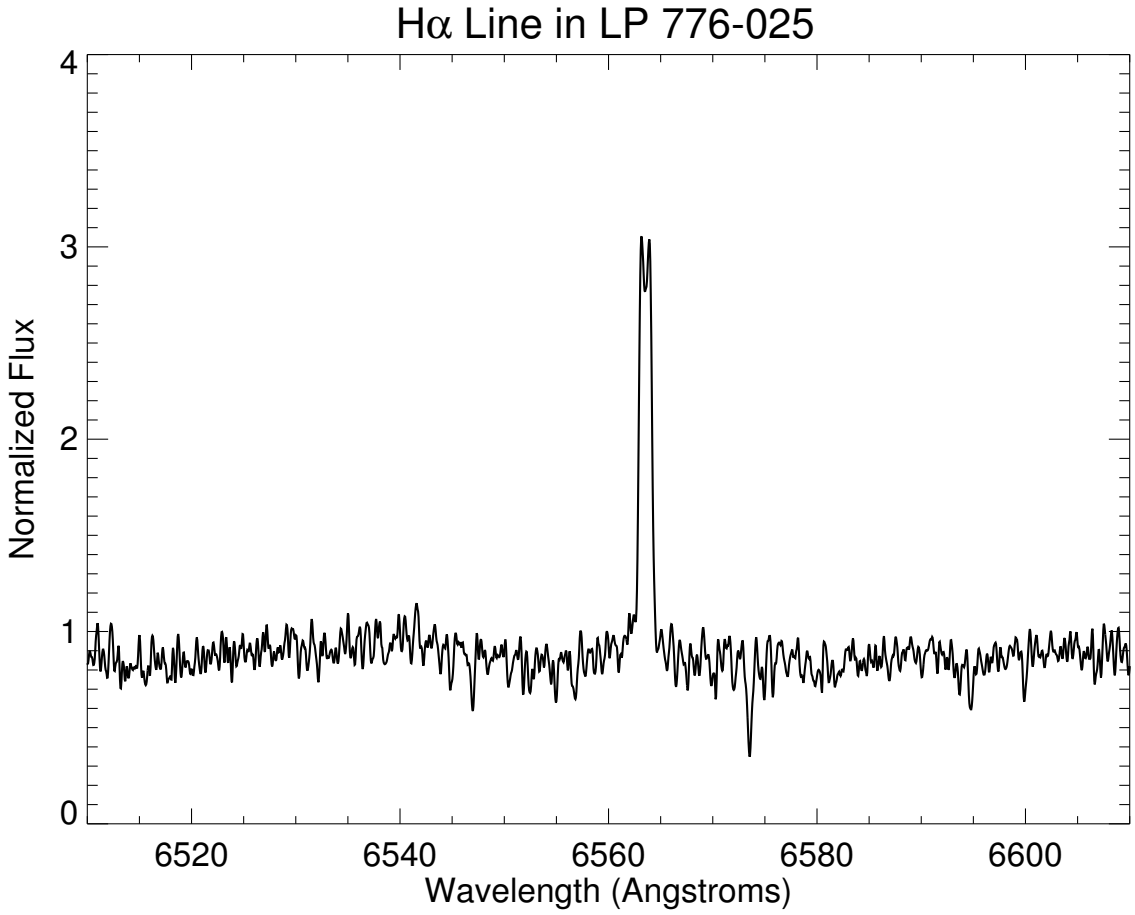

Figure 5.1: The Hα emission line at 6563Å in the spectrum of the known young star LP776-025.

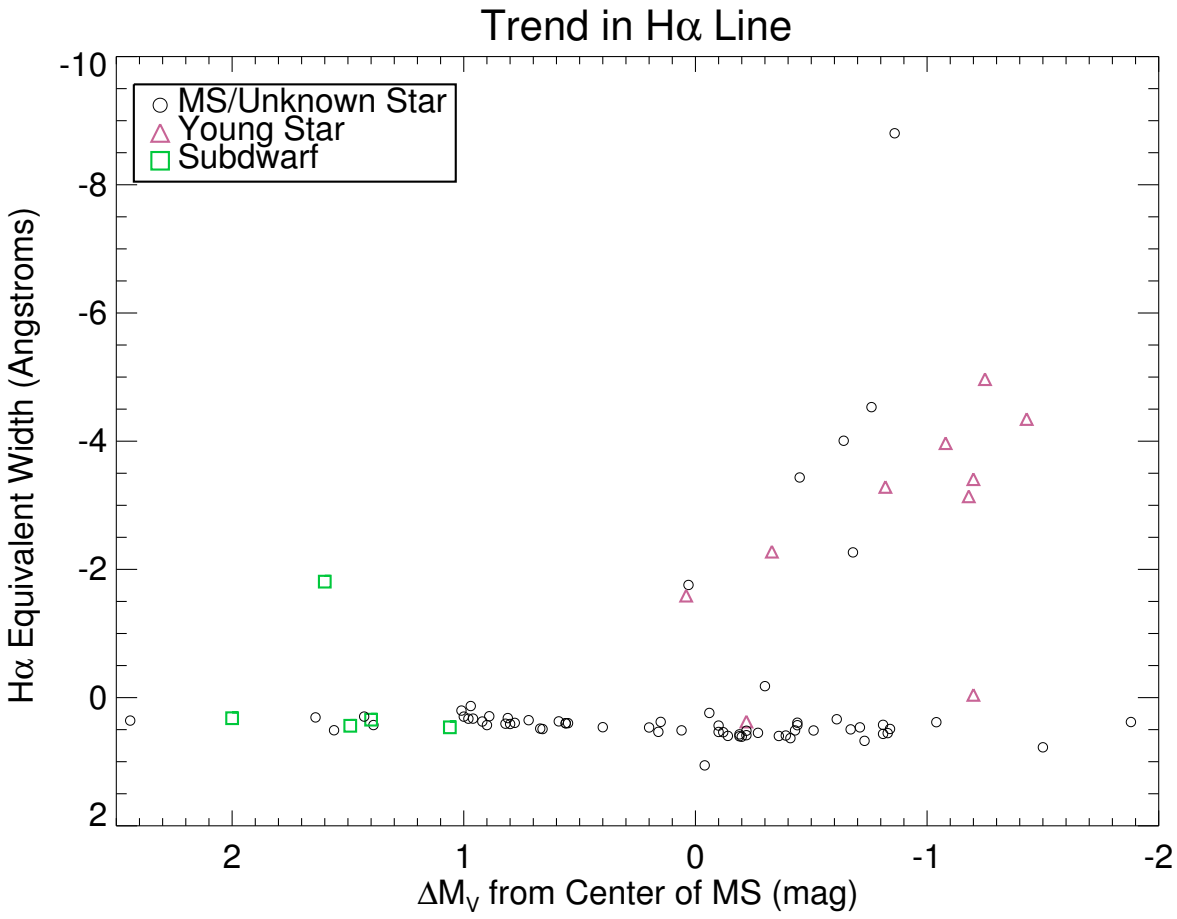

Figure 5.2: The measured EW of Hα for 80 red dwarfs versus the ΔM_V value for each star. Negative values indicate emission, so we reverse the values on the y-axis to better illustrate the increase in magnetic activity. The main sequence (or not yet identified as young of subdwarf) stars are indicated by black circles, subdwarfs by green squares, and young stars by the pink triangles.

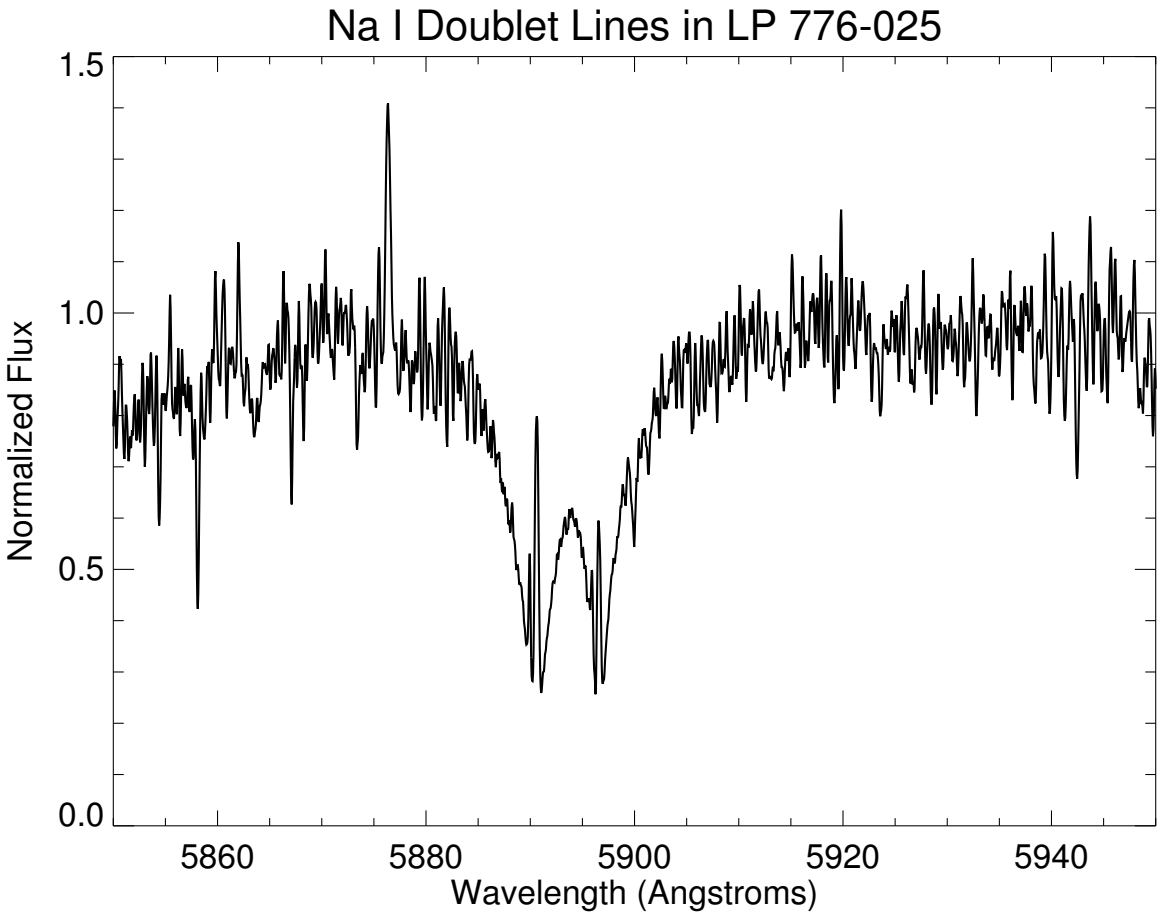

Figure 5.3: The Na I D doublet absorption lines with emission cores at 5890/5896Å in the spectrum of the known young star LP776-025.

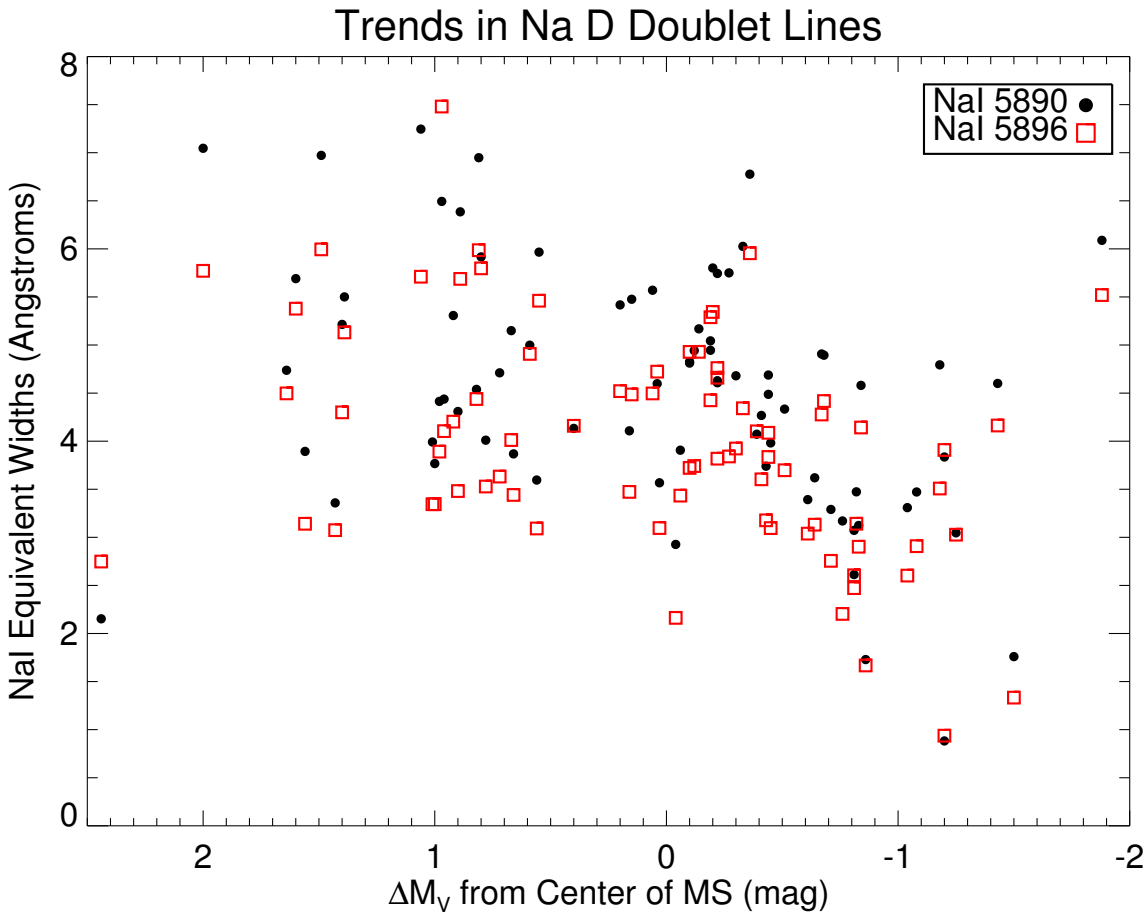

Figure 5.4: The measured EWs for the sodium doublet at 5890/5896Å, Na D (also known as the Fraunhofer D lines), in each spectrum versus the ΔM_V value for each star. Filled black circles indicate the EW measurements for the Na D feature at 5890Å and open red squares represent those for the Na D feature at 5896Å.

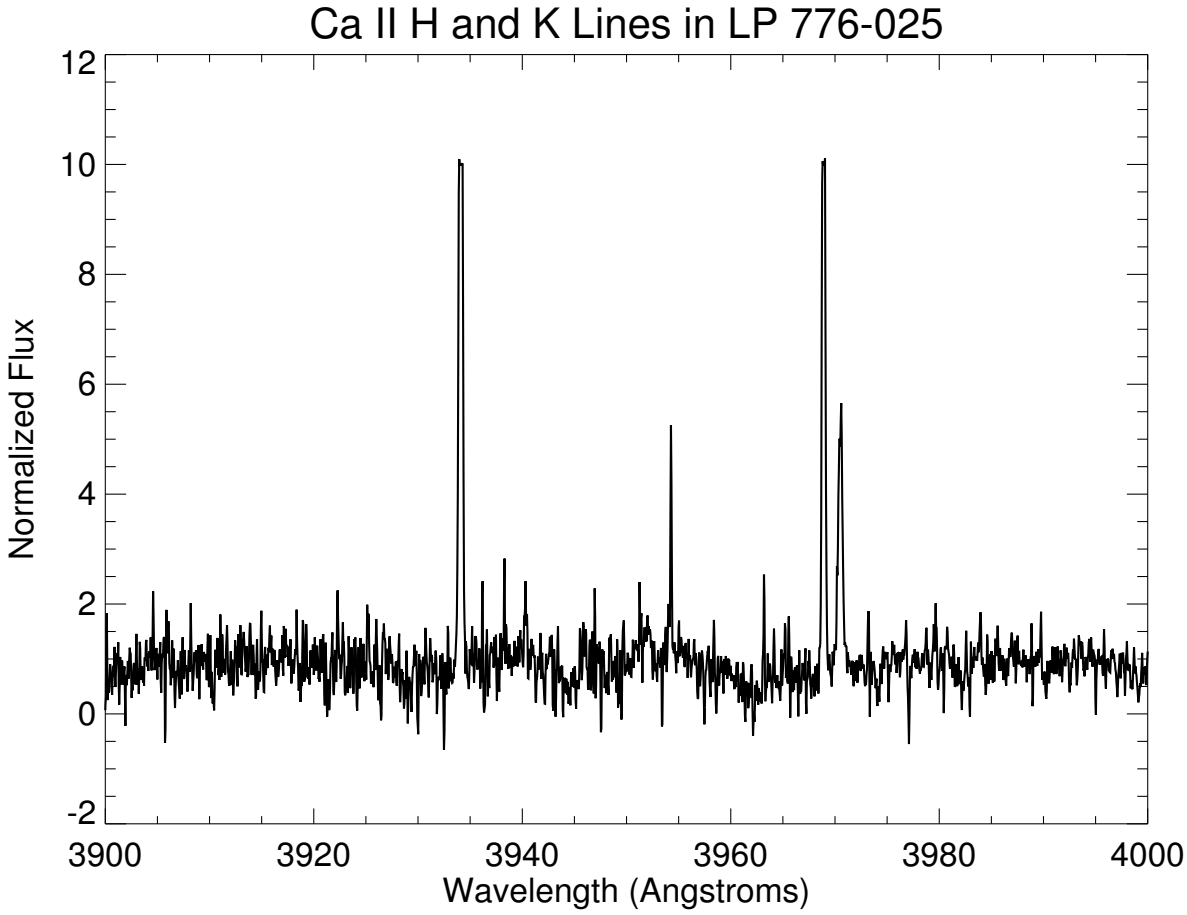

Figure 5.5: The Ca II K and H emission lines at 3933/3968Å in the spectrum of the known young star LP776-025. Note that the emission feature next to the Ca H line is caused by a Hydrogen Balmer line at 3970Å and does not interfere with the measurement of the Ca II feature.

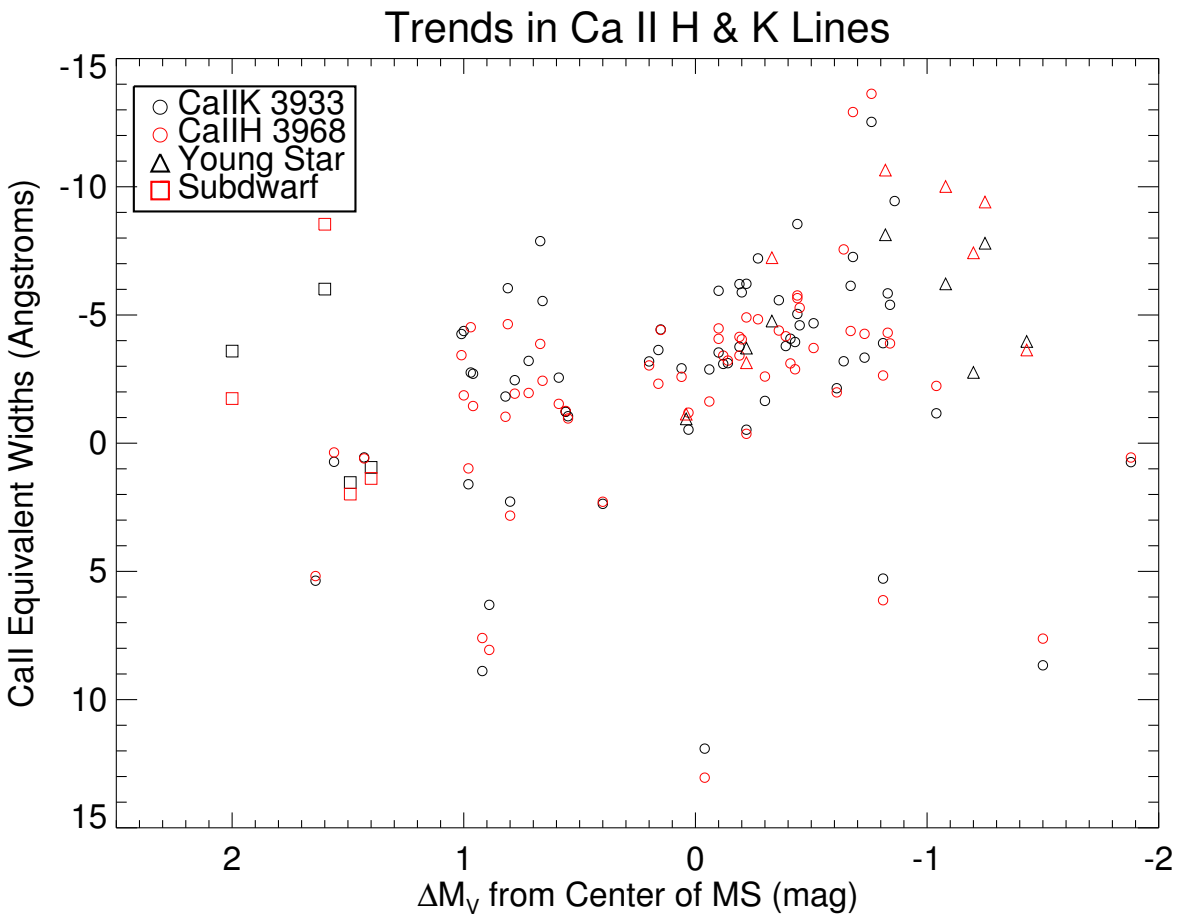

Figure 5.6: The measured EWs for the two Ca H and K features in each spectrum versus the ΔM_V value for each star. Negative values indicate emission, so we reverse the values on the y-axis to better illustrate the increase in magnetic activity. Black circles indicate measurements for the Ca K line at 3933Å and open red circles for the Ca H feature at 3968Å. Triangles indicate known young stars, while squares represent subdwarfs.

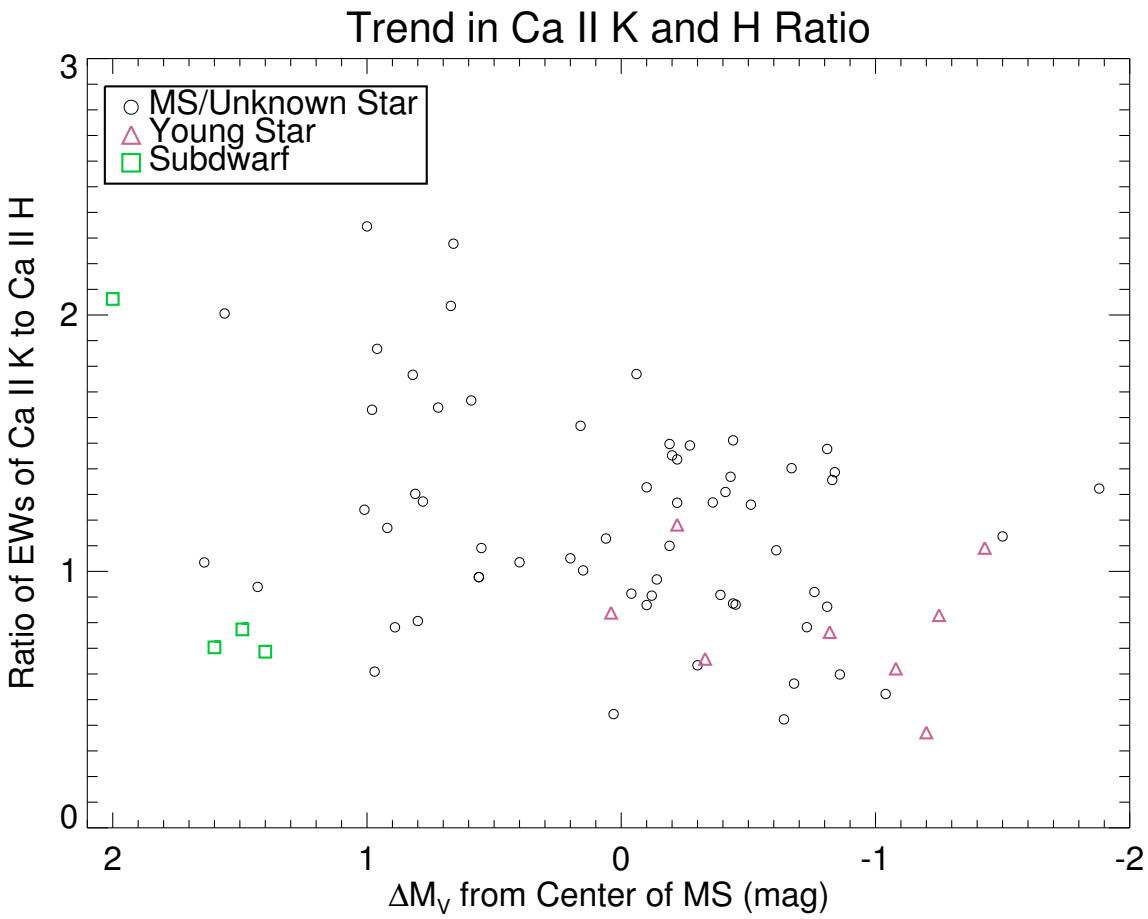

Figure 5.7: The ratio of the EWs of the two Ca H and K features in each spectrum versus the ΔM_V value for each star. Black circles indicate measurements for main sequence (or not yet identified as young of subdwarf) stars, pink triangles represent known young stars, and subdwarfs are indicated by the green squares.

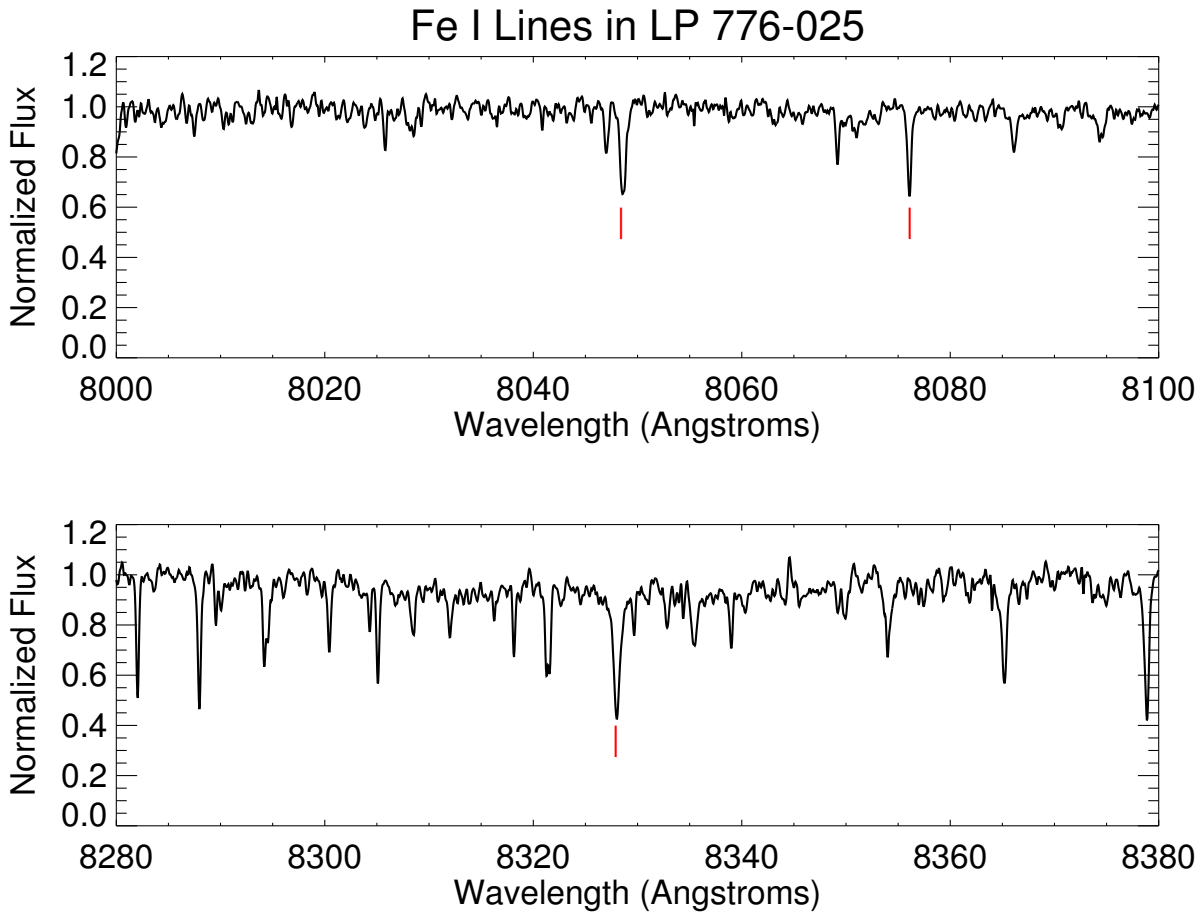

Figure 5.8: The Fe I absorption lines at 8046Å and 8075Å in the top panel and at 8327Å in the bottom panel in the spectrum of the known young star LP776-025.

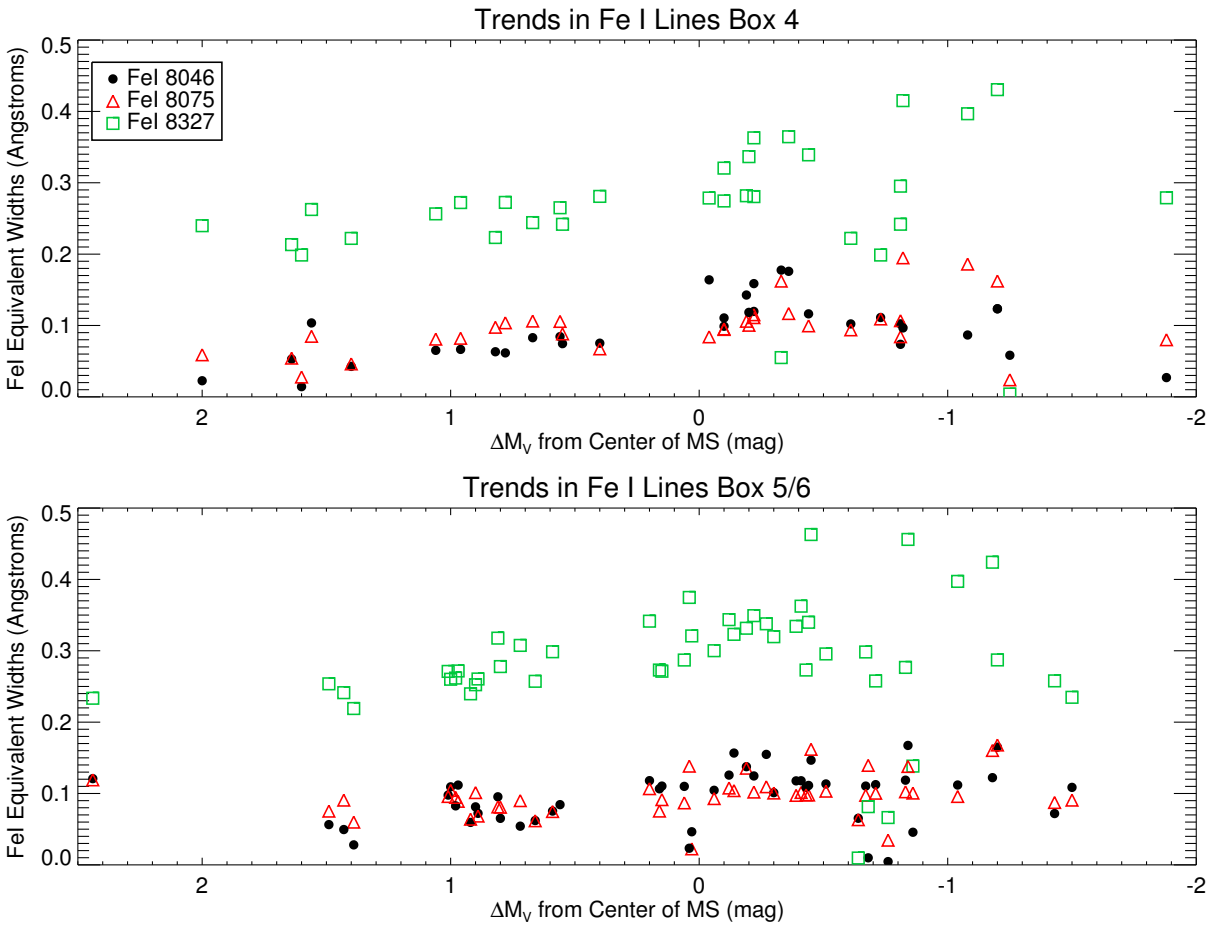

Figure 5.9: The measured EWs for three strong Fe I features for 80 red dwafrs versus the ΔM_V value for each star. Black circles indicate measurements for the Fe I line at 8046Å, red triangles for the feature at 8075Å, and green squares represent the Fe I line at 8327Å.

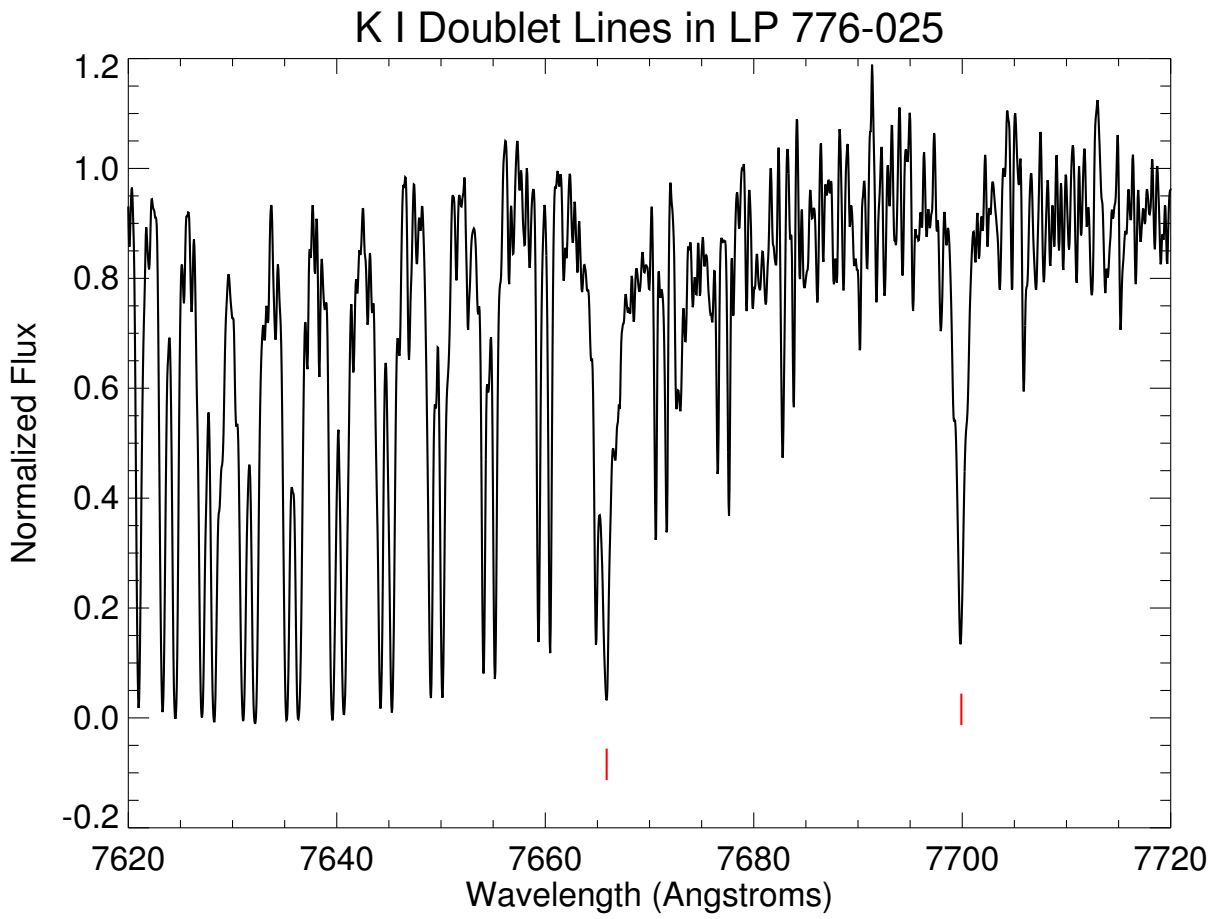

Figure 5.10: The K I doublet absorption lines at 7665/7699Å in the spectrum of the known young star LP776-025. The absorption features between 7620 and 7660Å are caused by water in the Earth's atmosphere.

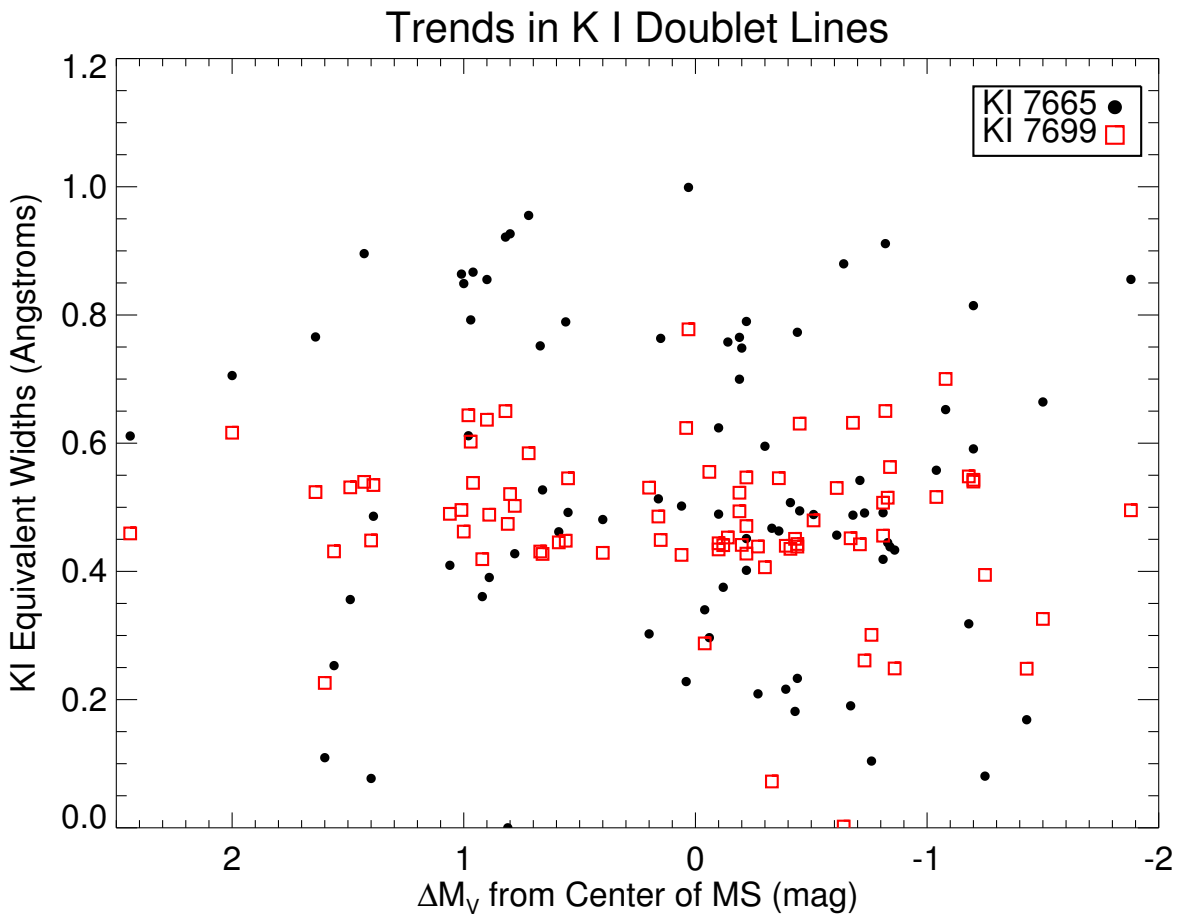

Figure 5.11: The measured EWs for the potassium doublet at 7665Å and 7699Å in each spectrum versus the ΔM_V value for each star. Filled black circles indicate the EW measurements for the K I feature at 7665Å and open red squares represent those for the K I feature at 7699Å.

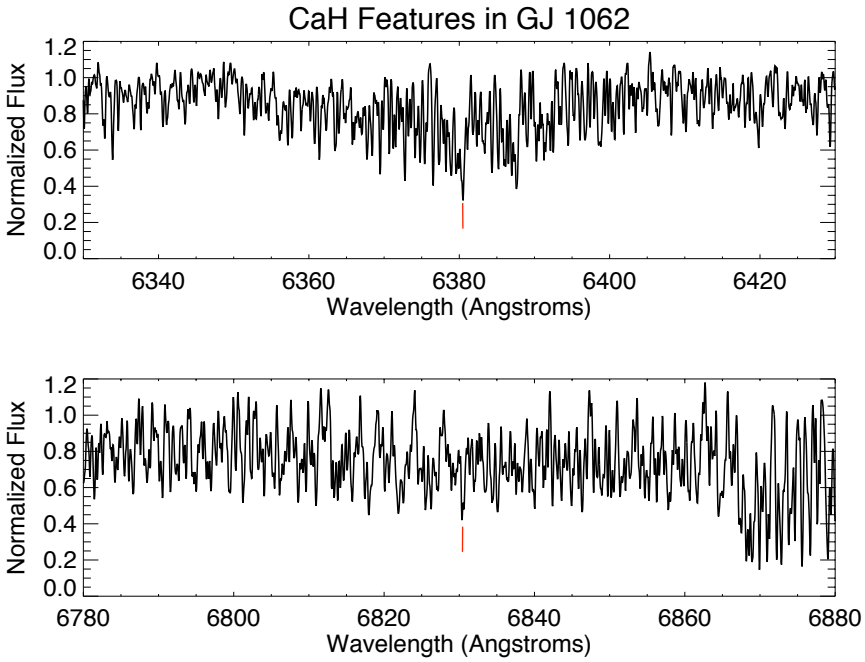

Figure 5.12: The CaH absorption features at 6382Å in the top panel and at 6830Å in the bottom panel in the spectrum of the known subdwarf GJ 1062.

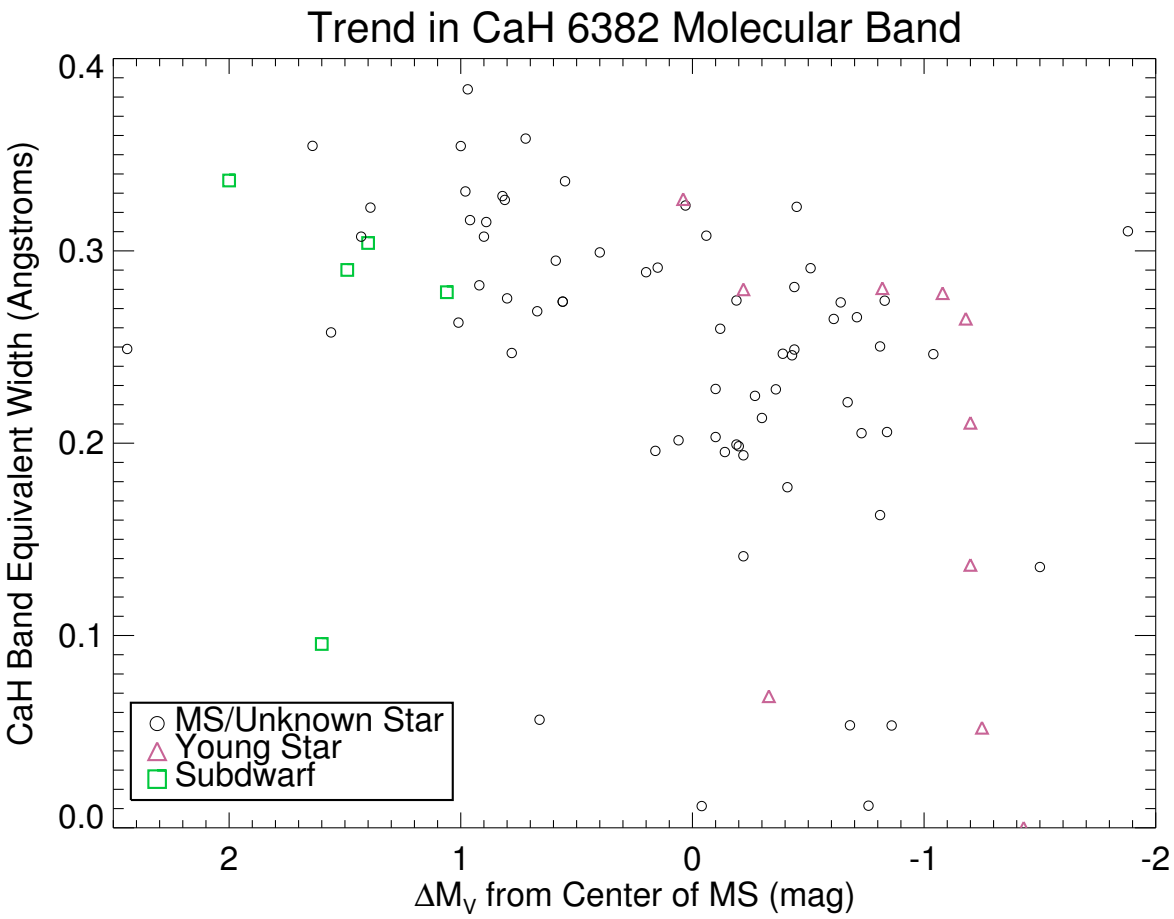

Figure 5.13: The measured EWs of the CaH molecular band at 6382Å for 79 red dwarfs versus the ΔM_V value for each star. Black circles indicate measurements for main sequence (or not yet identified as young of subdwarf), pink triangles represent known young stars, and subdwarfs are indicated by the green squares. The subdwarf outlier at EW $\sim$ 0.1 is LHS 482, the unusual subdwarf flare star.

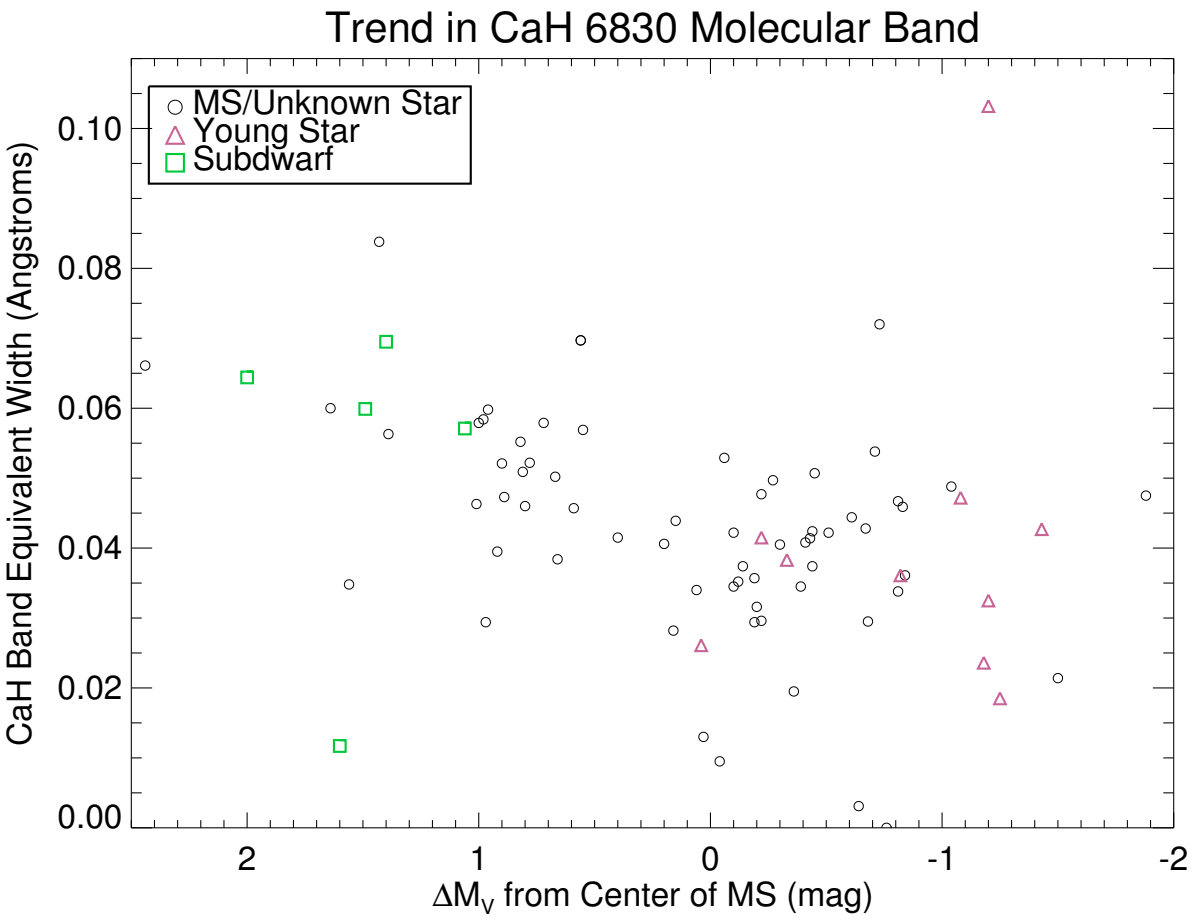

Figure 5.14: The measured EWs of the CaH molecular band at 6830Å for 78 red dwarfs versus the ΔM_V value for each star. Black circles indicate measurements for main sequence (or not yet identified as young or subdwarf) stars, pink triangles represent known young stars, and subdwarfs are indicated by the green squares. The subdwarf outlier at EW $\sim$ 0.01 is LHS 482, the unusual subdwarf flare star.

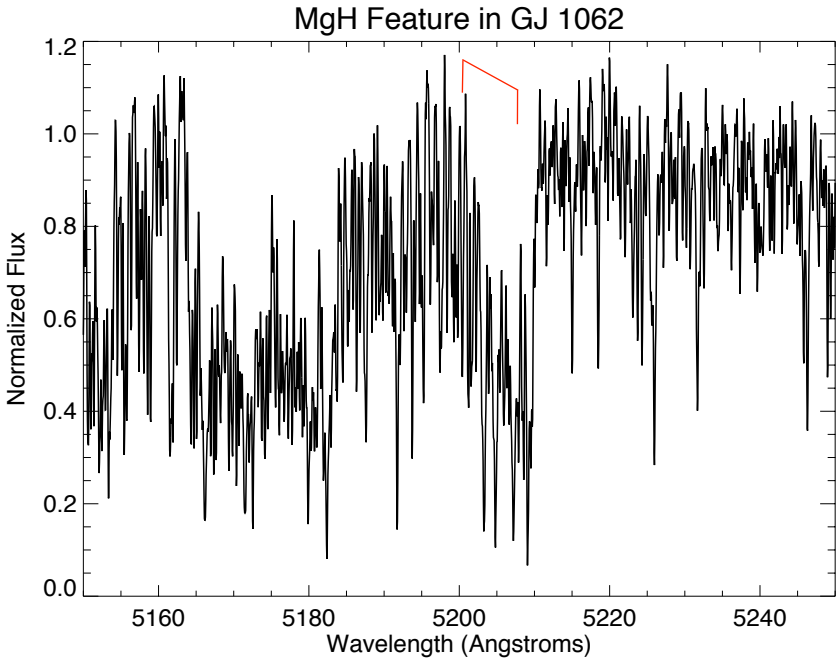

Figure 5.15: The MgH absorption band at 5200Å in the spectrum of the known subdwarf GJ 1062.

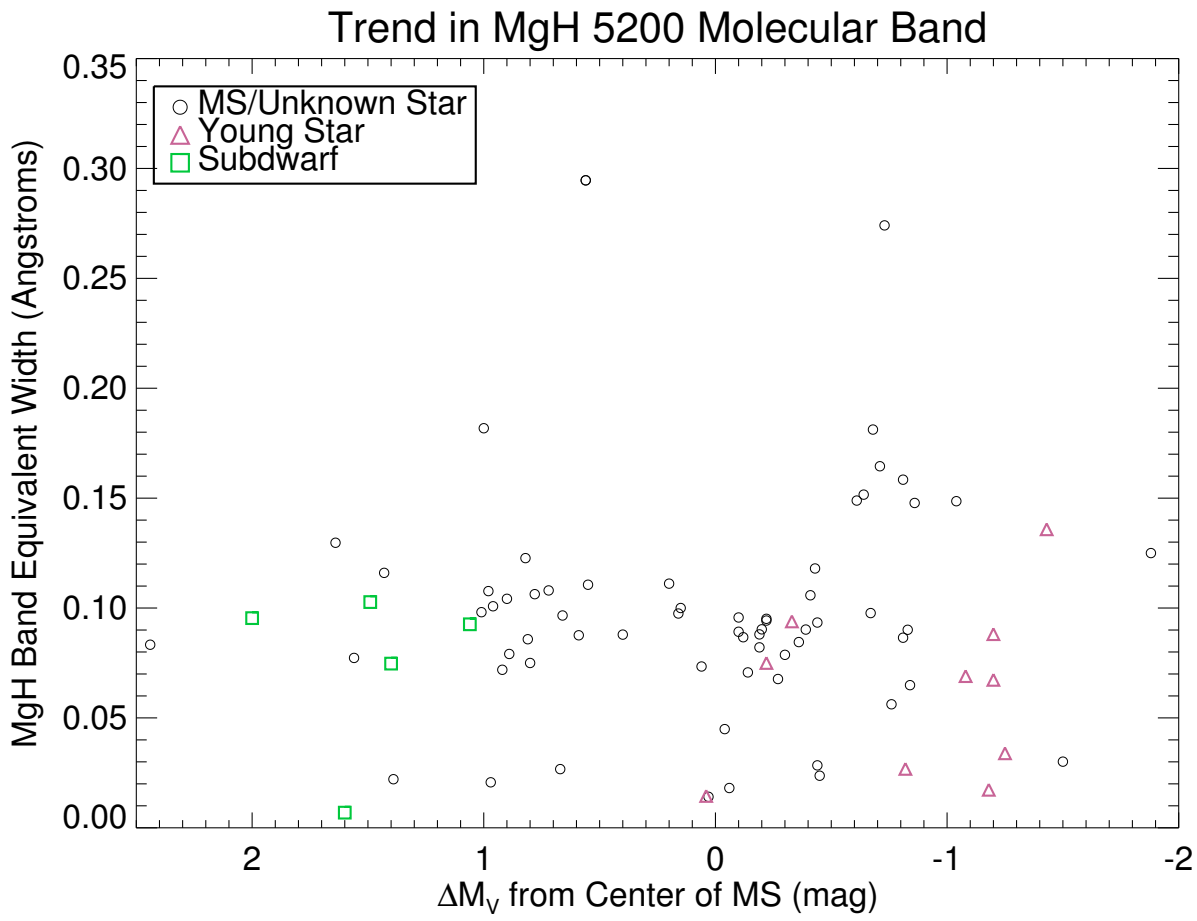

Figure 5.16: The measured EWs of the MgH molecular band at 5200Å for 79 red dwarfs versus the ΔM_V value for each star. Black circles indicate measurements for main sequence (or not yet identified as young or subdwarf) stars, pink triangles represent known young stars, and subdwarfs are indicated by the green squares.

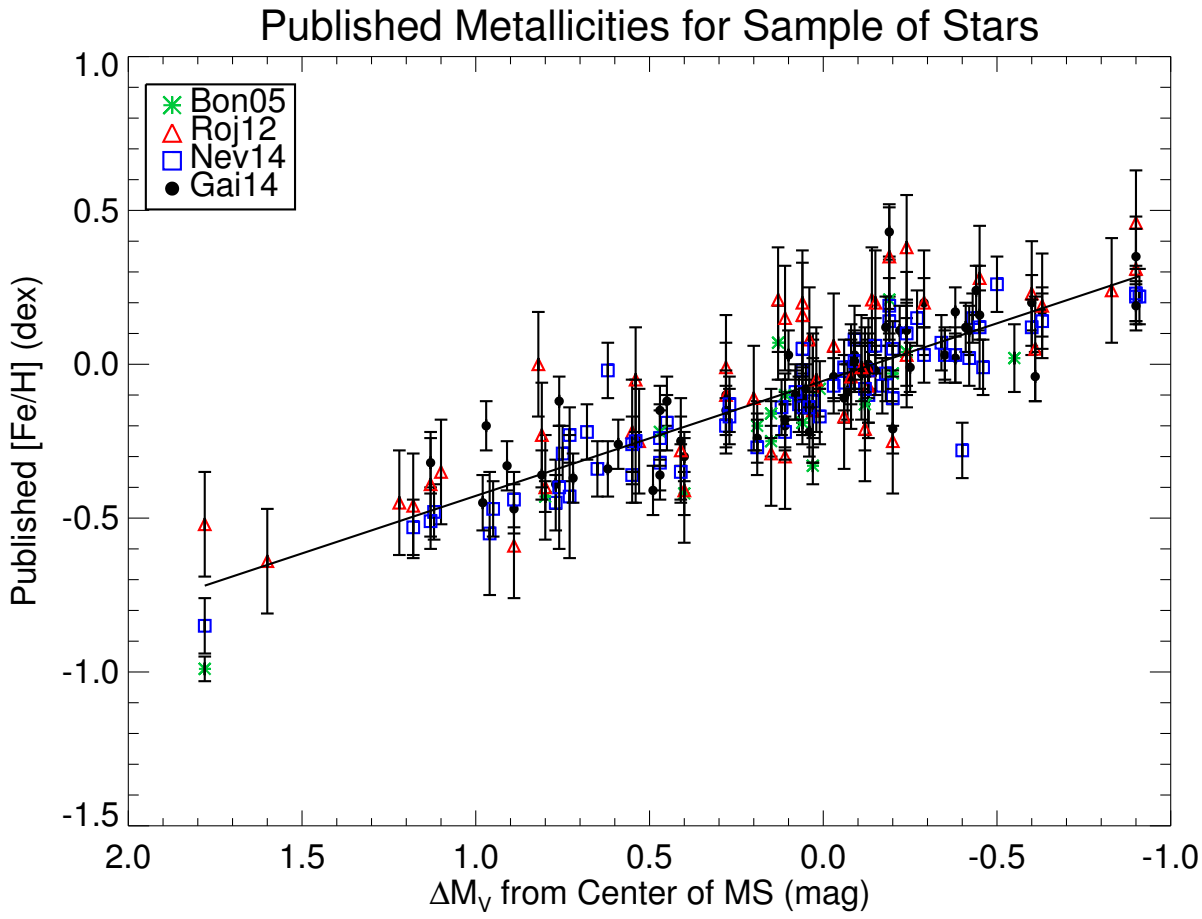

Figure 5.17: Metallicity versus distance from the central distribution of the main sequence (ΔM_V). The linear trend in metallicity is shown by the line fit through the data. Metallicities are as published in Bonfils et al. (2005), Rojas-Ayala et al. (2012), Neves et al. (2014), and Gaidos & Mann (2014), as detailed in §5.4.2 and in Table 5.3.

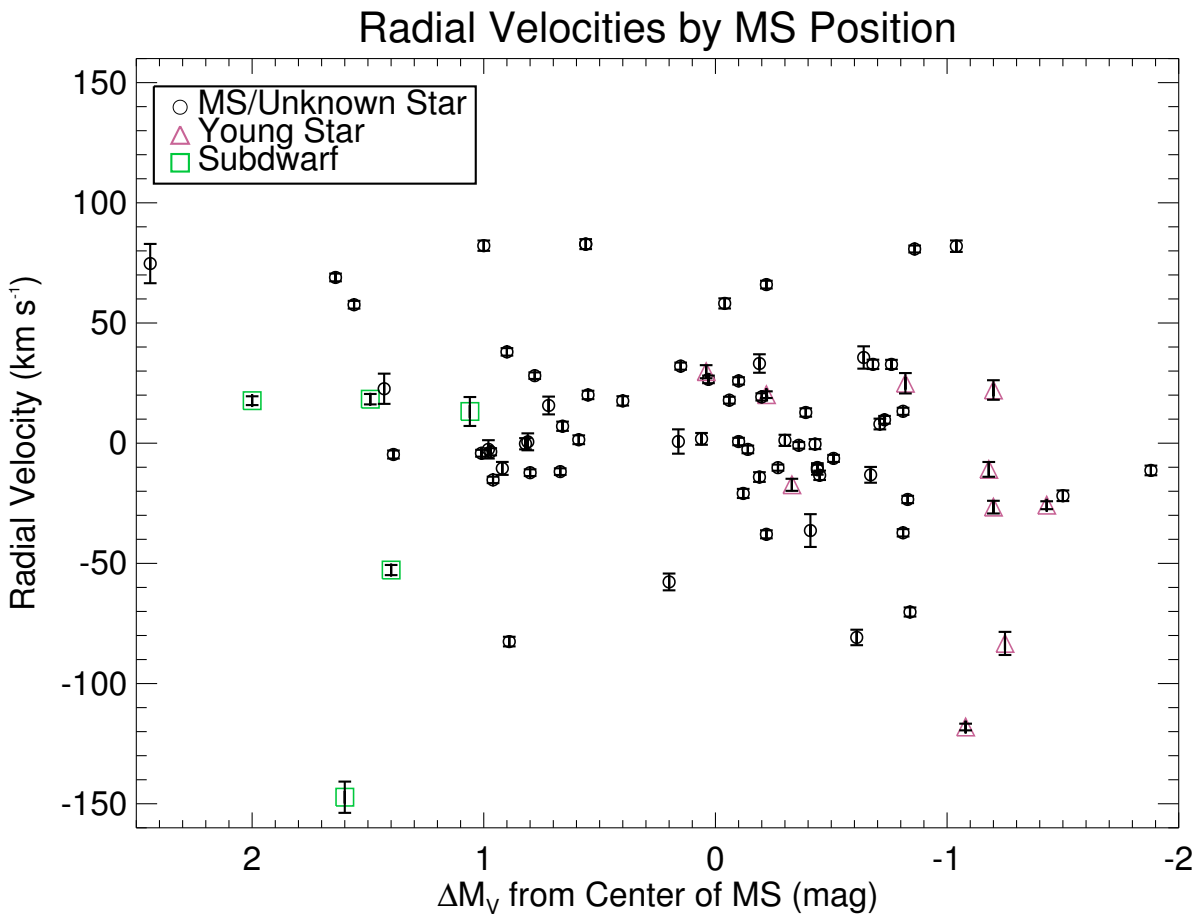

Figure 5.18: The mean of our radial velocity measurements produced by TAME versus the ΔM_V value for each star. The error bars are calculated as the standard deviations of measurements for a star divided by the square root of the number of measurements, as detailed in §5.4.3. Black circles indicate measurements for main sequence (or not yet identified as young or subdwarf) stars, pink triangles represent known young stars, and subdwarfs are indicated by the green squares. The subdwarf outlier at RV ~ -150 is LHS 482, the unusual subdwarf flare star.

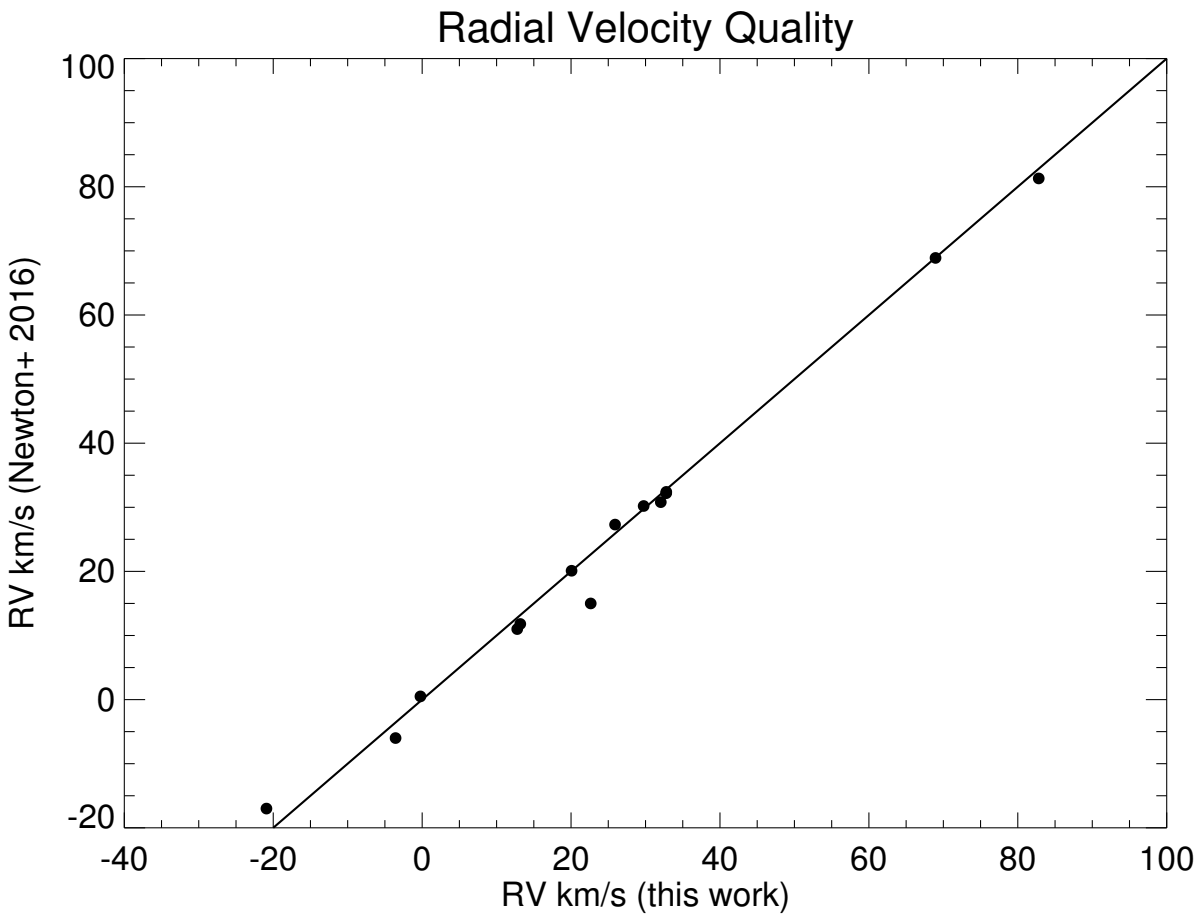

Figure 5.19: This figure serves to check the quality of our radial velocity measurements against those in the literature. We show the measurements of 14 of our radial velocity measurements that are also provided in Newton et al. (2016). The solid line is a one-to-one linear fit included to illustrate the quality of our measurements.

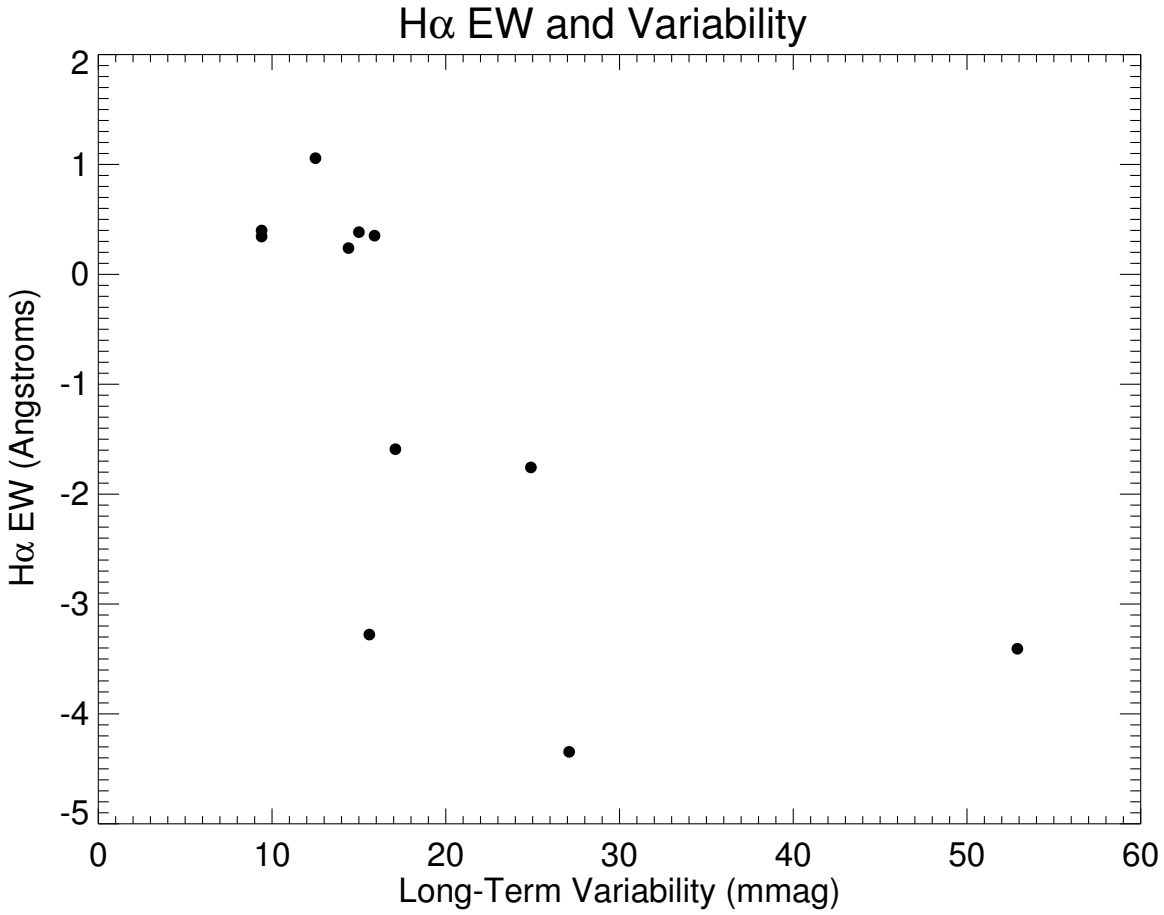

Figure 5.20: The Hα equivalent widths and variability measurements of the 11 stars with results on both the long-term variability study and this spectroscopy work. There is a hint of an increasing trend in the emission strength of Hα with increasing long-term variability measurements.

CHAPTER 6
CONCLUSIONS

6.1 Comparison to Other Works

The study of low mass stars is a vast field with many astronomers working to analyze, model, and better understand these abundant stars that make up at least 75% of the stars in the solar neighborhood (Henry et al. 2006). Their ubiquity has enabled many studies uncovering new properties, processes, and structures for these stars, as well as the theories surrounding how they might work. Considering this, finding something entirely new to study and discover about M dwarfs was not as difficult as would be expected, as there is still much that is not understood about them. While there have been many studies done on the abundances of and magnetic activity in low mass stars separately, very few have done so in reference to the notable widening of the main sequence at M0, and none have explored each of these properties together in the same regard. We were uniquely capable of closely analyzing the effects on the widening of the main sequence due to our access to the RECONS parallax program and all of the data acquired over the last two decades on the stellar population within 25 pc that has been incorporated into the RECONS 25 Parsec Database.

Our long term variability study was made possible by the two decades of parallax data obtained at the CTIO 0.9 m telescope by the RECONS team. This is a study that we were uniquely capable of carrying out with the precision, timescales, and cadences that we have achieved. Similar efforts to study the long term photometric changes and presence of cycles in low mass stars include the recent work by Suárez Mascareño et al. (2016), in which they

used lightcurves from the All Sky Automated Survey (ASAS) with timescales up to nine years for main sequence late-A to mid-M type stars. This rich dataset provided hundreds of photometric measurements for each lightcurve, allowing them to study both rotation periods as well as fitting long-term cycles to the data. Their results found periods for activity cycles of 17 M dwarfs with a mean length of 6.0 yrs for early type and 7.4 yrs for late type M dwarfs, as well as a mean rotation rate of 85.4 days. There have been other previous efforts to assess long-term variability such as those by Weis (1994), Jao et al. (2011), and Hosey et al. (2015). In the work of Weis (1994), photometric measurements of 43 M dwarf stars over an 11 year period were reported, 21 of which showed positive long-term variability detections and two that demonstrated cyclic activity with periods of less than three years. Jao et al. (2011) reported the first study of variability in red subdwarfs, including 130 stars from the RECONS program, and found that the cool subdwarfs are less photometrically variable than their main sequence counterparts. Hosey et al. (2015) examined the long-term variability of 264 M dwarfs in the VRI bands observed in the RECONS program and found that these stars display stronger variability in the V band than in R or I and that a majority of the M dwarfs exhibited low rates of variability, with the exception of a handful of known young stars. There have also been studies using spectroscopic observations to study the magnetic activity within the chromospheres of low mass stars on long-term scales, such as Gomes da Silva et al. (2011, 2012) and Robertson et al. (2013). Each of these studies used multiple measurements of activity indicators, such as Na I and Ca I lines and Hα, over timespans of two to about ten years to study long term activity cycles in these stars. To date, our

study (Clements et al. 2017) is the only one of its kind to analyze long-term variability with respect to the widened main sequence for low mass stars.

There have been several studies on the short term variability of low mass stars, searching for flares and microflares in M dwarf stars to better understand their activity levels, given that they are prime candidates for Earth-like extrasolar planets and understanding their environments is key to understanding the habitability of the planets around them. Such studies include the works of Robinson et al. (1995), Wargelin et al. (2008), Kowalski et al. (2009, 2013, 2016), and Hawley et al. (2014). These studies have been briefly discussed previously in Chapter 4 and particularly in §4.5. Robinson et al. (1995) reported rapid time sequence UV photometry for one M dwarf, CN Leo (GJ 406), over two hours and detected 32 small flare-like events. Wargelin et al. (2008) presented results of X-ray photometric monitoring of another M star, Ross 154 (GJ 729), and detected two large flares as well as evidence of microflare events. The work of Kowalski et al. (2009, 2013, 2016) examined M dwarf lightcurves simultaneously with spectroscopic observations to investigate stellar activity. In their first study, Kowalski et al. (2009) investigated 50,130 M dwarf light curves to examine the flare rate in these stars and found 271 flares with the flaring fraction increasing for redder stars. In each of Kowalski et al. (2013) and Kowalski et al. (2016), five M flare stars were monitored with photometric and spectroscopic techniques simultaneously, in the first they reported 20 flares and the second only detected a flare in one star; these studies found that Balmer emission presented with all of the flares. The effort carried out by Hawley et al. (2014) analyzed Kepler short-cadence M dwarf observations for both active and inactive

stars and found that the active stars showed numerous flares and starspots, while the inactive stars did not. They also found that there is no correlation between flare frequency or energy and starspot phase and that they occurred randomly. None of these works, however, have studied these short term variability measurements and how they relate to a stars' position above or below the main sequence, as we have done here.

Due to their complex atmospheres, which grow more complex with later spectral types, M dwarf abundances are ideally measured when the low mass star is part of a multiple system with an F-, G-, or K- primary because the metallicities of these higher mass stars are much more easily determined. It is inferred that the stars in each binary (or higher order multiple) system formed together from the same interstellar material and thus have the same or very close metallicity genetics. With the inferred metallicity values and a sufficient number of "calibrated" M dwarfs that function as metallicity tracers, spectral models can then be used to determine the abundances of other, single low mass stars. Such works to calibrate these metallicity markers in low mass stars using this method include those by Gizis (1997); Bonfils et al. (2005); Johnson & Apps (2009); Schlaufman & Laughlin (2010); and Newton et al. (2014). Gizis (1997) derived metallicities for solar type stars to the most extreme subdwarfs ([m/H] $\sim$ 0.0 to -2.0). In the work of Bonfils et al. (2005) they derived metallicities for 47 bright, single M dwarfs using their newly derived photometric calibration. Then, Johnson & Apps (2009) found that Bonfils et al. (2005) systematically underestimated the metallicities of high metallicity stars by an average of 0.32 dex and derived a new photometric calibration – they also found that planet hosting M dwarfs appear

to be metal rich. This work was followed by Schlaufman & Laughlin (2010), who also derived their own photometric metallicity calibration and found that metal rich M dwarfs are more likely to host low mass planets. The last study, Newton et al. (2014), had the largest sample with derived metallicities for 447 nearby M dwarfs and presented yet another new photometric color-color metallicity relation. The latter four of these studies each derived different relationships between the offsets of the stars from the mean main sequence and their metallicities to calibrate their metallicity measurements. Our work has done the opposite by taking previously published [Fe/H] values and studying how this property relates to a star's offset from the central distribution of the main sequence.

6.2 Overall Results

Through each of our three studies we have shown that the elevation of stars above the main sequence is strongly influenced by the magnetic activity of these stars. The effects of this activity have been confirmed on both long-term and short-term timescales through our studies detailed in Chapters 3 and 4, as well as at different layers of the stars. Activity within the photospheres, where starspots and flares may be observed, has been analyzed through our photometric studies, where we see strong trends on long-term timescales and a subtler trend in the short-term. Chromospheric activity has been analyzed and detected via our spectroscopy study detailed in Chapter 5 in particular through the Hα, Na I D_1/D_2, and Ca II H and K features, illustrated by Figures 5.2, 5.4, 5.6, and 5.7, respectively. Each of these three studies has confirmed our hypothesis that the over-luminous M dwarfs residing

above the main sequence, particularly the young stars, are driven more by magnetic activity than by high metallicity, given the weakening metallicity trends in Figures 5.9 and 5.17 and the strong activity trends in Figures 3.2, 3.4, 4.4, and 4.10. We theorize that heightened levels of activity serve to extend the outer chromospheric layer of the stars, increasing their luminosities through the effects of larger radii.

M dwarf stars are much more likely than high mass stars to present low metallicity measurements due to their longer lifetimes. The high mass stars will end their main sequence lives after only millions of years, adding the heavier elements they have created back into the interstellar medium to form new stars via their planetary nebulae and supernova explosions. All M dwarf stars have lifetimes that are longer than the current known age of the Universe, so those formed early enough to not have higher abundances of heavier elements in their primordial material are still burning hydrogen today. As discussed in §1.4, low metallicity stars, known as subdwarfs, have decreased opacities due to the lack of heavier elements in their upper atmospheres. As a result, we observe the deeper, hotter layers of the star, resulting in a temperature displacement that shifts these stars to the left on an H-R diagram, and thus below the mean distribution of the main sequence. Through our spectroscopy and metallicity analysis we have confirmed previous works and theories that much of the spread below the main sequence for low mass subdwarfs is driven by the effects of low metallicity. We see no trend in the variability of stars below the main sequence other than low overall variability levels, indicating that these stars have quiet photospheres (seen in Figures 3.2, 4.4, and 4.10). However, strong trends for subdwarfs are evident in both published metallicities

and spectral features that are known, or suspected, to be metallicity indicators, such as Fe I and CaH. As discussed in Chapter 5, we find that both the published metallicities and the measured EWs of the metallicity indicators show increasing trends in metallicity as stars are selected from below to on the main sequence, as illustrated by Figures 5.9, 5.13, 5.14, and 5.17. In each of these results, though, the trend appears to taper off or completely breaks down for stars above our determination of $\Delta M_V = -0.50$ for stars "on" the main sequence, suggesting that the role of metallicity is not as important in the vertical placement of these stars.

6.3 Potential Improvements

Each of the three studies conducted for this dissertation has room for improvements. For the long-term study, more time and data would greatly improve and add to our results. The short-term study could be improved with shorter cadences and perhaps time on larger telescopes (to achieve these cadences). Our spectroscopy study would be significantly improved with the addition of the CHIRON spectra obtained and the use of models and modeling programs to accurately derive the various stellar parameters of these stars.

The long-term study produced excellent results demonstrating the effects of internal magnetic field strangth on the vertical positions of M dwarf stars on the main sequence.The RECONS team plans to continue to observe several hundred M dwarfs at the 0.9 m. With more time and observations we could include more stars in the study than the 76 presented here, as many stars were not used because they had not yet been observed for at least three

years. Many of the newer stars added to the parallax survey will be ready for long term variability analysis in the next year or two. There were also several stars demonstrating interesting trends and cyclic activity that would benefit from further observations to more closely assess these trends and whether or not they continue over time. We also hope to be able to assess the cyclic activity of these stars and whether or not there is any trend present between the timescales of the stellar cycles and the ΔM_V values of our stars. With more observations we may be able to successfully carry out periodogram studies on these stars to calculate the periods of the observed stellar cycles.

Our short-term study produced some subtle results, but could be greatly improved by the use of larger telescopes and/or faster observing cadences. With larger telescopes we have the opportunity to observe more of the stars at the extreme vertical ends of the main sequence ($+1 < \Delta M_V$ and $\Delta M_V < -1$) to better sample these regions of the luminosity distribution. We can also achieve faster cadences with exposures of only a few seconds with larger telescopes, as our stars are generally faint and such integration times would not produce enough counts for our stars on smaller telescopes, such as the CTIO 0.9 m and the ARCES 0.5 m used for this dissertation work. Faster cadences will allow us a better opportunity to observe microflares and the resulting small changes in brightness that happen very quickly and were likely missed by the slower cadences of 30 – 300 s used in our work.

The spectroscopy component of this work produced clear trends in the measured EWs of both the spectral features known to be activity indicators as well as the metallicity indicators, but more work is needed. With the addition of the CHIRON data obtained, we can further

supplement our sample to produce more statistically significant results. We also have the opportunity to derive our own values for key stellar properties, such as [Fe/H], T_{eff}, log(g), and vsin$i$, and assess how these properties may be affecting the ΔM_V values of the stars. We can do this through the use of stellar models like the BT-Settl (Allard et al. 2011) and PHOENIX (Hauschildt et al. 1999) models created specifically for lower mass stars, and programs designed for comparing stellar spectra to spectral models, such as MOOG. The metallicity study could also benefit from the addition of more young stars and stars elevated far above the main sequence, as there are no stars beyond $\Delta M_V = -1$ with published metallicities in the studies we referenced. With more metallicity measurements for the over-luminous M dwarfs we may be able to better determine if the metallicity trend continues upwards or steadily levels out, as it appears to in Figure 5.17.

6.4 Future Work

As part of the ongoing work needed for this study more observations are a crucial part of expanding our research. One area where I would like to obtain more data for this project is the long-term variability study. With more observations we can not only add more stars to this interesting study, but we can also further explore other properties and their links to variability and ΔM_V values. We would be able to determine periods for the observed stellar cycles and assess any correlations between these periods and variability measurements, as well as whether there is a correlation between the length of the stellar cycle and the main sequence placement of the stars. We would also be afforded the opportunity to explore the

role of convection in the magnetic activity of these stars with the addition of more stars within Box 6 of this work.

We are currently working to compile and publish the results of our short-term study and hope to have that ready for publication next year. We also plan to find an effective way to reduce and analyze the CHIRON data so they can be added to our spectroscopy sample. We would like to incorporate the use of stellar models with respect to these data in order to derive even more information from these spectra so that these results may also be published in the future. The spectroscopy study is an ongoing project that will require more time and analysis to produce even more useful results. The ultimate goal is to gain a better understanding of why the main sequence widens significantly for low mass stars and what properties are influencing this disparity. With a better understanding of these properties we may be able to learn more about their environments, as they relate to planetary habitability, and their evolutionary tracks, because we will likely never have the opportunity to observe one of these stars after or even at the end of their main sequence lifetimes.

REFERENCES

Adams, F. C., Bodenheimer, P., & Laughlin, G. 2005, Astronomische Nachrichten, 326, 913

Ake, T. B., & Greenstein, J. L. 1980, ApJ, 240, 859

Allard, F., Homeier, D., & Freytag, B. 2011, ASPC, 448, 91

Alonso-Floriano, F. J. et al. 2015, A&A, 577, 128

Andretta, V., Doyle, J. G., & Byrne, P. B. 1997, A&A, 322, 266

Anglada-Escudé, G., Amado, P. J., Barnes, J., et al. 2016, Nature, 536, 437A

Anglada-Escudé, G., Boss, A. P., Weinberger, A. J., Thompson, I. B., Butler, R. P., Vogt, S. S., & Rivera, E. J. 2012, ApJ, 746, 37

Baraffe, I., Homeier, D., Allard, F., & Chabrier, G. 2015, A&A, 577, 42B

Barrado y Navascués, D., & Martín, E. L. 2003, AJ, 126, 2997

Bell, C. P. M., Mamajek, E. E., & Naylor, T. 2015, MNRAS, 454, 593B

Bessel, M. S. 1990, A&AS, 83, 357B

Beuzit, J.-L. et al. 2004, A&A, 425, 997

Bidelman, W. P. 1985, ApJ, 59, 197

Bonfils, X., Delfosse, X., Udry, S., et al. 2005, A&A, 442, 635

Bonfils, X., Lo Curto, G., Correia, A. C. M., et al. 2013, A&A, 556, 110

Cantrell, J. R., Henry, T. J., & White, R. J. 2013, AJ, 146

Casagrande, L., Flynn, C., & Bessell, M. 2008, MNRAS, 389, 585

Chabrier, G., & Baraffe, I. 1997, A&A, 327, 1039

Chabrier, G., Baraffe, I., & Plez, B. 1996, ApJ, 459, 91

Clements, T. D., Henry, T. J., Jao, W. C., et al. 2017, AJ, 154

Costa, E., Méndez, R. A., Jao, W.-C., et al. 2005, AJ, 130, 337

——. 2006, AJ, 132, 1234

Cram, L. E., & Mullan, D. J. 1979, ApJ, 234, 579

Cutispoto, G. 1990, A&AS, 84, 397

Cutispoto, G., & Giampapa, M. S. 1988, PASP, 100, 1452

D'Antona, F., & Mazzitelli, I. 1985, ApJ, 296, 502

David, T. J., Hillenbrand, L. A., Cody, A. M., et al. 2016, ApJ, 816, 21

Davison, C. L., White, R. J., Henry, T. J., et al. 2015, AJ, 149

Delfosse, X., Forveille, T., Beuzit, J.-L., Udry, S., Mayor, M., & Perrier, C. 1999, A&A, 344, 897

Dieterich, S. B. 2013, PhD thesis, Georgia State University

Dieterich, S. B., Henry, T. J., Golimowski, D. A., Krist, J. E., & Tanner, A. M. 2012, AJ, 144, 64

Dittmann, J. A., Irwin, J. M., Charbonneau, D., & Newton, E. R. 2016, ApJ, 818, 153

Fabricius, C., & Makarov, V. V. 2000, A&AS, 144, 45

Feiden, G. A., & Chaboyer, B. 2013, ApJ, 779, 183

——. 2014, ApJ, 789, 53

Gaidos, E., & Mann, A. W. 2014, ApJ, 791, 54

Gatewood, G. 2008, AJ, 136, 452

Gizis, J. E. 1997, AJ, 113, 806

——. 1998, AJ, 115, 2053

Goldman, B., Roeser, S., Schilbach, E., et al. 2013, A&A, 559A, 43

Gomes da Silva, J., Santos, N. C., Bonfils, X., Delfosse, X., Forveille, T., & Udry, S. 2011, A&A, 534, 30

Gomes da Silva, J., Santos, N. C., Bonfils, X., Delfosse, X., Forveille, T., Udry, S., Dumusque, X., & Lovis, C. 2012, A&A, 541, 9

Gould, A., & Chanamé, J. 2004, ApJS, 150, 455

Gray, R. O., Corbally, C. J., Garrison, R. F., McFadden, M. T., Bubar, E. J., McGahee, C. E., O'Donoghue, A. A., & Knox, E. R. 2006, AJ, 132, 161

Gray, R. O., Corbally, C. J., Garrison, R. F., McFadden, M. T., & Robinson, P. E. 2003, AJ, 126, 2048

Hanson, R. B. 1975, AJ, 80, 379

Hauschildt, P. H., Allard, F., & Baron, E. 1999, ApJ, 512, 377

Hawley, S. L. 1993, PASP, 105, 955

Hawley, S. L., Davenport, J. R. A., Kowalski, A. F., Wisniewski, J. P., Hebb, L., Deitrick, R., & Hilton, E. J. 2014, ApJ, 797, 121

Hawley, S. L., Gizis, J. E., & Reid, I. N. 1996, AJ, 112, 2799

Henry, T. J., Jao, W.-C., Subasavage, J. P., et al. 2006, AJ, 132, 2360

Henry, T. J., Kirkpatrick, J. D., & Simons, D. A. 1994, AJ, 108, 1437

Hosey, A. D., Henry, T. J., Jao, W.-C., et al. 2015, AJ, 150, 6

Houdebine, E. R., Mullan, D. J., Bercu, B., Paletou, F., & Gebran, M. 2017, ApJ, 837, 96

Houdebine, E. R., & Stempels, H. C. 1997, A&A, 326, 1143

Jao, W.-C., Henry, T., Winters, J., Subasavage, J., Riedel, A., Silverstein, M., & Ianna, P. 2017, accepted for publication in AJ

Jao, W.-C., Henry, T. J., Beaulieu, T. D., & Subasavage, J. P. 2008, AJ, 136, 840

Jao, W.-C., Henry, T. J., Subasavage, J. P., et al. 2005, AJ, 129, 1954

——. 2011, AJ, 141, 117

Johnson, J. A., & Apps, K. 2009, ApJ, 699, 933

Kang, W., & Lee, S.-G. 2012, MNRAS, 425, 3162

Kirkpatrick, J. D., Henry, T. J., & McCarthy, Donald W., J. 1991, ApJS, 77, 417

Klutsch, A., Freire Ferrero, R., Guillout, P., Frasca, A., Marilli, E., & Montes, D. 2014, A&A, 567, 52

Koen, C., Kilkenny, D., van Wyk, F., & Marang, F. 2010, MNRAS, 403, 1949

Kopp, R., & Pneuman, G. 1976, Sol. Phys., 59, 85

Kowalski, A. F., Hawley, S. L., Hilton, E. J., Becker, A. C., West, A. A., Bochanski, J. J., & Sesar, B. 2009, AJ, 138, 633

Kowalski, A. F., Hawley, S. L., Wisniewski, J. P., Osten, R. A., Hilton, E. J., Holtzman, J. A., Schmidt, S. J., & Davenport, J. R. A. 2013, ApJ, 207, 15

Kowalski, A. F., Mathioudakis, M., Hawley, S. L., Wisniewski, J. P., Dhillon, V. S., Marsh, T. R., Hilton, E. J., & Brown, B. P. 2016, ApJ, 820, 95

Lépine, S., Hilton, E. J., Mann, A. W., Wilde, M., Rojas-Ayala, B., Cruz, K. L., & Gaidos,

E. 2013, AJ, 145, 102

Liu, F., Yong, D., Asplund, M., et al. 2016, MNRAS, 457, 3934

Lurie, J. C., Henry, T. J., Jao, W.-C., et al. 2014, AJ, 148

Mann, A. W., Feiden, G. A., Gaidos, E., Boyajian, T., & von Braun, K. 2015, ApJ, 804, 64

McAlister, H. A., ten Brummelaar, T. A., Gies, D. R., et al. 2005, ApJ, 628, 439

Messina, S., & Guinan, E. F. 2002, A&A, 393, 225

Neves, V. et al. 2012, A&A, 538, 25

Neves, V., Bonfils, X., Santos, N. C., et al. 2014, A&A, 568, 121

Newton, E. R., Charbonneau, D., Irwin, J., Berta-Thompson, Z. K., Rojas-Ayala, B., Covey, K., & Lloyd, J. P. 2014, AJ, 147, 20

Newton, E. R., Irwin, J., Charbonneau, D., Berta-Thompson, Z. K., Dittmann, J. A., & West, A. A. 2016, ApJ, 821, 93

Nielsen, M. B., Gizon, L., Schunker, H., & Karoff, C. 2013, A&A, 557, 10

Nissen, P. E., Chen, Y. Q., Carigi, L., Schuster, W. J., & Zhao, G. 2014, A&A, 568, 25

Parker, E. N. 1955, ApJ, 122, 293

Perryman, M. A. C., Brown, A. G. A., Lebreton, Y., et al. 1998, A&A, 331, 81

Pettersen, B. R., Cochran, A. L., & Barker, E. S. 1985, AJ, 90, 2296

Prosser, Charles, F. 1992, ApJ, 103, 488

Rauscher, E., & Marcy, G. W. 2006, PASP, 118, 617

Reid, I. N., Hawley, S. L., & Gizis, J. E. 1995, AJ, 110, 1838

Reid, I. N., Kirkpatrick, J. D., Gizis, J. E., Dahn, C. C., Monet, D. G., Williams, R. J.,

Liebert, J., & Burgasser, A. J. 2000, AJ, 119, 369

Reid, N. 1993, MNRAS, 265, 785

Riedel, A. R., Finch, C. T., Henry, T. J., et al. 2014, AJ, 147

Riedel, A. R., Murphy, S. J., Henry, T. J., et al. 2011, AJ, 142

Riedel, A. R., Subasavage, J. P., Finch, C. T., et al. 2010, AJ, 140, 897

Robertson, P., Endl, M., Cochran, W. D., & Dodson-Robinson, S. E. 2013, ApJ, 764, 3

Robinson, R. D., Carpenter, K. G., Percival, J. W., & Bookbinder, J. A. 1995, ApJ, 451, 795

Rojas-Ayala, B., Covey, K. R., Muirhead, P. S., & Lloyd, J. P. 2012, ApJ, 748, 93

Schlaufman, K. C., & Laughlin, G. 2010, A&A, 519, 105

Schmitt, J. H. M. M., Kanbach, G., Rau, A., & Steinle, H. 2016, A&A, 589, 48

Shkolnik, E., Liu, M. C., & Reid, I. N. 2009, ApJ, 699, 649

Shkolnik, E. L., Allers, K. N., Kraus, A. L., Liu, M. C., & Flagg, L. 2017, AJ, 154, 69

Shkolnik, E. L., Anglada-Escudé, G., Liu, M. C., et al. 2012, ApJ, 758

Skrutskie, M. F., Cutri, R. M., Stiening, R., et al. 2006, AJ, 131, 1163

Smart, R. L., Ioannidis, G., Jones, H. R. A., Bucciarelli, B., & Lattanzi, M. G. 2010, A&A, 514, 84

Stassun, K. G., Kratter, K. M., Scholz, A., & Dupuy, T. J. 2012, ApJ, 756, 47

Stauffer, J. R., & Hartmann, L. W. 1986, ApJS, 61, 531

Stauffer, J. R., Schultz, G., & Kirkpatrick, J. D. 1998, ApJ, 499, 199

Stauffer, John, R., Giampapa, M. S., Herbst, W., et al. 1991, ApJ, 374, 142

Stetson, Peter, B. 1996, PASP, 108, 851

Suárez Mascareño, A., Rebolo, R., & González Hernández, J. I. 2016, A&A, 595, 12

Tarter, J. C. et al. 2007, Astrobiology, 7, 30

Taylor, B. J. 1994, PASP, 106, 600

Torres, C. A. O., Quast, G. R., da Silva, L., de La Reza, R., Melo, C. H. F., & Sterzik, M. 2006, A&A, 460, 695

van Altena, W. F. 1969, AJ, 74, 2

van Altena, W. F., Lee, J. T., & Hoffleit, D. 1995, Vizier Online Data Catalog, 1174, 0

van Leeuwen, F. 2007, Astrophysics and Space Science Library, 350

Voges, W., Aschenbach, B., Boller, T., et al. 1999, A&A, 349, 389

Wargelin, B. J., Kashyap, V. L., Drake, J. J., García-Alvarez, D., & Ratzlaff, P. W. 2008, ApJ, 676, 610

Weis, E. W. 1994, AJ, 107, 1135

——. 1996, AJ, 112, 2300

West, A. A., Hawley, S. L., Bochanski, J. J., et al. 2008, AJ, 135, 785

West, A. A., Hawley, S. L., Walkowicz, L. M., et al. 2004, AJ, 128, 426

Winters, J. G. 2015, PhD thesis, Georgia State University

Winters, J. G. et al. 2015, AJ, 149, 5

——. 2017, AJ, 153, 14

Zhao, J. K., Oswalt, T. D., Rudkin, M., Zhao, G., & Chen, Y. Q. 2011, AJ, 141, 107

APPENDIX
COMPLETE SAMPLE DATA

This appendix provides the properties of all of the 657 stars within the three boxes on Figures 1.1 and 1.2 that we have targeted for this work. Included in the Table is the name of each star (1), the 2000.0 coordinates (2, 3) , the V and I magnitudes (4, 5), the $V - K$ color (6), the absolute magnitude (7), and the ΔM_V value (8). The distances and references are given in the next columns (9, 10); some of the distances are calculated as the weighted mean of two or more published parallax values and are noted as such with two or three of the following: "Y" representing YPC95 (van Altena et al. 1995), "V" for vLe07 (van Leeuwen 2007), and "O" for other (any one or more of the other references given in the table). For references given as "RECXX" these distances are derived from parallax values obtained from the RECONS CTIOPI observing program but are yet to be published. In the next three columns (11, 12, 13) we note whether each star was in one of the three studies detailed in this dissertation, with a "yes" or "no" indicating whether or not the star is a part of each program. The long term study discussed in Chapter 3 is denoted by "LT" (11), the short term study from Chapter 4 is abbreviated to "ST" (12), and the spectroscopy study detailed in Chapter 5 is shortened to "Spec." (13). The final column (14) notes whether each star is known to be a young star (Y) or a subdwarf (S), or if it is suspected to be young ((Y)) or a subdwarf ((S)).

Table 1: Properties of the Low Mass Stars in the Sample.

Star Name (1)	R.A. 2000.0 (2)	Dec. 2000.0 (3)	V (4)	I (5)	$V-K$ (6)	M_V (mag) (7)	ΔM_V (mag) (8)	dist. (9)	dist. ref. (10)	LT Study (11)	ST Study (12)	Spec. Study (13)	Notes[a] (14)
GJ 1001A	00:04:36	−40:44:02	12.86	10.10	5.12	12.38	+0.04	12.5	Hen06	no	no	no	
GJ 2	00:05:11	+45:47:11	9.95	7.87	4.10	9.70	−0.09	11.2	YV	no	no	yes	
GJ 1	00:05:24	−37:21:26	8.54	6.41	4.02	10.37	+0.77	4.3	YV	no	no	yes	
HIP 000687	00:08:27	+17:25:27	10.80	8.93	3.82	9.12	−0.04	21.7	vLe07	no	no	no	
NLTT 372	00:08:52	+20:49:08	15.87	13.12	5.15	11.20	−1.20	85.8	Rie14	no	no	yes	Y
GJ 7	00:09:04	−27:07:19	11.69	9.78	3.83	9.89	+0.70	22.9	vLe07	no	yes	no	
LTT 17095	00:13:38	+80:39:56	11.11	8.94	4.21	9.66	−0.40	19.5	vLe07	no	no	no	
GJ 12	00:15:49	+13:33:22	12.62	10.05	4.81	12.32	+0.75	11.5	YVO	no	no	no	
GJ 1006A	00:16:14	+19:51:37	12.26	9.46	5.17	11.37	−1.09	15.1	YPC95	no	no	yes	
L 218-009	00:16:36	−50:16:08	12.35	10.14	4.18	10.62	+0.62	22.2	vLe07	no	no	no	
GJ 1007	00:16:56	+05:07:27	13.79	10.92	5.20	12.57	+0.05	17.5	YPC95	no	no	no	
LHS 1054	00:17:20	+29:10:58	11.52	9.35	4.28	9.73	−0.51	22.8	YV	no	yes	yes	
SCR 0017-6645	00:17:23	−66:45:12	12.45	10.00	4.75	9.49	−1.92	39.0	Rie14	yes	yes	no	Y
GJ 16	00:18:16	+10:12:10	10.91	8.78	4.17	9.82	−0.15	16.5	vLe07	no	no	no	
GJ 15A	00:18:23	+44:01:24	8.08	6.45	4.06	10.30	+0.59	3.6	YVO	no	yes	yes	
GJ 15B	00:18:26	+44:01:42	11.06	8.24	5.11	13.28	+0.97	3.6	YVO	no	yes	yes	
G 266-089A	00:19:37	−28:09:46	14.27	11.44	4.80	11.76	+1.23	31.8	Jao11	yes	no	no	(S)
GJ 2003	00:20:08	−17:03:41	11.66	9.64	3.97	9.84	+0.36	23.1	vLe07	no	no	no	
GJ 17.1	00:21:19	−45:44:47	10.40	8.49	3.86	9.21	−0.03	17.3	YV	no	no	no	
LHS 5004a	00:21:37	−46:05:33	12.24	9.73	4.79	10.81	−0.71	19.3	vLe07	no	yes	no	
GJ 1010A	00:23:28	+77:11:21	11.31	9.18	4.12	10.05	+0.19	17.9	YVO	no	no	no	
GJ 1010B	00:23:28	+77:11:21	14.10	11.37	4.99	12.84	+0.82	17.9	YVO	no	no	no	
GJ 21	00:26:52	+70:08:32	10.53	8.55	3.96	9.44	−0.04	16.5	YV	no	no	no	
GJ 2006A	00:27:50	−32:33:06	12.95	10.29	4.94	10.34	−1.54	33.2	Rie14	yes	yes	no	Y
GJ 2006B	00:27:50	−32:33:24	13.25	10.48	5.13	10.76	−1.59	31.5	Rie14	yes	yes	no	Y
GJ 1012	00:28:39	−06:39:49	12.17	9.51	4.98	11.57	−0.42	13.2	YPC95	no	no	no	
GJ 1013	00:31:35	−05:52:13	12.73	10.14	4.79	11.71	+0.21	16.0	YPC95	no	no	no	
GJ 22B	00:32:29	+67:14:08	12.19	···	5.81	12.17	−1.70	10.1	YVO	no	no	yes	
LHS 1101	00:34:44	+71:11:31	13.53	10.88	4.86	12.06	+0.37	19.7	YPC95	no	no	no	
GJ 1014	00:36:00	+10:28:08	15.32	12.00	5.95	14.34	+0.20	15.7	YPC95	no	no	no	
GJ 27.1	00:39:58	−44:15:12	11.39	9.36	4.00	9.46	−0.09	24.3	vLe07	no	no	no	
GJ 1015A	00:41:22	+55:50:08	14.02	···	4.98	12.21	+0.22	23.0	YPC95	no	no	no	
LHS 1134	00:43:25	−41:17:39	13.01	10.12	5.30	12.82	+0.07	10.9	Win17	no	no	no	
GJ 1019	00:43:35	+28:26:41	14.51	11.81	4.84	13.08	+1.44	19.3	YPC95	no	no	no	
G 001-021B	00:45:17	+01:40:34	14.04	11.85	4.20	12.22	+2.19	23.1	YPC95	no	yes	no	S
GJ 1021B	00:45:46	−47:33:07	12.43	9.73	4.79	11.54	+0.02	15.1	vLe07	no	no	no	
LTT 00453	00:48:13	−05:08:08	12.04	9.94	4.11	10.17	+0.34	23.7	vLe07	no	no	no	
LTT 00464	00:49:01	−50:08:41	10.73	8.86	3.78	9.07	+0.00	21.5	vLe07	no	no	no	
LTT 00534	00:56:50	−11:35:19	11.12	9.25	3.76	9.16	+0.14	24.7	vLe07	no	no	no	
GJ 46	00:58:27	−27:51:25	11.77	9.17	4.88	11.32	−0.41	12.3	vLe07	no	yes	no	
GJ 1025	01:00:56	−04:26:56	13.36	10.55	5.14	13.08	+0.71	11.4	Jao05	yes	yes	no	
GJ 49	01:02:38	+62:20:42	9.56	7.44	4.19	9.58	−0.43	9.9	YV	no	yes	yes	S
GJ 51	01:03:19	+62:21:56	13.78	10.43	6.06	13.80	−0.54	9.9	YV	no	no	no	
GJ 1028	01:04:59	−18:07:01	14.45	11.11	6.00	14.45	+0.23	10.0	YPC95	no	no	no	
GJ 1029	01:05:37	+28:29:34	14.79	11.35	6.24	14.29	−0.36	12.6	YPC95	no	no	no	
GJ 1030	01:06:41	+15:16:22	11.40	9.23	4.24	9.71	−0.43	21.8	vLe07	no	yes	yes	
GJ 53.1B	01:07:37	+22:57:17	13.60	11.00	4.93	11.99	+0.13	21.0	YV	no	no	no	
GJ 52.2	01:07:49	+34:12:54	13.37	11.06	4.29	11.65	+1.39	22.1	YPC95	no	no	yes	
LP 707-016	01:10:17	−11:51:16	12.71	10.03	5.05	11.37	−0.79	18.5	Win17	no	no	no	
LHS 1212	01:11:55	+04:55:05	12.88	10.27	4.93	11.87	+0.01	15.9	YPC95	no	no	no	
LHS 1213	01:11:58	+04:54:12	13.90	11.10	5.09	12.89	+0.65	15.9	YPC95	no	no	no	
L 221-060	01:14:34	−53:56:31	11.08	8.99	4.11	9.99	+0.16	16.5	vLe07	no	no	no	

[a]Notes in Column 14: Y = known young stars, (Y) = suspected young star, S = known subdwarf stars, (S) = suspected, but unconfirmed subdwarf stars.

Distance references: (Ang12) Anglada-Escudé et al. (2012); (Cos05) Costa et al. (2005); (Cos06) Costa et al. (2006); (Dav15) Davison et al. (2015); (Fab00) Fabricius & Makarov (2000); (Gat08) Gatewood (2008); (Gou04) Gould & Chanamé (2004); (Hen06) Henry et al. (2006); (Jao05) Jao et al. (2005); (Jao11) Jao et al. (2011); (Lur14) Lurie et al. (2014); (Rie10) Riedel et al. (2010); (Rie11) Riedel et al. (2011); (Rie14) Riedel et al. (2014); (Shk12) Shkolnik et al. (2012); (Sma10) Smart et al. (2010); (vLe07) van Leeuwen (2007); (Win15) Winters et al. (2015); (Win17) Winters et al. (2017); (YPC95) van Altena et al. (1995).

Table 1: Properties of the Low Mass Stars in the Short-Term Variability Study.

Star Name (1)	R.A. 2000.0 (2)	Dec. 2000.0 (3)	V (4)	I (5)	$V-K$ (6)	M_V (mag) (7)	ΔM_V (mag) (8)	dist. (9)	dist. ref. (10)	LT Study (11)	ST Study (12)	Spec. Study (13)	Notes[a] (14)
GJ 1034	01:16:29	+24:19:27	15.00	12.16	5.09	13.42	+1.16	20.7	YPC95	no	no	no	
L 797-030	01:17:15	−13:15:47	10.79	8.86	3.88	8.95	−0.35	23.3	vLe07	no	no	yes	
GJ 56.1	01:18:16	−12:53:59	11.79	9.55	4.24	10.08	−0.06	22.0	YV	no	no	no	
GJ 1035	01:19:52	+84:09:33	14.75	11.58	5.73	14.03	+0.34	13.9	YPC95	no	no	no	
HIP 006365	01:21:45	−46:42:51	11.40	9.31	4.11	9.66	−0.16	22.3	vLe07	no	no	no	
GJ 2022B	01:24:31	−33:55:02	15.50	12.33	6.48	13.44	−1.58	25.8	Rie14	no	no	no	Y
LHS 142	01:32:26	−21:54:18	11.18	9.08	4.08	9.89	+0.14	18.1	vLe07	no	no	no	
LHS 1268	01:37:20	−49:11:44	10.39	8.56	3.77	8.63	−0.41	22.5	vLe07	no	no	no	
LHS 1272	01:38:29	+00:39:05	13.22	10.62	5.90	11.69	−2.34	20.2	vLe07	no	no	no	
LHS 144	01:38:49	+11:21:38	16.30	13.70	4.22	12.79	+2.70	50.3	YPC95	no	no	no	S
LP 991-084	01:39:22	−39:36:08	14.45	11.06	6.18	14.78	+0.24	8.6	Win15	no	no	no	
LHS 1288	01:42:55	−42:12:12	11.19	9.27	3.79	9.46	+0.37	22.2	YVO	no	no	no	
LHS 1289	01:43:15	+27:50:31	10.40	8.55	3.80	8.75	−0.37	21.4	YV	no	yes	yes	
SCR 0143-0602	01:43:45	−06:02:40	13.01	10.25	5.10	11.53	−0.75	19.8	RECXX	no	no	no	
LEHPM 1-1882	01:47:42	−48:35:59	12.42	9.73	4.97	11.72	−0.24	13.8	Win17	no	no	no	
LHS 1302	01:51:04	−06:07:05	14.49	11.17	5.94	14.51	+0.40	9.9	Hen06	no	no	no	Y
GJ 78	01:51:48	−10:48:12	11.80	9.59	4.17	10.75	+0.78	16.2	YV	no	no	yes	
GJ 79	01:52:49	−22:26:05	8.88	7.08	3.70	8.67	−0.22	11.0	vLe07	no	no	yes	
GJ 82	01:59:23	+58:31:16	12.21	9.48	5.25	11.78	−0.86	12.2	YV	no	yes	yes	
L 173-019	02:00:38	−55:58:04	11.89	9.15	5.12	12.35	+0.03	8.1	RECXX	no	no	no	
LP 030-055	02:01:54	+73:32:32	14.12	···	5.75	13.84	+0.08	11.4	Gat09	no	no	no	
GJ 84.1B	02:05:21	−28:04:36	12.77	10.18	4.74	10.95	−0.42	23.1	vLe07	no	no	no	
GJ 84.1A	02:05:23	−28:04:11	10.88	9.04	3.72	9.06	+0.14	23.1	vLe07	no	no	yes	
GJ 87	02:12:20	+03:34:32	10.04	7.99	3.96	9.95	+0.47	10.4	YV	no	no	no	
GJ 91	02:13:53	−32:02:28	10.31	8.15	4.22	9.84	−0.24	12.4	vLe07	no	no	yes	
LHS 1376	02:16:35	−30:58:07	13.10	10.26	5.21	12.32	−0.23	14.3	vLe07	no	no	no	
LHS 1377	02:16:41	−30:59:18	12.03	9.41	4.90	11.25	−0.53	14.3	vLe07	no	no	no	
WT 84	02:17:28	−59:22:43	15.76	12.28	6.22	15.19	+0.58	13.0	Cos05	no	no	no	
GJ 93	02:17:34	−53:59:20	11.40	9.51	3.75	9.64	+0.64	22.5	vLe07	no	yes	no	
GJ 1047C	02:21:01	+36:52:47	14.29	11.63	4.88	12.62	+0.87	21.6	YPC95	no	no	no	
GJ 96	02:22:14	+47:52:48	9.41	···	3.86	9.05	−0.19	11.8	YV	no	yes	yes	
NLTT 08065	02:27:30	−30:54:35	10.89	8.88	3.96	9.32	−0.15	20.6	vLe07	no	no	no	
GJ 101	02:31:27	+57:22:43	13.22	10.58	4.80	11.83	+0.28	19.0	YO	no	no	no	
LHS 156	02:34:13	+17:45:51	14.92	12.61	4.20	12.10	+2.06	36.6	YPC95	no	no	no	S
GJ 105B	02:36:04	+06:53:12	11.71	8.88	5.14	12.42	+0.06	7.2	YVO	yes	no	yes	
APM 0237-5928	02:36:32	−59:28:05	14.47	11.08	6.13	14.56	+0.10	9.6	Hen06	no	no	no	
L 174-028	02:37:52	−58:45:11	12.43	9.76	4.92	11.55	−0.28	15.0	vLe07	yes	no	no	
LTT 17400	02:39:17	+07:28:17	14.27	11.52	5.24	12.83	+0.22	19.4	Shk12	no	no	no	
LHS 158	02:42:03	−44:30:59	13.64	···	3.91	10.23	+0.87	48.0	Jao05	no	no	no	S
GJ 1051	02:43:53	−08:49:45	11.91	9.83	3.99	9.94	+0.40	24.8	YV	no	no	no	
GJ 107B	02:44:11	+49:13:42	10.06	7.94	4.20	9.83	−0.20	11.1	YV	no	no	no	
LP 993-115	02:45:10	−43:44:32	12.38	9.61	5.11	12.13	−0.17	11.2	Rie14	yes	no	no	Y
LTT 17413	02:45:39	+44:56:55	10.85	9.10	3.87	9.04	−0.22	23.0	vLe07	no	yes	no	
SCR 0246-7024	02:46:02	−70:24:06	14.86	11.61	5.84	14.38	+0.45	12.5	Win17	no	no	no	
LHS 017	02:46:14	−04:59:20	16.33	12.76	6.18	15.24	+0.70	16.5	YPC95	no	no	no	
GJ 114.1	02:50:05	−53:08:20	10.72	8.55	4.23	10.15	+0.05	13.0	vLe07	no	no	yes	
GJ 118.2C	02:55:39	+26:52:23	13.90	11.06	5.24	12.04	−0.57	23.5	YV	no	yes	no	
GJ 119A	02:56:34	+55:26:14	10.48	8.55	3.89	8.90	−0.41	20.7	YVO	no	no	yes	
LP 771-095A	03:01:51	−16:35:36	11.22	8.66	4.72	11.99	+0.65	7.0	Hen06	yes	no	no	
LHS 1490	03:02:06	−39:50:52	15.85	12.44	5.97	15.12	+0.96	14.0	Win15	no	no	no	S
LHS 1491	03:04:04	−20:22:43	12.84	10.13	5.09	11.99	−0.27	14.8	Rie10	yes	no	no	
LHS 1499	03:08:23	+43:02:09	14.70	···	4.75	12.75	+1.34	24.5	YPC95	no	no	yes	
GJ 1055	03:09:00	+10:01:26	14.85	11.61	5.78	14.47	+0.66	11.9	YPC95	no	no	no	

[a] Notes in Column 14: Y = known young stars, (Y) = suspected young star, S = known subdwarf stars, (S) = suspected, but unconfirmed subdwarf stars.

Distance references: (Ang12) Anglada-Escudé et al. (2012); (Cos05) Costa et al. (2005); (Cos06) Costa et al. (2006); (Dav15) Davison et al. (2015); (Fab00) Fabricius & Makarov (2000); (Gat08) Gatewood (2008); (Gou04) Gould & Chanamé (2004); (Hen06) Henry et al. (2006); (Jao05) Jao et al. (2005); (Jao11) Jao et al. (2011); (Lur14) Lurie et al. (2014); (Rie10) Riedel et al. (2010); (Rie11) Riedel et al. (2011); (Rie14) Riedel et al. (2014); (Shk12) Shkolnik et al. (2012); (Sma10) Smart et al. (2010); (vLe07) van Leeuwen (2007); (Win15) Winters et al. (2015); (Win17) Winters et al. (2017); (YPC95) van Altena et al. (1995).

Table 1: Properties of the Low Mass Stars in the Short-Term Variability Study.

Star Name (1)	R.A. 2000.0 (2)	Dec. 2000.0 (3)	V (4)	I (5)	$V-K$ (6)	M_V (mag) (7)	ΔM_V (mag) (8)	dist. (9)	dist. ref. (10)	LT Study (11)	ST Study (12)	Spec. Study (13)	Notes[a] (14)
GJ 130	03:12:29	−38:05:20	11.43	9.18	4.25	10.95	+0.79	12.5	YPC95	no	no	no	
GJ 1057	03:13:22	+04:46:29	13.94	10.62	6.11	14.29	−0.13	8.5	YPC95	no	no	no	
LP 831-045	03:14:18	−23:09:31	12.56	9.91	4.94	11.58	−0.30	15.7	Win17	no	no	no	
LTT 11051	03:14:47	+48:31:11	11.43	···	4.02	9.94	+0.33	19.9	YPC95	no	no	no	
LHS 1521C	03:15:29	+57:51:33	15.24	12.53	4.97	14.40	+2.44	14.7	YV	no	no	yes	
LHS 1525	03:17:45	+25:15:06	11.78	9.63	4.11	10.11	+0.28	21.6	vLe07	no	no	no	
LP 887-070	03:18:03	−30:24:11	10.99	9.05	3.88	9.19	−0.09	22.9	vLe07	no	no	no	
GJ 134	03:18:07	+38:15:07	10.28	8.20	4.12	9.22	−0.62	16.3	YV	no	no	no	
GJ 1058	03:22:04	+02:56:35	14.78	11.82	5.27	13.64	+0.95	16.9	YPC95	no	yes	no	
GJ 1059	03:23:01	+42:00:27	15.31	12.04	5.71	14.39	+0.72	15.3	YPC95	no	no	no	
LTT 01628	03:25:39	−42:59:12	11.25	9.35	3.77	9.42	+0.38	23.2	vLe07	no	no	no	
GJ 143.2	03:29:22	−62:56:15	10.73	8.72	3.98	9.06	−0.46	21.6	YV	no	no	no	
GJ 1062	03:38:18	−11:29:49	13.01	10.79	4.18	11.99	+2.00	16.0	YPC95	no	yes	yes	S
LHS 178	03:42:29	+12:31:34	12.87	10.78	3.99	10.94	+1.39	24.3	YPC95	yes	yes	yes	S
GJ 150.1B	03:43:45	+16:40:02	10.71	8.70	4.02	9.52	−0.10	17.3	YV	no	no	no	
GJ 154	03:46:20	+26:12:55	9.58	7.75	3.74	8.76	−0.21	14.6	YV	no	no	yes	
GJ 155.1	03:47:58	+02:47:16	11.02	9.05	3.91	9.87	+0.51	17.0	YV	no	no	no	
LHS 1596	03:48:33	+73:33:18	11.32	9.19	4.15	10.25	+0.31	16.4	YPC95	no	no	no	
GJ 1065	03:50:43	−06:05:10	12.82	10.04	5.07	12.93	+0.73	9.5	YPC95	yes	yes	yes	
LHS 1610	03:52:41	+17:01:04	13.85	10.66	5.80	13.87	+0.03	9.9	Hen06	yes	no	no	
GJ 157.1	03:59:53	+26:05:24	12.62	10.09	4.80	10.83	−0.71	22.8	YPC95	no	no	yes	
LHS 186	04:03:38	−05:08:05	14.87	···	4.02	11.31	+1.71	51.5	YPC95	no	no	no	S
GJ 162	04:08:37	+33:38:13	10.20	8.19	4.02	9.56	−0.05	13.4	vLe07	no	no	no	
LP 889-037	04:08:56	−31:28:53	14.56	11.48	5.74	13.61	−0.11	15.5	Win15	no	no	no	
GJ 163	04:09:15	−53:22:25	11.84	9.34	4.71	10.96	−0.34	15.0	vLe07	no	no	no	
GJ 1068	04:10:28	−53:36:08	13.60	10.42	5.70	14.37	+0.73	7.0	Jao05	no	no	no	
WT 135	04:11:27	−44:18:10	14.10	11.82	4.27	12.06	+1.86	25.6	Jao11	no	no	no	S
2MA 0414-0906	04:14:17	−09:06:54	13.88	11.10	5.13	12.00	−0.34	23.8	Shk12	no	no	no	Y
GJ 166C	04:15:22	−07:39:35	11.24	8.31	5.28	12.75	+0.04	5.0	YV	yes	no	yes	
LTT 11399	04:19:59	+36:29:11	11.46	···	4.05	9.62	−0.06	23.3	vLe07	no	no	no	
LHS 5094	04:26:33	−30:48:01	14.17	10.99	5.76	13.55	−0.21	13.3	Win15	no	no	no	
LHS 1678	04:32:42	−39:47:05	12.46	10.25	4.20	11.00	+0.97	19.6	Win15	no	no	no	
LP 834-032	04:35:36	−25:27:34	12.44	9.74	5.03	11.25	−0.87	17.3	Win15	no	yes	no	Y
LHS 1686	04:36:39	+11:13:17	14.29	11.58	4.99	12.32	+0.31	24.8	YPC95	no	no	no	
GJ 173	04:37:41	−11:02:19	10.34	8.16	4.25	10.13	−0.03	11.0	vLe07	no	no	no	
GJ 1072	04:50:50	+22:07:22	15.20	11.80	6.22	14.47	−0.15	14.0	YPC95	no	no	no	
GJ 179	04:52:05	+06:28:35	11.98	9.33	5.04	11.53	−0.60	12.3	vLe07	no	yes	no	
LP 776-025	04:52:24	−16:49:21	11.63	9.12	4.74	10.58	−0.80	16.2	Shk12	yes	yes	yes	Y
GJ 1073	04:52:34	+40:42:24	13.44	10.58	5.13	12.89	+0.52	12.9	YPC95	no	no	no	
GJ 2036B	04:53:31	−55:51:37	12.12	9.32	5.23	11.89	−0.69	11.1	vLe07	no	no	no	Y
GJ 1074	04:58:45	+50:56:37	10.98	9.01	3.94	9.56	+0.14	19.2	vLe07	no	yes	no	
LHS 1731	05:03:20	−17:22:25	11.69	9.16	4.75	11.87	+0.45	9.2	Jao05	yes	no	no	
GJ 184	05:03:23	+53:07:42	9.98	8.10	3.81	9.30	+0.17	13.7	YV	no	no	yes	
BD-211074A	05:06:50	−21:35:09	10.41	8.25	4.29	9.10	−1.17	18.3	Rie14	yes	no	yes	Y
LP 015-315	05:08:18	+75:38:15	14.50	···	5.96	13.48	−0.67	16.0	Gat09	no	no	no	
GJ 191	05:11:40	−45:01:06	8.85	6.90	3.80	10.89	+1.78	3.9	YPC95	no	no	no	S
GJ 192	05:12:42	+19:39:56	10.75	8.53	4.28	10.13	−0.11	13.3	YVO	no	no	no	
LHS 1747	05:15:08	−07:20:48	11.54	9.51	4.02	9.79	+0.17	22.4	vLe07	no	no	no	
GJ 1077	05:16:59	−78:17:20	11.90	9.42	4.70	10.99	−0.30	15.2	Jao11	no	no	no	
LP 717-036	05:25:42	−09:09:12	12.59	9.92	4.97	11.04	−0.91	20.4	Shk12	no	no	no	Y
GJ 203	05:28:00	+09:38:38	12.47	9.78	4.93	12.54	+0.68	9.7	YV	yes	yes	no	
GJ 2043B	05:29:27	+15:34:38	14.68	11.81	5.26	13.50	+0.83	17.2	vLe07	no	no	no	
GJ 2043A	05:29:27	+15:34:38	10.63	8.73	3.85	9.45	+0.23	17.2	vLe07	no	no	no	

[a] Notes in Column 14: Y = known young stars, (Y) = suspected young star, S = known subdwarf stars, (S) = suspected, but unconfirmed subdwarf stars.

Distance references: (Ang12) Anglada-Escudé et al. (2012); (Cos05) Costa et al. (2005); (Cos06) Costa et al. (2006); (Dav15) Davison et al. (2015); (Fab00) Fabricius & Makarov (2000); (Gat08) Gatewood (2008); (Gou04) Gould & Chanamé (2004); (Hen06) Henry et al. (2006); (Jao05) Jao et al. (2005); (Jao11) Jao et al. (2011); (Lur14) Lurie et al. (2014); (Rie10) Riedel et al. (2010); (Rie11) Riedel et al. (2011); (Rie14) Riedel et al. (2014); (Shk12) Shkolnik et al. (2012); (Sma10) Smart et al. (2010); (vLe07) van Leeuwen (2007); (Win15) Winters et al. (2015); (Win17) Winters et al. (2017); (YPC95) van Altena et al. (1995).

Table 1: Properties of the Low Mass Stars in the Short-Term Variability Study.

Star Name	R.A. 2000.0	Dec. 2000.0	V	I	$V-K$	M_V (mag)	ΔM_V (mag)	dist.	dist. ref.	LT Study	ST Study	Spec. Study	Notes[a]
(1)	(2)	(3)	(4)	(5)	(6)	(7)	(8)	(9)	(10)	(11)	(12)	(13)	(14)
LHS 1767	05:31:04	−30:11:44	13.11	10.45	4.92	12.19	+0.35	15.3	Rie10	yes	no	no	
GJ 205	05:31:27	−03:40:38	7.95	5.88	3.91	9.17	−0.19	5.7	YV	no	no	yes	
LTT 11684	05:34:51	+13:52:25	11.81	9.21	4.87	11.34	−0.38	12.4	YPC95	no	no	no	
LHS 5109	05:36:00	−07:38:59	12.86	10.06	5.29	12.01	−0.73	14.8	Win17	no	no	no	
GJ 212	05:41:30	+53:29:23	9.76	7.75	4.00	9.33	−0.24	12.2	YV	no	yes	yes	Y
HIP 026844	05:41:58	+15:20:14	10.61	8.81	3.73	8.97	+0.01	21.3	vLe07	no	no	no	
GJ 213	05:42:09	+12:29:21	11.54	8.68	5.15	12.72	+0.32	5.8	YVO	yes	yes	no	
GJ 2045	05:42:13	−05:27:57	15.34	11.93	5.97	14.86	+0.69	12.5	Jao05	no	no	no	
APM 0544-4108	05:43:46	−41:08:08	14.12	11.25	5.25	12.55	−0.09	20.6	Rie10	no	no	no	
GJ 218	05:47:40	−36:19:42	10.74	8.62	4.13	9.87	+0.01	14.9	vLe07	no	no	no	
GJ 220	05:53:14	+24:15:32	10.84	8.71	4.21	9.40	−0.66	19.4	YPC95	no	yes	yes	
G 192-011A	05:59:37	+58:35:34	10.24	8.22	4.03	9.60	−0.03	13.4	VO	no	no	no	
G 099-049	06:00:03	+02:42:23	11.31	8.43	5.27	12.73	+0.05	5.2	Hen06	yes	yes	yes	
LHS 214	06:00:49	+68:09:24	12.94	10.33	4.87	11.43	−0.27	20.0	YPC95	no	no	no	
LHS 213	06:00:54	+68:08:00	13.32	10.65	4.99	11.81	−0.19	20.0	YPC95	no	no	no	
LHS 1805	06:01:11	+59:35:01	11.71	8.99	5.07	12.31	+0.10	7.6	YPC95	no	no	no	
LHS 1807	06:02:22	−20:19:44	13.26	10.62	4.89	12.53	+0.78	14.0	Rie10	no	no	no	
LHS 1809	06:02:29	+49:50:58	14.53	11.13	6.10	14.69	+0.29	9.3	YPC95	no	no	no	
AP Col	06:04:52	−34:33:36	12.97	9.60	6.10	13.35	−1.06	8.4	Rie11	yes	yes	no	Y
LP 838-016	06:07:43	−25:44:41	11.89	9.39	4.72	11.62	+0.28	11.3	vLe07	no	no	no	
GJ 229A	06:10:34	−21:51:52	8.14	6.14	3.97	9.32	−0.18	5.8	YV	no	no	no	
GJ 1088	06:10:52	−43:24:17	12.28	9.61	4.97	12.00	+0.04	11.4	Rie10	yes	no	no	
LHS 216	06:14:02	+15:09:54	14.63	12.54	3.97	12.02	+2.53	33.2	YPC95	no	no	no	S
G 192-022	06:14:02	+51:40:08	12.86	10.27	4.74	12.10	+0.72	14.2	YPC95	no	no	no	
GJ 231.3	06:19:21	−06:39:34	13.06	10.50	4.82	12.24	+0.64	14.6	YPC95	no	no	no	
GJ 232	06:24:41	+23:25:59	13.16	10.21	5.25	13.54	+0.90	8.4	YPC95	no	yes	yes	(S)
LHS 1848	06:25:53	+56:09:42	14.62	11.76	5.26	12.88	+0.21	22.3	YPC95	no	no	no	
L 032-008	06:33:46	−75:37:30	11.43	8.82	4.87	11.66	−0.06	9.0	vLe07	yes	no	no	
LHS 1857	06:36:07	+11:36:05	14.24	11.35	5.25	12.94	+0.31	18.2	YPC95	no	no	no	
LP 381-004	06:36:18	−40:00:23	10.59	8.72	3.80	9.14	+0.03	19.5	vLe07	no	no	no	
GJ 239	06:37:10	+17:33:53	9.64	7.75	3.78	9.68	+0.62	9.8	YV	no	no	no	
LP 780-032	06:39:37	−21:01:33	12.78	10.01	5.13	11.79	−0.57	15.8	RECXX	no	no	no	
NLTT 16863	06:39:37	−55:36:34	9.81	7.93	3.78	9.21	+0.13	13.2	vLe07	no	no	no	
G 108-022	06:42:09	+03:35:41	13.33	10.61	5.05	13.24	+1.08	10.4	YPC95	no	no	yes	
G 108-021	06:42:09	+03:35:41	12.06	9.55	4.73	11.97	+0.62	10.4	YPC95	no	yes	yes	
SCR 0642-6707	06:42:27	−67:07:20	16.01	12.42	6.20	15.33	+0.74	13.7	Win17	no	no	no	
GJ 2050	06:44:45	+71:53:15	10.95	8.99	3.95	9.24	−0.21	22.0	YV	no	yes	no	
LTT 11918	06:47:18	+23:46:44	12.65	11.15	3.94	10.99	+1.56	21.5	YPC95	no	yes	yes	
GJ 1092	06:49:05	+37:06:51	13.78	11.00	5.01	13.16	+1.11	13.3	YPC95	no	no	no	
GJ 251	06:54:48	+33:16:05	10.02	7.49	4.75	11.28	−0.12	5.6	YV	no	no	no	
LHS 1882	06:56:22	+54:57:38	12.47	10.24	4.21	11.29	+1.22	17.2	YPC95	no	yes	no	
LTT 11947	06:56:28	+40:04:27	11.10	9.16	3.91	9.14	−0.22	24.7	YV	no	no	no	
WT 207	07:02:36	−40:06:28	15.15	12.28	5.19	13.19	+0.69	24.7	Cos06	no	no	no	
LHS 225A	07:04:46	−38:36:08	12.87	10.51	5.00	11.61	−0.44	17.9	Jao05	no	no	no	
LHS 225B	07:04:46	−38:36:07	13.02	10.63	5.07	11.76	−0.45	17.9	Jao05	no	no	no	
GJ 2055	07:07:22	−21:27:27	11.08	8.87	4.28	9.90	−0.34	17.2	vLe07	no	no	no	
LTT 11972	07:07:50	+67:12:04	11.18	9.08	4.15	9.95	+0.04	17.6	vLe07	no	no	no	
LTT 17942	07:10:14	+37:40:19	14.57	···	5.10	12.65	+0.38	24.2	YPC95	no	no	no	
LHS 228	07:16:28	+23:42:10	15.51	13.23	4.21	11.75	+1.68	56.5	YPC95	no	no	no	S
SC R0717-0501	07:17:17	−05:01:04	13.30	10.40	5.26	13.13	+0.48	10.8	Win17	no	no	no	
LTT 12003	07:18:08	+39:16:29	10.33	···	3.96	9.54	+0.06	14.4	vLe07	no	no	no	
GJ 270	07:19:31	+32:49:48	10.08	8.27	3.70	8.67	−0.23	19.1	YV	no	yes	no	
GJ 272	07:23:14	+46:05:14	10.53	···	4.07	9.47	−0.26	16.3	YV	no	no	no	

[a] Notes in Column 14: Y = known young stars, (Y) = suspected young star, S = known subdwarf stars, (S) = suspected, but unconfirmed subdwarf stars.

Distance references: (Ang12) Anglada-Escudé et al. (2012); (Cos05) Costa et al. (2005); (Cos06) Costa et al. (2006); (Dav15) Davison et al. (2015); (Fab00) Fabricius & Makarov (2000); (Gat08) Gatewood (2008); (Gou04) Gould & Chanamé (2004); (Hen06) Henry et al. (2006); (Jao05) Jao et al. (2005); (Jao11) Jao et al. (2011); (Lur14) Lurie et al. (2014); (Rie10) Riedel et al. (2010); (Rie11) Riedel et al. (2011); (Rie14) Riedel et al. (2014); (Shk12) Shkolnik et al. (2012); (Sma10) Smart et al. (2010); (vLe07) van Leeuwen (2007); (Win15) Winters et al. (2015); (Win17) Winters et al. (2017); (YPC95) van Altena et al. (1995).

Table 1: Properties of the Low Mass Stars in the Short-Term Variability Study.

Star Name (1)	R.A. 2000.0 (2)	Dec. 2000.0 (3)	V (4)	I (5)	$V-K$ (6)	M_V (mag) (7)	ΔM_V (mag) (8)	dist. (9)	dist. ref. (10)	LT Study (11)	ST Study (12)	Spec. Study (13)	Notes[a] (14)
GJ 273	07:27:24	+05:13:32	9.85	7.14	4.99	11.95	−0.07	3.8	YVO	yes	yes	yes	
GJ 1097	07:28:45	−03:17:53	11.43	8.93	4.73	11.11	−0.25	11.6	YV	no	no	no	
GJ 277B	07:31:57	+36:13:47	11.78	9.06	5.03	11.42	−0.68	11.8	YV	no	yes	no	
GJ 275.1	07:32:02	+68:37:15	10.89	8.89	4.03	8.91	−0.73	24.9	vLe07	no	yes	yes	
GJ 277.1	07:34:27	+62:56:29	10.49	8.51	3.93	10.13	+0.72	11.8	YV	no	no	no	
GJ 282C	07:36:07	−03:06:38	9.87	7.92	3.94	9.12	−0.29	14.1	YVO	no	no	yes	
LHS 1932	07:36:12	−51:55:21	12.48	9.92	4.73	11.45	+0.10	16.1	Rie10	yes	yes	no	
SCR 0736-3024	07:36:57	−30:24:16	13.65	10.84	5.16	13.03	+0.62	13.3	Win17	no	no	no	
GJ 281	07:39:23	+02:11:01	9.58	7.80	3.71	8.77	−0.14	14.5	YV	no	no	yes	
SCR 0740-4257	07:40:12	−42:57:44	13.81	10.50	6.04	14.35	+0.05	7.8	RECXX	no	no	no	
GJ 289	07:48:16	+20:22:05	11.45	9.34	4.05	10.60	+0.91	14.8	YV	no	yes	no	
L 034-026	07:49:12	−76:42:06	11.31	8.79	4.73	11.18	−0.18	10.6	Rie14	yes	no	no	Y
GJ 1101	07:55:49	+83:23:19	13.13	10.29	5.22	12.66	+0.10	12.4	YPC95	no	no	no	
SCR 0757-7114	07:57:32	−71:14:54	12.45	9.77	5.03	10.73	−1.38	22.1	Rie14	yes	yes	no	Y
GJ 1105	07:58:12	+41:18:13	11.98	9.24	5.10	12.44	+0.15	8.1	YVO	no	no	no	
LHS 1976	08:03:20	+52:50:38	11.38	9.26	4.14	9.41	−0.49	24.8	Sma10	no	yes	no	
LHS 5133A	08:08:13	+21:06:18	9.40	7.83	3.32	8.29	+0.17	16.7	YPC95	no	no	no	
L 1321-040	08:09:30	+21:54:17	11.78	9.56	4.27	10.05	−0.16	22.2	vLe07	no	no	no	
GJ 299	08:11:58	+08:46:23	12.86	9.91	5.20	13.70	+1.18	6.8	YPC95	yes	no	no	(S)
LHS 2010	08:27:11	−44:59:21	11.86	9.19	4.99	11.18	−0.83	13.7	Rie10	yes	yes	no	
LHS 2038	08:40:55	+67:39:15	14.66	11.82	5.25	12.71	+0.08	24.5	YPC95	no	no	no	
GJ 317	08:40:55	−23:28:00	12.01	9.37	4.98	11.09	−0.91	15.3	Ang12	no	yes	no	
GJ 1114	08:51:43	+18:07:29	11.55	9.44	4.03	10.40	+0.77	17.0	YV	no	no	no	
LP 844-033	08:56:17	−23:26:57	15.95	12.52	6.13	14.09	−0.37	23.5	Cos06	no	no	no	
GJ 1118	08:59:05	−31:13:26	13.79	10.95	5.20	12.55	+0.02	17.7	Jao05	no	no	no	
LHS 259	09:00:52	+48:25:25	14.14	11.50	4.82	12.67	+1.08	19.7	YPC95	no	no	no	
LP 060-179	09:02:51	+68:03:18	12.65	9.92	4.94	12.31	+0.42	11.7	Sma07	no	no	no	
GJ 334	09:06:45	−08:48:24	9.50	7.68	3.74	8.71	−0.28	14.4	YV	no	no	yes	
GJ 1121	09:09:24	+40:06:05	14.53	11.65	5.23	12.84	+0.26	21.8	YPC95	no	no	no	
GJ 336.1	09:11:30	+46:37:01	10.94	9.04	3.88	8.99	−0.30	24.5	vLe07	no	no	no	
SCR 0914-4134	09:14:17	−41:34:38	15.06	11.75	5.94	14.66	+0.55	12.0	Win17	no	no	no	
LHS 2122	09:16:25	−62:04:16	12.57	9.94	5.03	11.42	−0.68	17.0	Rie10	no	yes	no	
GJ 1123	09:17:05	−77:49:23	13.15	10.05	5.70	13.38	−0.27	9.0	Jao05	yes	no	no	
LHS 265	09:17:45	+58:24:13	15.21	11.95	5.81	14.26	+0.40	15.5	YPC95	no	no	no	
LHS 267	09:20:58	+03:20:59	13.32	10.70	4.80	12.25	+0.71	16.4	YPC95	no	no	no	
GJ 341	09:21:37	−60:16:55	9.49	7.54	3.90	9.40	+0.06	10.4	YV	no	no	no	
GJ 1125	09:30:44	+00:19:22	11.72	9.13	4.85	11.74	+0.08	9.9	YV	no	yes	no	
GJ 353	09:31:56	+36:19:12	10.22	8.26	3.92	9.49	+0.11	14.0	YV	no	no	no	
GJ 354.1B	09:32:48	+26:59:44	16.50	···	7.03	15.25	−0.56	17.8	vLe07	no	no	no	
G 117-034	09:39:24	+31:45:17	11.91	···	4.23	10.01	−0.11	24.0	vLe07	no	no	no	
GJ 358	09:39:46	−41:04:03	10.78	8.27	4.72	10.89	−0.46	9.5	vLe07	yes	yes	no	
GJ 361	09:41:10	+13:12:34	10.40	8.20	4.27	10.13	−0.08	11.3	YV	no	no	no	
GJ 363	09:42:17	+55:58:31	12.50	9.83	4.97	11.58	−0.39	15.3	YPC95	no	no	no	
GJ 1128	09:42:46	−68:53:06	12.74	9.62	5.70	13.68	+0.03	6.5	Jao05	yes	no	no	
GJ 362B	09:42:51	+70:02:21	11.24	8.71	4.77	10.86	−0.60	11.9	YV	no	no	no	
LHS 272	09:43:46	−17:47:06	13.16	10.87	4.29	12.51	+2.26	13.5	Jao11	yes	no	no	S
LHS 2181	09:43:55	+26:58:08	12.05	9.47	4.86	11.32	−0.37	14.0	vLe07	no	no	no	
WT 244	09:44:23	−73:58:38	15.17	12.02	5.80	13.36	−0.47	23.0	Rie10	no	no	no	
GJ 1129	09:44:47	−18:12:48	12.46	9.67	5.20	12.33	−0.20	10.6	Jao11	yes	no	no	
G 161-071	09:44:54	−12:20:54	13.76	10.36	6.16	13.11	−1.40	13.5	RECXX	no	no	no	
WT 2458	09:45:59	−32:53:31	14.04	10.89	5.76	13.76	−0.01	11.4	Win17	no	no	no	
GJ 366	09:46:48	+76:02:38	10.64	8.59	4.01	9.63	+0.04	15.9	YV	no	no	no	
G 043-002	09:48:50	+15:38:44	13.24	10.66	4.77	12.02	+0.56	17.5	Shk12	no	no	no	

[a] Notes in Column 14: Y = known young stars, (Y) = suspected young star, S = known subdwarf stars, (S) = suspected, but unconfirmed subdwarf stars.

Distance references: (Ang12) Anglada-Escudé et al. (2012); (Cos05) Costa et al. (2005); (Cos06) Costa et al. (2006); (Dav15) Davison et al. (2015); (Fab00) Fabricius & Makarov (2000); (Gat08) Gatewood (2008); (Gou04) Gould & Chanamé (2004); (Hen06) Henry et al. (2006); (Jao05) Jao et al. (2005); (Jao11) Jao et al. (2011); (Lur14) Lurie et al. (2014); (Rie10) Riedel et al. (2010); (Rie11) Riedel et al. (2011); (Rie14) Riedel et al. (2014); (Shk12) Shkolnik et al. (2012); (Sma10) Smart et al. (2010); (vLe07) van Leeuwen (2007); (Win15) Winters et al. (2015); (Win17) Winters et al. (2017); (YPC95) van Altena et al. (1995).

Table 1: Properties of the Low Mass Stars in the Short-Term Variability Study.

Star Name	R.A. 2000.0	Dec. 2000.0	V	I	$V-K$	M_V (mag)	ΔM_V (mag)	dist.	dist. ref.	LT Study	ST Study	Spec. Study	Notes[a]
(1)	(2)	(3)	(4)	(5)	(6)	(7)	(8)	(9)	(10)	(11)	(12)	(13)	(14)
GJ 369	09:51:09	−12:19:47	10.06	8.11	3.91	9.36	+0.00	13.8	YV	no	no	no	
GJ 1130B	09:53:28	−31:45:08	14.14	11.48	4.86	12.23	+0.55	24.1	vLe07	no	no	no	
LP 847-048	09:55:23	−27:15:40	12.08	9.43	4.94	11.81	−0.07	11.3	vLe07	no	no	no	
GJ 373	09:56:08	+62:47:18	8.97	7.11	3.77	8.82	−0.22	10.7	YV	no	no	yes	
GJ 377	10:01:10	−30:23:24	11.44	8.98	4.74	10.42	−0.97	16.0	YV	no	yes	no	
GJ 378	10:02:21	+48:05:19	10.10	8.13	3.94	9.22	−0.21	15.0	YV	no	no	no	
LHS 2220	10:06:43	+41:42:52	11.33	9.36	3.93	9.76	+0.36	20.6	vLe07	no	no	no	
GJ 1131	10:07:59	+69:14:46	14.35	11.54	5.05	13.11	+0.96	17.7	YPC95	no	no	no	
LHS 2224	10:09:29	+51:17:19	13.48	10.71	4.96	12.88	+0.95	13.2	YPC95	no	no	no	
GJ 383	10:12:08	−18:37:04	9.95	8.14	3.76	8.69	−0.33	17.9	YVO	no	no	yes	
GJ 382	10:12:17	−03:44:44	9.29	7.11	4.28	9.80	−0.42	7.9	YV	no	no	yes	
GJ 2079	10:14:19	+21:04:29	10.04	8.24	3.78	8.23	−0.83	23.0	vLe07	no	no	yes	
GJ 1132	10:14:51	−47:09:24	13.49	10.69	5.17	13.09	+0.65	12.0	Jao05	no	no	no	
GJ 386	10:16:45	−11:57:42	10.51	8.13	4.06	9.91	+0.20	13.2	YV	no	no	no	
GJ 388	10:19:36	+19:52:11	9.29	6.78	4.70	10.84	−0.44	4.9	YPC95	no	no	yes	
GJ 389B	10:22:24	−60:10:37	12.63	10.12	4.73	11.15	−0.21	19.8	YV	no	no	no	
GJ 389A	10:22:24	−60:10:37	10.72	8.80	3.87	9.24	−0.04	19.8	YV	no	no	no	
GJ 390	10:25:10	−10:13:43	10.17	8.10	4.14	9.74	−0.15	12.2	YV	no	no	no	
LHS 2268	10:28:31	+48:14:10	13.25	10.52	5.02	11.65	−0.44	20.9	YPC95	no	no	no	
LTT 03855	10:30:50	−35:46:39	11.24	9.26	3.95	9.29	−0.16	24.6	vLe07	no	no	no	
LHS 283	10:35:06	+69:26:16	11.95	9.33	4.79	11.36	−0.15	13.1	YPC95	no	no	no	
GJ 398	10:36:01	+05:07:06	12.69	9.92	5.09	11.88	−0.38	14.5	YPC95	no	no	no	
LEHPM2-2758	10:38:51	−86:32:41	13.24	10.46	5.13	12.60	+0.26	13.4	Win17	no	no	no	
GJ 1134	10:41:37	+37:36:39	12.98	10.07	5.27	12.92	+0.24	10.3	YPC95	no	no	no	
GJ 1136A	10:41:51	−36:38:00	10.15	8.31	3.76	9.12	+0.09	16.1	vLe07	no	no	no	
LHS 288	10:44:21	−61:12:35	13.90	10.27	6.17	15.49	+0.96	4.8	Hen06	no	no	no	
LP 905-056	10:45:17	−30:48:27	11.22	9.03	4.23	10.49	+0.38	14.0	vLe07	no	no	no	
LHS 2317	10:50:26	+33:05:19	13.07	10.38	5.06	11.27	−0.91	22.9	YPC95	no	yes	no	
GJ 402	10:50:52	+06:48:29	11.70	8.85	5.33	12.54	−0.29	6.8	YV	yes	no	no	
GJ 403	10:52:04	+13:59:51	12.72	10.06	4.93	12.25	+0.40	12.4	Sma07	no	no	no	
LHS 2328	10:55:34	−09:21:25	13.55	10.86	4.94	12.21	+0.32	18.5	Rie10	no	no	no	
LP731-076	10:58:28	−10:46:30	14.44	11.24	5.80	13.76	−0.09	13.7	RECXX	no	no	no	
LHS 2337	10:59:04	+30:14:55	15.36	···	5.71	13.62	−0.04	22.3	YPC95	no	no	no	
LHS 296	11:01:23	+02:59:46	14.06	11.21	5.15	13.34	+0.94	13.9	YPC95	no	no	no	
GJ 1141B	11:02:21	+16:30:45	11.62	9.51	4.11	10.19	+0.36	19.3	YPC95	no	no	no	
GJ 1141A	11:02:21	+16:30:45	11.49	9.44	4.05	10.06	+0.38	19.3	YPC95	no	no	no	
GJ 410	11:02:38	+21:58:01	9.57	7.63	3.88	9.23	−0.07	11.7	YV	no	no	no	
GJ 411	11:03:20	+35:58:11	7.46	···	4.21	10.47	+0.41	2.5	YV	no	no	yes	
LP 491-051	11:03:21	+13:37:57	12.96	10.25	5.05	12.02	−0.13	15.4	Shk12	yes	no	no	
GJ 412A	11:05:28	+43:31:36	8.77	6.70	4.00	10.36	+0.80	4.9	YV	no	yes	yes	
NLTT 26359	11:07:27	−19:17:29	10.38	8.52	3.76	9.03	+0.01	18.6	vLe07	no	no	no	
GJ 414B	11:11:05	+30:26:45	9.98	7.82	4.25	9.60	−0.55	11.9	YV	no	yes	no	
2MA 1113+1025	11:13:00	+10:25:05	14.52	11.60	5.32	12.71	−0.09	23.0	Shk12	no	no	no	
GJ 421C	11:15:15	−18:07:34	13.61	11.02	4.85	12.64	+0.99	15.6	YPC95	no	no	no	
GJ 424	11:20:04	+65:50:47	9.32	7.43	3.79	9.57	+0.49	8.9	YV	no	yes	no	
LHS 2400	11:22:42	−32:05:40	16.35	12.93	6.19	14.59	+0.03	22.5	Cos06	no	no	no	
GJ 2085	11:23:44	+08:33:48	11.19	9.14	4.03	9.52	−0.12	21.6	YV	no	no	no	
LHS 2401	11:23:57	−18:21:48	13.10	10.54	4.78	11.79	+0.30	18.3	Rie10	yes	no	no	
LHS 2405A	11:25:29	+78:15:57	12.15	9.94	4.22	10.42	+0.33	22.2	YPC95	no	no	no	
LP 672-042	11:30:41	−08:05:42	12.06	9.46	4.91	11.46	−0.35	13.2	vLe07	no	no	no	
GJ 430.1	11:31:43	+22:40:01	10.27	8.29	3.95	9.26	−0.18	15.9	vLe07	no	yes	no	
GJ 431	11:31:46	−41:02:47	11.52	8.87	5.01	11.46	−0.60	10.3	vLe07	no	no	no	
LP 792-033	11:32:19	−16:58:07	11.45	9.43	3.98	9.66	+0.14	22.8	vLe07	no	no	no	

[a] Notes in Column 14: Y = known young stars, (Y) = suspected young star, S = known subdwarf stars, (S) = suspected, but unconfirmed subdwarf stars.

Distance references: (Ang12) Anglada-Escudé et al. (2012); (Cos05) Costa et al. (2005); (Cos06) Costa et al. (2006); (Dav15) Davison et al. (2015); (Fab00) Fabricius & Makarov (2000); (Gat08) Gatewood (2008); (Gou04) Gould & Chanamé (2004); (Hen06) Henry et al. (2006); (Jao05) Jao et al. (2005); (Jao11) Jao et al. (2011); (Lur14) Lurie et al. (2014); (Rie10) Riedel et al. (2010); (Rie11) Riedel et al. (2011); (Rie14) Riedel et al. (2014); (Shk12) Shkolnik et al. (2012); (Sma10) Smart et al. (2010); (vLe07) van Leeuwen (2007); (Win15) Winters et al. (2015); (Win17) Winters et al. (2017); (YPC95) van Altena et al. (1995).

Table 1: Properties of the Low Mass Stars in the Short-Term Variability Study.

Star Name (1)	R.A. 2000.0 (2)	Dec. 2000.0 (3)	V (4)	I (5)	$V-K$ (6)	M_V (mag) (7)	ΔM_V (mag) (8)	dist. (9)	dist. ref. (10)	LT Study (11)	ST Study (12)	Spec. Study (13)	Notes[a] (14)
TWA 8A	11:32:41	−26:51:56	12.23	9.79	4.80	8.87	−2.66	46.9	Rie14	yes	yes	no	Y
TWA 8B	11:32:41	−26:52:09	15.22	11.76	6.21	11.85	−2.74	47.1	Rie14	yes	yes	no	Y
LHS 2427	11:34:37	−23:52:15	11.17	9.19	3.91	9.92	+0.55	17.8	vLe07	no	no	no	
GJ 433	11:35:26	−32:32:23	9.84	7.69	4.22	10.09	+0.01	8.9	vLe07	no	no	no	
SCR 1138-7721	11:38:16	−77:21:48	14.78	11.24	6.26	15.21	+0.53	8.2	Hen06	no	no	no	
GJ 1147	11:38:24	−41:22:32	13.72	10.91	5.18	12.83	+0.36	15.1	Rie10	no	no	no	
GJ 1148	11:41:44	+42:45:07	11.92	9.18	5.10	11.67	−0.60	11.2	YV	no	yes	yes	
GJ 438	11:43:19	−51:50:25	10.35	8.27	4.03	10.18	+0.55	10.8	Rie10	yes	no	no	
GJ 442B	11:46:31	−40:30:01	12.88	9.99	4.92	13.06	+1.23	9.2	vLe07	no	no	no	
GJ 445	11:47:41	+78:41:28	10.79	8.13	4.84	12.17	+0.54	5.3	YV	no	yes	no	
GJ 450	11:51:07	+35:16:19	9.73	···	4.12	10.06	+0.20	8.6	YV	no	no	no	
GJ 452.1	11:54:08	+09:48:12	12.81	10.12	4.94	12.56	+0.68	11.2	YVO	no	no	no	
GJ 2086	11:55:49	−38:16:49	11.96	9.91	4.02	10.03	+0.43	24.3	vLe07	no	no	no	
LHS 2482	11:57:32	+11:49:39	11.84	9.64	4.27	9.91	−0.29	24.3	vLe07	no	no	no	
LHS 2484	11:58:27	−41:55:03	16.07	13.18	5.03	13.55	+1.44	31.9	Gou04	no	no	no	S
LHS 2497	12:02:18	+28:35:14	12.86	10.36	4.47	11.33	+0.63	20.2	YPC95	no	yes	no	S
LHS 320	12:02:34	+08:25:51	14.00	11.87	4.01	11.06	+1.46	38.8	YPC95	no	no	no	S
GJ 456.1B	12:09:54	−46:12:30	13.25	10.63	4.95	11.78	−0.14	19.7	vLe07	no	no	no	
LHS 2520	12:10:05	−15:04:16	12.09	9.30	5.23	11.55	−1.03	12.8	Rie10	yes	no	yes	
L 758-108	12:11:11	−19:57:38	12.62	9.99	4.88	12.14	+0.40	12.5	vLe07	no	no	no	
GJ 458A	12:12:20	+54:29:08	9.79	8.00	3.73	8.85	−0.11	15.4	vLe07	no	no	no	
GJ 458B	12:12:20	+54:29:08	13.33	10.63	4.94	12.39	+0.50	15.4	vLe07	no	no	no	
LP 852-057	12:13:32	−25:55:24	11.47	9.49	3.92	9.62	+0.24	23.4	vLe07	no	no	no	
SCR 1214-2345	12:14:08	−23:45:17	13.96	10.78	5.73	13.77	+0.07	10.9	Rie14	yes	yes	no	
GJ 1154	12:14:16	+00:37:26	13.64	10.31	6.10	14.02	−0.39	8.4	YPC95	yes	no	no	
SCR 1214-4603	12:14:40	−46:03:14	15.66	12.23	6.22	14.78	+0.17	15.0	Win17	no	no	no	
GJ 458.2	12:15:08	+48:43:57	10.53	8.70	3.76	8.56	−0.46	24.8	vLe07	no	yes	no	
GJ 1156	12:18:59	+11:07:34	13.80	10.34	6.23	14.74	+0.11	6.5	YPC95	yes	no	no	
NLTT 30359	12:20:34	−82:25:59	11.96	9.20	5.12	11.44	−0.88	12.7	Win17	no	no	no	
GJ 1157	12:23:01	−46:37:08	13.59	10.71	5.23	12.57	−0.02	16.0	Rie10	yes	no	no	
GJ 464	12:23:53	+12:34:48	10.39	8.59	3.76	8.79	−0.22	20.9	vLe07	no	no	no	
LP 377-100	12:29:27	+22:59:47	14.18	11.40	5.18	12.64	+0.18	20.3	Shk12	no	no	no	
GJ 1158	12:29:34	−55:59:37	13.26	10.41	5.20	12.67	+0.16	13.1	Jao11	no	no	no	
LHS 2568	12:29:54	−05:27:20	14.21	11.37	5.29	12.61	−0.12	20.9	Rie10	no	no	no	
LHS 2567	12:29:54	−05:27:24	13.08	10.33	5.12	11.48	−0.85	20.9	Rie10	no	yes	no	
GJ 471	12:31:15	+08:48:38	9.66	7.85	3.77	8.99	−0.05	13.6	YV	no	no	no	
GJ 476	12:35:00	+09:49:42	11.41	9.20	4.26	10.11	−0.07	18.2	vLe07	no	no	no	
GJ 1162	12:38:45	−04:19:38	13.56	10.82	5.11	12.09	−0.21	19.7	YPC95	no	no	no	
GJ 480	12:38:52	+11:41:46	11.51	8.98	4.82	10.78	−0.81	14.0	YV	no	yes	yes	
GJ 480.1	12:40:46	−43:33:59	12.24	9.58	4.83	12.72	+1.12	8.0	vLe07	yes	no	no	(S)
GJ 486	12:47:56	+09:45:05	11.40	8.67	5.04	11.78	−0.35	8.4	vLe07	yes	no	no	
LHS 2651	12:55:57	+50:55:22	14.42	11.76	4.82	12.85	+1.27	20.6	YPC95	no	no	no	
GJ 490B	12:57:39	+35:13:19	13.20	10.48	5.18	11.72	−0.76	19.8	YV	no	no	yes	
GJ 490A	12:57:40	+35:13:30	10.68	8.81	4.13	9.20	−0.67	19.8	YV	no	yes	yes	
HIP 063480	13:00:25	−34:36:24	10.63	8.69	3.92	9.16	−0.21	19.7	vLe07	no	no	no	
GJ 493.1	13:00:34	+05:41:08	13.41	10.29	5.75	13.87	+0.12	8.1	YPC95	no	no	no	
LHS 2668	13:01:19	−63:11:42	10.93	8.90	4.00	9.77	+0.21	17.1	vLe07	no	no	no	
LHS 346	13:09:20	−40:09:27	12.86	10.24	4.87	11.83	+0.11	16.1	Jao05	yes	no	no	
LHS 2686	13:10:13	+47:45:19	14.53	11.31	5.84	14.47	+0.54	10.3	Sma10	no	no	no	
GJ 1169	13:16:30	+27:52:44	13.26	10.64	4.82	12.27	+0.69	15.8	YPC95	no	yes	no	
GJ 505B	13:16:51	+17:01:01	9.60	···	3.85	9.37	+0.15	11.1	YV	no	no	no	
GJ 1170	13:17:58	+36:17:56	11.29	9.31	3.94	9.63	+0.19	21.5	vLe07	no	no	no	
GJ 507A	13:19:33	+35:06:36	9.52	7.54	3.96	8.90	−0.57	13.3	YV	no	no	no	

[a] Notes in Column 14: Y = known young stars, (Y) = suspected young star, S = known subdwarf stars, (S) = suspected, but unconfirmed subdwarf stars.

Distance references: (Ang12) Anglada-Escudé et al. (2012); (Cos05) Costa et al. (2005); (Cos06) Costa et al. (2006); (Dav15) Davison et al. (2015); (Fab00) Fabricius & Makarov (2000); (Gat08) Gatewood (2008); (Gou04) Gould & Chanamé (2004); (Hen06) Henry et al. (2006); (Jao05) Jao et al. (2005); (Jao11) Jao et al. (2011); (Lur14) Lurie et al. (2014); (Rie10) Riedel et al. (2010); (Rie11) Riedel et al. (2011); (Rie14) Riedel et al. (2014); (Shk12) Shkolnik et al. (2012); (Sma10) Smart et al. (2010); (vLe07) van Leeuwen (2007); (Win15) Winters et al. (2015); (Win17) Winters et al. (2017); (YPC95) van Altena et al. (1995).

Table 1: Properties of the Low Mass Stars in the Short-Term Variability Study.

Star Name (1)	R.A. 2000.0 (2)	Dec. 2000.0 (3)	V (4)	I (5)	$V-K$ (6)	M_V (mag) (7)	ΔM_V (mag) (8)	dist. (9)	dist. ref. (10)	LT Study (11)	ST Study (12)	Spec. Study (13)	Notes[a] (14)
GJ 507.1	13:19:40	+33:20:47	10.62	···	4.23	9.47	−0.64	17.0	YV	no	yes	no	
LHS 2718	13:20:03	−35:24:44	12.84	10.24	4.86	12.17	+0.49	13.6	Rie10	yes	no	no	
L 977-016A	13:20:24	−01:39:27	11.57	9.51	4.04	9.91	+0.24	21.5	vLe07	no	no	no	
LHS 350	13:22:54	+24:28:00	12.96	10.21	5.00	12.29	+0.25	13.6	YPC95	no	yes	no	
LHS 2729	13:23:38	−25:54:45	12.89	10.14	5.11	12.17	−0.13	13.9	Rie10	no	yes	no	Y
GJ 510	13:25:48	−28:22:26	11.00	8.86	4.12	9.89	+0.03	16.7	YV	no	no	no	
LP 855-014	13:27:53	−26:57:01	11.78	9.59	4.24	10.17	+0.04	21.0	vLe07	no	no	no	
GJ 512A	13:28:21	−02:21:37	11.42	8.93	4.81	10.74	−0.82	13.7	YV	no	no	yes	
GJ 514	13:29:59	+10:22:37	9.05	7.01	4.01	9.65	+0.05	7.6	YV	no	no	no	
LEP 1330-2039	13:30:41	−20:39:03	12.46	9.75	5.07	11.33	−0.87	16.8	Win17	no	no	no	
GJ 520C	13:37:40	+48:07:54	14.47	11.74	5.17	12.73	+0.28	22.3	vLe07	no	no	no	
GJ 521	13:39:24	+46:11:11	10.23	···	3.95	9.68	+0.24	12.9	YV	no	no	no	
GJ 1174	13:40:08	+43:46:38	12.78	10.07	4.99	11.77	−0.23	15.9	YPC95	no	no	no	
LHS 2784	13:42:43	+33:17:24	11.97	9.27	4.99	12.15	+0.14	9.2	vLe07	no	no	no	
SCR 1343-4002	13:43:41	−40:02:28	15.06	11.88	5.81	13.88	+0.01	17.2	Win17	no	no	no	
GJ 526	13:45:43	+14:53:29	8.46	6.39	4.05	9.80	+0.13	5.4	YVO	no	no	no	
LHS 2794	13:45:50	−17:58:05	11.86	9.19	4.96	11.82	−0.12	10.2	vLe07	no	no	no	
GJ 1179	13:48:13	+23:36:48	15.32	11.87	6.14	14.92	+0.45	12.0	YPC95	no	no	no	
LP798-051	13:52:53	−18:20:16	11.77	9.64	4.16	9.94	+0.00	23.2	vLe07	no	no	no	
GJ 534.2	13:53:47	+78:51:06	10.61	8.76	3.80	8.70	−0.41	24.1	vLe07	no	yes	no	
SSS 1358-3938	13:58:05	−39:37:55	14.04	11.20	5.09	13.79	+1.53	11.2	Win15	no	no	no	
GJ 536	14:01:03	−02:39:17	9.68	7.65	4.00	9.68	+0.12	10.0	YV	no	no	no	
HIP 068570	14:02:19	+13:41:22	10.66	8.74	3.95	9.18	−0.28	19.8	vLe07	no	no	no	
LHS 2852	14:02:47	−24:31:50	12.13	9.85	4.29	10.95	+0.69	17.2	YPC95	no	yes	no	S
GJ 540	14:08:12	+80:35:50	10.35	8.33	4.02	9.22	−0.40	16.8	YV	no	yes	no	
LHS 2866	14:08:16	+75:51:14	11.59	9.51	4.03	9.61	−0.02	24.9	YPC95	no	yes	no	
NLTT 36465	14:10:57	−31:17:25	10.83	8.73	4.14	9.72	−0.17	16.7	vLe07	no	no	no	
GJ 2106	14:13:12	−56:44:31	10.19	8.11	4.05	9.87	+0.17	11.6	vLe07	no	no	no	
GJ 545	14:20:07	−09:37:13	12.84	10.15	4.86	12.11	+0.41	14.0	YO	yes	no	no	
LHS 370	14:20:53	+36:57:16	15.36	···	5.11	13.87	+1.56	19.9	Sma07	no	no	no	
LHS 2899	14:21:15	−01:07:19	13.12	10.39	5.03	12.50	+0.40	13.3	Rie10	yes	no	no	
GJ 2107	14:23:06	−68:22:57	10.27	8.49	3.71	8.42	−0.49	23.4	vLe07	no	no	no	
GJ 548A	14:25:43	+23:37:01	9.76	7.91	3.79	8.73	−0.36	16.1	YV	no	yes	no	
GJ 548B	14:25:46	+23:37:13	10.01	8.07	3.92	8.98	−0.40	16.1	YV	no	yes	no	
GJ 552	14:29:29	+15:31:57	10.68	8.46	4.29	9.93	−0.32	14.1	YV	no	no	no	
GJ 553.1	14:31:01	−12:17:45	11.95	9.30	4.99	11.78	−0.23	10.8	vLe07	no	no	no	
LHS 375	14:31:38	−25:25:33	15.64	13.35	4.07	13.74	+4.01	24.0	YPC95	no	no	no	S
SCR 1444-3426	14:44:07	−34:26:47	14.17	11.26	5.29	13.38	+0.65	14.4	Win17	no	no	no	
GJ 1185	14:47:53	−03:09:15	13.33	10.99	4.27	11.86	+1.64	19.7	YPC95	no	yes	yes	
GJ 563.2B	14:49:31	−26:06:42	12.07	9.92	4.18	10.33	+0.34	22.3	YVO	no	yes	no	
GJ 563.2A	14:49:32	−26:06:20	11.68	9.62	4.04	9.94	+0.28	22.3	YVO	no	yes	no	
LHS 381	14:50:29	−08:38:37	15.10	13.07	3.86	12.29	+3.04	36.5	YPC95	no	no	no	S
LHS 2999	14:54:53	+09:56:36	11.29	9.35	3.90	9.34	+0.00	24.5	vLe07	no	no	no	
LHS 3001	14:56:27	+17:55:00	15.81	12.52	5.96	14.57	+0.42	17.7	Rie10	no	no	no	
LHS 3005	14:57:20	+14:58:55	14.83	11.99	5.17	12.84	+0.39	25.0	YPC95	no	no	no	
GJ 1187	14:57:53	+56:39:24	15.53	11.98	6.26	15.28	+0.60	11.2	YPC95	no	no	no	
LHS 3018	15:04:18	+60:23:04	10.99	8.88	4.10	9.74	−0.07	17.8	vLe07	no	yes	no	
LHS 3033	15:11:53	+17:56:39	13.49	10.96	4.72	11.63	+0.29	23.5	YPC95	no	no	no	
LHS 3056	15:19:12	−12:45:06	12.87	10.04	5.29	11.24	−1.50	21.2	RECXX	no	no	yes	
GJ 581	15:19:26	−07:43:20	10.55	8.03	4.71	11.59	+0.27	6.2	YV0	yes	no	no	
GJ 586C	15:27:45	−09:02:00	15.41	···	5.78	13.86	+0.06	20.4	YV	no	no	no	
GJ 587.1	15:28:01	+25:47:23	11.12	9.24	3.83	9.17	+0.00	24.5	vLe07	no	no	no	
LHS 3073	15:28:14	+16:43:11	13.92	12.47	3.52	10.07	+1.55	58.8	YPC95	no	yes	no	S

[a] Notes in Column 14: Y = known young stars, (Y) = suspected young star, S = known subdwarf stars, (S) = suspected, but unconfirmed subdwarf stars.

Distance references: (Ang12) Anglada-Escudé et al. (2012); (Cos05) Costa et al. (2005); (Cos06) Costa et al. (2006); (Dav15) Davison et al. (2015); (Fab00) Fabricius & Makarov (2000); (Gat08) Gatewood (2008); (Gou04) Gould & Chanamé (2004); (Hen06) Henry et al. (2006); (Jao05) Jao et al. (2005); (Jao11) Jao et al. (2011); (Lur14) Lurie et al. (2014); (Rie10) Riedel et al. (2010); (Rie11) Riedel et al. (2011); (Rie14) Riedel et al. (2014); (Shk12) Shkolnik et al. (2012); (Sma10) Smart et al. (2010); (vLe07) van Leeuwen (2007); (Win15) Winters et al. (2015); (Win17) Winters et al. (2017); (YPC95) van Altena et al. (1995).

Table 1: Properties of the Low Mass Stars in the Short-Term Variability Study.

Star Name	R.A. 2000.0	Dec. 2000.0	V	I	$V-K$	M_V (mag)	ΔM_V (mag)	dist.	dist. ref.	LT Study	ST Study	Spec. Study	Notes[a]
(1)	(2)	(3)	(4)	(5)	(6)	(7)	(8)	(9)	(10)	(11)	(12)	(13)	(14)
LP 802-069	15:29:07	−17:22:54	10.52	8.70	3.72	8.55	−0.38	24.8	vLe07	no	no	no	
GJ 1193	15:34:30	+14:16:18	13.89	11.13	5.08	12.32	+0.09	20.6	YPC95	no	no	no	
LP 099-392	15:35:26	+60:05:08	13.46	10.73	5.05	12.05	−0.10	19.1	vLe07	no	no	no	
LHS 3091	15:35:41	+22:08:54	12.73	10.11	4.81	11.39	−0.17	18.5	YPC95	no	no	no	
GJ 592	15:37:01	−14:07:53	12.70	9.93	5.13	12.08	−0.27	13.3	YPC95	no	no	no	
GJ 1194A	15:40:03	+43:29:39	12.48	9.43	4.92	11.84	+0.01	13.4	YPC95	no	no	no	
GJ 595	15:42:07	−19:28:18	11.84	9.29	4.67	11.84	+0.62	10.0	YV	no	no	no	
GJ 2116	15:43:18	−20:15:32	13.06	10.93	4.04	11.42	+1.75	21.3	Jao11	no	yes	no	S
G 202-016	15:49:36	+51:02:57	12.05	9.94	4.30	10.66	+0.38	19.0	vLe07	no	no	no	
LHS 3130B	15:53:06	+34:44:47	13.17	10.50	4.99	11.43	−0.59	22.3	YPC95	no	yes	no	
GJ 606	15:59:53	−08:15:11	10.49	8.39	4.15	9.81	−0.11	13.7	vLe07	no	no	no	
SCR 1601-3421	16:01:56	−34:21:57	16.18	12.86	6.20	14.50	−0.08	21.7	Win17	no	no	no	
GJ 609	16:02:50	+20:35:21	12.58	9.70	5.21	12.58	+0.03	10.0	YPC95	yes	yes	no	
LHS 3149	16:04:20	−06:16:45	15.65	12.28	6.10	14.54	+0.13	16.7	YPC95	no	no	no	
GJ 611	16:04:47	+39:09:35	14.23	11.48	5.07	13.42	+1.21	14.5	YV	no	no	no	
GJ 1198	16:08:12	−10:28:06	14.69	11.78	5.16	13.06	+0.63	21.2	YPC95	no	no	no	
HIP 079126	16:09:03	+52:56:37	10.19	8.31	3.86	9.05	−0.19	16.9	vLe07	no	no	no	
LP 804-027	16:12:41	−18:52:31	11.37	8.92	4.78	10.59	−0.90	14.3	vLe07	no	no	no	
GJ 615.2D	16:13:56	+33:46:24	12.33	···	3.99	10.55	+1.00	22.7	YVO	no	yes	yes	
LHS 3169	16:14:21	−28:30:36	12.95	10.29	4.84	11.59	−0.04	18.7	Rie10	yes	no	no	
GJ 618.4	16:22:40	−48:39:20	11.84	9.70	4.20	9.97	−0.08	23.7	YV	no	no	no	
GJ 620	16:23:07	−24:42:35	10.22	8.34	3.83	9.15	−0.03	16.4	vLe07	no	no	no	
GJ 625	16:25:24	+54:18:14	10.11	7.89	4.28	11.05	+0.81	6.5	YV	no	yes	yes	
GJ 2120	16:27:33	−10:00:28	10.85	8.84	4.02	9.06	−0.54	22.8	vLe07	no	no	yes	
GJ 2121	16:30:13	−14:39:49	12.35	9.84	4.75	10.60	−0.82	22.4	vLe07	no	yes	yes	
GJ 628	16:30:18	−12:39:45	10.07	7.37	5.00	11.90	−0.12	4.3	YV	yes	no	yes	
LHS 3218	16:35:24	−27:18:54	14.18	11.28	5.18	12.84	+0.37	18.5	Rie10	no	no	no	
GJ 1204	16:36:05	+08:48:34	13.81	10.92	5.30	12.89	+0.13	15.3	YPC95	no	no	no	
SCR 1636-4041	16:36:58	−40:41:06	13.44	10.70	5.13	11.68	−0.67	22.5	Win17	no	no	no	
LHS 5319	16:39:30	+50:34:03	11.83	9.95	3.97	10.22	+0.72	21.0	vLe07	no	no	no	
LTT 14949	16:40:48	+36:19:00	11.50	9.45	4.30	10.08	−0.19	19.2	vLe07	no	no	no	
GJ 634	16:41:28	−43:59:31	11.58	9.38	4.25	10.38	+0.22	17.4	YPC95	no	no	no	
LHS 425	16:42:04	+10:25:59	15.12	12.93	3.82	12.18	+3.02	38.8	YPC95	no	no	no	S
LP 154-205	16:47:55	−65:09:11	13.98	11.16	5.10	13.13	+0.85	14.8	Win17	no	no	no	
GJ 637	16:48:24	−72:58:33	11.35	9.26	4.13	10.36	+0.49	15.8	vLe07	no	no	no	
LP 806-008	16:48:45	−15:44:20	10.94	8.99	4.17	9.64	−0.32	18.2	vLe07	no	no	no	
G 169-029	16:50:57	+22:26:48	14.08	10.91	5.77	14.06	+0.27	10.1	Win17	no	no	no	
GJ 643	16:55:25	−08:19:21	11.77	9.01	5.05	12.71	+0.56	6.5	YVO	yes	yes	yes	
GJ 645	16:56:48	−37:03:20	11.44	9.34	4.10	10.28	+0.48	17.1	YPC95	no	no	no	
GJ 1207	16:57:05	−04:20:56	12.25	9.43	5.13	12.56	+0.21	8.67	Hen06	yes	yes	no	Y
GJ 649	16:58:08	+25:44:39	9.69	7.63	4.07	9.65	−0.07	10.2	YV	no	no	no	
HIP 083405	17:02:49	−06:04:06	10.82	8.89	3.88	9.50	+0.22	18.4	vLe07	no	no	no	
GJ 654B	17:05:13	−05:05:39	10.08	7.96	4.11	9.95	+0.14	10.6	YVO	no	no	no	
L 268-067	17:10:59	−52:30:55	10.02	7.99	3.99	9.55	+0.00	12.4	vLe07	no	no	no	
LTT 15087	17:11:34	+38:26:33	11.61	9.15	4.81	11.21	−0.35	12.0	vLe07	no	no	no	
GJ 1214	17:15:18	+04:57:50	14.71	11.50	5.93	14.16	+0.06	12.9	YPC95	no	no	no	
L 1205-067	17:16:00	+11:03:27	10.83	8.77	4.01	9.59	−0.01	17.7	vLe07	no	no	no	
LP 138-036B	17:17:39	+52:24:22	14.04	···	5.11	12.73	+0.43	18.3	vLe07	no	no	no	
HIP 084652	17:18:21	−01:46:53	10.59	8.72	3.88	9.17	−0.11	19.2	vLe07	no	no	no	
GJ 669A	17:19:54	+26:30:03	11.42	8.76	5.00	11.25	−0.78	10.8	YV	no	no	no	
GJ 1216	17:20:46	+49:15:20	14.53	11.70	5.15	13.38	+0.97	17.0	YPC95	no	no	yes	
HIP 085042B	17:22:51	−02:23:17	12.18	9.64	4.74	10.73	−0.66	19.5	vLe07	no	no	no	
GJ 672.1	17:23:49	−32:15:16	11.64	9.55	4.12	9.78	−0.07	23.5	vLe07	no	no	no	

[a] Notes in Column 14: Y = known young stars, (Y) = suspected young star, S = known subdwarf stars, (S) = suspected, but unconfirmed subdwarf stars.

Distance references: (Ang12) Anglada-Escudé et al. (2012); (Cos05) Costa et al. (2005); (Cos06) Costa et al. (2006); (Dav15) Davison et al. (2015); (Fab00) Fabricius & Makarov (2000); (Gat08) Gatewood (2008); (Gou04) Gould & Chanamé (2004); (Hen06) Henry et al. (2006); (Jao05) Jao et al. (2005); (Jao11) Jao et al. (2011); (Lur14) Lurie et al. (2014); (Rie10) Riedel et al. (2010); (Rie11) Riedel et al. (2011); (Rie14) Riedel et al. (2014); (Shk12) Shkolnik et al. (2012); (Sma10) Smart et al. (2010); (vLe07) van Leeuwen (2007); (Win15) Winters et al. (2015); (Win17) Winters et al. (2017); (YPC95) van Altena et al. (1995).

Table 1: Properties of the Low Mass Stars in the Short-Term Variability Study.

Star Name	R.A. 2000.0	Dec. 2000.0	V	I	$V-K$	M_V (mag)	ΔM_V (mag)	dist.	dist. ref.	LT Study	ST Study	Spec. Study	Notes[a]
(1)	(2)	(3)	(4)	(5)	(6)	(7)	(8)	(9)	(10)	(11)	(12)	(13)	(14)
GJ 1219	17:27:39	+14:29:02	13.73	11.11	4.77	12.24	+0.77	19.9	YPC95	no	yes	no	
GJ 1218	17:28:07	−62:27:14	12.74	9.95	5.17	11.68	−0.78	16.3	Jao05	no	no	no	
LHS 3295	17:29:27	−80:08:57	12.18	9.53	4.88	11.70	−0.05	12.5	Rie10	yes	no	no	
GJ 676A	17:30:11	−51:38:13	9.59	7.76	3.77	8.53	−0.50	16.3	vLe07	no	yes	yes	
GJ 676B	17:30:11	−51:38:13	13.40	10.50	5.38	12.34	−0.61	16.3	vLe07	no	yes	no	
GJ 678.1	17:30:22	+05:32:54	9.30	7.40	3.88	9.32	+0.04	9.9	YV	no	no	no	
GJ 685B	17:35:34	+61:40:53	9.97	8.01	3.90	9.24	−0.11	14.0	YVO	no	no	no	
GJ 686	17:37:53	+18:35:30	9.61	7.55	4.04	10.07	+0.41	8.1	YV	no	no	no	
L 204-148	17:38:33	−58:32:34	12.52	9.91	4.85	11.57	−0.10	15.5	Win17	no	no	no	
L 1422-016A	17:39:30	+27:45:44	11.12	9.37	3.86	9.14	−0.11	24.9	vLe07	no	no	no	
L 1422-015B	17:39:32	+27:46:37	12.72	10.32	4.75	10.74	−0.67	24.9	vLe07	no	yes	no	
GJ 694.2	17:45:33	+46:51:19	10.72	8.80	3.93	9.07	−0.32	21.4	YV	no	no	no	
GJ 2130A	17:46:12	−32:06:09	10.50	8.34	4.25	9.75	−0.41	14.1	Hen06	yes	no	no	
GJ 693	17:46:34	−57:19:08	10.77	8.20	4.75	11.95	+0.53	5.8	YV	yes	no	yes	
LHS 3333	17:50:13	+23:46:16	13.50	10.80	5.05	11.76	−0.40	22.3	YPC95	no	no	no	
GJ 1222	17:54:17	+07:22:45	13.12	10.36	5.15	12.02	−0.37	16.6	YPC95	no	no	no	
BARNARDS	17:57:48	+04:41:36	9.57	6.79	5.05	13.29	+1.14	1.8	YVO	no	no	no	
GJ 1223	18:02:46	+37:31:03	14.79	11.55	5.90	14.41	+0.37	11.9	YPC95	no	no	no	
G 154-043	18:03:36	−18:58:47	14.13	10.90	5.86	13.54	−0.41	13.1	Win17	no	no	no	
G 182-037	18:04:17	+35:57:25	10.83	8.99	3.96	9.21	−0.27	21.1	vLe07	no	no	no	
GJ 701	18:05:07	−03:01:52	9.37	7.30	4.06	9.91	+0.19	7.8	YV	no	no	yes	
GJ 1224	18:07:31	−15:58:15	13.51	10.32	5.68	14.13	+0.53	7.5	YPC95	no	no	no	
LP 334-011	18:09:40	+31:52:12	11.41	9.40	3.98	9.77	+0.26	21.3	vLe07	no	no	no	
LP 390-016	18:13:06	+26:01:51	13.32	10.58	5.26	12.16	−0.50	17.1	Shk12	no	no	no	
LHS 3370	18:13:52	−77:08:20	15.38	12.55	5.03	13.54	+1.43	23.3	Cos06	no	no	no	
LTT 15403	18:15:43	+18:56:19	10.82	8.57	3.86	9.04	−0.20	22.7	YV	no	no	no	
GJ 709	18:16:31	+45:33:28	10.28	9.55	3.83	9.13	−0.04	17.0	YV	no	no	no	
LHS 461B	18:18:03	+38:46:36	13.54	10.71	5.17	13.27	+0.82	11.3	YPC95	no	no	yes	
GJ 1227	18:22:27	+62:03:02	13.46	10.35	5.72	13.89	+0.22	8.2	YPC95	no	no	no	
LTT 15449	18:25:04	+24:38:04	10.79	9.08	3.81	9.10	−0.04	21.8	vLe07	no	no	no	
LHS 3385	18:25:31	+38:21:12	11.27	9.37	3.78	9.32	+0.26	24.5	vLe07	no	no	no	
LP 630-081	18:26:17	+01:46:21	14.90	11.79	5.74	13.55	−0.16	18.6	Lep09	no	no	no	
WT 562	18:26:19	−65:47:41	15.36	12.13	5.92	14.20	+0.13	17.1	Rie10	no	no	no	
LTT 07341	18:30:12	−58:16:28	9.81	7.93	3.85	8.97	−0.24	14.7	Win17	no	no	no	
GJ 720A	18:35:18	+45:44:38	9.86	7.99	3.78	8.92	−0.14	15.4	YV	no	no	no	
GJ 720B	18:35:18	+45:44:38	13.02	10.33	4.95	12.08	+0.18	15.4	YV	no	no	no	
GJ 723	18:40:17	−10:27:54	11.47	9.38	4.01	9.80	+0.21	21.6	YV	no	no	no	
LHS 3402B	18:40:55	+31:32:05	11.63	9.51	4.24	9.77	−0.36	23.6	YV	no	no	no	
GJ 724	18:40:57	−13:22:46	10.62	8.56	4.07	9.53	−0.21	16.5	YV	no	no	no	
G 141-029	18:42:45	+13:54:17	12.84	9.94	5.29	12.61	−0.12	11.1	Rie14	no	yes	no	Y
LTT 07419A	18:43:12	−33:22:31	10.25	8.28	3.92	9.34	−0.05	15.2	Win17	yes	no	yes	
LHS 3409	18:45:44	+52:28:20	15.13	12.37	4.91	13.59	+1.78	20.3	YPC95	no	no	no	S
GJ 729	18:49:49	−23:50:10	10.50	7.68	5.13	13.11	+0.76	3.0	YV	yes	yes	yes	
LHS 3413	18:49:51	−57:26:48	12.68	9.88	5.23	12.27	−0.31	12.1	Rie10	no	no	no	
GJ 730	18:50:00	+03:05:17	10.74	8.80	3.88	9.17	−0.13	20.6	YV	no	no	no	
HIP 092451	18:50:26	−62:03:03	10.70	8.69	4.00	9.67	+0.11	16.1	vLe07	no	no	no	
GJ 731	18:51:51	+16:34:59	10.15	8.28	3.83	9.24	+0.06	15.2	YV	no	no	yes	
L 489-043	18:52:25	−37:30:36	12.71	9.86	5.15	11.79	−0.62	15.3	Win17	no	no	no	
GJ 740	18:58:00	+05:54:29	9.21	7.31	3.85	9.02	−0.21	10.9	YV	no	no	yes	
GJ 741	19:03:16	−13:34:12	14.78	12.08	5.24	13.39	+0.76	19.0	YPC95	no	no	no	
GJ 745A	19:07:05	+20:53:17	10.78	8.54	4.26	11.08	+0.90	8.7	YV	no	yes	yes	
GJ 745B	19:07:13	+20:52:37	10.76	8.53	4.24	11.06	+0.91	8.7	YV	no	yes	yes	
GJ 747.4	19:12:25	−55:52:07	11.30	9.35	3.92	9.65	+0.26	21.4	vLe07	no	no	no	

[a] Notes in Column 14: Y = known young stars, (Y) = suspected young star, S = known subdwarf stars, (S) = suspected, but unconfirmed subdwarf stars.

Distance references: (Ang12) Anglada-Escudé et al. (2012); (Cos05) Costa et al. (2005); (Cos06) Costa et al. (2006); (Dav15) Davison et al. (2015); (Fab00) Fabricius & Makarov (2000); (Gat08) Gatewood (2008); (Gou04) Gould & Chanamé (2004); (Hen06) Henry et al. (2006); (Jao05) Jao et al. (2005); (Jao11) Jao et al. (2011); (Lur14) Lurie et al. (2014); (Rie10) Riedel et al. (2010); (Rie11) Riedel et al. (2011); (Rie14) Riedel et al. (2014); (Shk12) Shkolnik et al. (2012); (Sma10) Smart et al. (2010); (vLe07) van Leeuwen (2007); (Win15) Winters et al. (2015); (Win17) Winters et al. (2017); (YPC95) van Altena et al. (1995).

Table 1: Properties of the Low Mass Stars in the Short-Term Variability Study.

Star Name	R.A.	Dec.	V	I	$V-K$	M_V	ΔM_V	dist.	dist. ref.	LT Study	ST Study	Spec. Study	Notes[a]
	2000.0					(mag)	(mag)						
(1)	(2)	(3)	(4)	(5)	(6)	(7)	(8)	(9)	(10)	(11)	(12)	(13)	(14)
LHS 3443	19:13:07	−39:01:53	12.39	9.85	4.73	10.83	−0.54	20.5	Rie10	yes	no	no	
LHS 3446	19:14:39	+19:18:22	13.28	10.57	4.95	11.93	+0.03	18.6	YVO	no	no	no	
LHS 3445	19:14:39	+19:19:04	11.59	9.05	4.78	10.24	−1.24	18.6	YVO	no	yes	yes	(Y)
LHS 475	19:20:54	−82:33:16	12.69	10.00	5.00	12.29	+0.25	12.0	Jao11	yes	no	no	
GJ 756	19:21:51	+28:39:58	11.86	9.84	4.31	10.11	−0.21	22.4	YV	no	no	no	
GJ 1236	19:22:02	+07:02:31	12.39	9.86	4.70	12.24	+0.95	10.7	YPC95	no	yes	yes	
LTT 18490	19:39:32	+71:52:19	10.98	9.23	3.79	9.25	+0.16	22.2	YV	no	no	no	
LP 869-042	19:39:36	−26:45:07	10.48	8.58	3.83	8.65	−0.53	23.2	vLe07	no	no	yes	
LTT 15769	19:45:49	+32:23:13	10.86	8.91	4.09	10.45	+0.68	12.1	YVO	no	no	yes	
GJ 767A	19:46:23	+32:01:01	10.23	7.67	4.19	9.55	−0.47	13.7	YVO	no	no	no	
LHS 479	19:46:49	+12:04:59	14.26	···	3.76	10.94	+1.91	46.1	YPC95	no	no	no	S
GJ 1243	19:51:09	+46:29:00	12.83	10.09	5.06	12.47	+0.29	11.8	YPC95	no	no	no	
LHS 3499	19:55:52	+51:16:22	11.86	9.79	4.01	9.90	+0.30	24.7	YV	no	yes	no	
GJ 773B	19:57:19	−12:34:04	15.36	11.95	6.04	14.00	−0.30	18.7	YV	no	no	no	
GJ 1248	20:03:51	+05:59:44	12.11	9.84	4.24	11.63	+1.48	12.5	YPC95	no	yes	yes	(S)
GJ 774B	20:04:02	−65:36:48	12.83	10.24	4.70	12.24	+0.95	13.1	YPC95	no	yes	no	
GJ 774A	20:04:02	−65:36:48	11.35	9.06	4.29	10.76	+0.49	13.1	YPC95	no	yes	no	
LHS 482	20:05:02	+54:26:03	12.00	9.98	3.89	10.91	+1.61	16.5	YPC95	no	no	yes	S
GJ 781.1A	20:07:44	−31:45:14	12.22	9.73	4.82	11.27	−0.33	15.5	vLe07	no	yes	no	
GJ 781.1B	20:07:48	−31:45:28	12.51	9.70	4.92	11.56	−0.28	15.5	vLe07	no	yes	no	
GJ 1250	20:08:17	+33:18:13	14.93	11.71	5.85	13.26	−0.68	21.6	YPC95	no	no	no	
2MA 2009-0113	20:09:18	−01:13:38	14.47	11.16	5.96	14.38	+0.23	10.4	Rie14	no	no	no	Y
HIP 099316B	20:09:34	+16:48:20	9.92	···	3.98	8.05	−1.46	23.7	vLe07	no	no	no	
GJ 783.2B	20:11:06	+16:11:16	13.98	11.17	5.10	12.43	+0.16	20.4	YV	no	no	no	
LP 754-050B	20:12:09	−12:53:35	11.28	9.50	3.66	9.30	+0.50	24.9	YV	no	no	no	
GJ 784.2A	20:13:58	+06:41:25	13.33	10.55	5.16	11.59	−0.84	22.3	YPC95	no	yes	no	
GJ 1253	20:26:05	+58:34:23	14.04	10.84	5.95	14.20	+0.07	9.3	YPC95	no	no	no	
LHS 491	20:27:29	+35:59:25	14.75	···	3.89	11.30	+2.00	49.0	YPC95	no	no	no	S
GJ 1252	20:27:42	−56:27:25	12.20	9.93	4.29	10.73	+0.48	19.7	Jao05	no	no	no	
L 755-019	20:28:43	−11:28:31	12.47	9.81	4.97	11.10	−0.86	18.8	Rie14	no	no	no	Y
GJ 792	20:31:25	+38:33:44	13.48	10.65	5.12	12.61	+0.28	14.9	YPC95	no	no	no	
SCR 2033-2556	20:33:37	−25:56:52	14.87	11.57	5.99	11.45	−2.76	48.3	Rie14	no	no	no	Y
GJ 1254	20:33:40	+61:45:14	12.54	9.79	5.14	11.55	−0.84	15.8	YPC95	no	no	no	
LHS 3564	20:34:43	+03:20:51	11.92	9.62	4.29	10.27	+0.00	21.4	YV	no	no	no	
GJ 1256	20:40:33	+15:29:59	13.45	10.36	5.70	13.49	−0.15	9.8	YPC95	no	no	no	
G 262-026	20:43:41	+64:16:54	11.38	9.63	3.77	9.76	+0.72	21.1	vLe07	no	no	no	
GJ 806	20:45:04	+44:29:56	10.77	8.57	4.24	10.34	+0.21	12.2	YV	no	no	yes	
GJ 803A	20:45:09	−31:20:27	8.65	6.61	4.12	8.67	−1.18	9.9	YV	no	yes	yes	Y
SC R2049-4012	20:49:10	−40:12:07	13.53	10.31	5.83	13.73	−0.16	9.1	RECXX	no	no	no	
LEP 2050-3424	20:50:16	−34:24:43	13.75	10.55	5.75	13.84	+0.09	9.6	RECXX	no	no	no	
GJ 808	20:51:41	−79:18:39	11.81	9.64	4.15	10.59	+0.68	17.5	Jao11	yes	no	no	
LP 816-060	20:52:33	−16:58:29	11.50	8.64	5.30	12.72	−0.04	5.7	vLe07	yes	no	no	
2MA 2053-0133	20:53:09	−01:33:04	15.79	12.46	6.00	14.50	+0.28	18.1	Shk12	no	no	no	
GJ 809	20:53:19	+62:09:15	8.56	6.58	3.94	9.30	−0.13	7.1	YV	no	no	yes	
GJ 810B	20:55:37	−14:03:54	14.63	11.40	5.72	14.09	+0.42	12.8	Jao11	no	no	no	
GJ 812A	20:56:48	−04:50:49	11.94	9.27	4.88	10.83	−0.90	16.7	YV	no	yes	no	
LTT 16135	20:58:41	+34:16:27	11.06	9.18	3.81	9.15	+0.02	24.1	vLe07	no	no	no	
GJ 2151	21:03:13	−56:57:48	12.84	10.15	4.94	12.22	+0.34	13.3	vLe07	no	no	no	
GJ 817	21:04:53	−16:57:31	11.45	9.42	3.91	10.19	+0.84	17.9	YV	no	no	no	
LHS 064	21:07:55	+59:43:19	13.23	11.19	3.84	11.34	+2.14	23.9	YPC95	no	no	no	S
GJ 821	21:09:17	−13:18:09	10.87	8.83	3.96	10.46	+0.98	12.1	YV	no	no	no	
GJ 818.1C	21:09:22	−73:10:22	13.50	···	6.16	12.02	−2.49	19.8	vLe07	no	no	no	
L 1433-004B	21:16:03	+29:51:46	13.49	10.72	5.04	12.07	−0.06	19.2	Shk12	no	no	no	

[a] Notes in Column 14: Y = known young stars, (Y) = suspected young star, S = known subdwarf stars, (S) = suspected, but unconfirmed subdwarf stars.

Distance references: (Ang12) Anglada-Escudé et al. (2012); (Cos05) Costa et al. (2005); (Cos06) Costa et al. (2006); (Dav15) Davison et al. (2015); (Fab00) Fabricius & Makarov (2000); (Gat08) Gatewood (2008); (Gou04) Gould & Chanamé (2004); (Hen06) Henry et al. (2006); (Jao05) Jao et al. (2005); (Jao11) Jao et al. (2011); (Lur14) Lurie et al. (2014); (Rie10) Riedel et al. (2010); (Rie11) Riedel et al. (2011); (Rie14) Riedel et al. (2014); (Shk12) Shkolnik et al. (2012); (Sma10) Smart et al. (2010); (vLe07) van Leeuwen (2007); (Win15) Winters et al. (2015); (Win17) Winters et al. (2017); (YPC95) van Altena et al. (1995).

Table 1: Properties of the Low Mass Stars in the Short-Term Variability Study.

Star Name (1)	R.A. 2000.0 (2)	Dec. 2000.0 (3)	V (4)	I (5)	$V-K$ (6)	M_V (mag) (7)	ΔM_V (mag) (8)	dist. (9)	dist. ref. (10)	LT Study (11)	ST Study (12)	Spec. Study (13)	Notes[a] (14)
L 117-123	21:20:09	−67:39:05	10.89	8.86	4.06	9.30	−0.40	20.8	YV	no	no	no	
GJ 828B	21:26:52	−44:48:47	13.53	10.76	5.19	11.68	−0.80	23.4	vLe07	no	no	no	
GJ 828.2	21:27:16	−06:50:39	11.10	9.15	3.93	10.03	+0.61	16.4	vLe07	no	no	yes	
LHS 3677	21:27:46	+07:17:16	11.64	9.64	4.10	9.69	−0.10	24.5	YPC95	no	no	no	
LHS 510	21:30:47	−40:42:29	13.12	10.34	4.99	12.74	+0.74	11.9	Jao05	no	no	no	
GJ 832	21:33:33	−49:00:32	8.66	6.48	4.16	10.21	+0.27	4.9	YV	no	no	yes	
HIP 106803	21:37:55	−63:42:42	10.62	8.62	3.98	8.99	−0.53	21.2	vLe07	no	no	yes	
LHS 512	21:38:43	−33:39:55	12.55	9.88	4.98	12.14	+0.16	12.1	Jao05	yes	no	no	
GJ 1263A	21:46:40	−00:10:25	12.64	9.87	5.15	12.26	−0.14	11.9	YPC95	no	no	no	
LTT 16369	21:46:56	+46:38:06	13.36	10.62	5.15	12.27	−0.12	16.5	Pra09	no	no	no	
LHS 3711	21:47:53	+50:15:16	13.33	10.68	4.78	11.68	+0.20	21.4	YPC95	no	no	no	
LTT 16412	21:57:26	+08:08:13	11.03	8.91	4.19	9.41	−0.60	21.1	YVO	no	yes	yes	
GJ 842.2	21:58:24	+75:35:20	10.57	8.69	3.84	9.00	−0.20	20.6	YV	no	no	no	
LHS 3739A	21:58:50	−32:28:17	14.72	11.88	5.16	13.26	+0.83	19.6	Rie10	no	yes	no	
GJ 842	21:59:34	−59:45:10	9.74	7.75	3.98	9.34	−0.18	12.0	YV	no	no	no	
G 188-038	22:01:13	+28:18:24	12.05	9.16	5.27	12.28	−0.42	9.0	YV	yes	no	no	
GJ 846	22:02:10	+01:24:00	9.17	7.27	3.85	9.13	−0.09	10.2	YV	no	no	yes	
LHS 3746	22:02:29	−37:04:51	11.76	9.04	5.04	12.41	+0.27	7.4	Hen06	yes	no	no	
LHS 3748	22:03:27	−50:38:38	12.09	9.86	4.28	10.60	+0.36	19.9	vLe07	no	no	no	
SCR 2204-3347	22:04:02	−33:47:39	15.44	13.41	3.84	11.60	+2.40	58.6	Cos05	no	yes	no	S
LTT 08848	22:05:51	−11:54:51	10.11	8.28	3.71	8.38	−0.54	22.2	vLe07	no	no	yes	
GJ 849	22:09:40	−04:38:26	10.38	7.87	4.79	10.61	−0.89	9.0	YV	yes	no	yes	
G 214-012	22:09:45	+41:02:21	12.62	10.08	4.75	10.85	−0.57	22.6	YPC95	no	no	no	
G 232-062	22:16:03	+54:40:00	14.00	···	5.07	12.34	+0.14	21.5	vLe07	no	no	no	
GJ 1266	22:16:20	+70:56:40	12.12	9.96	4.10	10.40	+0.59	22.1	YPC95	no	no	no	
LHS 3799	22:23:07	−17:37:01	13.30	10.04	5.98	13.95	−0.24	7.4	YPC95	yes	yes	no	Y
GJ 855	22:23:33	−57:13:14	10.72	8.72	3.99	9.33	−0.22	19.0	YV	no	no	no	
LTT 16590	22:28:45	+18:55:54	10.74	8.91	3.76	9.03	+0.00	22.0	vLe07	no	no	no	
LP 640-074	22:29:05	+01:39:48	10.49	8.65	3.74	8.85	−0.14	21.3	vLe07	no	no	no	
GJ 1270	22:29:49	+41:28:49	13.24	10.40	5.20	12.56	+0.03	13.7	YPC95	no	no	no	
GJ 863	22:33:02	+09:22:40	10.38	8.34	4.02	9.76	+0.14	13.3	YV	no	no	yes	
GJ 867C	22:38:45	−20:37:16	11.45	8.78	4.96	11.75	−0.18	8.7	YV	no	no	no	
GJ 871.1A	22:44:57	−33:15:01	12.11	9.32	5.18	10.27	−2.20	23.3	vLe07	no	yes	no	Y
LHS 3850	22:46:26	−06:39:25	16.03	12.76	6.18	14.67	+0.13	18.7	YPC95	no	no	no	
GJ 873	22:46:49	+44:20:02	10.22	7.55	4.92	11.73	−0.12	5.0	YVO	no	no	no	
GJ 875	22:50:19	−07:05:24	9.86	8.02	3.76	9.11	+0.10	14.1	YV	no	no	yes	
GJ 1274	22:50:37	+34:51:21	11.72	9.52	4.21	10.44	+0.38	18.0	YV	no	no	no	
GJ 875.1	22:51:53	+31:45:15	11.62	9.11	4.75	10.77	−0.63	14.8	YV	no	no	yes	
LHS 5394	22:52:48	−28:47:42	11.87	9.65	4.29	10.41	+0.14	19.6	vLe07	no	no	no	
GJ 876	22:53:16	−14:15:49	10.18	7.40	5.17	11.82	−0.63	4.7	YVO	yes	no	yes	
GJ 878	22:54:21	+60:59:44	12.78	10.23	4.81	11.87	+0.31	15.2	YPC95	no	no	no	
LHS 3872	22:54:46	−05:28:26	13.89	11.12	5.08	12.03	−0.20	23.5	YXO	no	no	no	
HIP 113201	22:55:27	−52:18:09	11.51	9.44	4.09	9.55	−0.24	24.7	vLe07	no	no	no	
L 1150-065A	22:55:55	+05:45:22	11.21	9.22	3.97	9.27	−0.22	24.4	vLe07	no	no	no	
GJ 1277	22:56:24	−60:03:49	14.00	10.79	5.89	13.96	−0.07	10.2	Jao11	yes	no	no	
GJ 880	22:56:34	+16:33:12	8.65	6.55	4.13	9.49	−0.38	6.8	YV	no	no	yes	
L 718-071	23:00:33	−23:57:10	11.57	9.48	4.16	10.03	+0.08	20.3	vLe07	no	no	no	
L 718-070	23:00:36	−23:58:10	11.61	9.49	4.19	10.07	+0.05	20.3	vLe07	no	no	no	
HI P113850	23:03:20	−49:43:34	10.67	8.75	3.86	9.13	−0.11	20.3	vLe07	no	no	no	
GJ 887	23:05:52	−35:51:11	7.34	5.32	3.88	9.75	+0.47	3.3	YV	no	no	yes	
HIP 114066	23:06:04	+63:55:34	10.82	8.99	3.84	8.87	−0.33	24.5	vLe07	no	no	yes	Y
GJ 889B	23:07:07	−23:09:34	13.65	11.01	4.91	12.05	+0.23	20.9	vLe07	no	no	no	
GJ 889.1	23:08:06	+03:19:44	10.91	8.98	3.84	9.92	+0.71	15.8	vLe07	no	no	no	

[a] Notes in Column 14: Y = known young stars, (Y) = suspected young star, S = known subdwarf stars, (S) = suspected, but unconfirmed subdwarf stars.

Distance references: (Ang12) Anglada-Escudé et al. (2012); (Cos05) Costa et al. (2005); (Cos06) Costa et al. (2006); (Dav15) Davison et al. (2015); (Fab00) Fabricius & Makarov (2000); (Gat08) Gatewood (2008); (Gou04) Gould & Chanamé (2004); (Hen06) Henry et al. (2006); (Jao05) Jao et al. (2005); (Jao11) Jao et al. (2011); (Lur14) Lurie et al. (2014); (Rie10) Riedel et al. (2010); (Rie11) Riedel et al. (2011); (Rie14) Riedel et al. (2014); (Shk12) Shkolnik et al. (2012); (Sma10) Smart et al. (2010); (vLe07) van Leeuwen (2007); (Win15) Winters et al. (2015); (Win17) Winters et al. (2017); (YPC95) van Altena et al. (1995).

Table 1: Properties of the Low Mass Stars in the Short-Term Variability Study.

Star Name	R.A. (2000.0)	Dec. (2000.0)	V	I	$V-K$	M_V (mag)	ΔM_V (mag)	dist.	dist. ref.	LT Study	ST Study	Spec. Study	Notes[a]
(1)	(2)	(3)	(4)	(5)	(6)	(7)	(8)	(9)	(10)	(11)	(12)	(13)	(14)
GJ 890	23:08:19	−15:24:35	10.84	9.01	3.73	9.06	+0.11	22.7	YV	no	no	no	
GJ 891	23:10:15	−25:56:52	11.27	8.06	4.28	10.26	+0.04	15.9	vLe07	no	no	no	
GJ 1281	23:10:42	−19:13:34	12.45	10.20	4.22	10.52	+0.44	24.3	Jao05	no	no	no	
LHS 3909	23:12:11	−14:06:11	12.97	10.40	4.75	11.67	+0.25	18.2	Rie10	no	no	no	
GJ 2154A	23:14:16	−19:38:39	10.48	8.56	3.86	9.00	−0.25	19.8	vLe07	no	no	no	
LHS 3925	23:17:50	−48:18:47	13.61	10.92	4.91	11.97	+0.17	21.3	Rie10	no	no	no	
GJ 894.1	23:18:17	+46:17:21	10.89	8.98	3.87	8.94	−0.33	24.6	vLe07	no	no	no	
LHS 543	23:21:37	+17:17:25	11.65	8.89	5.14	11.48	−0.90	10.8	YV	no	yes	no	
GJ 895	23:24:30	+57:51:15	10.00	7.95	4.13	9.43	−0.44	13.0	YV	no	no	no	
G 190-027	23:29:25	+41:27:48	12.42	9.56	5.25	11.58	−1.07	14.7	YPC95	no	yes	no	
G 190-028	23:29:26	+41:28:20	11.89	9.31	4.82	11.05	−0.55	14.7	YPC95	no	yes	no	
GJ 1284	23:30:13	−20:23:27	11.12	8.60	4.79	10.09	−1.43	16.1	Rie14	yes	yes	yes	(Y)
LHS 3978	23:35:44	+06:11:46	16.17	12.90	6.01	14.27	+0.02	24.0	YPC95	no	no	no	
HIP 116491B	23:36:18	−48:35:17	12.39	9.64	5.20	10.58	−1.94	23.0	vLe07	no	no	no	
LTT 16952	23:36:25	+55:29:43	11.70	9.62	4.12	9.73	−0.12	24.8	vLe07	no	no	no	
GJ 1290	23:44:23	+21:36:14	13.29	10.66	5.07	11.58	−0.62	22.0	YPC95	no	yes	no	
GJ 907	23:48:03	+49:00:57	12.08	9.92	4.15	10.98	+1.06	16.6	YV	no	no	yes	(S)
GJ 908	23:49:12	+02:24:04	8.98	6.95	3.94	10.09	+0.67	6.0	YV	no	no	yes	
L 085-031	23:53:25	−70:56:41	13.01	10.18	5.23	12.51	−0.09	12.6	Win17	no	no	no	
LHS 4039A	23:54:01	−33:16:24	13.46	10.85	4.85	11.67	+0.01	22.8	Sub09	no	no	no	
LHS 4057	23:59:50	+47:45:09	16.12	12.76	6.19	14.7	+0.14	19.2	YPC95	no	no	no	
LHS 4058	23:59:51	−34:06:42	12.84	10.08	5.09	11.85	−0.41	15.8	Rie10	yes	no	no	

[a]Notes in Column 14: Y = known young stars, (Y) = suspected young star, S = known subdwarf stars, (S) = suspected, but unconfirmed subdwarf stars.

Distance references: (Ang12) Anglada-Escudé et al. (2012); (Cos05) Costa et al. (2005); (Cos06) Costa et al. (2006); (Dav15) Davison et al. (2015); (Fab00) Fabricius & Makarov (2000); (Gat08) Gatewood (2008); (Gou04) Gould & Chanamé (2004); (Hen06) Henry et al. (2006); (Jao05) Jao et al. (2005); (Jao11) Jao et al. (2011); (Lur14) Lurie et al. (2014); (Rie10) Riedel et al. (2010); (Rie11) Riedel et al. (2011); (Rie14) Riedel et al. (2014); (Shk12) Shkolnik et al. (2012); (Sma10) Smart et al. (2010); (vLe07) van Leeuwen (2007); (Win15) Winters et al. (2015); (Win17) Winters et al. (2017); (YPC95) van Altena et al. (1995).